UNIVERSITY OF SOUTHAMPTON

An experimental study of phase conjugation via stimulated Brillouin scattering applied to a high power Nd:YAG oscillator/amplifier laser system

by

Ian David Carr

A thesis submitted for the degree of
Doctor of Philosophy

Department of Physics
Faculty of Science

December 1984

To my parents

His thinking does not result in smoke after the flashing fire, but in light emerging from the smoke.

Horace 65-68 BC

UNIVERSITY OF SOUTHAMPTON

ABSTRACT

Faculty of Science
Physics

Doctor of Philosophy
An experimental study of phase conjugation via stimulated Brillouin scattering applied to a high power Nd:YAG oscillator/amplifier laser system

by Ian David Carr

In the thesis we investigate the use of phase conjugation techniques for the correction of amplifier aberrations in a Nd:YAG oscillator/amplifier system. The phase conjugation process examined was stimulated Brillouin scattering in methane gas.

In the first part of the thesis a TEMoo, single longitudinal mode, pre-lase Q-switched oscillator is described, which gave a high-quality output beam. We discuss the properties of Nd:YAG laser amplifiers of the type used to amplify this output, and the ensuing beam distortions. The processes of phase conjugation and stimulated Brillouin scattering are then explained. In the latter part of the thesis experimental investigations of these processes are described. These include the effects of depolarisation due to thermally induced birefringence in the laser amplifier and the extent to which the phase conjugation process can tolerate this depolarisation. The effect of the process upon the laser linewidth, and *vice versa* , are also discussed. When a single amplifier stage was used in a two-pass arrangement incorporating either a conventional mirror or a phase conjugate mirror, the latter gave a factor of four improvement in beam brightness over the former. This factor was increased to sixteen when the phase conjugate mirror was used in a four-pass configuration.

CONTENTS

CHAPTER 1

Introduction

Since the invention of the laser two and a half decades ago, much research effort has been devoted to improving the properties of the output beam. Brightness, spatial and temporal coherence and monochromaticity are of particular importance. In many applications, (noteworthy examples being most non-linear optical processes and holography), high values of all these parameters are required.

High spatial and temporal coherence and monochromaticity can be obtained from a laser by suitable design of the oscillator. The output power, and therefore brightness, however, are limited by the volume of the active material and the pumping efficiency. One way to achieve higher powers, widely used with solid state lasers, is to follow the laser oscillator with an amplifier or a chain of amplifiers. The extreme is reached in the large neodymium-in-glass lasers used in fusion experiments, where the output of an oscillator, of a few millijoules, is raised to energies measured in hundreds of kilojoules in long amplifier chains.

One of the most widely employed of all lasers is the pulsed solid state neodymium:YAG (Nd:YAG) laser, which has a usual operating wavelength of 1.06 μm and applications which vary from satellite-ranging to surgery. This type of laser has been used in the studies described in the thesis. Unfortunately, and in common with other solid state lasers such as ruby and Nd:glass, it can suffer from poor beam quality when used in oscillator/amplifier configurations. This arises because the amplifier rods, even if they do not possess intrinsic optical distortions, acquire thermally-induced distortions when pumped. Thus, even though the oscillator may have an output beam of high spatial coherence, the amplified beam is aberrated. In severe cases the initially Gaussian beam breaks up into several parts.

One application of phase conjugation is the correction of linear optical distortions of the type encountered in solid state amplifiers. Beam aberrations can be corrected and the spatial quality of the oscillator beam recovered, by double-passing the distorting medium (the amplifier) using a phase conjugate mirror.

One process in which phase conjugation occurs and which is also readily applied to high power pulsed lasers is stimulated Brillouin scattering (SBS). Many investigations and studies of phase conjugation using SBS have been made, and it has been applied successfully to lasers having severe aberrations. Indeed, a feature of many experiments has been the deliberate introduction of highly distorting elements in order to demonstrate the remarkable correction that phase conjugation can provide. However, what is not apparent from the literature is whether it is a worthwhile exercise applying phase conjugation to a typical laboratory laser, such as a Nd:YAG oscillator/amplifier, in which the amplifier has modest, but still troublesome, distortions. Some of the published work suggests that unless a beam is severely aberrated, it cannot be phase conjugated with high efficiency. Nevertheless, phase conjugation may still give significant benefits over the use of a conventional mirror.

A further question, which arises in applications where narrow linewidth and high temporal coherence are important, is whether the process of phase conjugation via SBS degrades the monochromaticity of the beam, either by line broadening or by introduction of new frequency components. It is also important to know the upper limits on laser linewidth that still allow successful phase conjugation. The work described in this thesis was therefore aimed at investigating the value of phase conjugation via stimulated Brillouin scattering when applied to a typical laboratory Nd:YAG oscillator/amplifier.

The initial work, described in Chapter 2, concerned the development of a Nd:YAG oscillator, incorporating a telescopic resonator and giving the maximum possible TEMoo mode energy. The theory of

single longitudinal mode (SLM) selection is given, and the conversion of the oscillator to SLM operation then explained. This oscillator thus provided an output of high spatial and temporal coherence for subsequent amplification.

The theory of pulse amplification in a laser amplifier and the possible temporal changes in envelope shape are presented in Chapter 3. More importantly, the static and thermally induced optical distortions which occur in a pumped laser rod, such as thermal lensing and stress birefringence, are discussed. It is in part due to these that the beam becomes aberrated.

The process of phase conjugation and the way it can be used to compensate unwanted optical distortions is elucidated in Chapter 4. The non-linear optical interactions that give rise to phase conjugation are outlined briefly, followed by a more detailed account of stimulated Brillouin scattering. This includes the basic theory required to predict threshold powers and a review of some of the relevant work on the subject published to date. The latter provides both an insight into the importance of certain pulse parameters (duration or polarization for example) on the SBS phase conjugation process and indicates where there are shortcomings in current understanding.

Chapter 5 comprises accounts of the three basic experimental arrangements tested, the measurements made on these and the results obtained. Details are given of the high-pressure methane cell used as the phase conjugate mirror. Firstly, a two-pass amplifier scheme was examined, both when a conventional mirror and the phase conjugate mirror were employed, so that a comparison could be made of the performance with and without phase conjugation. Secondly, a four-pass configuration was assessed in a similar manner. Thirdly, a two-pass system incorporating 'four-wave Brillouin mixing' for improved conjugation of a depolarized beam was evaluated. The observations and measurements made during the course of the experiments are compared with the theory set out in Chapter 4 and

both theoretical and experimental results obtained by other workers. These observations enable very positive conclusions to be drawn and these are given in Chapter 6.

CHAPTER 2

High Power Single Mode Nd:YAG Oscillator Development

2.1. Theory of the telescopic resonator

2.1.1. Stable TEMoo mode operation

As mentioned previously, two important aims in the design of a laser are that it should have high output energy and low beam divergence. The latter is equivalent to ensuring that the resonator oscillates only on the TEMoo mode of the cavity. The simplest resonator consists of two curved mirrors, and the spot-sizes on them are given by (Kogelnik and Li, 1966):

$$\frac{\pi w_{1,2}^2}{\lambda} = L\left[\frac{g_{2,1}}{g_{1,2}(1-g_1 g_2)}\right]^{1/2} \qquad 2.1.$$

where $$g_{1,2} = 1 - \frac{L}{R_{1,2}} \qquad 2.2.$$

and R_1 , R_2 are the mirror radii and L is the cavity length. This cavity has two disadvantages: firstly, one requires that to fill a laser rod of diameter D, the spot-size should be $w \simeq D/3$, which leads to a typical cavity length of 10m for $D = 6mm$ and a wavelength of $1\mu m$, which is excessive. Secondly, the laser rod acts as a (positive) lens whose focal length depends upon the flashlamp pump energy and repetition rate, and whose focal length can vary from shot to shot. This variation arises from fluctuations in flashlamp pump power and coolant flow and temperature. The variation in resonator parameter causes changes in both the output beam divergence and in the output energy, because the spot size in the gain medium changes. In 1972 Steffen, Lörtscher and Herziger suggested incorporating a telescope in a cavity to simultaneously compensate for thermal lensing of the rod

and to minimise the fluctuations of this focal length, in the configuration of Fig. 2.1. This resonator can be analysed in terms of ray transfer matrices (Hanna et al, 1981) and the TEMoo spot sizes expressed (Baues, 1969) as follows, where the approximation has been made that the rod is a thin lens adjacent to mirror 2, ($l_1 = 0$) and is also in the focal plane of the telescope objective ($l_2 = f_2$). The dimensions l_1 and l_2 are indicated on figure 2.1. The results are:

$$W_1' \equiv \left[\frac{\pi W_1^2}{\lambda L'}\right]^{1/2} = \left[\frac{M^2 G_2}{G_1 (1 - G_1 G_2)}\right]^{1/4} \qquad 2.3.$$

$$W_2' \equiv \left[\frac{\pi W_2^2}{\lambda L'}\right]^{1/2} = \left[\frac{M^2 G_1}{G_2 (1 - G_1 G_2)}\right]^{1/4} \qquad 2.4.$$

$$W_3' \equiv \left[\frac{\pi W_3^2}{\lambda L'}\right]^{1/2} = \left[\frac{W_2'}{M}\right] \qquad 2.5.$$

where λ is the laser wavelength, M is the telescope magnification, $L' = L - f_1^*$ (f_1 being the focal length of the negative telescope lens); $G_1 = M\left[1 - \frac{L'}{R_1}\right]$; $G_2 = M\left[1 - \frac{L'}{R_2'}\right]$.

$\frac{1}{R_2'}$ in the formula for G_2 is given by:

$$\frac{1}{R_2'} = \frac{1}{f_T} + \frac{1}{f_R} + \frac{1}{R_2} \qquad 2.6.$$

where $f_T = \frac{f_2^2}{\delta}$

* Note that L is no longer the cavity length, see fig. 2.1.

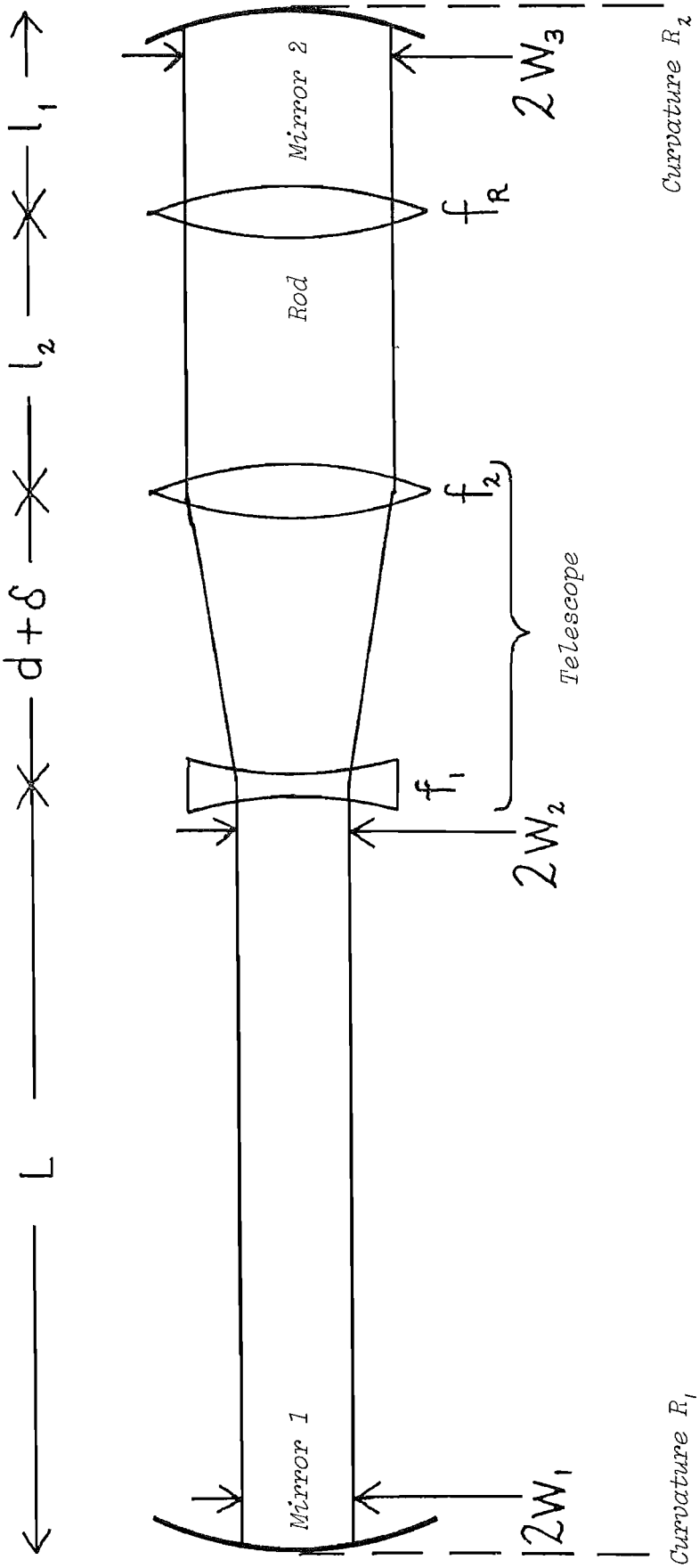

Figure 2.1 The telescopic resonator.

and δ is the defocussing of the telescope from the infinity setting (δ is positive when the telescope lens separation is greater than $f_2 + f_1$). It should be noted that the least variation of w with f_R occurs when $G_1G_2 = 1/2$, when $dw/df_R = 0$, this condition is satisfied by choosing appropriate values of M, L', R_1, R_2 and δ. There is no advantage in using curved mirrors, so putting $R_1 = R_2 = \infty$ and setting $G_1G_2 = 1/2$ with $G_1 = M$ and $G_2 = \frac{1}{2M}$ simplifies the above equations to:

$$w_1 = \left(\frac{\lambda L'}{\pi}\right)^{1/2} \qquad 2.7.$$

$$w_2 = \left(\frac{\lambda L' . 2M^2}{\pi}\right)^{1/2} \qquad 2.8.$$

$$w_3 = \left(\frac{2\,\lambda L'}{\pi}\right)^{1/2} = \sqrt{2}\, w_1 \qquad 2.9.$$

which are the basic design equations for the telescopic resonators used in the work described in this thesis. In practice L' and M must be chosen so that w_2 is large enough to fill the laser rod, but w_1 is not so small that damage occurs at mirror 1.

Although certain approximations are made in deriving the formulae above, it has been shown by Hanna, Sawyers and Yuratich (1981) that only negligible changes occur when these approximations are taken into account.

2.1.2. Transverse mode selection

The theoretical results above predict the TEMoo spot sizes for the telescopic resonator. Since a laser oscillating on this mode has the highest brightness, it

is desirable that it oscillates on the TEMoo mode only. Higher order modes have a larger transverse dimension, so selection of the TEMoo mode consists of simply inserting a circular aperture into the cavity, so that the loss per round trip is significantly higher for the higher order modes than for the TEMoo mode. Li in 1965 showed that the maximum discrimination between the TEMoo mode and the next highest mode, TEM_{01} , occurs in the confocal resonator, and Sawyers (1981) showed that the telescopic resonator is equivalent to a symmetric confocal resonator provided that the aperture is at one end mirror. By choosing $3w = D$, where D is the diameter of the aperture, one finds that for typical numbers of round trips in a Q-switched laser there is adequate discrimination in favour of the TEMoo mode, without this mode being significantly truncated. This condition is therefore used for our telescopic resonators.

2.2. Experimental work on high power TEMoo mode telescopic resonators

When designing a high power laser there are several factors which need to be taken into account. Firstly, as will be shown later, it is helpful to keep the length of the resonator to a minimum, because this maximises the adjacent longitudinal mode frequency spacing, which facilitates single longitudinal mode selection. Secondly, as was shown earlier (equation 2.7.), the spot size on one mirror may become so small, especially if L is kept short, that damage occurs here because the laser intensity becomes too high. This mirror is often used as the output coupler of the resonator and consists of a plane parallel uncoated glass or fused silica resonant reflector. This is chosen for its high damage threshold, which for these materials is ~ 5 GW cm^{-2} for 10 ns pulses under ideal conditions. Now for a resonator 1m long, L is approximately 0.5m, leading to a spot size of ~ 0.4mm on this mirror (equation 2.7). Thus for a 30 ns pulse duration, the 'ideal' damage threshold is reached at an output

energy of ~250 mJ. In practice it is found that due to the effects of dust and intensity modulation of the pulse when more than one longitudinal mode is oscillating, the maximum safe output energy is limited to the 100 mJ level. The Nd:YAG rod used in the oscillator under development had dimensions of 1/4" x 3", and could be pumped with a maximum flashlamp energy of 50 J in a standard single flashlamp pumping chamber manufactured by JK lasers. At this pumping level it was found that the telescopic resonator produced approximately 300 mJ of non-Q-switched output. Hence it was anticipated that if the problems of damage at the narrow beam end of the resonator could be overcome, an increase of possibly as much as 200 mJ in Q-switched output energy could be achieved. As a first step in this direction it was noted that the energy incident on the output mirror inside a cavity consisting of a total (100%) reflector and a low reflectivity output coupler (as is the case in a Q-switched Nd:YAG laser where the gain is very high) is much greater than that incident on the total reflector. The ratio of these two energies is of the order of the single pass gain in the cavity, which is typically a factor of four in a Q-switched Nd:YAG laser. Thus, for an output energy of 100 mJ, 25 mJ is incident on the 100% mirror. This suggested placing a 100% reflector at the narrow beam end of the resonator. By using such a reflector with a damage threshold greater than 25 mJ in a 30 ns pulse on a spot of radius 0.4mm, it was hoped to increase the output energy of the telescopic resonator. Taking the laser output from the large beam end of the resonator has the additional advantages that the beam divergence angle θ, given by:

$$\theta = \frac{2\lambda}{\pi W_o} \qquad 2.10.$$

is smaller; and the larger beam radius reduces the danger of damage to optical components used outside the resonator (for beam steering for example).

Several types of 100% reflector were incorporated into telescopic resonators and the results of their use are described below. Initially, however, a resonator with the output from a resonant reflector at the small beam end was tested to provide a comparison for the other schemes. This is shown in Figure 2.2.

An aperture of diameter 5mm was used with the 6mm diameter rod, the telescope had a magnification of three, and the spot sizes in the rod and at the resonant reflector were 1.67mm and 0.39mm respectively. With these spot sizes it was found that the maximum safe operating level was at an output energy of 100 mJ in a TEMoo mode. Running at energies of up to 150 mJ was possible, but damage then occurred after a number of shots, if not on the first shot.

The oscillator of Figure 2.2. was now modified by simply exchanging the positions of the two mirrors, so that the output was taken from the large beam end of the resonator. In this arrangement the coated 100% mirror damaged when the output energy was 70 mJ. As a first step towards increasing the available output, a lower reflectivity (higher transmission) output coupler was chosen. The lower the output mirror reflectivity, the lower the intra-cavity intensity for a given output energy. As shown by Koechner (1976), the output power under steady-state conditions is given by:

$$P_{out} = A I (1-R) R^{-1/2} \qquad 2.11.$$

where A is the area of the beam at the output mirror; I is the geometric mean power density inside the optical resonator, given by $I = (I_1 I_4)^{1/2}$, where I_1 and I_4 are the intensities of the beams travelling in opposite directions in the laser resonator; and R is the output mirror reflectivity. The power reflectivity of a resonant reflector is given by:

$$R = \left[\frac{n^2 - 1}{n^2 + 1}\right]^2 \qquad 2.12.$$

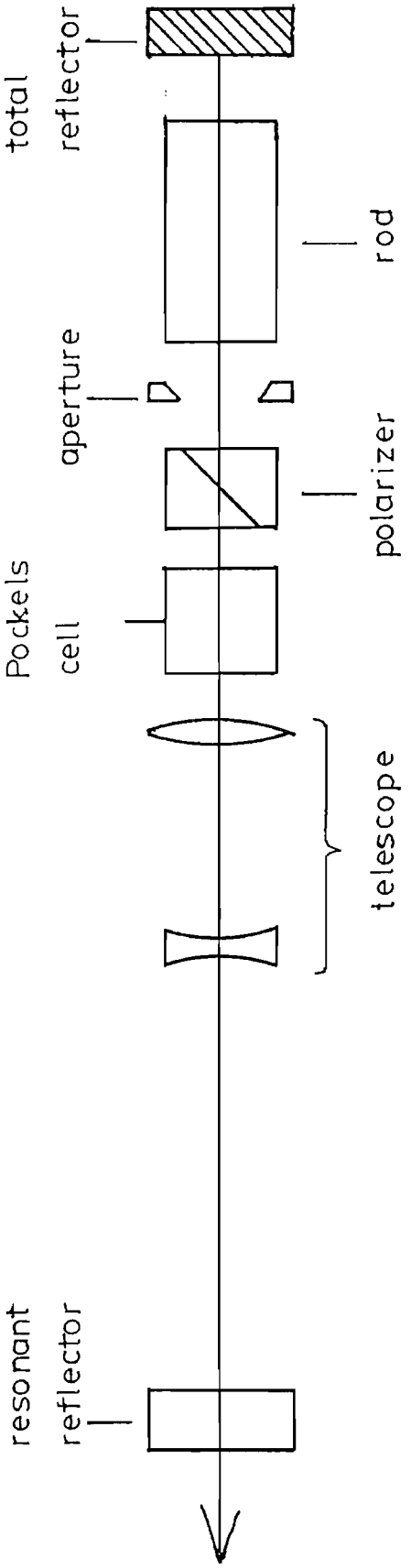

Figure 2.2 The telescopic resonator with output from the contracted beam end.

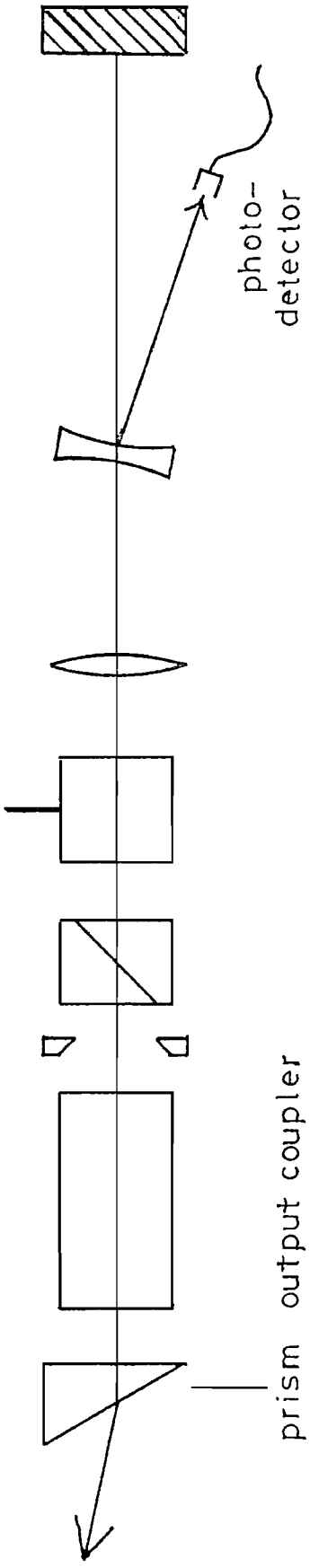

Figure 2.3 Indirect measurement of the energy incident on the total reflector

where n is the refractive index, for n = 1.5, R = 15%, and P_{out}/I = 2.19 A. For a single glass surface, R ≃ 4%, and P_{out}/I = 4.8 A. It can be shown that the intensity at the 100% mirror is proportional to I. Thus one anticipates that approximately twice as much steady state power may be extracted from a resonator by changing the output coupler from resonant reflector to single surface reflector when the output is limited by damage to the 100% reflector. In fact, equation 2.11., being derived in the steady-state, is not directly applicable to a pulsed laser. However, we can use it as a rough guide as long as we also take account of the effect on pulse duration, and therefore on power and damage, of a lower reflectivity output coupler. For a given pumping rate, the pulse duration Δt_p depends on the cavity photon lifetime τ_c, and the initial, final and threshold inversions n_i, n_f, n_t, (Koechner 1976), being given by:

$$\Delta t_p = \tau_c \cdot \frac{n_i - n_f}{n_i - n_t \left[1 + \ln\left(n_i / n_t\right)\right]} \qquad 2.13.$$

where τ_c is given by

$$\tau_c = \frac{2 l'}{c\left(L - \ln R\right)} \qquad 2.14.$$

in which l' is the cavity optical path length, c the velocity of light, and L the fractional round trip loss;

$$n_t = \frac{1}{c\,\sigma\,\tau_c} \qquad 2.15.$$

in which σ is the emission cross-section;

$$n_i = \frac{E_{stored} \cdot \lambda}{V h c} \qquad 2.16.$$

where V is the rod's volume; and n_f is found graphically.

Given L = 30%, we calculate that:

$$\frac{\Delta t_p (R = 4\%)}{\Delta t_p (R = 15\%)} \simeq 0.6$$

for the typical operating conditions of our oscillator. Taking both the above factors into account leads to an expected energy increase of ~ 1.3 in going to the lower reflectivity mirror, i.e. ~ 90 mJ instead of 70 mJ.

As a low reflectivity mirror one surface of a 30^0 prism was aligned in the cavity. This wedge angle was chosen to prevent the reflection from the second surface from returning into the laser rod. The output energy now increased to 105 mJ before the 100% mirror damaged, an increase by a factor of 1.5, and the pulse duration was shortened to ~ 25 ns.

A parameter of interest was the energy incident on the 100% mirror. This was found by measuring the amount of light reflected off one surface of the negative telescope lens, as shown in Figure 2.3. The lenses in a high power laser resonator must generally be tilted by a small angle, so that there is no danger of a reflection from a curved surface being focussed to a small spot in another optical component and causing damage. For this reason the reflection from the negative telescope lens is accessible and has an energy of $\sim 4\%$ of the intracavity intensity, this being the reflection coefficient for an uncoated glass surface. This way the damage threshold of the coated 100% mirror was found to be 26 mJ in a 25 ns pulse.

By expanding the beam onto the 100% mirror, it was hoped that this problem of damage could be overcome. Two methods of doing this were attempted, using either a second telescope or a series of beam expanding prisms (Figure 2.4.).

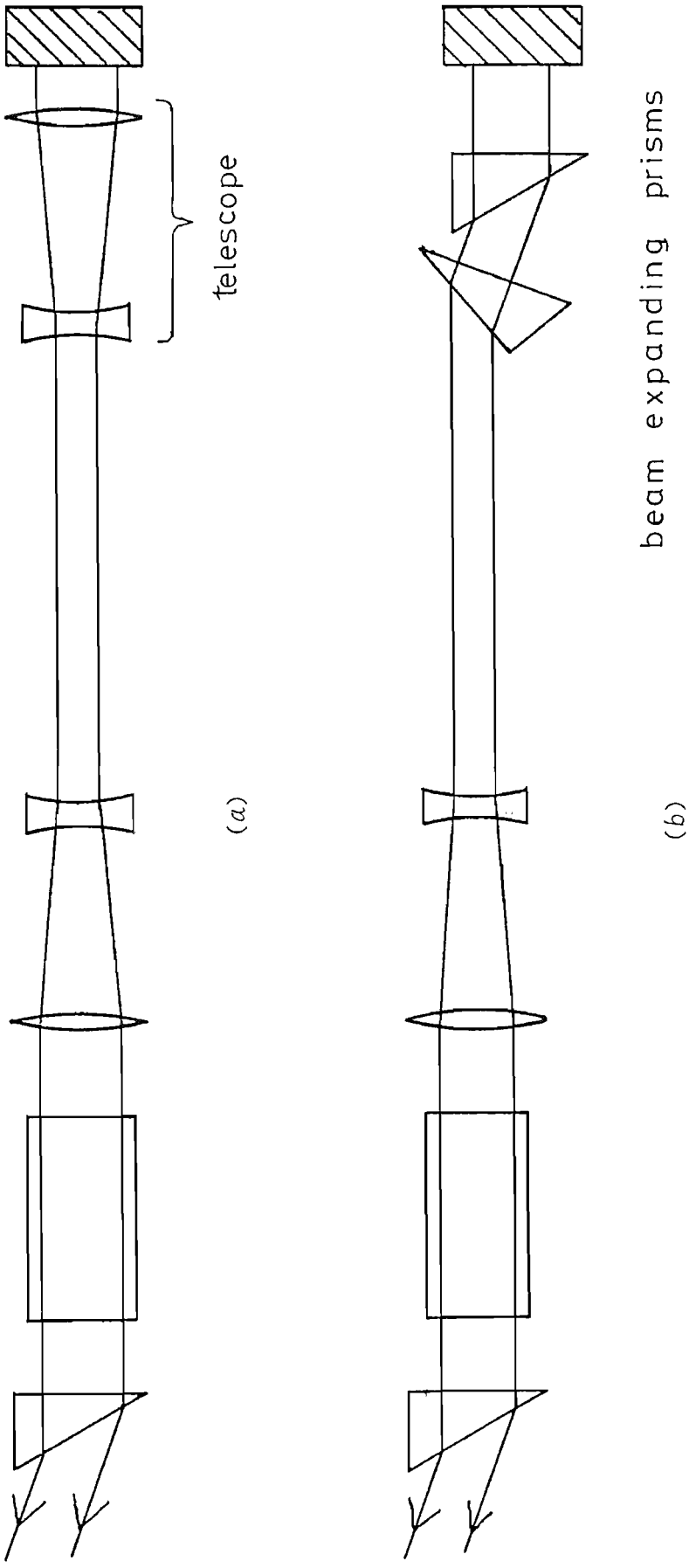

Figure 2.4 Reducing the intensity on the total reflector using either a beam expanding telescope (a), or prisms (b).

Unfortunately it proved impossible to obtain a good TEMoo beam with the telescopic arrangement, because the alignment of and the spacing between the two lenses of the expanding telescope was critical.

Prisms with internal angles of 30^{o}, 60^{o} and 90^{o} were used as beam expanders. The external angle of incidence on face a (see Figure 2.5.) for a 90^{o} angle of incidence on face b is 48^{o} if the refractive index is 1.5, which gives the maximum expansion. In the plane of expansion the beam increases in dimension by a factor of 1.29, and this is also the factor by which the area increases. It was found that with two prisms, giving an increase in beam area of $(1.29)^{2} = 1.66$, the output energy from the laser could be increased to 140 mJ before the mirror damaged. The energy incident on it was 40 mJ, monitored by using one of the reflections from the prism faces. The power reflection from the face a for light polarized in the incident plane can be calculated to be 0.5%, the value is low because 48^{o} is close to the Brewster angle of 56^{o}. For the face b the reflectivity is $\sim$ 4%, so the round trip loss introduced by each prism is $\sim$ 9%. When three or four beam expanding prisms were used, the output energy could not be increased beyond 145 mJ, because the increased pumping required to overcome the higher losses was such that superradiance depleted the inversion in the rod before Q-switching took place. It is anticipated that the performance of the laser incorporating beam expanding prisms could be significantly improved if the prisms were constructed in such a way that the incident beam was at Brewsters angle on face a, and by having face b anti-reflection-coated (on at least some of the prisms) to reduce the losses.

2.2.1. A prism reflector of high damage threshold

The next approach to the problem of damage in the contracted beam end of the resonator was the design and construction of a prism reflector giving total reflection without the use of coatings or roof edges. This is

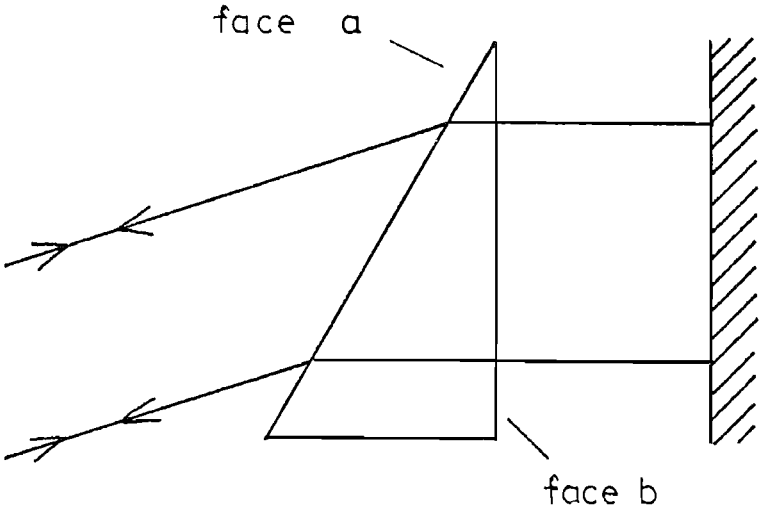

Figure 2.5 A beam expanding prism.

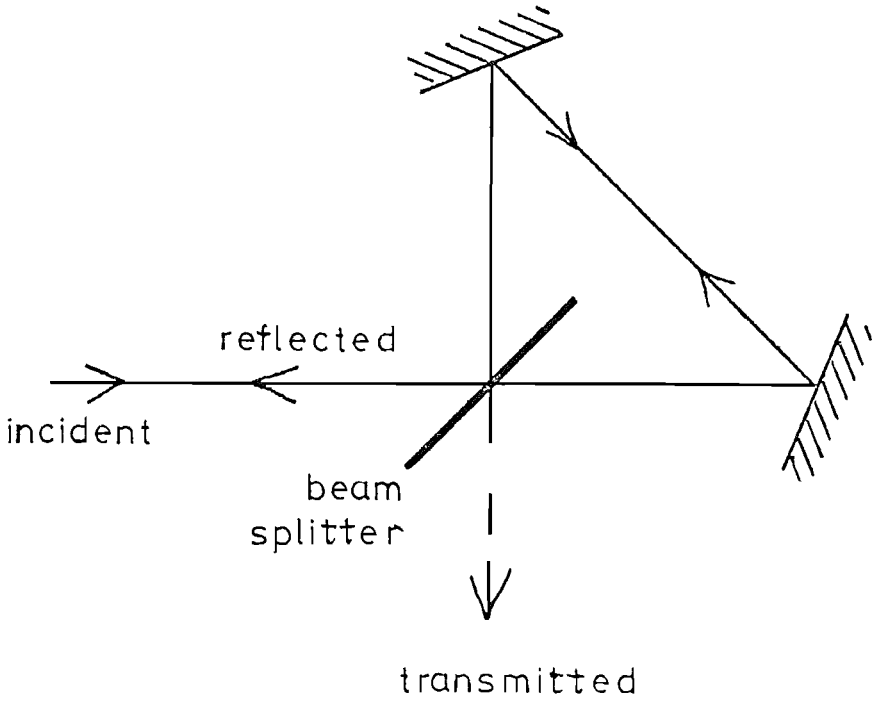

Figure 2.6 An anti-resonant ring.

described in Appendix I and some of the details are discussed below. The reflector consists of an anti-resonant ring (Figure 2.6.), in which a beam-splitter divides the incident beam into two counter-propagating beams, which then re-combine at the beam-splitter. The transmitted beam is the superposition of the clockwise circulating beam, which undergoes two reflections at the beam-splitter, and the anti-clockwise circulating beam, which undergoes two transmissions through the beam-splitter. For the device to work it is necessary that the intensity in the transmitted beam be zero, then the reflected beam carries all the power. Two conditions must be satisfied for this to be the case: the two beams must be in exact antiphase, and they must be of equal intensity. In 1970 McGeoch used frustrated total internal reflection (FTIR) to form the beam splitter and in 1981 Vanherzeele et al employed the same technique. We, however, chose to use an air spaced Fabry-Perot interferometer, formed by the two surfaces of adjacent identical prisms, which also perform the task of circulating the beams. This arrangement has the advantage that all the reflecting surfaces can be accurately aligned relative to each other during manufacture; and also the Fabry-Perot beam-splitter is more convenient than one utilizing FTIR, which requires a very narrow liquid or air space of typically a quarter of a wavelength thickness.

What is not obvious at first sight is that the two beams which constitute the transmitted beam do indeed cancel each other to give zero intensity, when the angle of incidence upon the Fabry-Perot and its spacing are such that the incident beam is split into two equal parts. This we will now show.

Consider an anti-resonant ring as shown in Figure 2.7.a. Figure 2.7.b. shows the Fabry-Perot surfaces in more detail. We will consider a single ray incident on the interface as shown. The refractive index of the gap is n_2 and that of the medium either side (in this case glass) is n_1. The amplitude reflectivity in going from n_1 to n_2 is r, while that going from n_2 to n_1 is r', and the transmission in either direction is t. We want to find the amplitude of the transmitted light beam. We let the optical path length round the ring from point A to point D ($\overline{AD}$) (which is equal to that from C to F, or G to H etc.) be α. First we consider rays that reflect twice from the etalon, like this:

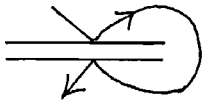

The transmitted field resulting from a reflection at A, circulating round the ring to D and the subsequent multiple reflections, is:

$$E_{to} = E e^{i\omega t} \cdot \left[\frac{r\,(1 - e^{-i\delta})}{1 - r^2 e^{-i\delta}} \right] e^{-i\alpha} \cdot r \qquad 2.17.$$

In this expression, the term in brackets is the usual result of multiple reflections from a single ray incident (in this case at point D) on an etalon. The phase shift $e^{-i\alpha}$ results from the optical path length round the ring, and r is the amplitude reflection coefficient at point A. δ is the usual Fabry-Perot phase shift

$$\delta = \frac{2\pi}{\lambda} \cdot 2 n_2 d \cos\theta$$

where d is the etalon spacing and θ the angle of incidence on the internal face.

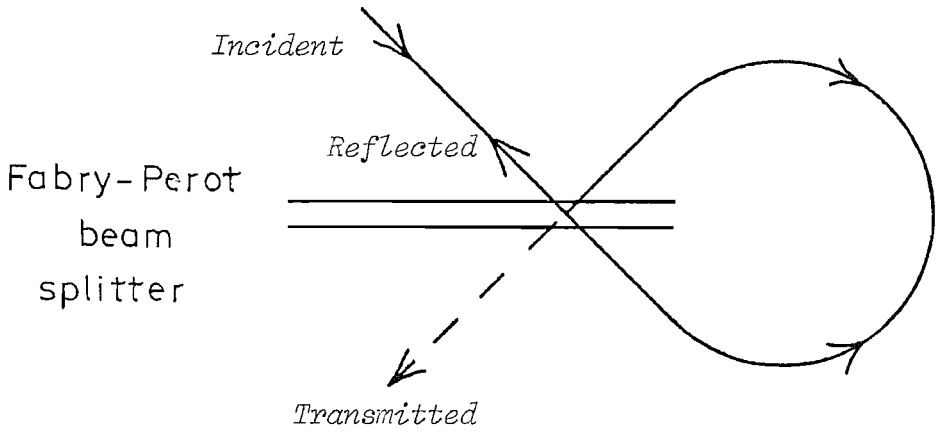

Figure 2.7(a) *Anti-resonant ring incorporating Fabry-Perot beam splitter.*

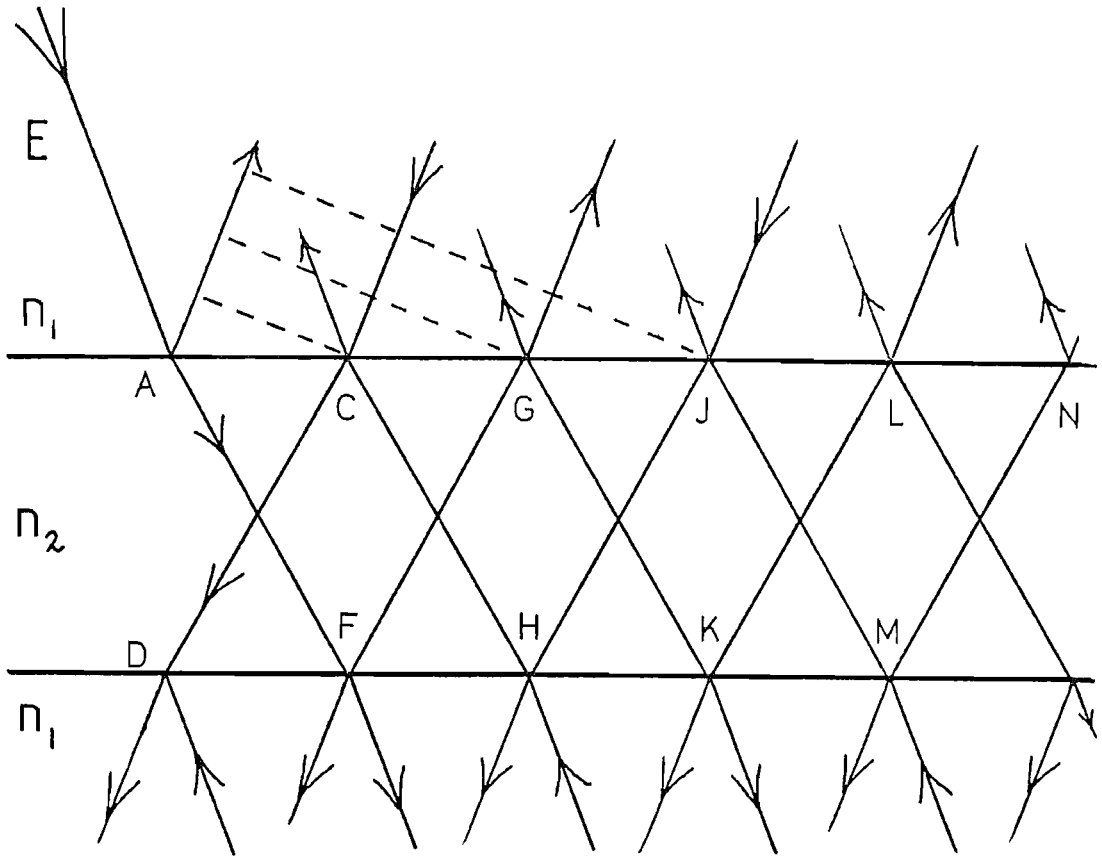

Figure 2.7(b) *Ray diagram for the Fabry-Perot interface.*

There is another term resulting from the ray path AFGH:

$$E_{t_1} = E e^{i\omega t}\left[\frac{r(1-e^{-i\delta})}{1-r^2e^{-i\delta}}\right] t^2 r' e^{-i\alpha} e^{-i\delta} \qquad 2.18$$

and AFGKLM:

$$E_{t_2} = E e^{i\omega t}\left[\frac{r(1-e^{-i\delta})}{1-r^2e^{-i\delta}}\right] t^2 r'^3 e^{-i\alpha} e^{-2i\delta} \qquad 2.19.$$

and so on.

The sum of all these terms is:

$$E_t = E_{to} + E_{t1} + E_{t2} + \ldots$$

which simplifies, remembering that $r = -r'$, to

$$E_t = E e^{i\omega t} e^{-i\alpha}\left[\frac{r(1-e^{-i\delta})}{1-r^2e^{-i\delta}}\right]^2 \qquad 2.20$$

This is the product of two Fabry-Perot reflection expressions as one would expect.

The second contribution to the transmitted intensity results from two transmissions through the Fabry-Perot, like this:

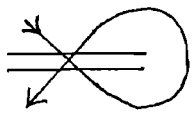

The first term is due to the ray path AFCD:

$$E'_{t_0} = E e^{i\omega t}\left[\frac{t^2}{1-r^2e^{-i\delta}}\right] e^{-i\alpha} e^{-i\delta} t^2 \qquad 2.21.$$

This time the term in brackets is the usual expression for multiple ray transmission from a single ray incident on a Fabry-Perot. The next terms are AFGK̄JH:

$$E'_{t_1} = Ee^{i\omega t}\left[\frac{t^2}{1-r^2e^{-i\delta}}\right] e^{-i\alpha} e^{-i\delta}\, t^2\, r'^2\, e^{-i\delta} \qquad 2.22.$$

and

$$E'_{t_2} = Ee^{i\omega t}\left[\frac{t^2}{1-r^2e^{-i\delta}}\right] e^{-i\alpha} e^{-i\delta}\, t^2\, r'^4\, e^{-2i\delta} \qquad 2.23.$$

and so on.

The sum of these terms $E'_t = E'_{to} + E'_{t1} + E'_{t2} + \cdots$ simplifies to:

$$E'_t = Ee^{i\omega t} e^{-i\alpha}\left[\frac{t^2}{1-r^2e^{-i\delta}}\right]^2 e^{-i\delta} \qquad 2.24$$

which, as expected, is the product of two Fabry–Perot transmission expressions. The total transmitted amplitude is the sum $E_T = E_t + E'_t$:

$$E_T = Ee^{i\omega t} e^{-i\alpha}\left\{\left[\frac{r(1-e^{-i\delta})}{1-r^2e^{-i\delta}}\right]^2 + \left[\frac{t^2}{1-r^2e^{-i\delta}}\right]^2 e^{-i\delta}\right\} \qquad 2.25$$

A similar analysis gives an expression for the reflected field amplitude:

$$E_R = 2Ee^{i\omega t} e^{-i\alpha} e^{-i\delta/2}\left[\frac{r(1-e^{-i\delta})}{1-r^2e^{-i\delta}}\right]\left[\frac{t^2}{1-r^2e^{-i\delta}}\right] \qquad 2.26.$$

and the intensities are found to be: $\frac{I_T}{E^2} = \frac{E_T E_T^*}{E^2} = T =$

$$\frac{r^4(6-8\cos\delta+2\cos 2\delta) + 4r^2t^4(\cos\delta-1) + t^8}{B} \qquad 2.27.$$

$$\frac{I_R}{E^2} = \frac{E_R E_R^*}{E^2} = \frac{8t^4 r^2 (1-\cos\delta)}{B} = R \qquad 2.28.$$

where $B = (1 - 2r^2 \cos\delta + r^4)^2$ 2.29.

and $\delta = \frac{2\pi}{\lambda} \cdot 2 n_2 d \cos\theta_1$; $r = \frac{\tan(\theta_1 - \theta_2)}{\tan(\theta_1 + \theta_2)}$

for light polarized in the plane of incidence, θ_1 and θ_2 are the internal and external angles at the Fabry-Perot surfaces.

Now, given λ and n_2, if any combination of θ_1 and d are chosen so that the power reflectivity (and transmissivity) of the Fabry-Perot beam splitter is 0.5, it turns out that R = 1 (and T = 0) which is precisely what is required for the anti-resonant ring to work.

Having shown that an anti-resonant ring incorporating a Fabry-Perot should work, a practical device was designed and this is shown in Figure 2.8. The parameters θ_2, d, and the prisms' dimensions and angles were decided upon as follows. Firstly, we notice that at one point the circulating beams cross the Fabry-Perot interface at normal incidence and at this point the reflectivity can be arranged to be zero by setting d as a multiple of $\lambda/2$. We chose $d = \lambda = 1.06\ \mu m$. Then θ_2 was fixed at 40.56° to give 50% reflectivity, the prism material being BK7 glass with a refractive index of 1.507 at 1.06 μm. A Brewster angle entrance was required and this determined the angle $\alpha = 6.98^\circ$, and in turn $\beta = 110.28^\circ$.

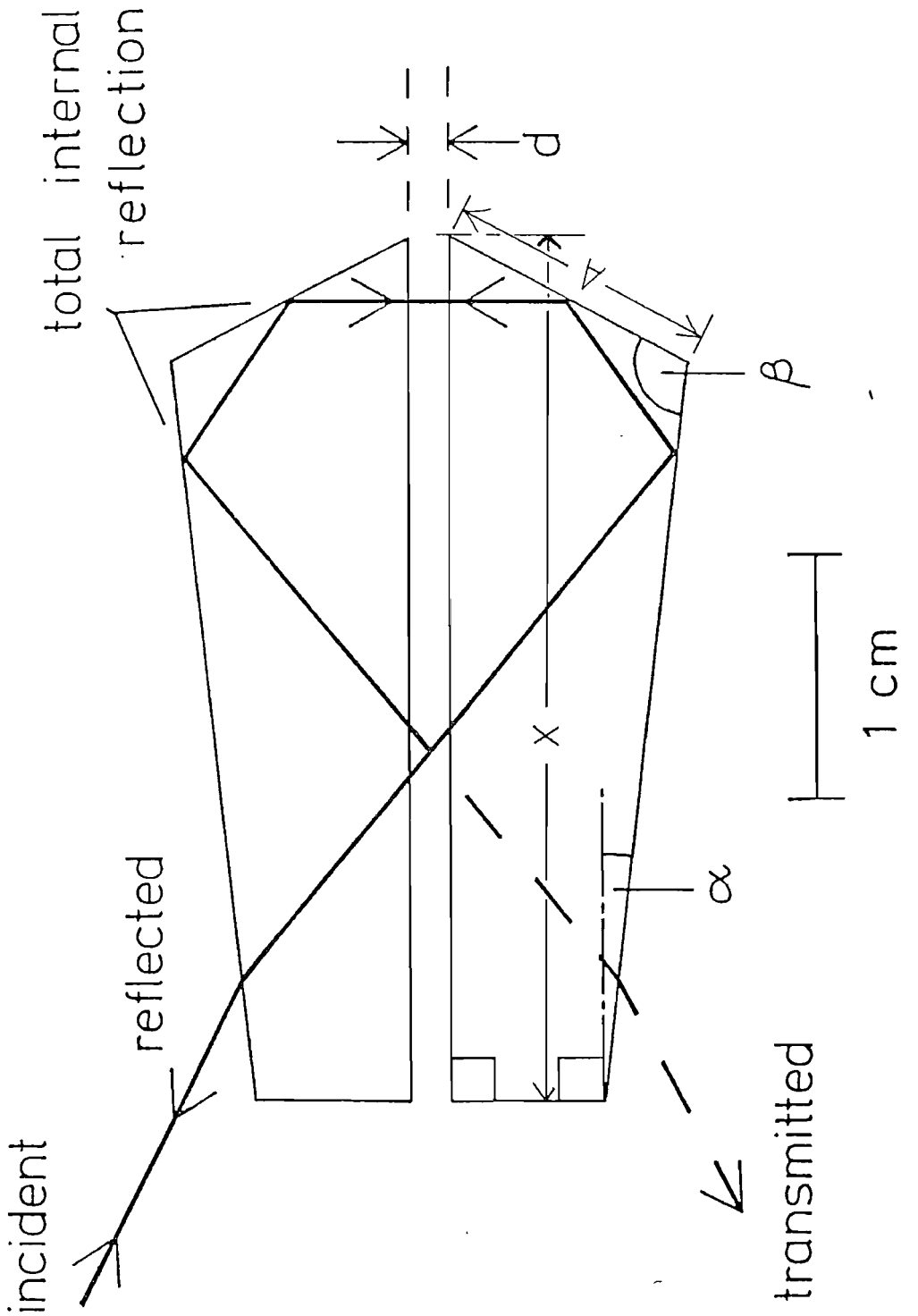

Figure 2.8 The prism reflector design actually constructed and tested

Geometrical considerations show that the maximum TEMoo spot size w that can be accommodated by the prisms is limited by the length of the face A according to:

$$A = 9.87\ w \qquad 2.30.$$

and that the lengths A and X are related by:

$$X = 2.37\ A \qquad 2.31.$$

Here it is assumed that, if the effective aperture presented by the prisms is greater than 3w, negligible truncation of the beam occurs. The reflector was designed to cater for spot sizes of up to w = 1.5mm. Allowing 0.5mm at each end of the face A led to dimensions of: A = 15.8mm, X = 37.5mm.

Two identical prisms were manufactured by I.C. Optical Systems by cutting a single prism in half. The angles α and β were accurate to $\pm$ 1 minute of arc while the bases were perpendicular to the reflecting surfaces to $\pm$2 seconds of arc. The gap of λ between the two prisms was created by evaporating two dielectric coatings along each edge of the longest face of one prism (the longest faces being the Fabry-Perot surfaces) to leave the centre of the face clear and then firmly clamping the two prisms together. The prisms were mounted together on an optical flat to ensure that all the reflecting surfaces were perpendicular to the same plane. They were then clamped into a holder giving access to the transmitted beam and this in turn was mounted in a conventional mirror mount having micrometer angular adjustments.

The reflector was tested firstly for accuracy of construction and the reflectivity was also measured before it was used in a laser oscillator. The most critical dimension of the reflector is the Fabry-Perot spacing, since this determines the reflectivity of the interface and the reflectivity of the device. The reflectivity as a function of $\frac{\lambda}{d}$ can be estimated using equation 2.28., remembering that this equation was derived assuming zero reflection at the normal incidence traversal of the beam splitter. However, if $\frac{\lambda}{d}$ varies from 0.8 to 1.2, the reflection at this point is less than 5%, and R, as given by 2.28, is always greater than 99%.

The parallelism between the prisms and between the prisms and their base was checked by visually observing any interference fringes created between these surfaces. The beam-splitter faces had no fringe across the length of the face, indicating an excellent parallelism to less than approximately 1 second of arc. The parallelism between the prism bases and the optical flat was estimated to be as much as 5 seconds out, nevertheless this did not appear to significantly degrade the reflector performance.

The device reflectivity was measured in two ways, firstly by using as the incident beam the horizontally polarized TEMoo output from a Nd:YAG laser. A beam-splitter was used to monitor the incident and reflected beams and measurement indicated a reflectivity of greater than 95%, although this was of limited accuracy ($\pm$ 5%). The transmitted beam contained approximately 1% of the incident energy and consisted mainly of light polarized orthogonally to the incident beam. This suggests that some strain-induced birefringence was present. In a second more accurate reflectivity measurement, the

reflector was used as one mirror of a Nd:YAG laser. The lasing threshold was compared with that obtained when one mirror was a conventional 100% multilayer mirror, and the two threshold energies were equal to within $< 0.5\%$, indicating a reflectivity of $> 99\%$.

Having demonstrated that the prism pair had the desired reflectivity, it was incorporated into the Q-switched oscillator described above, to test its power handling capability and to try and increase the output energy of this laser. A Q-switched TEMoo output of 185 mJ was obtained before damage occurred, which was ~ 45 mJ greater than previously possible. At this level the energy incident on the reflector was measured to be 47 mJ, i.e. about twice that which a multilayer total reflector could sustain. Reliable damage-free performance was possible if the output was maintained at or below 150 mJ. The damage occurred at the Fabry-Perot beam splitting surface at the point where the incident beam hits it. At this point there are two sets of overlapping standing waves arising from the incident and reflected waves and from the beams circulating in opposite directions around the ring (Boling et al, 1973). Thus, the maximum intensity at this point is considerably higher than the incident intensity.

An interesting possible further development of the reflector is shown in Figure 2.9. By making the spacing d variable and controlled, for example, by piezo-electricity, the reflector could be made tunable over a wide range of wavelengths, limited only by the transmission range of the material, and in addition the reflectivity could be varied continuously from 0 to 100% at any particular wavelength.

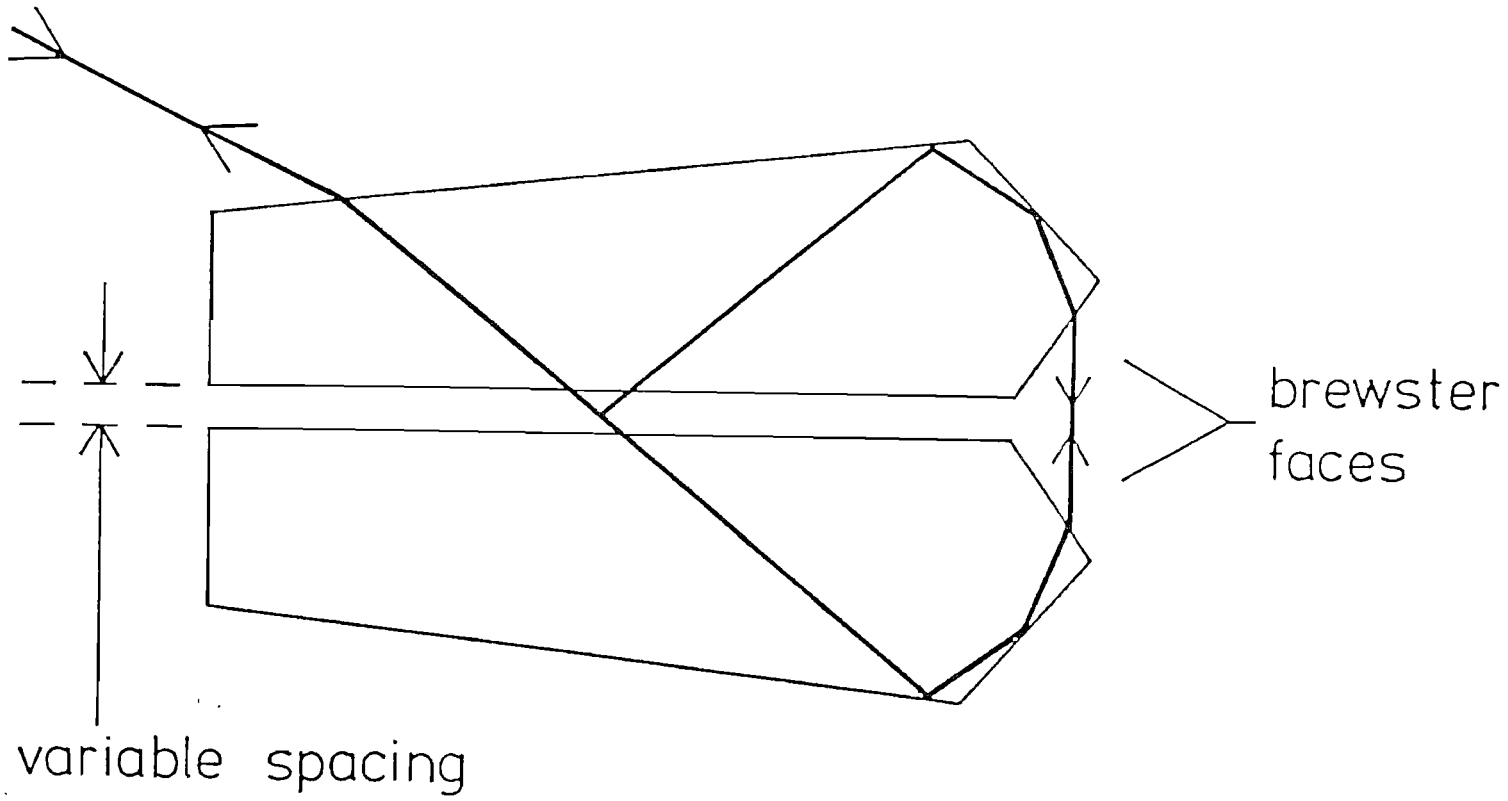

Figure 2.9 *A design for a reflector with reflectivity tunable over the transmission range of the prism material.*

To conclude this section we summarise the three telescopic oscillator configurations that give good high power TEMoo mode performance. Taking the output from the contracted beam end of the resonator through a resonant reflector gives up to 100 mJ in a 30 ns pulse. Taking the output from the expanded beam end of the resonator through a single air/glass surface output coupler again gives up to approximately 100 mJ in a slightly shorter 25 ns pulse when a conventional 100% mirror is used in conjunction with beam expanding prisms in the contracted beam end. If the 100% mirror with beam expanders are replaced with the prism reflector, the output level is increased to 150 mJ in a 25 ns pulse.

Which of the three designs is the most appropriate for a particular application depends upon the chief requirement. If high power is of primary importance, then clearly the third design incorporating the prism reflector would be the choice. However, the first design is simpler and cheaper and lends itself more readily to modification by introduction of line narrowing components. Thus, in applications where a narrow linewidth is desirable, this design may be the most sensible choice. We discuss narrow linewidth operation of high power Q-switched lasers in the next section.

2.3
Narrow linewidth and single longitudinal mode operation

The principle of single longitudinal mode operation of a laser is similar to that of single transverse mode operation mentioned briefly above - it is necessary to increase the round trip losses for all the unwanted modes, so that during the lasing period none of them attains an intensity which is significant compared to the dominant mode intensity. The amount of round trip loss

necessary depends upon the number of round trips during the lasing period, a small number of round trips demands a high round trip loss for the unwanted modes; while many round trips means that less loss need be introduced. Because the longitudinal modes of a laser cavity differ from each other in frequency, the losses for the unwanted modes are introduced by using frequency selective components such as etalons or resonant reflectors.

A high gain laser such as Nd:YAG is generally "fast" Q-switched. By this we mean that a switchable intra-cavity loss mechanism prevents *any* lasing until a large population inversion has built up at the end of the flashlamp pump pulse. The loss is then suddenly switched off allowing the build up of a giant high power pulse in a duration of a few tens of round trip times. The problem is that, because there is such a small number of round trips, the amount of loss that must be introduced for the unwanted modes is greater than is conveniently possible using etalons or resonant reflectors. These components can provide only a small amount of discrimination between adjacent cavity modes, because the mode frequency spacing is small. The adjacent mode frequency spacing is:

$$\Delta \nu_L = \frac{c}{2L} \qquad 2.32.$$

which, for a 1m long cavity, is only 150 MHz (0.005 cm^{-1}) The solution to this problem lies in increasing the number of round trips taken for the Q-switched pulse to build up, so that even with moderate discrimination between modes, one mode will dominate all the others. This technique is described as pre-lase Q-switching (Hanna et al, 1972, two papers).

Theory of pre-lase Q-switching

In pre-lase Q-switching, the intracavity losses are not kept at such a high level that all lasing is prevented until the moment of Q-switching, as in fast Q-switching. Instead, they are kept at a level such that there comes a time during the flashlamp pump pulse when the population inversion, and therefore the gain, have increased to the point where the gain just exceeds the loss and lasing is able to take place at a very low intensity. This low intensity lasing continues for hundreds of round trips, during which time a single longitudinal mode can become dominant if a moderate amount of mode selection is present. The cavity loss is then switched off completely, and the oscillating single mode is amplified into a giant Q-switched pulse. Thus in pre-lase Q-switching the Q-switched pulse builds up from an established single mode, whereas in fast Q-switching it builds up from multimode noise.

To calculate the amount of mode selection necessary in a pre-lase Q-switched laser, it is useful to know how many round trips take place and what the powers in different modes are at the end of this period. It was shown by Sawyers (1981) that if a mode n reaches threshold at time t_n and then continues to grow over q_n round trips each of time τ, then the power P_n in that mode is given by:

$$P_n(t_n+q_n\tau) = P_{no}(R_{1n}R_2)^{q_n}\exp\left[2\sigma_n l\sum_{p=1}^{q}N(t_n+(q-p)\tau)\right] \quad 2.33.$$

Here P_{no} is the noise power in mode n, σ_n is the stimulated emission cross section for the n'th mode, l is the length of the lasing medium and N(t) is the population inversion at time t. R_{1n} and R_2 are the

resonator mirror reflectivities. The effect of frequency selective elements in the resonator is accounted for by writing them as equivalent frequency - dependent (and therefore mode number dependent) mirror reflectivity R_{1n}; R_2 is frequency independent.

For fast Q-switching the inversion is almost constant during the few tens of round trips it takes to build up an appreciable laser intensity from noise (see for example Koechner, 1976), so equation 2.33 simplifies to:

$$P_n(t) = P_{no}(R_{1n}R_2)^{q_n} \exp\left[2\sigma_n l N(t_s) q_n\right] \qquad 2.34.$$

where t_s is the time at which Q-switching occurs. Now the linewidth Γ_F of Nd:YAG is 120 GHz (4 cm^{-1}) which is about 800 cavity mode spacings for a 1m laser cavity, so σ_n is approximately constant for adjacent cavity modes near the centre of the gain curve. Therefore, if we compare 2.34 with a similar expression for the adjacent mode m, the exponential terms (which describe gain narrowing) will be much less significant than the terms $(R_{1n}R_2)^{qn}$ and $(R_{1m}R_2)^{qm}$ which describe the narrowing due to frequency selective elements. We notice that these terms depend strongly on q_n and q_m and they therefore become very important in pre-lase Q-switching when q_n and q_m become large. However, 2.34 is not valid in pre-lase Q-switching because the inversion is not constant during the build up time. We assume it can be approximated by a linear relationship of the form:

$$N(t) = \gamma t + \text{constant} \qquad 2.35.$$

where $\gamma = \frac{dN(t)}{dt}$ is the pumping rate. By using 2.35

in 2.33 it can be shown that the ratio of powers in two adjacent modes n and m is given by:

$$\frac{P_n(t_s)}{P_m(t_s)} = \left[\frac{R_{1n}}{R_{1m}}\right]^{q_{eff}} \qquad 2.36.$$

where $q_{eff.} = \frac{q_n + q_m}{2} = q_n - \frac{\epsilon}{4\sigma(\omega_o)\gamma l \tau}$

$$= \left[\frac{\ln(P_n/P_{no})}{\sigma(\omega_o)\gamma l \tau}\right]^{1/2} - \frac{\epsilon}{4\sigma(\omega_o)\gamma l \tau} \qquad 2.37.$$

Here it has been assumed that mode n reaches threshold first; that $\sigma_n \approx \sigma_m = \sigma(\omega_o)$ and that R_{1n}/R_{1m} can be written in the form $1 + \epsilon$. 2.36 and 2.37 are the main results of the theory. For SLM operation a certain power ratio P_n/P_m is required. R_{1n}, R_{1m} are decided by the mode selectors chosen, and q_{eff} is influenced by them also, via the number ϵ in 2.37.

2.3.1.

Application of mode selection

We now discuss how the application of mode selecting elements influences the linewidth of the laser output. In general the spectrum of the laser will contain a number of longitudinal modes (as in Figure 2.10) each with frequency spacing $\Delta\nu_L$. The linewidth Γ is defined as the FWHM of the envelope, in other words:

$$P\left(\omega_o \pm \frac{\Gamma}{2}\right) = \frac{P(\omega_o)}{2} \qquad 2.38.$$

For SLM operation one can demand that:

$$\Gamma < 2\Delta\nu_L \qquad 2.39.$$

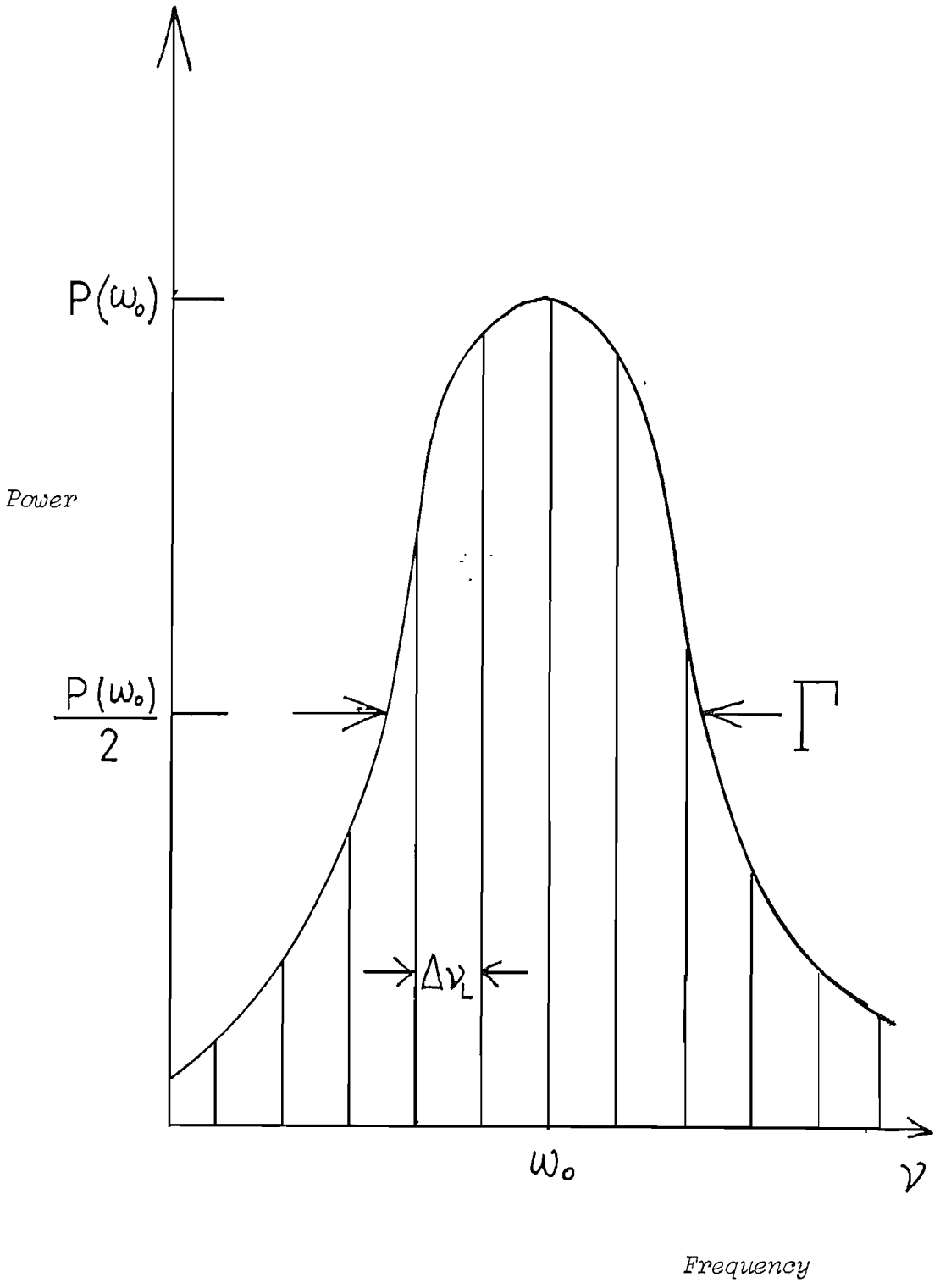

Figure 2.10 *General output spectrum of a laser, consisting of a number of longitudinal modes separated by* $\Delta\nu_L$.

but then the adjacent mode may still contain a significant amount of power. A more useful criterion is that the ratio of powers N between dominant and adjacent modes:

$$N = \frac{P_n}{P_{n\pm1}} \qquad 2.40.$$

be smaller than some arbitrary value. In our work this corresponds to less than 1% modulation on the temporal profile of the Q-switched pulse. It can be shown (Hanna et al 1981) that:

$$N \simeq \frac{16}{K^2} \qquad 2.41.$$

where K is the fractional modulation in the temporal power output. Thus for 1% modulation K = 0.01 and $N \approx 10^5$. Using this in 2.36 gives the condition necessary for SLM operation

$$\left[\frac{R_{1n}}{R_{1n+1}}\right]^{q_{eff.}} \geqslant 10^5 \qquad 2.42.$$

To calculate laser linewidths all we need to know now are values for R_{1n}. Frequency selective losses are introduced into laser cavities using either etalons with their frequency selective transmission, or resonant reflectors with frequency selective reflection. They are specified by the free spectral range Δ_E the finesse F_E and the contrast C_E:

$$\Delta_E = \frac{1}{2nt} \qquad 2.43.$$

$$F_E = \frac{\pi\sqrt{R}}{(1-R)} \qquad 2.44.$$

$$C_E = \left(\frac{1+R}{1-R}\right)^2 \qquad 2.45.$$

where $R = \sqrt{R_1 R_2}$ (R_1 and R_2 are the face reflectivities), n is the refractive index and t the thickness. It can be shown (Sawyers, 1981) that for an etalon:

$$\frac{R_{ln}}{R_{lm}} \simeq 1 + \epsilon_T \qquad 2.46.$$

where $$\epsilon_T = 2\left(\frac{2\Delta F_E}{\Delta_\epsilon}\right)^2 \qquad 2.47.$$

is the fractional discrimination per round trip, in which Δ is the frequency difference between modes n and m; and for a resonant reflector:

$$\frac{R_{ln}}{R_{lm}} \simeq 1 + \epsilon_R \qquad 2.48.$$

where $$\epsilon_R = \left(\frac{\pi \Delta}{\Delta_\epsilon}\right)^2 \cdot \frac{1}{C_E} \cdot \qquad 2.49.$$

Substituting 2.46, 2.48 and 2.38 into equations of the form of 2.33 or 2.34 leads, after some manipulation, to expressions for the laser linewidths under various conditions of fast or pre-lase Q-switched with or without mode selection. These we summarize below:

1. Fast Q-switched without mode selection:

$$\Gamma_{FQ} \simeq \Gamma_F \left(\frac{\ln 2}{2\sigma(\omega_o)\, l\, N(t_s)\, q}\right)^{1/2} \qquad 2.50.$$

Using typical values for $N(t_s) \simeq 3 \times 10^{17}$ cm^{-3} and q = 30 we find $\Gamma_{FQ} \simeq 0.3$ cm^{-1}.

2. Fast Q-switched with mode selection:

With a resonant reflector:

$$\Gamma_{FQRR} = \left(C_E \frac{\ln 2}{q}\right)^{1/2} \cdot \frac{2\Delta_E}{\pi} \qquad 2.51.$$

A typical resonant reflector might have parameters R = 4%, t = 6mm, n = 1.5, so C_E = 1.17, Δ_E = 0.555 cm^{-1}, and then Γ_{FQRR} = 0.058 cm^{-1}.

With an etalon:

$$\Gamma_{FQE} = \left(\frac{\ln 2}{q}\right)^{1/2} \cdot \frac{\Delta_E}{F_E} \qquad 2.52.$$

A typical etalon with R = 65%, t = 1cm, n = 1.5cm, F_E = 7.24, Δ_E = 0.333 cm^{-1} leads to a linewidth of Γ_{FQE} = 0.007 cm^{-1}.

3. Pre-lase Q-switched with or without mode selection:

It turns out that the three relevant equations are once again 2.50, 2.51 and 2.52, but of course q is now much greater, being of the order of 600. We find that without mode selection Γ_{PLQ} = 0.067 cm^{-1}, and with mode selection using the same examples as above Γ_{PLQRR} = 0.013 cm^{-1} and Γ_{PLQE} = 0.0016 cm^{-1}.

In practice, if one wants narrow linewidth or SLM operation, it is necessary to use both an etalon and a resonant reflector. This is because to ensure sufficient discrimination between adjacent modes, the transmission (or reflection) bandwidth Δ_E/F_E has to be narrow, which implies a small free spectral range Δ_E.

(The finesse of an etalon is limited because as R is increased, so the etalon has to be tilted further to prevent lasing off its surfaces, so increasing insertion and walk-off losses; also the intensity inside the etalon increases leading to possibility of damage.) If Δ_E is small then lasing may occur on a longitudinal mode one free spectral range of the etalon away, as in Figure 2.11, although not on the adjacent mode. In this situation a resonant reflector with a broad reflection bandwidth centred on w_0, shown dotted in figure 2.11, will prevent the lasing of the modes with frequency $w_0 \pm \Delta_E$. Alternatively, a thick resonant reflector for adjacent mode selection can be used with a thin low finesse etalon. Another alternative, though more costly approach, is to use a thick etalon of high finesse with $\lambda/4$ plates either side, separated from the laser rod by a polarizer (Hanna, Koo, Pratt, 1983). In this way the etalon can be used at or near normal incidence minimising walk-off losses.

In the theory above it is assumed that the longitudinal mode of interest (in the case of SLM operation) lies on the centre of the laser gain curve and also at the centre of the pass or reflection-band of the mode selecting elements. Of course, in a real laser this is not automatically the case, the modes drift about due to thermal variations in the optical length of the cavity. Hence even if the criterion for SLM operation (equation 2.42) is satisfied, a certain proportion of shots will be 2-mode. The ratio r of SLM shots to shots containing an unacceptable amount of mode beating is (Hanna and Koo, 1982):

$$r = \epsilon \cdot \frac{q_{eff}}{\ln N} - 1 \qquad 2.53.$$

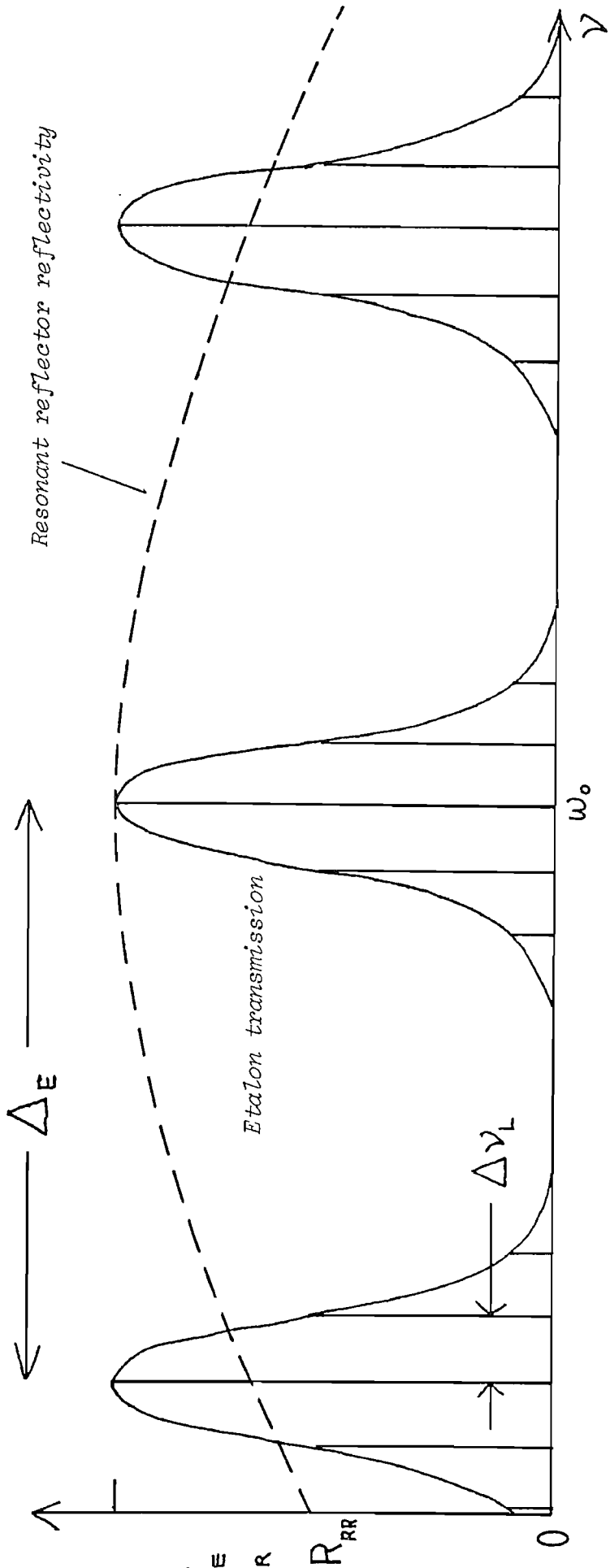

Figure 2.11 Single longitudinal mode selection using an etalon and a resonant reflector.

Clearly, however much mode selection is used, there will always be occasions when two longitudinal modes fall symmetrically either side of an etalon passband peak, resulting in 2-mode oscillation. It would appear that only by stabilizing the cavity optical length to a fraction of a wavelength can SLM operation be guaranteed on every laser shot. The principal cause of variation in the cavity length is heating and consequent expansion of the laser rod as it absorbs energy from the flashlamps during the pumping pulse. The cavity length tends to sweep during the pump pulse because of this and Hanna and Koo (1982) have exploited this phenomenon to actually improve SLM operation. Enough mode selection is used to ensure that, at most, two longitudinal modes can oscillate at one time. The mode selection is chosen so that if two modes do oscillate together, they are adjacent modes. The pre-lase period of lasing consists of a sequence of relaxation oscillations, which are about 0.5 μs long at intervals of ~ 5 μs, each of which is then either single or two-mode. These are monitored using a photodiode and the signal is amplified and filtered electronically before being used to trigger the pockels cell Q-switch. The filter is tuned to the adjacent mode beat frequency $\Delta\nu_L$ which is around 130 MHz, and if beating is detected no trigger signal is fed to trigger the pockels cell open. However, if no beating is detected the pockels cell is triggered open. This way the laser is Q-switched only when a SLM prelase pulse is available for amplification. Since the laser cavity length is sweeping during the pump pulse, then there will always come a time when one longitudinal mode has been swept to the centre of an etalon or resonant reflector band peak, giving a SLM pre-lase pulse. Hence, every laser shot is SLM.

In the next section we describe how spatial hole burning in SLM lasers can be overcome.

2.3.2. Spatial hole burning and its prevention

An effect encountered when a laser is run on an SLM is that of spatial hole burning in the laser rod. The radiation inside the cavity would normally consist of a plane-polarized standing wave, which depletes the inversion at the antinodes, but not at the nodes, leaving planes of undepleted inversion separated by $\lambda/2$. A second longitudinal mode of a different frequency whose nodes fall at the antinodes of the first mode may then feed on this unused inversion. This second mode appears as a second smaller pulse emerging from the laser after the main Q-switched pulse (with a delay of typically 200 ns) although sometimes the two overlap causing beating. Spatial hole burning may be eliminated by placing quarter wave plates round the rod, which produce a helical nodeless standing wave which utilizes all the inversion. This arrangement is shown in Figure 2.12.

The fast (or slow) axis of the plate A nearest the polarizer must be at 45^{o} to the polarization axis. The fast axis of the second plate B must be either parallel or perpendicular to that of A, though it doesn't matter which, as we will now see. Consider axes as in Figure 2.12, with a beam plane polarized at 45^{o} to the x and y axes and incident upon A travelling along the positive z direction. If we write the electric field in region 1 in the form:

$$Ex_1 = \hat{x} \sin(kz-wt) \qquad 2.54$$

$$Ey_1 = \hat{y} \sin(kz-wt) \qquad 2.55$$

where $\hat{x}$, $\hat{y}$ are unit vectors in the x and y directions then the field in 2 after passing through A (with fast axis parallel to $\hat{x}$) is:

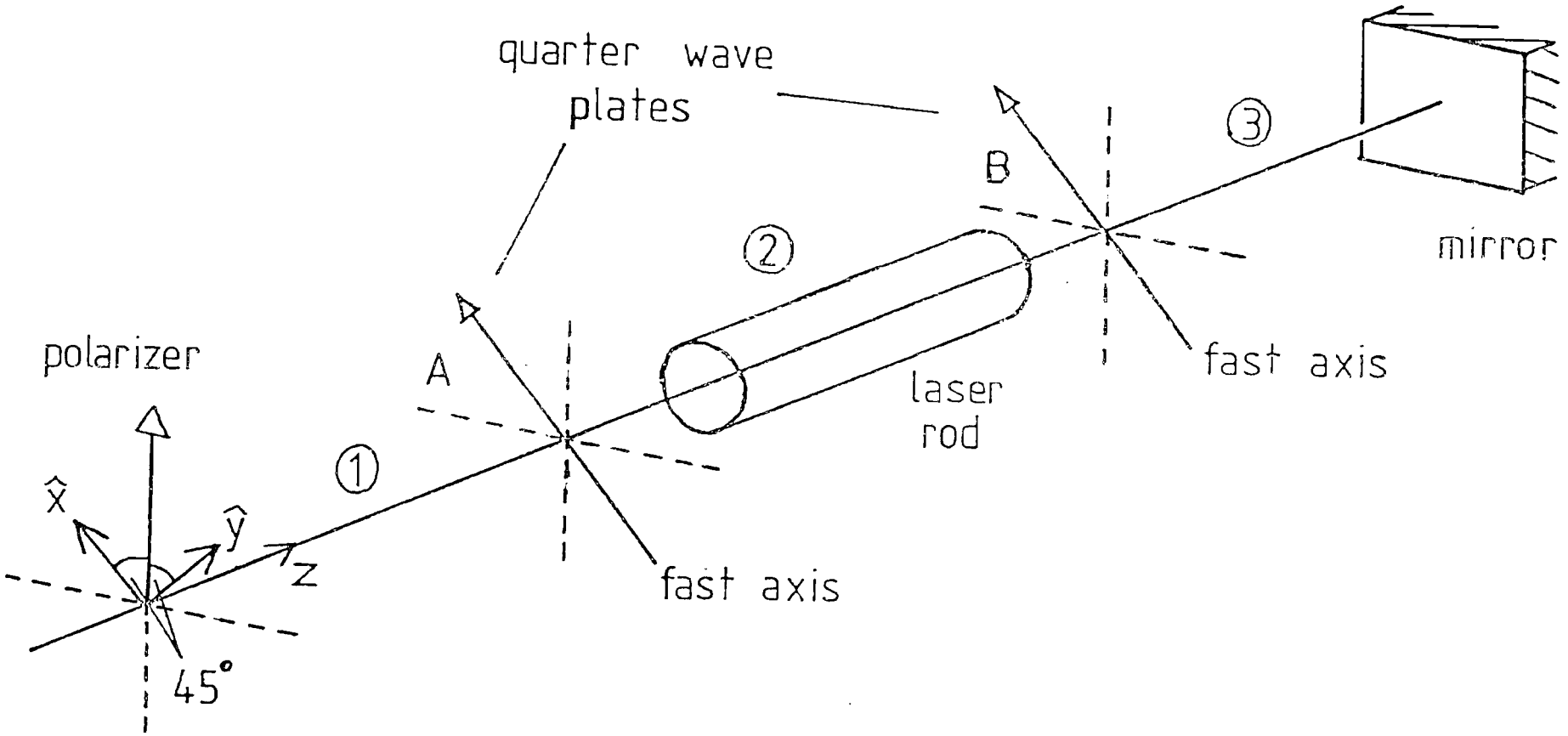

Figure 2.12 Scheme for elimination of spatial hole-burning by using quarter wave plates around the laser rod

$$Ex_2 = \hat{x}\ \sin(kz-wt) \qquad 2.56$$

$$Ey_2 = \hat{y}\ \sin(kz-wt+\tfrac{\pi}{2}) = \hat{y}\cos(kz-wt) \qquad 2.57$$

Suppose, firstly, that plate B has its fast axis parallel to $\hat{x}$, that is, parallel to A's fast axis (as in figure 2.12), then in 3 the field is:

$$Ex_3 = \hat{x}\ \sin(kz-wt) \qquad 2.58$$

$$Ey_3 = \hat{y}\ \sin(kz-wt+\pi) = -\hat{y}\sin(kz-wt) \qquad 2.59$$

After reflection the fields have the form:

$$E'x_3 = \hat{x}\ \sin(kz+wt) \qquad 2.60$$

$$E'y_3 = -\hat{y}\sin(kz+wt) \qquad 2.61$$

$$E'x_2 = \hat{x}\ \sin(kz+wt) \qquad 2.62$$

$$E'y_2 = -\hat{y}\sin(kz+wt-\tfrac{\pi}{2}) = \hat{y}\cos(kz+wt) \qquad 2.63$$

(Note that in 2.63 $E'y_2$ has a phase relative to $E'x_2$ of $-\frac{\pi}{2}$ (not $+\frac{\pi}{2}$) since the waves are now travelling in the negative z direction) and

$$E'x_1 = \hat{x}\ \sin(kz+wt) \qquad 2.64$$

$$E'y_1 = -\hat{y}\sin(kz+wt-\pi) = \hat{y}\sin(kz+wt) \qquad 2.65$$

The total field in 2, where the laser rod is situated, is therefore:

$$\begin{aligned} E_{x2T} &= \hat{x}\ \sin(kz-wt) + \hat{x}\ \sin(kz+wt) \\ &= 2\hat{x}\ \sin(kz)\cos(wt) \end{aligned} \qquad 2.66$$

$$E_{y2T} = \hat{y}\cos(kz-wt) + \hat{y}\cos(kz+wt)$$
$$= 2\hat{y}\cos(kz)\cos(wt) \qquad 2.67$$

This represents a helical standing wave with no nodes or antinodes, therefore no spatial hole burning occurs.

Now suppose plate B has its fast axis parallel to $\hat{y}$, that is, perpendicular to that of A, the outward wave in 3 now becomes:

$$Ex_3 = \hat{x}\sin(kz-wt+\frac{\pi}{2}) = \hat{x}\cos(kz-wt) \qquad 2.68$$

$$E_{y3} = \hat{y}\sin(kz-wt+\frac{\pi}{2}) = \hat{y}\cos(kz-wt) \qquad 2.69$$

and the reflected wave in 3 is:

$$Ex'_3 = \hat{x}\cos(kz+wt) \qquad 2.70$$

$$Ey'_3 = \hat{y}\cos(kz+wt) \qquad 2.71$$

and in 2 it is:

$$Ex'_2 = \hat{x}\cos(kz+wt-\frac{\pi}{2}) = \hat{x}\sin(kz+wt) \qquad 2.72$$

$$Ey'_2 = \hat{y}\cos(kz+wt) \qquad 2.73$$

and in 1 for completeness:

$$Ex'_1 = \hat{x}\sin(kz+wt) \qquad 2.74$$

$$Ey'_1 = \hat{y}\cos(kz+wt-\frac{\pi}{2}) = \hat{x}\sin(kz+wt) \qquad 2.75$$

Hence the field in 2 is exactly as for the case of parallel fast axes, and once again no spatial hole burning occurs.

This result, i.e. no spatial hole burning for either orientation of plate B, was verified experimentally.

2.4. Experimental work on the single mode oscillator

The first experiments devised with the ultimate aim of a reliable single longitudinal mode oscillator examined the possible use of a three surface resonant reflector. Subsequently a pre-lase Q-switched laser was built incorporating an etalon and resonant reflector, and later the single mode detector circuit was added to this.

As discussed above, sufficient discrimination between adjacent modes can be achieved by using a resonant reflector of narrow reflection bandwidth, which implies that it must be thick. However, in this case, the reflection maxima are so close together that they too must be discriminated against, either by a thin low finesse etalon or a thin resonant reflector. The latter was attempted using a three surface resonant reflector (Figure 2.13) consisting of a 6mm glass resonant reflector aligned with one face of a wedged glass plate, these two components being separated by air to provide the large spacing, which could therefore be varied.

The arrangement was used in a fast Q-switched telescopic resonator, with the output from the small beam end. When the plate was misaligned every laser pulse was very strongly modulated in accordance with multimode operation. (Notice this is the situation used in the example on page 37, in which the linewidth was calculated as 0.058 cm^{-1}, equivalent to 12 longitudinal modes). When the plate was aligned 13 cm from the solid resonant reflector, (about one eighth of the cavity optical length), 10% of pulses exhibited modulation with a period of 7 ns corresponding to adjacent mode beating. In this situation one finds from equation 2.51 that $\Gamma_{FQRR} = 0.004\ cm^{-1}$, implying single mode operation. When the air space was increased to 25 cm, ($\Gamma_{FQRR} = 0.002\ cm^{-1}$) no adjacent

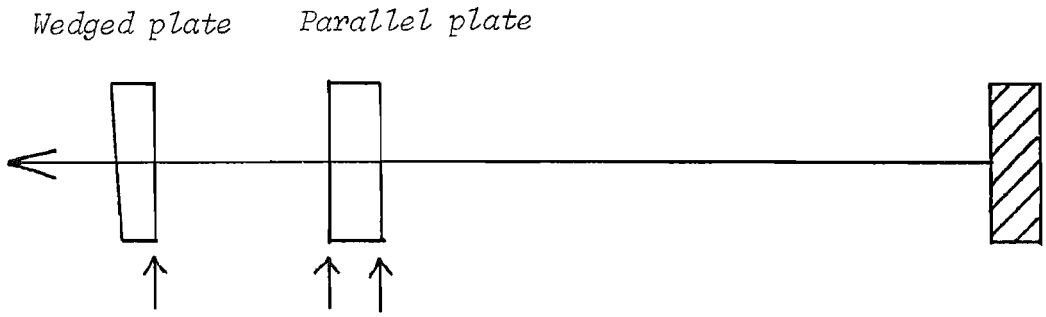

Figure 2.13 Three-surface resonant reflector.

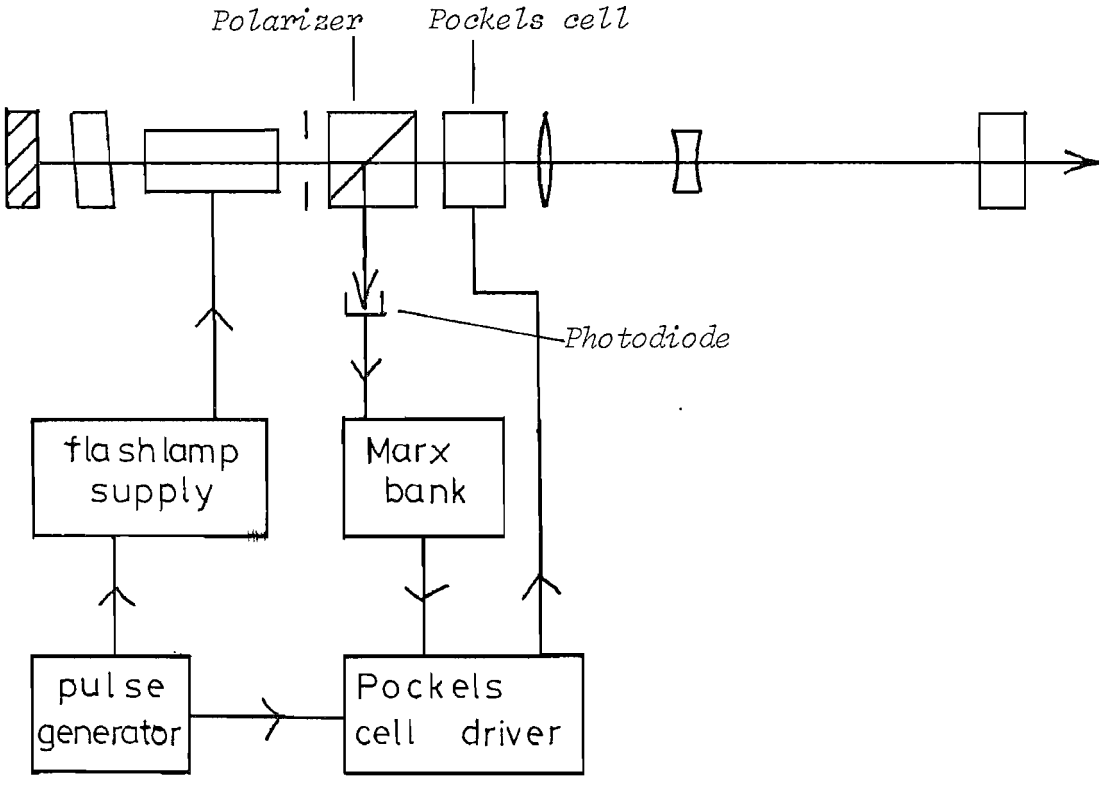

Figure 2.14 Schematic diagram of pre-lase Q-switching electronics.

mode beating was seen, but slight ripples of shorter period could be observed on 10% of shots. Now the FSR of a 25 cm resonant reflector is 0.02 cm^{-1}, which is only 4 adjacent mode spacings, and it was suspected that the laser was oscillating on two modes at this frequency spacing and that the beating, being instrument-limited, was not observable. To check this the laser output was frequency doubled to the visible 532 nm, in the green, transmitted through a Fabry-Perot etalon and focussed onto a screen. The resulting ring pattern confirmed that the laser was indeed running for some of the time on two modes with this frequency spacing. Out of interest a thin tilted intracavity etalon was inserted to prevent this, although admittedly it defeated the object of the three-surface resonant reflector. This eliminated the problem temporarily, but after several minutes variation of air pressure and temperature detuned the resonant reflector relative to the etalon. In fact an inherent defect of the three surface resonant reflector is that the thick air spaced part needs to be kept in tune with the thin glass resonant reflector and this can only be done using temperature and pressure controllers. Consequently, this scheme for a single mode fast Q-switched laser was abandoned in favour of more modest mode selection used with pre-lase Q-switching.

Because of its simplicity and ease of alignment the telescopic resonator with the output from the narrow beam end was used as the basis for a pre-lase Q-switched laser. A schematic diagram of the electronics is shown in Figure 2.14. Firstly, the pulse generator triggers the Pockels cell driver to close the cavity (high voltage on the Pockels cell) and at the same time triggers the flashlamps so that the inversion builds up in the rod. Pre-lasing is detected with a PIN photodiode using the light ejected from the cavity off the polarizer. When the power reaches a certain level (of the order of a few Watts, typically) the signal from the photodiode is enough (1V across 100 Ω) to trigger the Marx bank, which in turn triggers the Pockels cell open. For mode selection a 6mm resonant reflector was used, together with a 10mm tilted etalon with face reflectivity of 72% placed between the 100% mirror and the laser rod. From

equation 2.52 we find that $\Gamma_{PLQE} = 0.0012\ cm^{-1}$ with this etalon, which is comparable to the linewidth of a single longitudinal mode, so this should be quite adequate for SLM operation. Notice, however, that we have ignored the effects of walk-off (Arnaud et al, 1974). This laser produced SLM output on about 80% of shots. The other 20% showed varying amounts of adjacent mode beating. Equation 2.53 predicts that 85% of shots will be SLM. To increase this percentage to 100% the beat detection circuit was built with the guidance of J. Koo and D.J. Pratt and added to the laser. The circuit is shown schematically in Figure 2.15. The system worked in that every pulse from the laser was single mode. Observations of the pre-lase signal revealed that the laser was usually Q-switching on the first pre-lase pulse, sometimes on the second and occasionally on the third or fourth pulse. Moreover, there were shots when the laser did not Q-switch at all, meaning that no SLM pre-lase pulses with intensity great enough to trigger the Marx bank occured during the pre-lase period. The number of pre-lase pulses could be increased by lowering the Pockels cell hold-off voltage, but then the energy lost during pre-lasing is increased - measured at $\sim 2\%$ of the total energy in each pre-lase pulse. The obvious remedy is to increase the optical mode selection by, for example, using a thick (say 7.5 cm) resonant reflector with a thin tilted intracavity etalon. Although this, in theory, does not give a significantly narrower linewidth, ($\Gamma_{PLQRR} = 0.0011\ cm^{-1}$ from equation 2.51), a resonant reflector does not suffer from walk-off loss so its mode selectivity is higher.

The effect of spatial hole burning was observed on the laser when it was pre-lase Q-switched and oscillated on a single mode - a second pulse emerged about 200 ns after the first, containing perhaps 20% of the energy. This was eliminated when suitably orientated quarter wave plates were placed around the laser rod, when the energy in the Q-switched pulse increased by an amount corresponding to that in the second pulse when the plates were absent. The energy available from this laser was still limited to 100 mJ by damage to the resonant reflector.

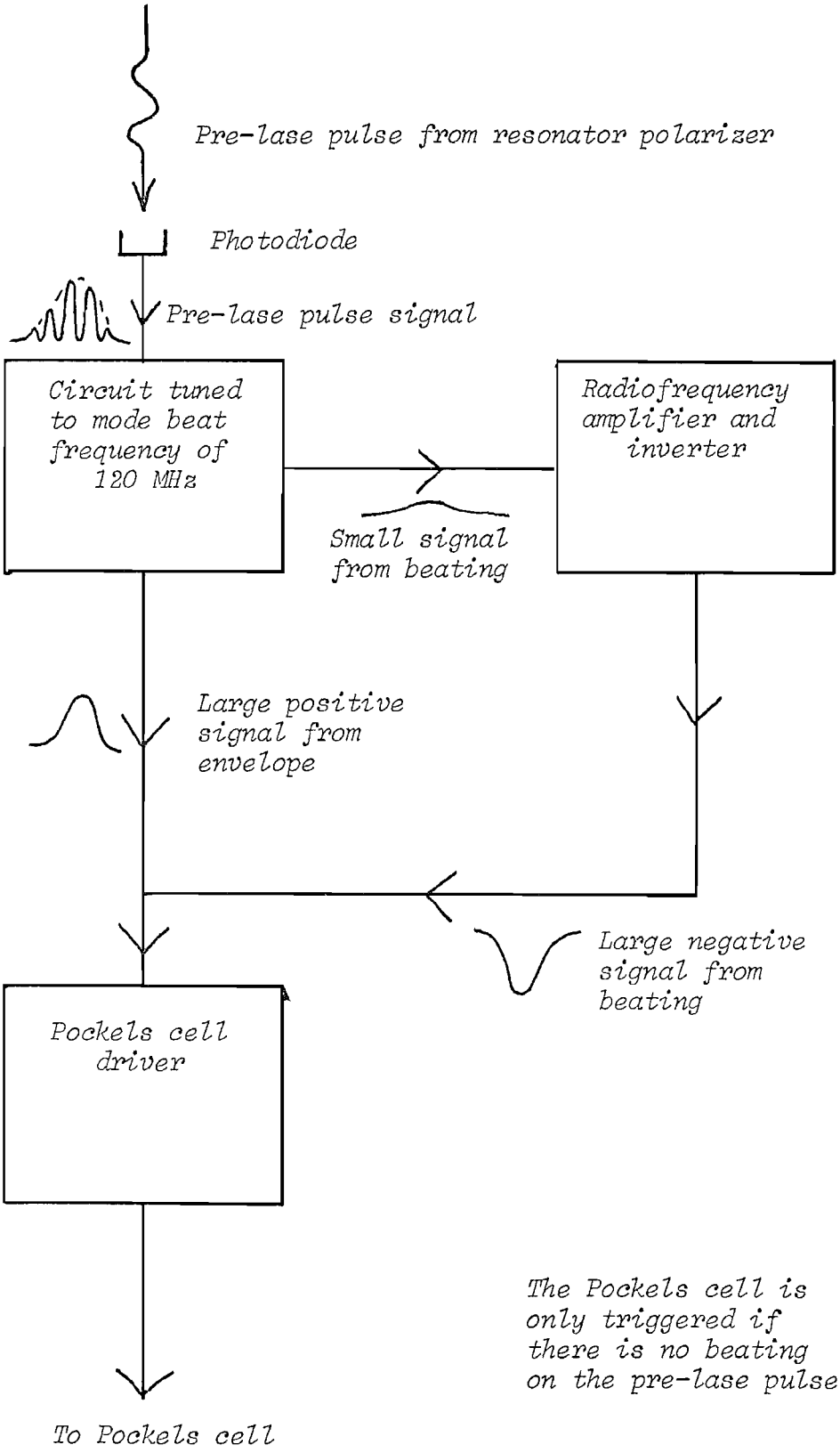

Figure 2.15 *Schematic diagram of the beat detection circuit for single-mode operation of the laser oscillator.*

Having arrived at and built an efficient high power single transverse and longitudinal mode oscillator, the next step was to increase the energy and power by amplifying its output. In the next chapter we examine and discuss the properties and problems of amplifiers.

CHAPTER 3

Laser amplification

In its simplest form a laser amplifier consists of a length of pumped gain medium through which the oscillator output passes once. Its purpose is to increase the beam brightness $B = P/A\Omega$, where P is the power of the output from area A, with beam solid-angle divergence Ω. Clearly then, gain and energy extraction are the main considerations when designing or choosing an amplifier. In an ideal amplifier these would be the only considerations, but in a real system it is also necessary to take into account distortions of wavefront, pulse shape and polarization state, as well as superradiance or pre-lasing caused by feedback.

We first consider pulse amplification in which saturation effects cause temporal changes and then go on to examine thermally induced wavefront and polarization distortions.

3.1. Theory of pulse propagation in a laser amplifier

We refer to the paper by Frantz and Nodvik (1963) in which the growth of a radiation pulse traversing a medium with an inverted population is described by non-linear time dependent photon transport equations, which are solved for an arbitary input pulse and initial population inversion distribution. We modify the theory for a four-level system.

A beam of monochromatic light is incident on the surface of the gain medium, which occupies the space $0 \leqslant x \leqslant L$. The number density of active atoms in the excited state is $N(x,t)$, while the density of ground state atoms may be taken as zero. The photon density is $n(x,t)$. If c is the velocity of light in the medium and σ the emission cross section, then the photon transport equation is:

$$\frac{\partial n}{\partial t} + c\left(\frac{\partial n}{\partial x}\right) = \sigma c n N \qquad 3.1.$$

We assume the laser line is homogeneously broadened and that there is negligible absorption.

Spontaneous emission is neglected because the radiative lifetime of the excited state is long compared to the duration of Q-switched pulses. The rate of increase of photons given by the right hand side of 3.1 is equal to the rate of decrease of excited state atoms so:

$$\frac{\partial N}{\partial t} = \sigma c n N \qquad 3.2.$$

The boundary conditions are the initial upper level population $N_o(x)$ before the beam enters the medium:

$$N(x,-\infty) = N_o(x) \qquad 0 \leqslant x \leqslant L \ ; \qquad 3.3.$$

and the photon density arriving at the x = o boundary of the medium:

$$n(o,t) = n_o(t) \qquad 3.4.$$

We will not enter into the details of the solution of the equations 3.1 and 3.2 but simply state the general solutions which are:

$$n(x,t)=\frac{n_o(t-x/c)}{1-\left(1-\exp\left[-\sigma\int_o^\infty N_o(x')\,dx'\right]\right).\exp\left[-\sigma c\int_{-\infty}^{t-x/c} n_o(t')\,dt'\right]} \qquad 3.5.$$

$$N(x,t)=\frac{N_o(x).\exp\left(-\sigma\int_o^\infty N_o(x')\,dx'\right)}{\exp\left(\sigma c\int_{-\infty}^{t-x/c} n_o(t')\,dt'\right)+\exp\left(-\sigma\int_o^\infty N_o(x')\,dx'\right)-1} \qquad 3.6.$$

in the region $0 \leqslant x \leqslant L$.

Further analytical results are obtainable from 3.5 and 3.6 for the simplest case of a square pulse and this is a useful approximation to a Q-switched pulse when information is required about energy and gain, but knowledge of the temporal shape is less important.

However, if knowledge of the temporal evolution of input pulses of more complex Gaussian or exponential shapes is needed, then 3.1 and 3.2 can be solved numerically (R.V. Ambartsumyan et al, 1966). Taking a square input pulse of duration τ and magnitude n_0,

$$n_0(t) = \begin{cases} n_0 & 0 \leq t \leq \tau \\ 0 \text{ otherwise} \end{cases} \qquad 3.7.$$

and a uniform initial population inversion

$$N_0(x) = N_0 = \text{const}, \quad 0 \leq x \leq L \qquad 3.8.$$

3.5. can be evaluated as:

$$n(x,t) = \frac{n_0}{1-[1-\exp(-\sigma N_0 x)].\exp[-\sigma\eta(t-x/c)/\tau]}, \quad 0 \leq t-\frac{x}{c} \leq \tau, \qquad 3.9$$

$$= 0 \qquad \text{, otherwise.}$$

Here $\eta = n_0 c\tau$ is the total number of photons per unit area in the pulse.

Light which enters the amplifier at time t leaves it at time $t = \frac{L}{c}$, so for an input pulse $n_0(t)$ the output pulse is:

$$n_L(t) = n(L, t+L/c) \qquad 3.10.$$

or

$$n_L(t) = \frac{n_0}{1-[1-\exp(-\sigma N_0 L)].\exp(-\sigma\eta t/\tau)} \qquad 3.11.$$

To make use of this equation we need to estimate N_0 and η from experimentally known parameters. To estimate N_0 we need to know the stored energy per unit volume in the amplifier rod. To do this (Koechner 1976) we proceed from 3.11 and obtain an expression relating the single pass gain G, the saturation energy density E_s,

the input energy density E_{in} and the small signal single pass gain G_0, all of which are experimentally observable. The last of these, G_0, can be used to calculate the stored energy E_{st} and thence N_0. This value of N_o can then be re-inserted into 3.11 and the temporal change of the square pulse can be calculated.

Now the energy gain for a light beam passing through an amplifier of length L is defined by:

$$G = \frac{1}{n_o \tau} \int_{-\infty}^{\infty} n_L(t)\, dt \qquad 3.12.$$

Using 3.11 in 3.12 and integrating we find:

$$G = \frac{1}{\sigma n_o \tau} \ln\left\{1 + \left[\exp(\sigma n_o \tau) - 1\right] \exp(N_o \sigma L)\right\} \qquad 3.13.$$

We rewrite this in terms of measurable parameters. The input energy per unit area is:

$$E_{in} = n_o \tau h\nu \qquad 3.14.$$

and the saturation energy density is defined by:

$$E_s = \frac{h\nu}{\sigma} \qquad 3.15.$$

The small signal gain coefficient g_0 is related to the single pass gain G_0 by $G_0 = \exp(g_0 L)$ and is given by $g_0 = N_0 \sigma$.

Now 3.13 can be rewritten as:

$$G = \frac{E_s}{E_{in}} \ln\left\{1 + \left[\exp\left(\frac{E_{in}}{E_s}\right) - 1\right] G_o\right\} \qquad 3.16.$$

The stored energy is given by:

$$E_{st} = h\nu N_o = g_o E_s \qquad 3.17.$$

Equation 3.16 is a unique relationship between G, E_{in}, E_s and $G_0 = \exp(g_0 L)$, and is valid for square input pulses over the entire régime from small signal input to complete saturation and is significant because once one data point is known for an amplifier, the performance at any other operating point can be calculated. Thus, for example, the small signal gain can be found from large signal measurements.

The amplifier used for the experiments described later in this thesis consisted of a Nd:YAG rod with dimensions of 7.5 cm and a diameter of 9 mm. It was pumped by twin flashlamps with a pump energy of up to 100 J per shot. The performance of the amplifier as far as energy gain was concerned was evaluated by measuring the single pass energy gain at various pumping levels for two input energies, one of which was close to the small signal régime, defined by $G_0 E_{in}/E_s \ll 1$. The results were inserted in 3.16 to give an estimate for G_0, and via 3.17, for N_0. From 3.15 the saturation energy density of Nd:YAG (ν = 2.83 x 10^{14} Hz, σ (effective) = 3.5 x 10^{-19} cm^2 (Svelto, 1982)) is 0.536 J cm^{-2}. The results of the measurements are shown in Figure 3.1. The input beam had a spot size of w = 3mm, and Q-switched inputs of 3.5 mJ ($\equiv$ 12.4 mJ cm^{-2}) and 50 mJ ($\equiv$ 177 mJ cm^{-2}) were used. (At this point we note that we are stretching a calculation which assumes a uniform transverse intensity distribution to the case of a Gaussian intensity profile). For the smaller input the maximum gain was 16, so $G E_{in}/E_s$ = 0.37, and 3.16 can be approximated to $G \sim G_0 \equiv \exp(g_0 L)$. If we re-arrange 3.16, G_0 can be calculated exactly:

$$G_o = \frac{\exp\left(G E_{in} / E_s \right) - 1}{\exp\left(E_{in} / E_s \right) - 1} \qquad 3.18.$$

At the maximum pumping level, the smaller input gives G_0 = 19, the larger gives G_0 = 23. The stored energy is related to G_0 by (3.17) $E_{st} = g_0 E_s$ or:

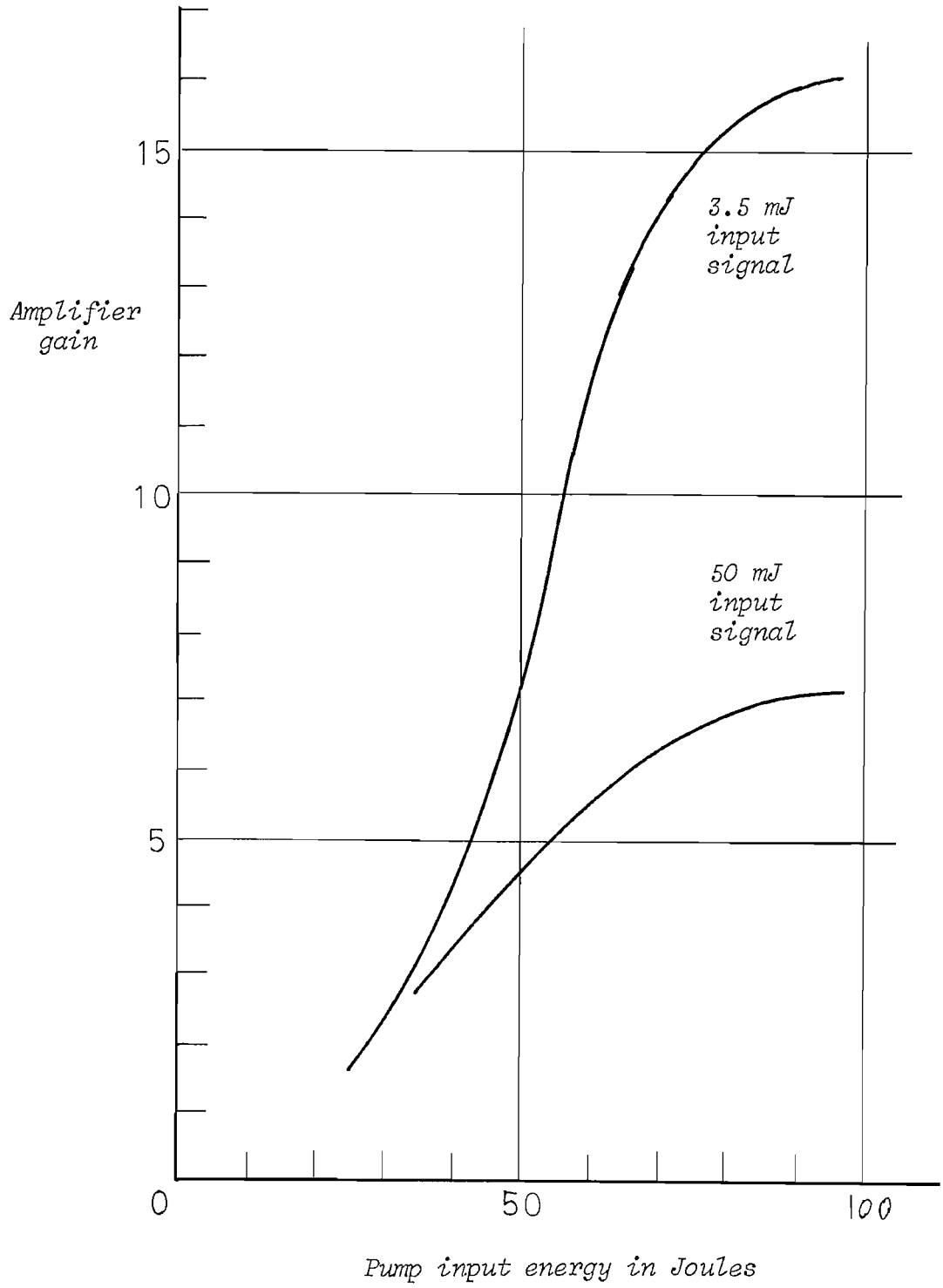

Figure 3.1 Amplifier energy gain versus pump input energy.

$$E_{st} = \frac{\ln G_o}{L} \cdot E_s \qquad 3.19.$$

and the corresponding results are 210 and 220 mJ cm^{-3}. Thus the total stored energy in the rod volume of 4.77 cm^3 is ~1J. The inversion N_o is:

$$N_o = \frac{E_{st}}{h\nu} = 1{\cdot}1 \times 10^{18} \quad cm^{-3}$$

Having found N_o we also need to know η in order to deal with equation 3.11. This is simply:

$$\eta = \frac{E_{in}}{h\nu} \qquad 3.20.$$

Evaluation of 3.11 for various values of N_o and n_o reveals that a square pulse generally experiences different gains at different positions within the pulse, so that the leading edge is amplified more than the trailing edge. This occurs for the simple reason that the leading edge acquires photons by stimulated emission, which depletes the population inversion, this depleted inversion being that seen subsequently by the trailing edge of the pulse. Hence less energy is added to the later part of the pulse than to the earlier part. The degree of distortion occuring through this effect depends upon the energy of the incident pulse compared to the initial population inversion. If the pulse energy is small compared with the energy stored in the gain medium, then relatively few atoms will be stimulated into emission by the leading edge of the pulse and the trailing edge will still see a substantial inversion. If, on the other hand, the pulse energy is comparable to the stored energy, the leading edge heavily depletes the inversion and the trailing edge receives much less amplification. These situations are illustrated in Figure 3.2. In Appendix IV we perform a calculation using equation 3.11 based on the experimental results described in Chapter 5.

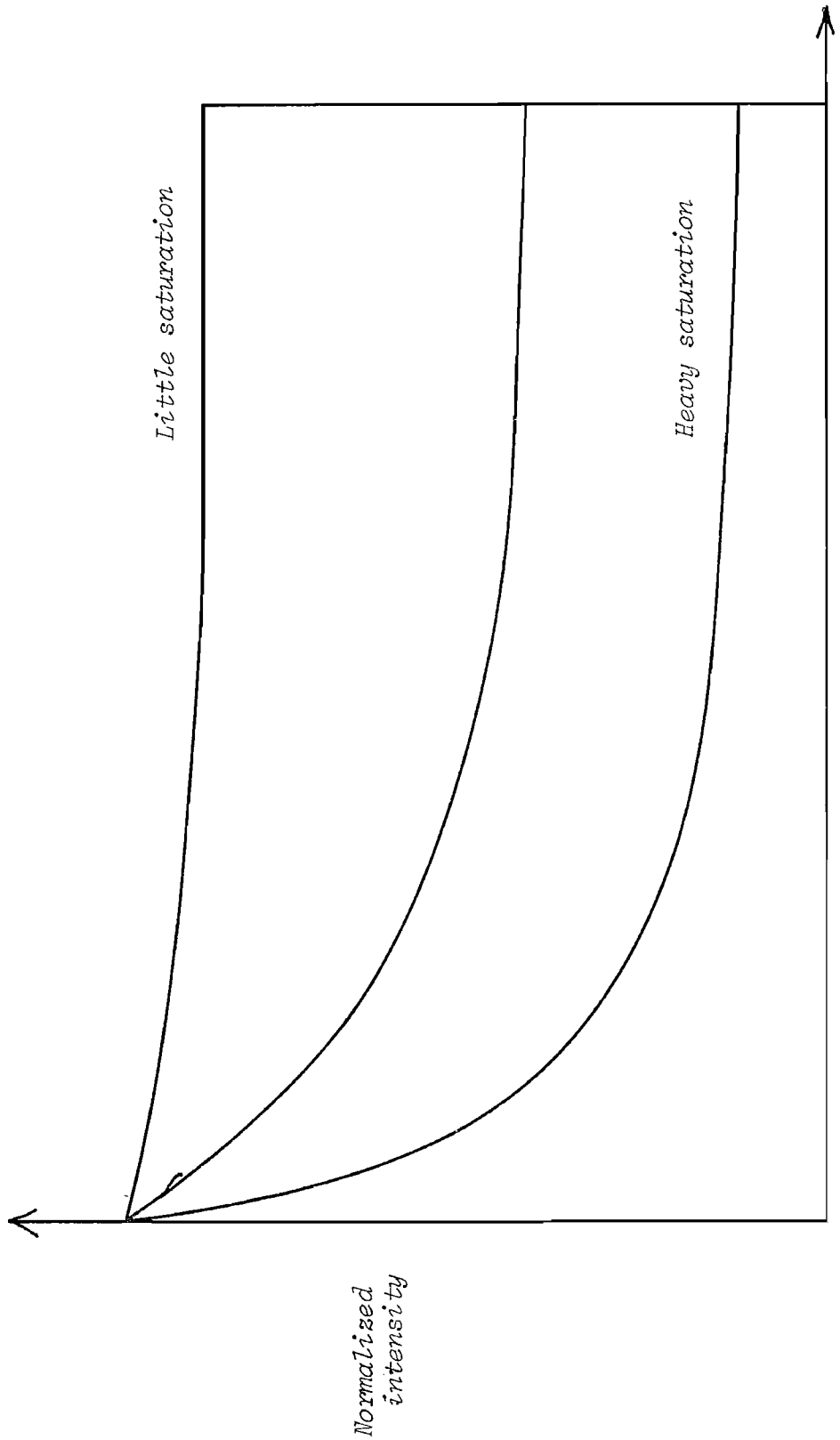

Figure 3.2 Distortion of a square pulse shape in a saturated amplifier.

When the input pulse shape is of a more complex form than a square shape then, as mentioned before, 3.1. and 3.2 must be solved numerically. R.V. Ambartsumyan et al (1966) did this for several input pulse shapes and discovered that the evolution of the pulse shape depends strongly on the shape of the rising edge of the pulse. Their results can be summarised by saying that a Gaussian shaped pulse (which approximates the output pulse shape of a Q-switched single-mode laser) suffers a forward shift of the peak and is then shortened as it traverses the gain medium; a pulse with exponential rising edge assumes a stationary shape; and a pulse with a stepped rise leading edge is first narrowed (as described above) and then broadens infinitely, given a long enough amplifier.

Having discussed the temporal structure of a pulse as it traverses an amplifier, we now go on to talk about thermally induced wavefront and polarization distortions.

3.2. Thermal effects in pumped laser rods

Thermal effects in laser rods arise because of heat generation in the rod by absorption of pump radiation and the removal of this excess heat by coolant flowing around the rod surface. The resulting non-uniform temperature distribution in the rod causes optical distortion of the beam due to temperature - and stress - dependent variation of the index of refraction. These distortions are predominantly thermal lensing and thermally induced birefringence. The temperature profile set up in the laser rod depends upon the flashlamp energy and pulse repetition rate of the laser. Nd:YAG lasers of the type described in this thesis are generally operated at repetition rates of up to $\sim$15 Hz. If the laser is operated at a repetition rate such that the time between shots is comparable to or less than the thermal relaxation time of the rod, then at the time of one pulse there will be a residual temperature distribution from the previous pulse and over a number of shots a steady state condition will be reached. When the pulse repetition period is much less than

the thermal relaxation time, the thermal effects depend upon the average input power (Koechner, 1976) and they may be quantified using a steady-state theory. It is in this régime that the thermal effects become troublesome. The thermal time constant of the rod is $\tau = r_o^2/k$ where r_o is the radius and k the thermal diffusivity, which for Nd:YAG is $k = 0.046$ at a temperature of 300K. Thus for a 6mm rod $\tau = 2s$, and for a 9mm rod as used for the amplifier described later in this thesis, $\tau = 4.4s$. Hence, even at repetition rates down to less than 1 Hz the condition is steady state.

Firstly we need to know the temperature distribution, which will in turn give the stress distribution. These two distributions both contribute to thermal lensing, while birefringence is caused by the stress distribution alone.

The temperature distribution in a cylindrical rod of thermal conductivity K in which heat is uniformly generated at a rate Q per unit volume is obtained from the one dimensional heat equation (see Koechner, 1976):

$$\frac{d^2T}{dr^2} + \left(\frac{1}{r}\right)\left(\frac{dT}{dr}\right) + \frac{Q}{K} = 0 \qquad 3.21.$$

Solving this gives the steady state temperature as a function of radial position r. The boundary condition is the temperature at the rod surface $T(r_o)$. It follows that:

$$T(r) = T(r_o) + \frac{Q}{4K}\cdot(r_o^2 - r^2) \qquad 3.22.$$

Note that the temperature distribution is parabolic and the temperature gradients inside the rod are independent of the surface temperature. The heat generated per unit volume may be written as:

$$Q = \frac{P_a}{\pi r_o^2 L} \qquad 3.23.$$

where P_a is the total heat dissipated by the rod of length L.

The temperature distribution 3.22 leads to thermal stresses in the radial (σ_r), tangential (σ_ϕ) and axial (σ_z) directions. These stresses in turn generate thermal strains in the rod, which produce refractive index variations through the photoelastic effect. The refractive index ellipsoid is modified in shape, size and orientation by the thermal strains. It can be shown that the refractive index changes in the radial and tangential directions (Figure 3.3.) are:

$$\Delta n_r = -\frac{1}{2}\, n_o^3\, \frac{\alpha Q}{K}\, C_r\, r^2 \qquad 3.24.$$

$$\Delta n_\phi = -\frac{1}{2}\, n_o^3\, \frac{\alpha Q}{K}\, C_\phi\, r^2 \qquad 3.25.$$

where C_r and C_ϕ are functions of the elasto-optical coefficients of Nd:YAG and are C_r = 0.017, C_ϕ = -0.0025, α is the thermal expansion and n_o is the refractive index at the centre of the rod.

3.2.1. Thermal lensing

The change of refractive index along a path through the rod at radial distance r from the axis consists of two parts:

$$n(r) = n_o + \Delta n(r)_T + \Delta n(r)_\epsilon \qquad 3.26.$$

where $\Delta n(r)_T$ and $\Delta n(r)_\epsilon$ are the temperature and stress dependent changes of the refractive index respectively. It can be shown that an optical beam suffers a quadratic spatial phase variation, which is equivalent to a spherical lens, and that if the focal length is long compared to the length of the rod, then the focal length is given by:

$$f' = \frac{K}{QL}\left(\frac{1}{2}\cdot\frac{dn}{dT} + \alpha C_{r,\phi}\, n_o^3\right)^{-1} \qquad 3.27.$$

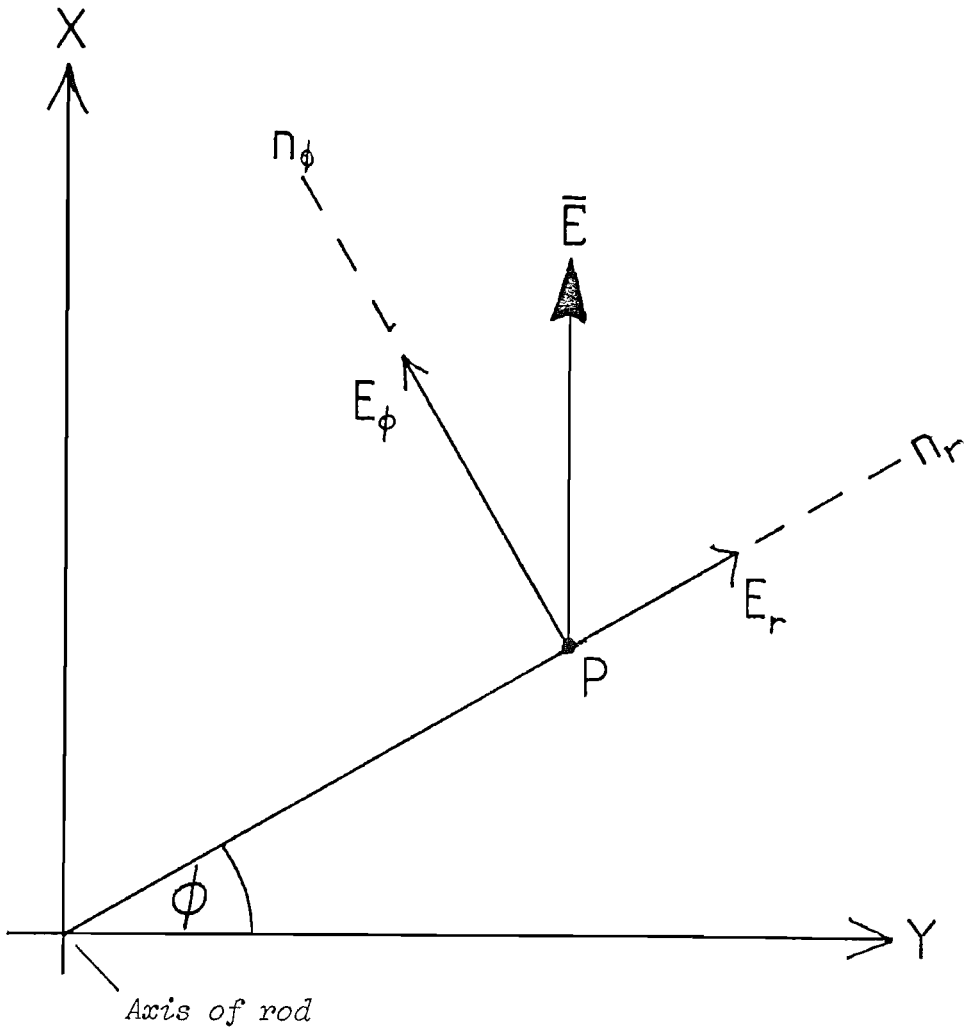

Figure 3.3 The axes of birefringence at a point P in the rod cross-section.

Notice that f' has two values, corresponding to the values of $C_{r,\phi}$ for either radially or tangentially polarized light. A further contribution to the focal length is the result of curvature of the rod faces - the stress distribution at the ends differs from that in the bulk of the rod. Including this modifies 3.27 to:

$$f = \frac{KA}{P_a}\left(\frac{1}{2}\frac{dn}{dT} + \alpha C_{r,\phi} n_o^3 + \frac{\alpha r_o (n_o - 1)}{L}\right)^{-1} \qquad 3.28.$$

where A is the cross sectional area of the rod and P_a the total heat dissipated in the rod. For Nd:YAG the temperature-dependent refractive index contributes 74% of the lensing, the stress-dependent part is 20% and the end face curvature contributes 7%. Equation 3.28 may be written as:

$$f = M P_{in}^{-1} \qquad 3.29.$$

in which M contains the material parameters and an efficiency parameter η such that $P_a = \eta P_{in}$. For Nd:YAG it is found that $\eta \simeq 0.05$. Putting the material parameters into 3.28 we find that for a rod of dimensions $r_o = 0.45$ cm, L = 7.5 cm,

$$f_r = \frac{3.4 \times 10^5}{P_{in}} \qquad 3.30.$$

$$f_\phi = \frac{4.2 \times 10^5}{P_{in}} \qquad 3.31.$$

for the radial and tangential polarizations respectively. The two focal lengths of a pumped Nd:YAG rod have been observed by Koechner (1970).

In the amplifier used in the experiments the pump energy was supplied by the discharge of two 100 μF capacitors charged to a voltage V of up to 1000 V. Hence $P_{in} = \frac{V^2 R}{10^4}$ where R is the pulse repetition rate.

Equations 3.30 and 3.31 now become:

$$f_r = \frac{3.4 \times 10^7}{V^2 R} \quad m \qquad 3.32.$$

$$f_\phi = \frac{4.2 \times 10^7}{V^2 R} \quad m \qquad 3.33.$$

Theoretically $f_\phi / f_r = 1.2$, but workers have found values varying from 1.35 to 1.5.

3.2.2. Stress birefringence

We now calculate the degree of stress - dependent birefringence induced in a Nd:YAG rod and the resultant depolarization suffered by a beam passing through it. We saw earlier in equations 3.24 and 3.25 that the principle axes of birefringence are orientated radially and tangentially at any point in the rod cross section as in Figure 3.3., and the magnitude increases quadratically with r. We assume the input to the rod is a beam plane polarized in the x direction. At each point P the radiation must be resolved into two components along the directions n_r and n_ϕ. Since $\Delta n_r \neq \Delta n_\phi$ these two components exit from the rod with some phase difference (unless P lies on the x or y axes) and the radiation will therefore be elliptically polarized. (If P lies on the x or y axes there is a component of E only along n_r or n_ϕ respectively). The phase difference δ between the two components due to the refractive index difference is:

$$\delta = \frac{2\pi}{\lambda} \cdot L \left(\Delta n_\phi - \Delta n_r\right) \qquad 3.34.$$

which, using 3.24, 3.25 and 3.23 may be written as:

$$\delta = \frac{n_o^3 \alpha \left(C_\phi - C_r\right) P_a}{\lambda K} \left(\frac{r}{r_o}\right)^2 \qquad 3.35.$$

Laser rods in either oscillators or amplifiers are often used in conjunction with polarizers and the depolarization caused by thermally induced birefringence then leads to a loss, because the depolarized part of the beam is coupled out of the system via the polarizer. Thus it is useful to know how much of the beam ends up being in the "wrong" polarization after one or more passes through the rod. With reference to Figure 3.3, calculation of this quantity involves writing down the polarization component in the y direction after (for example) one pass through the rod at point P, then integrating the expression over the cross section of the rod. Calculations of this type will be performed in Chapter 5 and Appendix III, but for now it is sufficient to say that the magnitude of the effect can be up to 25% of the beam being in the "wrong" polarization after a single pass through a strongly pumped rod.

3.3. Further signal distortion in amplifiers

Although thermal lensing and thermally induced birefringence are the most apparent aberrations of Nd:YAG amplifier rods, there are several other spatial distortions of smaller magnitude which we briefly describe.

1. Nonuniformities in the active material may cause permanent phase aberrations. Nd:YAG has for some time been available of such high optical quality that these are not of noticeable proportions.

2. Gain saturation. In most situations the beam being amplified has a Gaussian transverse intensity distribution, having originated from a TEMoo mode oscillator. Those parts of the beam near the edge of the rod have a smaller energy density compared to the saturation energy density than does the centre of the beam. Hence, as discussed in section 3.1, these weaker parts of the beam may be

amplified more than the centre. The beam radius w defined by $I(w) = I(r=0)/e^2$ is as a consequence increased. The maximum distortion occurs when $I_{in} = I_s$. For very weak signals where even the central maximum intensity is in the small signal régime, no distortion occurs because the gain is the small signal gain g_o for all parts of the signal. Also, when the amplifier is very heavily saturated, very little extra energy relative to the initial energy is added to the signal and again little or no distortion occurs.

3. Diffraction effects. The amplifier is a truncating aperture for the beam and if its radius is too small compared to the beam spot size, it causes diffraction rings which can strongly influence the beam uniformity. It can be shown (Trenholm, 1973) that, if an aperture cuts off those parts of the beam with an intensity less than K times the maximum intensity, then the peak to peak magnitude of the diffraction ripple is of the order of $40K^{1/2}\%$. Thus for an aperture of radius $r_o = 1.5w$ (which transmits 98.9% of the total Gaussian beam power), the peak to peak diffraction ripple is $\sim 4\%$; and for $r_o = 2w$ (which transmits 99.9% of the total power) it is 0.7%. Thus matching the beam spot size to the amplifier radius becomes a compromise between wanting a large beam which extracts more of the energy and keeping the beam small enough to avoid diffraction effects.

In the next Chapter we discuss the process of phase conjugation and the possibilities it offers for compensation of the main aberrations described above. In Chapter 5 we go on to describe experiments carried out with the aim of achieving this.

CHAPTER 4

Phase conjugation and stimulated Brillouin scattering

In this chapter we start with a brief explanation of what phase conjugation is and what it can achieve, and mention the various processes by which it can occur. One of these processes, stimulated Brillouin scattering (SBS) is particularly useful and convenient for the application discussed in this thesis, so this process is dealt with in more detail. Lastly, the different media in which SBS occurs are discussed.

4.1. What is phase conjugation?

We describe below firstly in mathematical, and then in physical terms, what we mean by phase conjugation.

Consider a monochromatic wave whose field amptitude $\underline{E}_p$ is of the form:

$$\begin{aligned} \underline{E}_p(\underline{r},t) &= \frac{1}{2}\underline{\mathcal{E}}_p(\underline{r})\exp\left[i(\omega t - \underline{k}_p.\underline{r})\right] + \text{c.c.} \\ &\equiv \frac{1}{2}\Psi_p(\underline{r})\exp(i\omega t) + \text{c.c.} \end{aligned} \qquad 4.1.$$

where $k_p = \omega c/n$ is the wavevector, $\underline{\mathcal{E}}_p(\underline{r})$ is the slowly varying complex field amplitude, and c.c. is the complex conjugate.

Now suppose that this beam has its propagation direction reversed, but that its other parameters, in particular the shape of the wavefront, remain unchanged. In this case its field amplitude $\underline{E}_c$ would be written as:

$$\begin{aligned} \underline{E}_c(\underline{r},t) &= \frac{1}{2}\Psi_p(\underline{r})\exp(-i\omega t) + \text{c.c.} \\ &\equiv \frac{1}{2}\underline{\mathcal{E}}_p(\underline{r})\exp\left[i(-\omega t - \underline{k}_p.\underline{r})\right] + \text{c.c.} \\ &\equiv \frac{1}{2}\underline{\mathcal{E}}_p^*(\underline{r})\exp\left[i(\omega t + \underline{k}_p.\underline{r})\right] + \text{c.c.} \\ &\equiv \frac{1}{2}\Psi_p^*(\underline{r})\exp(i\omega t) + \text{c.c.} \end{aligned} \qquad 4.2.$$

This is known as the 'conjugate wave' or 'phase conjugate' or 'time reversed replica' of the input beam. It is obtained either by reversing the sign of time in the time dependent part of the input, or by taking the complex conjugate of the space dependent part of the input.

A device which creates the phase conjugate of its input is described as a 'phase conjugator' or 'phase conjugate mirror' (PCM).

To show more clearly what is meant physically by the phase conjugate wave, consider the simple case of a beam diverging from a point source on the left towards a conventional plane mirror on the right, as in Figure 4.1. (a). The wavefronts are spherical, having the source at the centre of curvature. After reflection from the mirror the beam continues to diverge, now from right to left, and the centre of curvature of the wavefronts is now the image of the source, the image being to the right of the mirror. So what happens if the conventional mirror is replaced by a phase conjugate mirror? In this case, Figure 4.1. (b), the reflected beam does not continue to diverge. Because the reflected wavefronts are identical in shape to the incident wavefronts, but travel in the opposite direction, the beam converges to the source. The centre of curvature of the wavefronts is still the source. If the source moves around the reflected beam follows it, always retracing the same path as the incident beam. So, if the beam arrives at the phase conjugator having traversed a complex optical system, the return beam will travel back through the system along exactly the same path. More generally, if the wavefront is not spherical, but has some other perhaps very complicated shape, the shape is reproduced in the reflected beam.

A consequence of wavefront reversal in an ideal phase conjugator is that the polarization state of the input wave is also conjugated. Take, for example, a right hand circularly polarized beam close to normal incidence on a conventional mirror (Figure 4.2. (a)). The reflected beam is left circularly polarized. If, however, the same beam were incident upon an ideal phase conjugate mirror (Figure 4.2.

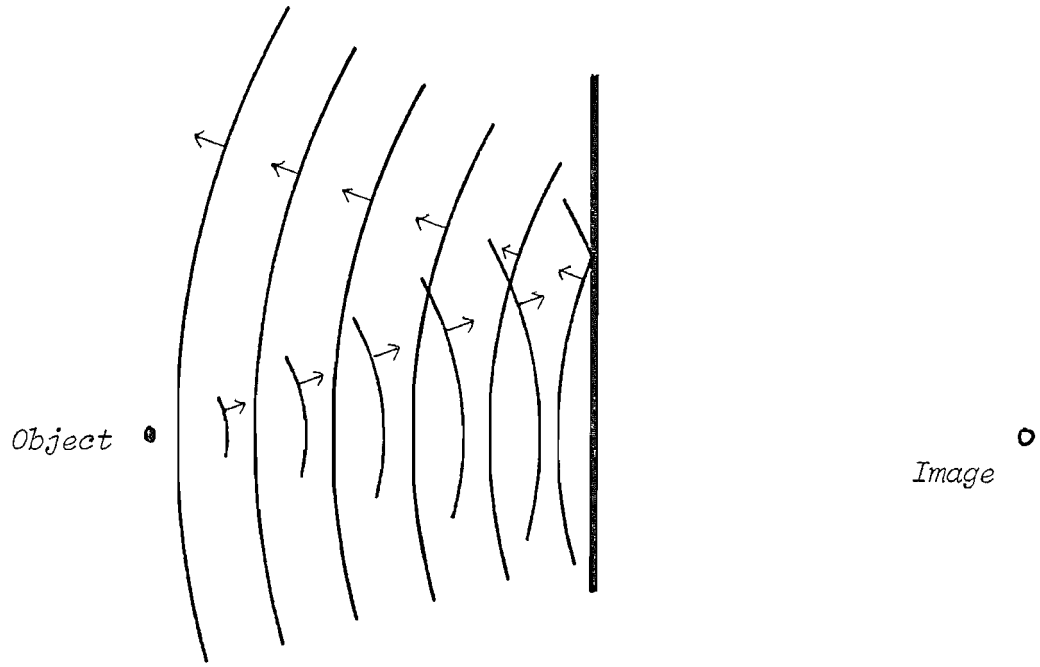

Figure 4.1(a) *Spherical waves reflected from a conventional mirror.*

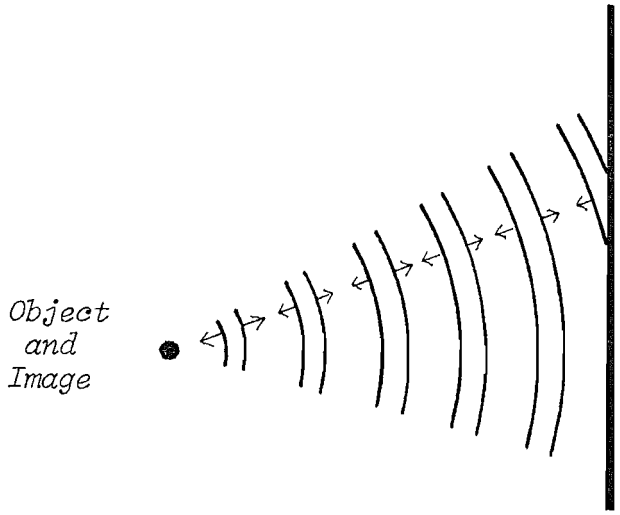

Figure 4.1(b) *Spherical waves reflected from a phase conjugate mirror.*

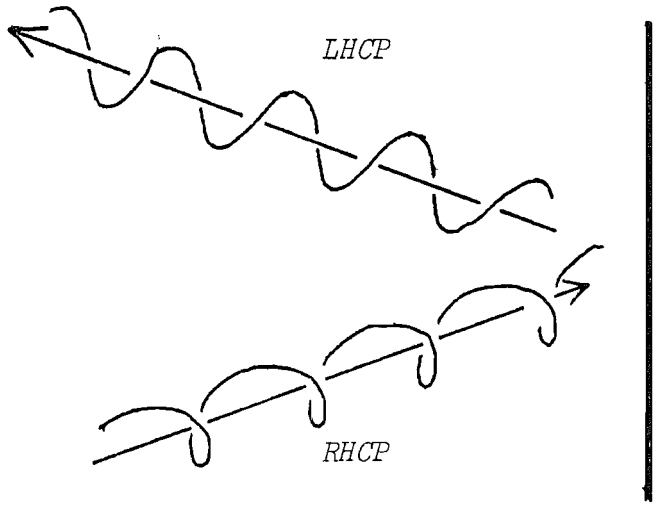

Figure 4.2(a) *Reflection of circularly polarized light from a conventional mirror.*

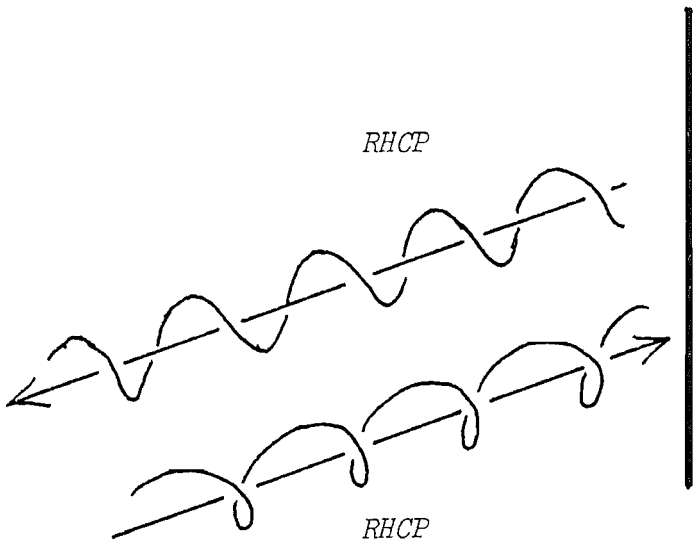

Figure 4.2(b) *Reflection of circularly polarized light from a phase conjugate mirror.*

(b)), the reflected beam, like the input, would also be right hand circularly polarized.

We have assumed above that the medium through which the beams propogate is linear and lossless. If this is the case then the wavefront reversal properties of a phase conjugator can be used to compensate for optically induced phase distortions in the following manner.

Suppose that a high quality beam with, for example, a plane wavefront (1) in Figure 4.3. (a) is incident from the left upon a spatially dependent linear phase aberrator. After passing through the aberrator the wavefront is distorted (2). This distorted wavefront is time reversed by the PCM (3) and after passing back through the same aberrating medium the beam recovers its initial plane wavefront (4). For comparison (Figure 4.3. (b)) a similar arrangement is shown with a conventional plane mirror instead of a PCM. In this situation it can be seen that, after reflection from the mirror, the wavefront (5) is reversed from left to right when compared with that in diagram 3(a) (3), so that after the second pass through the aberrator the wavefront distortion is doubled in magnitude (6).

Similar arguments show that a polarization state may be restored after polarization "scrambling" in an aberrator. Additionally, if the system includes losses or, more significantly, gains with no transverse spatial variation, then the scheme can still restore the wavefront, its amplitude being either reduced or increased. Thus an obvious application of phase conjugation is to correct out the linear distortions of an optical amplifier by double-passing it using a PCM, and this arrangement forms the basis of the investigations and experiments described in this thesis.

Further applications of optical phase conjugation are described in Fisher, 1983, and numerous references therein, and Pepper, 1982, and include, in the spatial domain: compensated imaging, lensless imaging, spatial information processing, optical signal processing, interferometry; and in the temporal and frequency domain: frequency

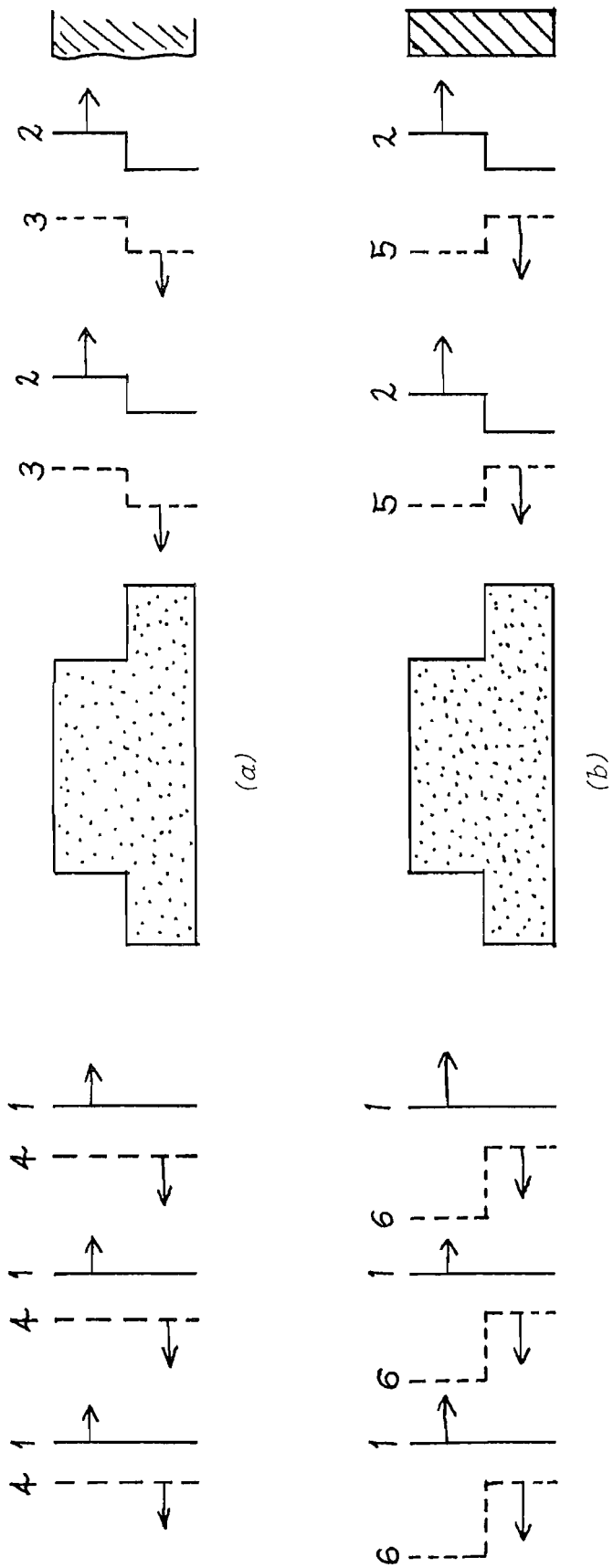

Figure 4.3 A phase conjugate mirror allows compensation of phase distortions (a), where a conventional mirror increases their effect (b).

filtering, temporal signal processing, optical bistability, laser spectrocopy, to name but some. We will concentrate on aberration compensation, but first we need to know something about the non-linear optical processes by which optical phase conjugation can occur.

4.2. Non-linear optics

We first state the standard equation for an electromagnetic wave in a homogeneous, nonmagnetic, nonconducting medium with no free charges:

$$\nabla^2 \underline{E} - \mu_0 \epsilon \frac{\partial^2 \underline{E}}{\partial t^2} = \mu_0 \frac{\partial^2 \underline{P}_{NL}}{\partial t^2} \qquad 4.3.$$

Here ϵ is set by the linear medium permittivity. In the absence of non-linear polarization, equation 4.3. becomes the standard wave equation where linearity implies that different waves present do not interact with one another. If there is a non-linear polarization, it appears as a driving term on the right of 4.3.. Because electric fields can create a non-linear polarization, and vice versa, coupling between different waves can occur in a non-linear medium.

Equation 4.3. can be reduced to a simpler first order equation by making a few approximations. Optical periods are so short, of the order of 10^{-15} s (1fs), that the pulse envelope amplitude changes little during an optical cycle. We write the non-linear polarization in the plane wave form:

$$P_{NL} = \tfrac{1}{2} \mathcal{P}(z,t) \exp[i(wt-kz)] + c.c. \qquad 4.4.$$

where w and k are also the frequency and wavevector of the electric field. $\mathcal{P}(z,t)$ describes the envelope function and the exponential function describes the fast optical variation in space and time. Similarly $\mathcal{E}(z,t)$ describes the envelope function of the electric field. The approximation described above (known as the slowly varying envelope approximation) may be written as:

$$\left| k^2 \mathcal{E} \right| \gg \left| k \frac{\partial \mathcal{E}}{\partial z} \right| \gg \left| \frac{\partial^2 \mathcal{E}}{\partial z^2} \right| \qquad 4.5.$$

and

$$\left|\omega^2 \mathcal{E}\right| \gg \left|\omega \frac{\partial \mathcal{E}}{\partial t}\right| \gg \left|\frac{\partial^2 \mathcal{E}}{\partial t^2}\right| \qquad 4.6.$$

Applying these to 4.3., multiplying by exp[i(wt-kz)] and integrating over one optical period leads to the linear equation:

$$\left(\frac{\partial}{\partial z} + \sqrt{\mu_o \epsilon}\,\frac{\partial}{\partial t}\right) \mathcal{E} = i \cdot \frac{\omega}{2} \cdot \sqrt{\frac{\mu_o}{\epsilon}} \cdot \mathcal{P} \qquad 4.7.$$

for a wave travelling in the positive z direction. For a wave travelling in the opposite direction the equation is:

$$\left(\frac{\partial}{\partial z} - \sqrt{\mu_o \epsilon}\,\frac{\partial}{\partial t}\right) \mathcal{E} = -i \cdot \frac{\omega}{2} \cdot \sqrt{\frac{\mu_o}{\epsilon}} \cdot \mathcal{P} \qquad 4.8.$$

If many plane electric fields are present, each travelling in arbitary direction, the total field has the form:

$$\underline{E}(\underline{r},t) = \frac{1}{2} \sum_i \mathcal{E}_i(\underline{r},t) \exp\left[i(\omega_i t - \underline{k}_i \cdot \underline{r})\right] + \text{c.c.} \qquad 4.9.$$

and the total non-linear polarization has a similar form. Each component i of the non-linear polarization couples to the corresponding component i of the electric field. The growth of an electric field at a particular frequency and wavevector $\underline{k}$ is determined only by the non-linear polarization with the same frequency and wavevector. Discovering what happens in a particular situation consists of finding the general non-linear polarization and then picking out the part with the appropriate frequency and wavevector. This is inserted into 4.7 or 4.8 to calculate the electric field generated.

The general non-linear polarization may be written in the form:

$$P(E) = E\chi(E) = \chi^{(1)}E + \chi^{(2)}E^2 + \chi^{(3)}E^3 + \ldots \qquad 4.10.$$

where E is the total field composed of waves of different frequency, wavevector and polarization. The susceptibilities $\chi^{(1)}$, $\chi^{(2)}$,

$\chi^{(3)}$ (and so on) describe linear effects (for example absorption or birefringence), second-order effects (for example frequency doubling) and third-order effects, respectively. Each order of χ can take a number of different values, one or more for each different combination of frequencies present in the medium, so is written as a function of the frequency w_i of the induced non-linear polarization and of the frequencies w_1, w_2 .... of the input waves, viz $\chi(w_i, w_1, w_2, \ldots)$. Of the many non-linear processes possible, three are especially useful for phase conjugation, all of which are third order effects. They are: stimulated Brillouin scattering, stimulated Raman scattering, and four-wave mixing. We will describe the latter two very briefly before going more deeply into stimulated Brillouin scattering.

4.2.1. Four wave mixing

In some media (referred to as Kerr media) the refractive index is linearly dependent upon the light intensity:

$$n = n_0 + n_2 \langle E^2 \rangle \qquad 4.11.$$

If several beams are present, they form an interference pattern of varying intensity, which in turn sets up a grating of varying refractive index. This grating can scatter beams into new directions or into each other. In particular consider the configuration of Figure 4.4, where two intense counter-propogating waves E_1 and E_2, of frequency w, pump a Kerr medium. It turns out (Yariv, 1978; Pepper, 1982 for example) that for this geometry any weak probe wave E_p also of frequency w incident on the medium is phase conjugated. Under the right conditions energy can be extracted from the pump waves so that the reflected phase conjugate wave is more intense than the input. Phase conjugation via four wave

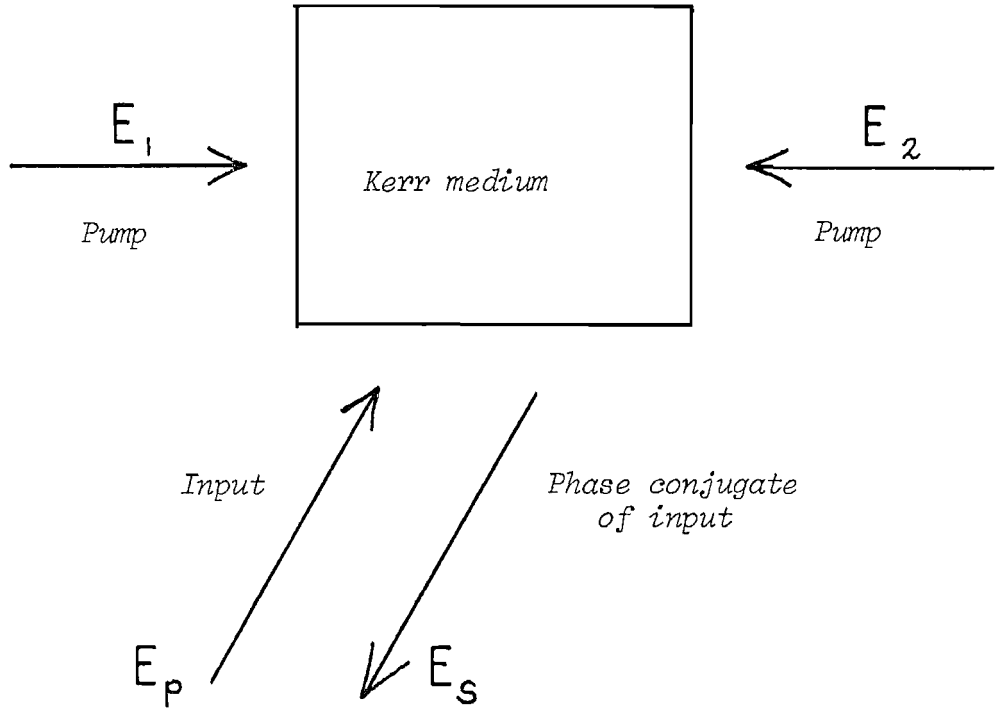

Figure 4.4 Phase conjugation via four-wave mixing.

mixing may be thought of as a form of holography, in which the phase grating created by the object and reference beams (E_1 and E_p in Figure 4.4) is "read" simultaneously by a second counter-propagation "readout" beam (E_2 in Figure 4.4), which scatters from the grating to give the image or phase-conjugate beam E_s.

4.2.2. Stimulated scattering

The stimulated Raman effect and the stimulated Brillouin effect have a number of similarities in that they are both inelastic scattering processes involving a transition between energy levels of the medium. The energy levels involved may be electronic, rotational or vibrational molecular levels (in Raman scattering), or they may correspond to bulk excitations such as optical phonons (in Raman scattering), or acoustic phonons (in Brillouin scattering). The spontaneous Raman process is illustrated in Figure 4.5 (a) in which an incident photon of frequency w_L excites the medium from the initial state $|a\rangle$ to an intermediate state in the vicinity of an excited state $|c\rangle$. The medium then decays to a different state $|b\rangle$ at an energy difference $\hbar\Omega$ above $|a\rangle$, and emits a photon at the reduced frequency $w_s = (w_L - \Omega)$. The medium gains energy at the expense of the photon energy. In the stimulated process (Figure 4.5 (b)) two waves with frequencies of w_L and w_s are simultaneously incident on the medium. The photon at w_L excites the medium to the intermediate state. The medium is then stimulated into emission by one of the photons at w_s, creating another photon at w_s. Because it is a stimulated process the new photon at w_s is identical to the photon stimulating the decay from state $|c\rangle$. Thus, the medium behaves as a gain medium

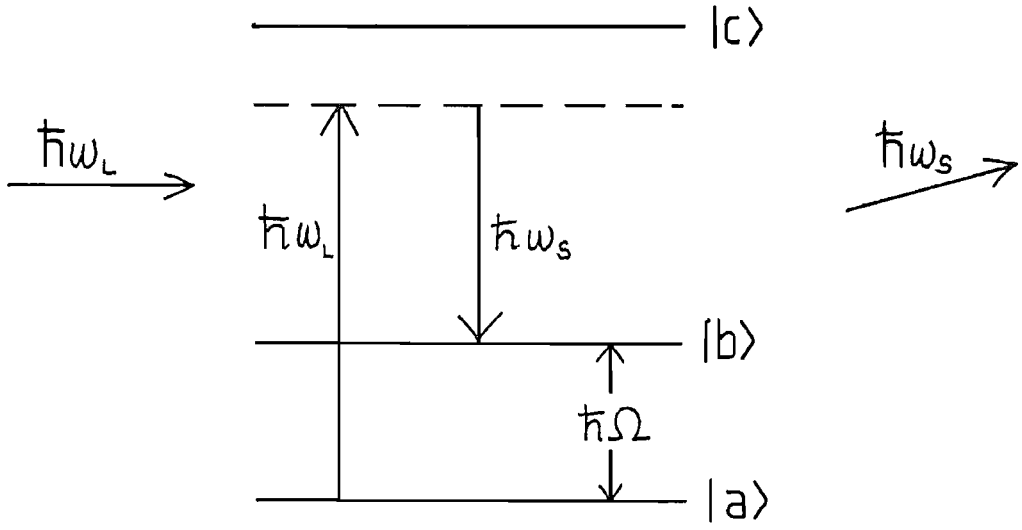

Figure 4.5(a) *The spontaneous Raman process.*

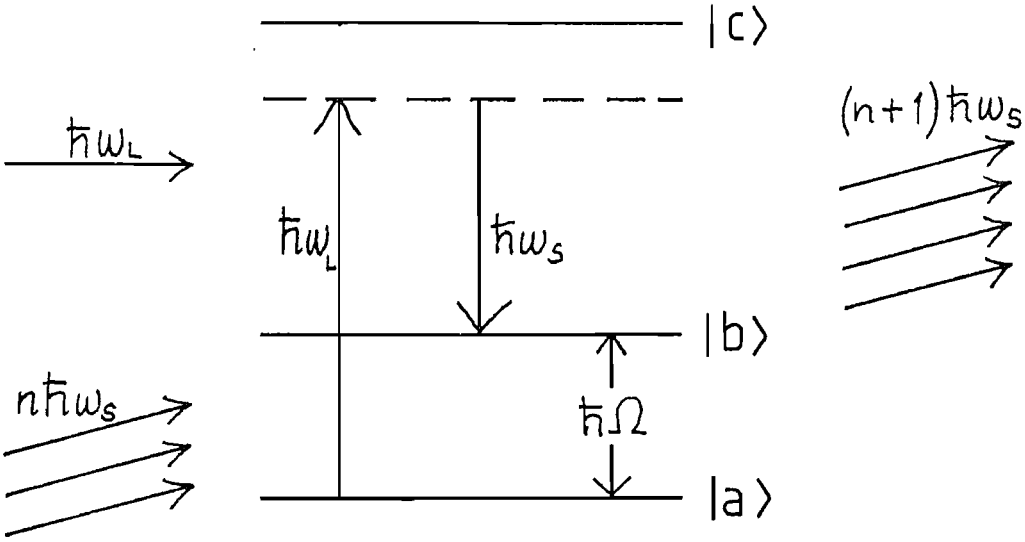

Figure 4.5(b) *The stimulated Raman process.*

for the beam at w_S pumped by the beam at w_L, and a weak beam at w_S will experience exponential gain as it travels through the medium. The wave at w_S is referred to as the Stokes wave and it can develop from spontaneous scattering, so that a laser pump beam incident alone on a Raman medium will generate it. The Stokes wave can propogate in either the forward or backward direction and it turns out that it has a spatial dependence which is the complex conjugate of that of the pump wave. This was not appreciated until long after the discovery of Raman scattering. Were it not for the different frequency of the Stokes wave, it would be the phase conjugate (equation 4.2) of the pump (equation 4.1). Unfortunately 'phase conjugation' via stimulated Raman scattering (SRS) is of little use in practice, because of the magnitude of the frequency shift Ω, which may be up to several tens of percent of the pump frequency w_L. Thus, even if the Stokes wave matches the pump in the interaction region, it will diffract and propogate differently outside. Phase conjugation via SRS is described by Sokolovskyaya et al (1978).

4.2.3. Stimulated Brillouin scattering

In stimulated Brillouin scattering the medium excitation is an acoustic phonon of energy $\hbar\Omega$. (In its most frequently encountered form, the excitation in Raman scattering consists of many isolated atomic or molecular transitions.) In a Brillouin medium there is an acousto-optic interaction between light waves and acoustic waves, which arises because the polarizability is a function of pressure - this is the basis of the electrostrictive effect. An acoustic wave is a pressure variation in the medium, causing a similar variation in the polarization. One or more electric waves can couple

to this polarization wave. If an input light wave is present, a scattered light wave and an acoustic wave coupling the two light waves can grow in intensity from noise at the expense of the input intensity. The interference between the input and scattered waves produces the sound wave (via electrostriction), which is effectively a moving grating, from which the input is scattered. A large fraction of the input may be transferred to the scattered wave this way.

The interaction may be thought of as the reflection of light from a moving Bragg mirror, the movement causing a Doppler shift of the light frequency. Because the speed of sound is of the order of 10^5 - 10^6 times less than that of light, the fractional frequency shift suffered by the light is very small, so its wavevector only changes by about 1 in 10^5 - 10^6, so $k_L \simeq k_S$. Thus the phonon energy is much less than the photon energy, so that $\Omega \ll w_L \simeq w_S$. It can be shown (see Yariv, 1975) that the gain is largest for the wave scattered in the backward direction, that is, opposite in direction to the input wave, in which case the frequency shift Δw is given by:

$$\Delta w = 2 w_L \cdot \frac{nv}{c} \qquad 4.12.$$

Δ w is typically of the order of 0.1 cm^{-1} ($\sim$ 5 GHz).

The phase conjugating property of SBS was demonstrated by Zel'dovich et al in 1972. (The peculiar focussing property of the reflected beam in SBS had been noticed in earlier experiments, but the full implications of this were not realized at the time.) They showed that the back-scattered wave that is the phase conjugate of the pump has a gain factor at least twice that of any other back-scattered wave. This assumes that the pump satisfies certain conditions, which we discuss a little

later on. Now a typical detector threshold level is when the noise signal intensity is amplified by a factor of $\exp(gIl) = \exp(30)$ where g is now the intensity gain coefficient. Thus, when the signal with maximum gain g_0 reaches threshold, any other signal will be at least a factor of $\exp(30)/\exp(7.5) = 10^9$ times weaker at this time. Thus, in SBS, only the phase conjugate of the input reaches any significant power.

4.3. Why is stimulated Brillouin scattering a useful mechanism for phase conjugation?

Probably the most attractive feature of SBS for phase conjugation is the simplicity of the process - the only input beam required is the beam to be phase conjugated. If this is not significantly aberrated it can be focussed simply, using a lens, into the SBS medium (otherwise a waveguide may be necessary, as will be explained later). No pump beams are required as in four-wave mixing. Because the frequency shift is so small (unlike that in SRS), the scattered wave frequency still lies well within the gain curve of most amplifying media, making double or multiple pass configurations a possibility. A further useful feature of SBS is that it occurs in liquids and gases where other undesirable non-linear effects such as SRS or self-focussing do not occur to an appreciable extent. The power handling capability of such media is very high, being limited only by the breakdown intensity. This makes the application of SBS to high power lasers very straightforward.

4.4. Theory of stimulated Brillouin scattering

A full theoretical treatment of SBS is so complex that to date analyses have had to incorporate various simplifying assumptions. Ideally, one would like to be able to predict what happens to both the reflectivity of the SBS mirror and the fidelity of phase

conjugation when changes occur in the SBS medium (gas pressure for example), in the input pulse (intensity, duration, temporal structure, linewidth, transverse spatial profile, polarization state) and in the interaction geometry (tight focussing conditions or guided). Theory exists in which one or several of these parameters are varied, while others are held constant, and we try below to give a general idea of what happens in the SBS process by referring to the work of several authors. Firstly, we show how the intensity threshold for SBS is calculated for a focussed pump beam, and discuss steady-state and transient scattering. The non-linear medium used in the majority of experiments described in this thesis was methane gas, so we apply this theory specifically to it. (The choice of methane is explained at the end of the Chapter.)

Steady-state and transient threshold

The parameter of most importance initially is the threshold pump power for SBS, since knowing it tells us whether a particular experiment will work at all. We calculated this from published data and found good agreement with experimental results. Under steady state conditions, defined by $(\Delta\nu_p)^{-1} \gg \tau_B$, where $\Delta\nu_p$ is the pump pulse bandwidth and τ_B the acoustic phonon lifetime, equation 4.7 simplifies to:

$$\frac{\partial \mathcal{E}}{\partial z} = i \frac{\omega}{2}\sqrt{\frac{\mu_o}{\epsilon}}\,\mathcal{P} \qquad 4.13.$$

The third order polarization induced at the Stokes frequency in a Raman or Brillouin medium is given by (see e.g. Bloembergen, 1967):

$$\mathcal{P}_s(\omega_s, \underline{k}_s) = \frac{3}{2}\epsilon_o \chi^{(3)} |\mathcal{E}_p|^2 |\mathcal{E}_s| \qquad 4.14.$$

where p now refers to the incident pump wave. Substitution of 4.14 into 4.13 gives an equation describing the exponential gain of the Stokes wave. A similar equation found by inserting the non-linear polarization at the pump frequency:

$$\mathcal{P}_p(\omega_p, \underline{k}_p) = \frac{3}{2}\epsilon_o \chi^{(3)} |\mathcal{E}_s|^2 |\mathcal{E}_p| \qquad 4.15.$$

into 4.14 describes the exponential decay of the pump wave as it traverses the non-linear medium. The two coupled equations can be solved simultaneously to allow for pump depletion (Von der Linde et al, 1969); Maier et al, 1969). However, up to the threshold condition pump depletion is negligible and so $\mathcal{E}_p(z) = \mathcal{E}_p(o) = \mathcal{E}_0$, a constant. In this case only the equation describing the growth of the Stokes wave is needed and becomes:

$$\frac{d\mathcal{E}_s(z)}{dz} = \frac{3i\omega_s}{4cn_s}\chi^{(3)}\mathcal{E}_o^2\mathcal{E}_s(z) \qquad 4.16.$$

This equation is integrated over the interaction length L (the pump enters the cell at z = L) to give the result:

$$\mathcal{E}_s(L) = \mathcal{E}_o \exp\left(\frac{3i\omega_s}{2\epsilon_o c^2 n_s n_p}\chi^{(3)} I_o L\right) \qquad 4.17.$$

where $\mathcal{E}_0$ is the noise amplitude at the start of the integration path and I_0 is the pump intensity. In terms of intensities we have:

$$I_s(L) = I_0 \exp(g I_0 L) \qquad 4.18.$$

where:

$$g = \frac{3\omega_s}{\epsilon_o c^2 n_s n_p} \cdot \chi^{(3)*} \qquad 4.19.$$

in which $\chi^{(3)*}$ is the imaginary part of the susceptibility. $\chi^{(3)*}$ must be found in terms of the material parameters and the result for the steady-state Brillouin gain coefficient is (Minck, Hagenlocker, Rado, 1967; Kaiser and Maier, 1972):

$$g_B = \frac{\omega_s \Delta\omega \tau_B}{2v^2 n^2 c^2 \rho}\left[\rho\frac{\partial\epsilon}{\partial\rho}\right]^2 = \frac{\omega^2 \tau_B}{c^3 n v \rho}\left[\rho\frac{\partial\epsilon}{\partial\rho}\right]^2 \qquad 4.20.$$

where v is the acoustic phonon velocity, ρ the density, $\frac{\partial\epsilon}{\partial\rho}$ the change in permittivity due to density change, $\Delta\omega$ the frequency shift (equation 4.12). Sometimes $v^2\rho$ is written as the bulk modulus.

Below we calculate values of τ_B and $\rho \frac{\partial \epsilon}{\partial \rho}$, and show that in methane under typical conditions τ_B can be of the same order as $(\Delta\nu_p)^{-1}$ so that a transient analysis is necessary. Many theoretical treatments of transient Raman and Brillouin scattering exist (see section 4.4.1). The results are usually expressed in the form of a transient gain coefficient G_T, which is a function of the steady state gain coefficient g_B:

$$G_T = 2\left(\frac{G_B t_p}{\tau_B}\right)^{1/2} - \frac{t_p}{\tau_B} \qquad 4.21.$$

where $G_B = g_B I_p L$ and t_p is the pump duration, so we still need to know the steady state gain coefficient. Again the threshold condition is $G_T = 30$.

The phonon lifetime in a gas may be expressed (see for example Damzen and Hutchinson, 1983) as:

$$\tau_B = \frac{\rho}{4 k_L^2 \left[\eta(T) + K(T)\left(\frac{1}{C_v(T)} - \frac{1}{C_p(T)}\right)\right]} \qquad 4.22.$$

where η (T) is the viscosity, K(T) the thermal conductivity, C_p(T) and C_v(T) the specific heats at constant pressure and volume respectively. Notice that τ_B is proportional to pressure. Inserting the parameters for methane gives:

$$\tau_B(\text{ns}) = 0.313\ P(\text{Atm}) \qquad 4.23.$$

so that τ_B is roughly equal in duration to a typical 30 ns Q-switched pulse at a pressure of 100 atmospheres. Working at pressures much in excess of this is not experimentally convenient, so the transient theory must be used in the majority of situations.

An expression for $\rho \frac{\partial \epsilon}{\partial \rho}$ is found by differentiating the Clausius-Mosotti equation for non-polar gases with respect to the density ρ, giving:

$$\rho \left.\frac{\partial \epsilon}{\partial \rho}\right|_\rho = \epsilon_r - 1 \qquad 4.24.$$

which for methane is $(\epsilon_r - 1) = 8.54 \times 10^{-4}$ at STP. $(\epsilon_r - 1)$ is proportional to pressure, and it is this term which gives the P^2 dependence of the steady state Brillouin gain. By relating pressure to density using the Ideal Gas Law and inserting the relevant parameters into 4.20 we find:

$$g_B(P) = 9.09 \times 10^{-6} P \text{ (atm)} \quad \text{cm/MW} \qquad 4.25.$$

Before we can use equations 4.25 and 4.21 to predict threshold powers we need to take account of the fact that, in many experiments, the input beam is not a plane wave, but is a focussed Gaussian beam from a TEMoo laser. Cotter et al (1975) performed a calculation which showed that the threshold pump power in this situation is:

$$P_{p,th} = \frac{\lambda_p}{4 g_B} \left[1 + \left(1 + \frac{30}{\tan^{-1}(L/b_p)}\right)^{1/2}\right]^2 \qquad 4.26.$$

where the beam is focussed with a confocal parameter b_p to the centre of a medium of length L, and it has been assumed that $k_s \simeq k_p$, $w_p \simeq w_s$.

Trutna and Byer (1980) derive a slightly different expression:

$$P_{p,th} = \frac{15\,\lambda_p}{g_B \tan^{-1}(L/b_p)} \qquad 4.27.$$

Now equations 4.26 and 4.27 predict the steady state threshold, but as mentioned above the transient threshold is often required. Inserting the expression for the transient gain coefficient G_T, (equation 4.21) into 4.26 and 4.27 they become:

$$P_{p,th} = \frac{\lambda_p}{4 g_B} \left\{1 + \left[1 + \frac{\tau_B}{4 t_p \tan^{-1}(L/b_p)} \left(30 + \frac{t_p}{\tau_B}\right)^2\right]^{1/2}\right\}^2 \qquad 4.28$$

and

$$P_{p,th} = \frac{\lambda_p \tau_B (30 + t_p/\tau_B)^2}{8 g_B t_p \tan^{-1}(L/b_p)} \qquad 4.29.$$

respectively.

In a typical experiment, as described later, the relevant parameters are t_p = 30 ns, λ_p = 1.06 μm, the gas cell length L = 1m, b_p =

0.13m. In Figure 4.6 equations 4.26, 4.28 and 4.29 have been used to calculate the SBS threshold as a function of gas pressure for this experiment. In Chapter 5 we compare the experimental results with these curves. We note that at the higher pressures up to 50 atmospheres, the power requirement to reach threshold is really quite modest, representing an energy of ~ 15 mJ in a 30 ns pulse. Although at these higher pressures the process becomes more transient ($\Upsilon_B = 0.313$ P), this is offset by the fact that $g_B \propto P^2$.

It is not possible to achieve significant reductions in threshold by varying the focussing conditions because the best one can do is to make $\arctan\left(\frac{L}{b_p}\right) = \frac{\pi}{2}$ in equation 4.28.

However, the important point is that, with the laser used in the experiments, there is enough energy, especially after a single pass through an amplifier, to comfortably exceed threshold.

In the sections below we review some of the work in which the effects of the parameters of the input pulse upon the SBS process have been investigated.

4.5. The effect of input pulse parameters on SBS

4.5.1. Power

In 1967 Hagenlocker, Minck and Rado measured the Brillouin gain coefficients in nitrogen as a function of phonon lifetime, and the Stokes power as a function of ruby laser power, finding that their results agreed well with a transient analysis using a modified gain coefficient of the form of equation 4.21 (see Kroll (1965)). They measured the gain coefficients by measuring the threshold power for SBS. They concluded that transient conditions must be considered even when the phonon lifetimes are two or three orders of magnitude

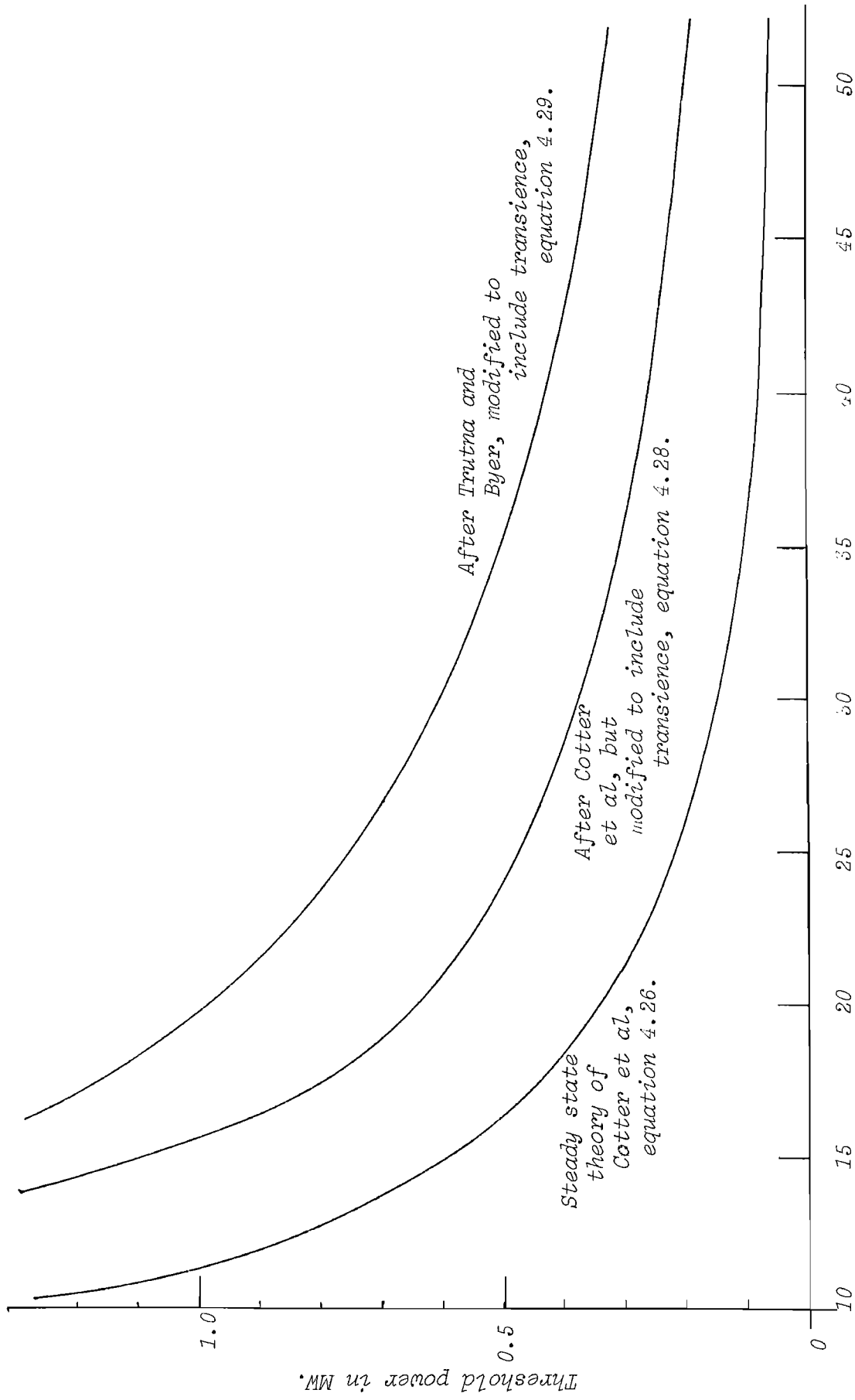

Figure 4.6 Threshold power versus gas pressure for stimulated Brillouin scattering in methane, using the theories indicated.

less than the pulse duration of the laser, a conclusion which Maier did not reach the following year.

The effect of the input laser power upon the reflectivity of the SBS mirror was investigated by Maier in 1968. He measured the back-scattered Brillouin power for Q-switched ruby laser light focussed in CS_2, n-hexane and ethyl ether and successfully applied a steady state theory to his results by solving the coupled wave equations 4.13 and allowing for pump depletion.

For these liquids the phonon lifetimes are 16 ns, 4.5 ns and 3.5 ns respectively, suggesting that a transient theory might have been necessary. A typical result for CS_2 was that, above threshold, the Brillouin power depended linearly upon the laser power and was proportional to it, minus a roughly constant amount. Thus, well above threshold, the reflectivity was almost independent of input power. Maier observed that after the SBS process had begun, the Brillouin pulse shape closely followed the incident pulse shape, and that this was so, even when structure down to 2 ns in length appeared on the laser pulse due to mode beating.

The apparent discrepancy between the findings of Hogenlocker et al and Maier was cleared up in 1971, when Maier and Renner found that, for low conversion efficiency (as in threshold measurements), a transient theory is necessary; whereas in the saturation régime, where the conversion effiency is high, a quasi-steady-state is reached which can be described with steady-state theory. If $\Gamma = 1/\tau_B$ is the Brillouin linewidth, then in the <u>low</u> conversion regime there are two regions of transient stimulated scattering:

(i) for $10 < \Gamma t_p < 100$ the maximum gain is reduced only slightly.

(ii) for $\Gamma t_p < 10$ a strong reduction of gain occurs.

If the laser power is high - how high above threshold one needs to be is a question which still needs to be answered - then a transient onset of SBS occurs with a rapidly rising Brillouin pulse edge, after which the Brillouin pulse closely follows the shape of the input pulse, indicating that a quasi-steady state is reached in the saturation region. The higher the laser power, the less time is taken to reach the saturation steady state.

This change in the transient Stokes gain as the laser power increases is explained in a theoretical paper on SRS by Wang (1969). Once threshold is reached, an abrupt increase in the transient gain can occur, leading to efficient conversion of a high intensity pump into the Stokes wave.

Having seen how the power efficiency of SBS depends upon the incident laser power, one would like to know how the fidelity of phase conjugation depends upon this parameter. Basov et al (1979)(α) carried out a very qualitative experiment in which they observed the phase conjugate of the focussed beam from a Nd:glass laser scattered by acetone or carbon tetrachloride, finding that just above threshold the wavefront reversal was almost perfect, but that as the laser power increased the fidelity of conjugation deteriorated.

Kochemasov and Nikolaev (1979) calculated the fidelity of phase conjugation for steady state SRS and SBS in a waveguide and showed that, as the back-scattering reflection coefficient increases, (which it does as threshold is exceeded by greater amounts until complete saturation occurs), the better the phase conjugation. Similar results were obtained by Zel'dovich and Shkunov (1977), by Baranova et al (1978) and by Mays and Lysiak (1980), all experimentally.

Lehmberg (1982), in an interesting and informative paper, describes a numerical calculation which models the phase conjugation of a focussed aberrated beam, including the effect of pump depletion. He too found that pump depletion improved the fidelity, which improved monotonically with reflectivity. He also compared the near and far-field beam profiles.

In several papers (e.g. Baranova and Zel'dovich 1978, Lehmberg and Holder, 1980) spatial gain narrowing is mentioned, this being the tendency of a focussed pump wave to enhance the back-scattered radiation in the stronger central part of its intensity distribution. This appears to be the main cause of inexact phase conjugation in focussed experiments. This is one reason why sometimes a waveguide geometry is preferred which mixes the stronger and weaker parts of the beam. However, if the back-scattered Stokes wave saturates the pump, the Stokes wave receives more gain in the wings, where the saturation is less than in the centre, and this can compensate for spatial gain narrowing.

Dolgopolov et al (1979) noticed three regimes of SBS phase conjugation dependent upon the laser intensity when they examined the quality of wavefront reversal of a

focussed aberrated beam with transverse intensity variations. At input power levels just above threshold, only the more intense parts of the beam were phase conjugated, the weaker parts being below threshold for SBS. Thus a Gaussian beam with a small amount of energy in modes other than TEMoo returned as a purer Gaussian, because the higher order modes were not conjugated. At higher pumping levels (2-4 times threshold) the fidelity improved because the weaker parts of the beam then contained enough energy to exceed the SBS threshold. At still higher pumping levels ($>$ 4 times threshold) saturation effects became apparent, reducing the gain for the more intense parts of the beam and reducing the fidelity. In these experiments an excimer laser pumped the gain medium, which was compressed nitrogen.

4.5.2. Linewidth

We now consider the effect of the laser linewidth - and therefore also the detailed temporal structure of the laser pulse - upon the SBS phase conjugation process. We have already referenced work where the régimes for steady state or transient scattering theory are investigated, in which the pulse duration is compared to the phonon lifetime, but there are several papers in which the effect of a non-bandwidth limited pulse is taken into account.

Several papers have been written on the effect of laser linewidth on SRS (e.g. Carman et al, 1970), Akhmanov et al, 1971, Grasyuk et al, 1972), which are also applicable to SBS experiments. Akhmanov et al (1974) drew some interesting conclusions in his paper on SRS (and SBS) stimulated by a broadband focussed pump, as follow.

The SBS gain with a noisy pump is the same as that for a monochromatic pump of the same mean intensity I_p, provided that the length of the gain medium, $30/g_B I_p$, over which an e^{30}-fold Stokes growth occurs is much less than the coherence length $L_{coh} = c/\Delta\nu_p$ of the pump. For a focussed beam with confocal parameter b_p, this requirement is supplemented by the need to keep the effective length of gain medium, which is b_p, less than the coherence length of the laser, $b_p < L_{coh}$. If this condition is relaxed, then an increase in the required threshold power is seen, because the effective length of gain medium is limited by the coherence length of the laser, instead of the physical length of the interaction region. Nevertheless, what is still unclear is what effect this has when one operates at power levels well above threshold, and how far above threshold it is necessary to go to obtain good reflectivity and fidelity of phase conjugation.

A further point arises when conjugation of a narrow linewidth laser, such as a single mode laser, is considered, and it is desired that the conjugated wave is also of narrow linewidth. In this situation one needs to know how much broadening, if any, arises from the process.

4.5.3. Transverse spatial profile

For our purposes the usefulness of phase conjugation lies in its ability to reverse the wavefront of a spatially distorted laser beam, so perhaps the most important questions to ask are what are the limits on beam aberration that can be corrected and how does the fidelity depend upon the degree of aberration? Clearly, a beam could be so severely aberrated that it would be

impossible to get all of it into the phase conjugator. On the other hand it is quite possible, as we mentioned with regard to spatial gain narrowing, for an "ideal" Gaussian input to be incorrectly conjugated.

Zel'dovich et al (1972) argued that perfect phase conjugation can only occur if the spatial intensity of the pump wave shows considerable transverse modulation. If the pump wave has an irregular local divergence θ_0, then the characteristic transverse dimension of the inhomogeneity is of order $\Delta r_\perp \simeq (k\theta_0)^{-1}$ and the characteristic length in the direction of beam propagation is $\Delta z \simeq (k\theta_0^2)$ (see Fisher, 1983). These dimensions must be much smaller than the interaction region for good wavefront reversal. The effective gain coefficient g_{eff} for the scattered wave $\mathcal{E}_s(\underline{r},z)$ is given by the intensity overlap integral:

$$g_{eff.} = \frac{\int G \left|\mathcal{E}_0(\underline{r},z)\right|^2 \left|\mathcal{E}_s(\underline{r},z)\right|^2 d^2\underline{r}}{\int \left|\mathcal{E}_s(\underline{r},z)\right|^2 d^2\underline{r}} \qquad 4.30.$$

where G = const, $\mathcal{E}_0(\underline{r},z)$ is the pump amplitude. A scattered wave $\mathcal{E}_s$ whose profile $\left|\mathcal{E}_s(\underline{r},z)\right| = \text{const}\left|\mathcal{E}_0(\underline{r},z)\right|$ has a gain roughly twice that of any other scattered wave that does not correlate with $\mathcal{E}_0(r,z)$. As mentioned earlier in this Chapter, this implies an intensity ratio of at least 10^9 between the conjugate wave at threshold and any non-conjugate wave. This does seem rather a stringent criterion to define good phase conjugation and once again the question is raised of how much this condition can be relaxed in an experiment without the loss of satisfactory phase conjugation. Both Sidorovich (1976) and Zel'dovich and Shkunov (1978)(a) showed in theoretical papers that the necessary condition for the existence of a phase conjugate wave is weak amplification over the longitudinal length of inhomogeneities:

$$g\,\Delta z \equiv \frac{g}{k\theta_0^2} \leqslant 1 \qquad 4.31.$$

Because the threshold condition is 2gL = 30, this can be written as:

$$\frac{L}{\Delta z} \geqslant 15 \qquad 4.32.$$

However, it is not clear how poor the phase conjugation is when this condition is not satisfied.

Hellwarth (1978) calculated the fidelity of conjugation when scattering is stimulated in a waveguide by a steady state, multimode, monochromatic beam, and also for the case of a focussed beam. Pump depletion was not taken into account. He found that, in his model, even for the worst possible transverse intensity distribution in the waveguide (the distribution giving the poorest fidelity), less than 8% of the back-scattered energy was 'lost', i.e. not phase conjugated. As a result he suggested that the conditions above, as stated by previous workers, were too restrictive.

In the paper already mentioned by Lehmberg (1982) a numerical study of phase conjugation in stimulated back-scattering with pump depletion indicated that the fidelity of conjugation can be lower than this, however no conditions on the transverse intensity modulation of the beam were looked for.

The effect on threshold of a focussed aberrated beam, compared to a Gaussian beam, can be estimated by considering its intensity-length product IL. In Appendix II we show that for a beam which is M times diffraction limited this is given approximately by:

$$IL \sim \frac{2P}{\lambda M} \qquad 4.33.$$

where P is the power. Since the phase conjugate of the aberrated beam experiences a gain roughly twice that of the conjugate of a single spatial mode (Hellwarth, 1978), the threshold is increased by a factor of roughly $\frac{M}{2}$. If the increase in threshold is great enough to inhibit the process of phase conjugation, the intensity-length product can be increased by confining the transverse dimensions of the beam in a waveguide. In this case we can show (Appendix II) that the intensity-length product is approximately given by:

$$IL \simeq \frac{4PL}{\pi D^2} \qquad 4.34.$$

where L is the length of the guide and D its diameter. We have assumed that the losses are negligible. Waveguiding also has the advantage that the weak parts of the beam are mixed with the strong and are phase conjugated, even when in a tight focussing geometry they may be too weak to reach threshold.

4.5.4. An aside - Four-wave Brillouin mixing

The interesting phenomenon of the phase conjugation of a weak signal (with power below threshold for SBS) in the presence of a strong signal was described by Basov et al (1979) **(b)**. They extended the theory of Sidorovich (1976) to include a pump wave with two components, one strong and one weak, and showed that reflection of the weak wave should be as efficient as the strong wave. They verified this experimentally using radiation from a neodymium laser in a waveguide. In fact the arrangement is a form of four-wave mixing, as described in section 4.2.2. (see Figure 4.4.) in which the pump waves are the strong beam and its phase conjugate propogating in the opposite direction and the probe wave E_p is the weak

beam. Pilipetskii et al (1979, two papers) measured how weak the weak beam can be in such an arrangement and still be conjugated, and found that even a beam of power 3W was conjugated. This was a power 10^6 times smaller than the strong beam. Efimkov et al (1979) and Gyulamiryan et al (1981) carried out experiments in which the strong beam had a relatively long duration compared to the phonon lifetime (so steady-state theory applied to it), while the weak beam had a pulse duration roughly equal to the phonon lifetime (transient), and obtained satisfactory phase conjugation of the weak beam though the process was less efficient in terms of reflectivity than with a longer weak pulse. This technique of four-wave Brillouin mixing is potentially valuable in the light of what follows regarding the phase conjugation of a depolarised beam.

4.5.5. Polarization

At the beginning of the Chapter it was stated that an 'ideal' phase conjugator conjugates the polarization state of the input beam as well as its wavefront. However, SBS is not an 'ideal' phase conjugator, not only because of the frequency shift of the conjugate beam relative to the input (albeit small), but also because the polarization state is not reversed. Thus, it is found experimentally that if a right hand circularly polarized beam is incident on an SBS conjugate mirror, the reflected beam is left hand circularly polarized, as it would be if it had been reflected from a conventional plane mirror. Unfortunately, however, the polarization state of the conjugate beam is not always like that of a beam reflected from a conventional mirror. For example, it may differ if the input has spatial variations in the polarization state over the cross section of the beam, as

is the case for a beam that has traversed a birefringent amplifier.

Zel'dovich and Shkunov (1978)(b) calculated how a depolarized pump is reproduced in stimulated scattering without pump depletion, and showed that the scattered wave effectively consists of three components (into which the input wave can be decomposed), each of different polarization state. Two of these components (the components linearly polarized perpendicular to each other) have gain coefficients which depend upon the pump polarization degree p defined by:

$$p = \frac{I_1 - I_2}{I_1 + I_2}$$

where I_1, I_2 are the intensities in these two components in the pump wave. The third component itself depends upon p, so in general the polarization state is not reproduced in the conjugate wave, but is only reproduced in special cases (e.g. unidirectional linear polarization across the whole of the input beam cross-section). Moreover, the three components are uncorrelated in phase so the polarization state of the conjugate wave can vary randomly. Blaschuk et al (1978) measured the wavefront reversal of a depolarized pump and partly agreed with the theory, showing that polarization distortion does occur. However, limits upon the possible degree of pump depolarization for a given polarization distortion of the reflected wave are not clear, especially for the case of saturation of the pump.

In 1978 Basov et al devised a scheme for phase conjugation of a depolarized pump, based on four-wave Brillouin mixing, noting that a uniformly linearly polarized pump suffers no distortion of polarization when it is conjugated. The pump, with a small amount of

depolarization, was separated into two beams, one strong and one weak, of orthogonal polarizations, using a birefringent wedge. One of these beams was then polarization-rotated by 90^{o} so that both beams had the same polarization. Thus, the initially depolarized beam was transformed into two beams with uniform polarization. These two beams were combined and phase conjugated together in a four-wave Brillouin mixing scheme in a light pipe. Being of uniform polarization, they suffered less polarization distortion and produced better fidelity of conjugation than the situation where they had orthogonal polarizations. However, the depolarization of the phase conjugate beam was not measured, so the performance of the scheme cannot be quantified.

4.6. Media for stimulated Brillouin scattering

Stimulated Brillouin scattering can in principle occur in any medium, solid, liquid or gas. In choosing a suitable medium it is obvious that a high Brillouin gain coefficient is of importance, but there are a number of other points to consider. Ideally it should also have low absorption at the laser wavelength, be free from other competing non-linear effects, have a high damage threshold (or breakdown) intensity, and be convenient to use.

Solids tend to be excluded from use with high power lasers, because they are liable to suffer from irreversible optically-induced damage.

Many liquids exhibit SBS, (Pine, 1966, Kaiser and Maier (1972), Wiggins et al, 1967). Unfortunately some of these suffer from self focussing and consequent breakdown, caused by an intensity dependent refractive index of the form of equation 4.11. One of these, CS_2, has one of the highest Brillouin gains found in liquids. ($\sim$ 0.13cm/MW at a wavelength of 6943Å). The problem of self focussing can be overcome in some cases by guiding the beam in a light pipe, but even

then the beam has to be focussed to some extent into the entrance of the light pipe. Some liquids are Raman active also. Most liquids are inefficient when used for SBS with Nd:YAG lasers, because they have absorption bands in the near infra-red which extend down to the laser wavelength of 1.06 μm. Two exceptions to this seem to be CS_2 and CCl_4, (Zubarev 1980). Even these, though, require precautions in their use, for unless bought as spectroscopic grade chemicals they contain impurities which do absorb at 1.06 μm; such impurities dissolve in them and are likely to be present in apparatus used to contain them (Dr. T. Gilson, personal communication).

Several gases possess high Brillouin gains, and methane emerges as the most convenient and efficient at 1.06 μm (see Pepper (1982), Hon (1982)). Other gases are discussed by Damzen and Hutchinson (1983), Wiggins et al (1966), and Minck et al (1967). Of these nitrogen has rather a low gain at moderate gas pressures (tens of atmospheres) and only gives high efficiency of reflection at a pressure of the order of two hundred atmospheres (Wiggins, 1966). Methane, on the other hand, has a relatively high gain at moderate pressures. Above ten atmospheres the Brillouin gain exceeds the Raman gain (for methane is Raman active also) for typical Q-switched pulse lengths ($\sim$ 30 ns). Other non-linear effects are negligible. Additionally methane is readily available and relatively cheap. These factors make it an excellent medium for phase conjugation via SBS and therefore it was chosen for the initial experiments, and subsequently further experiments described in the following Chapter.

To conclude this Chapter we remark that, despite the wealth of published work on SBS and its use as a phase conjugation mechanism, many of the details are not clearly understood. In particular the effect of the transverse spatial structure of the beam on conjugation fidelity has not been experimentally investigated carefully, expecially in the saturation régime; and since this is the situation in which the application of the process is most likely to be of use, is a question that needs to be answered. Likewise, with the present state of understanding, it is difficult to place limits on the

linewidth and polarization requirements of the aberrated beam, so that it is not a simple matter to predict whether, with a given laser, the process will work satisfactorily. In the next Chapter experiments are described in which the process was applied to a typical laboratory Nd:YAG laser.

CHAPTER 5

Experimental work on phase conjugation using a Nd:YAG oscillator/amplifier

In this Chapter we describe firstly (Section 5.1) a two-pass amplifier arrangement in which a conventional plane mirror was used to double pass the amplifier and a similar set-up incorporating a phase conjugate mirror instead. In Sections 5.2. the measurements carried out are described, the results of which (Section 5.3.) enable a comparison to be made of the two systems, and which also quantify the performance of the phase conjugator.

In Sections 5.4. a four-pass amplifier configuration utilizing a phase conjugator is described, the aim being to extract more energy from the amplifier than with the two-pass arrangement.

In Section 5.5. a two-pass system is described, incorporating depolarization compensation based on the four-wave Brillouin mixing schemes mentioned in Section 4.5.4. of the previous Chapter.

5.1. Two-pass amplifier scheme

5.1.1. The basic experiment

The experimental two-pass amplifier arrangement is shown in Figure 5.1. The output from the oscillator, which will be described in Section 5.1.2. was plane polarized in the plane of the diagram. We will henceforth refer to this as horizontal polarization. The beam was expanded and passed through a dielectric polarizer before traversing the amplifier, which was doubled passed using either a conventional plane 100% mirror or the phase conjugator. The beam was extracted (and isolated

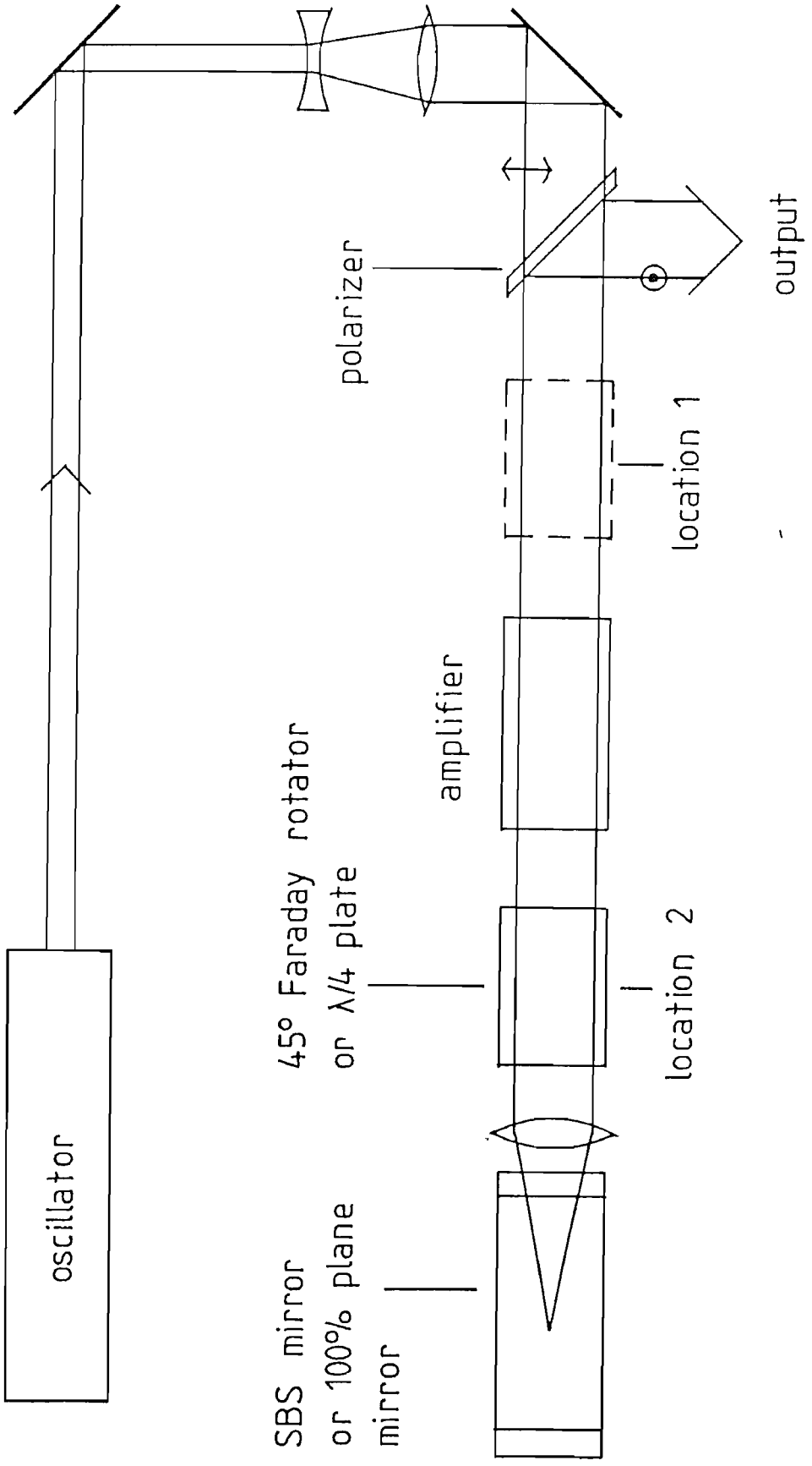

Figure 5.1 The two-pass amplifier arrangement

from the oscillator) after the double pass by rotating the plane of polarization of the beam by a total of 90^{o} before it returned to the polarizer, so that it was reflected off the polarizer as output.

Using a conventional mirror and assuming that there are no depolarizing elements between the polarizer and mirror, this 90^{o} rotation can be accomplished most simply using a suitably orientated quarter wave plate at location 1 or 2 in Figure 5.1. However, as we saw in Chapter 3, the amplifier rod itself suffers from thermally induced birefringence which is non-uniform over the rod cross-section, so one cannot expect perfect beam extraction and isolation. An alternative to the quarter wave plate is a Faraday rotator inducing 45^{o} of polarization rotation for each pass. If it is placed at location 2 after the first pass of the amplifier, it can in principle provide complete compensation for the birefringence of the amplifier when a conventional mirror is used. We shall explain this further in Section 5.2.4. If the plane mirror is replaced with a phase conjugator however, the phase conjugator may distort the polarization state of the beam if the polarization state is not uniform over the cross section of the beam, as was mentioned in Chapter 4 (Section 4.4.5.). Thus, one might expect imperfect depolarization correction when a Faraday rotator is used in conjunction with an SBS phase conjugate mirror. Both a quarter wave plate and a Faraday rotator were used separately at location 2 in the experiments, to enable a comparison to be made.

5.1.2. The oscillator

The oscillator incorporated a telescopic resonator and mode selection elements and electronics as described in

Chapter 2 (see Figure 2.14.). The Nd:YAG rod size was 3" x 1/4", the telescope had a magnification of 3, consisting of 15cm and -5cm lenses, and the spacing bewtween the telescope and output coupler was 35cm. The output coupler was a 6mm uncoated resonant reflector and was used together with a tilted 10mm intracavity etalon of face reflectivities 72%, and pre-lase Q-switching, to give single mode operation. The beat detection circuit was also used for continuous single mode shot operation when required. The laser linewidth could be increased if necessary by removing the etalon and/or using fast Q-switching instead of pre-lase Q-switching. These cases were chosen for the examples on linewidth calculations used in Chapter 2 and are summarised with the results calculated from equations 2.51 and 2.52 in Table 5.1.

This oscillator produced up to 100 mJ of TEMoo mode energy in a 30 ns pulse.

5.1.3. The methane gas cell

The phase conjugator consisted of a gas cell filled with methane at pressures of up to 50 atmospheres and is shown in Figure 5.2. The main structure of the cell was made of a length of 'Aminco' tubing with an 'Aminco' 'T' piece at each end, all of stainless steel. The side port of one 'T' piece was used to mount a Psika pressure gauge reading up to 70 atmospheres, and a Hoke gas tap was fitted to the other 'T' piece. The cell could thereby be filled using a remote gas handling system and be a portable self-contained unit during experimental work. The enlarged part of Figure 5.2. shows how windows were fitted to the cell. These were manufactured from spectrosil B by I.C. Optical Systems Ltd., with

TABLE 5.1.

The calculated oscillator linewidth

(A tick indicates the mode selection or Q-switching method used)

6mm resonant reflector	10mm 72/72% etalon	Pre-lase Q-switching	Fast Q-switching	Linewidth	
				cm^{-1}	MHz
✓	✓	✓		0.0015	45
✓	✓		✓	0.007	210
✓		✓		0.013	390
✓			✓	0.058	1740

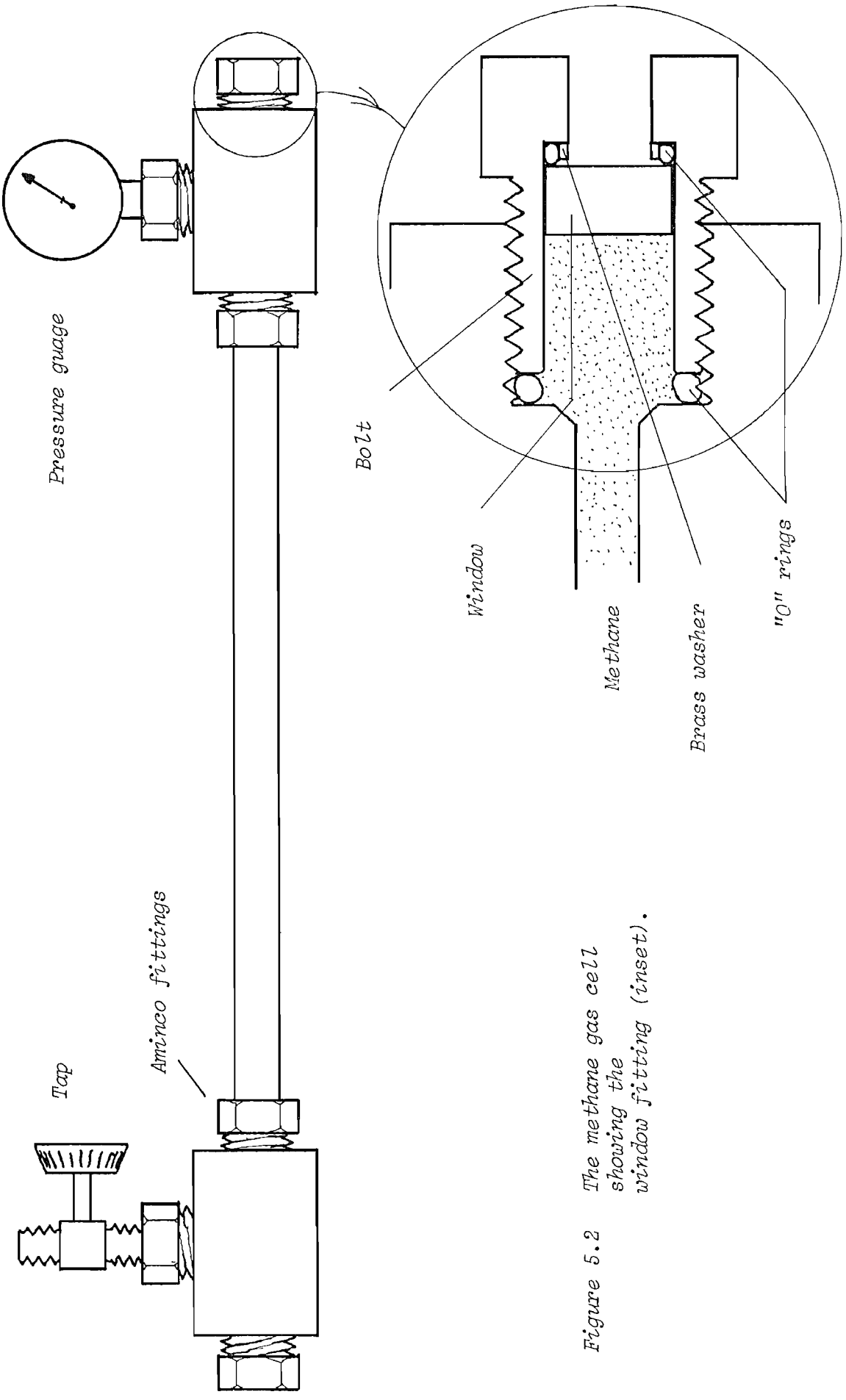

Figure 5.2 The methane gas cell showing the window fitting (inset).

dimensions of 12.5mm thick by 21mm in diameter. The window surfaces were wedged at an angle of 5 minutes to prevent etalon effects, and polished flat to $\lambda/4$. This diameter fitted snuggly inside a standard Aminco bolt, which screwed into the 'T' piece. Inside the bolt there was a convenient lip on which a closely fitting O ring could sit to provide a gas seal between the window and bolt. The pressure inside the cell forced the window against the O ring, improving the seal as the pressure increased. It was initially found that, at a pressure of around 20 atmospheres, the O ring would suddenly deform inwards towards the bolt axis, releasing the gas. This problem was tackled by machining a simple brass washer slightly smaller than the O ring, to provide support for it on the inside surface, subsequently no further 'blow outs' occurred. Another O ring was placed inside the 'T' piece as shown, to provide a seal between it and the bolt - a gas tight seal was easily made simply by screwing the bolt down onto the O ring. The total length of the cell was approximately 1m, the plan being to focus the beam to a waist at the cell centre using a 50cm focal length lens. It was a simple matter to reduce or increase the length by inserting tubes of different length. The effective aperture of the cell was 7mm.

5.1.4. Setting up the experiment

In order to extract as much energy as possible from the amplifier, it is necessary to fill the amplifier rod with the beam for both passes. The amplifier rod had a diameter of 9mm, so the appropriate spot size for the beam was ~ 3mm. Double passing the amplifier with a plane mirror implied that there should be a beam waist at the mirror, so that the beams travelling in each

direction through the amplifier both filled it by the same amount. In fact, a spot size of 3mm gives a divergence angle of $\theta = \lambda/\pi w_0 \simeq 0.1$ mrad, so the spot size changed negligibly over the length of the experiment, and an essentially parallel input filled the rod on both passes. Use of a computer programme enabled spot sizes to be quickly calculated at any point in the experiment, and it was found that placing a x 2 beam expansion telescope 1.5m from the oscillator output would give a ~ 3mm spot size over the length of the amplifier and Faraday rotator. This telescope was made using a + 20cm and -10cm lens, one of which was mounted on a translation stage, so that the telescope could be accurately focussed to give the correct spot size in the amplifier.

The spot size at the entrance window of the methane cell was kept as large as possible, to minimise the possibility of damage, but was limited by the internal diameter of the 'T' piece to a value of ~ 2mm. This spot size was attained by using a x 1.7 beam reducing telescope after the Faraday rotator, followed by a space of 30cm, the 50cm focussing lens being placed close to the cell window. The calculated spot sizes at the optical components are given in Table 5.2. Typical energy inputs to the cell were 200 mJ, giving a mean power density of 50MW cm^{-2} on the cell window, well below the damage threshold of spectrosil B. The optical components were aligned initially using a helium-neon laser, fixed behind the oscillator so that the two laser beams - HeNe and Nd:YAG - were collinear. Alignment was completed with the laser running. The spot size before and after the amplifier and Faraday rotator could be conveniently measured as the beam expanding telescope was being adjusted by using a diode array and oscilloscope to display the beam profile.

TABLE 5.2.

Calculated spot sizes at various locations in the two-pass amplifier

Position	Distance from oscillator output, m	Spot-size w, mm
Oscillator output	0	0.43
- 10 cm lens	1.5	1.26
20 cm lens	1.6	2.59
Amplifier	2.28	2.84
F.R.	2.69	3.00
15 cm lens	3.17	3.18
- 9 cm lens	3.23	1.93
50 cm lens	3.53	2.12
Focus in cell	4	0.15

The pulsed Faraday rotator was driven with a standard JK Lasers power supply and triggered from a pulse generator. The oscillator and amplifier power supplies were triggered from the Faraday rotator via a delay box, because it took the Faraday rotator some time (~ 1ms) to turn fully 'on'. The voltage (and therefore current) for 45^{o} of polarization rotation per pass of the Faraday rotator was set by double passing it with a plane mirror and measuring the amount of light passing back through the polarizer. Ideally this should have been zero. In practice, adjusting the voltage to the optimum value, 785V, resulted in only 0.25% of the light incident on the polarizer passing through it, the rest being reflected. The transmission of the Faraday rotator was measured to be 91% per pass.

SBS threshold

As stated in Chapter 4, a knowledge of the threshold power for SBS is useful. This was measured at pressures of up to 30 atmospheres by Berry (1983) and repeated here up to 50 atmospheres , both for a single longitudinal mode and a multimode pump. For the multimode case the oscillator was run fast Q-switched, with a 6mm resonant reflector as the only mode selection, giving a linewidth of 0.058 cm^{-1} or ~ 1700 MHz (Table 5.1). The input energy to the cell was varied using a two-plate beam attenuator.

Threshold was measured by observing the back-scattered light reflected from a beam splitter in the input beam onto a phosphor card, this signal appearing when threshold was reached. The results are shown in Figure 5.3, together with theoretical curves calculated from the analysis of Cotter et al (equation 4.28) and Trutna and

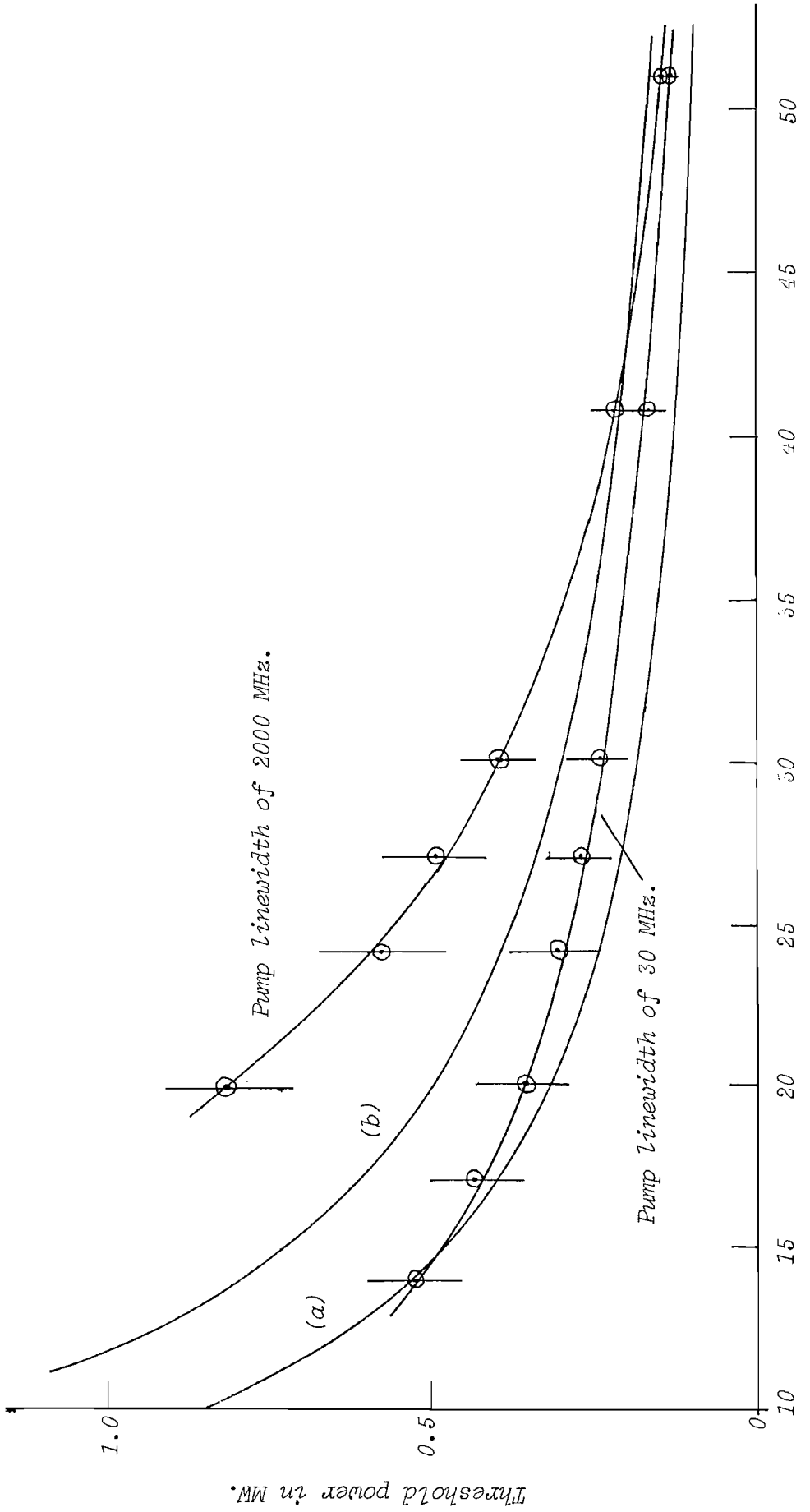

Figure 5.3 *Experimentally measured threshold powers for stimulated Brillouin scattering in methane. The theoretical curves are based on equation 4.28 (curve (a)) after Cotter et al, and on equation 4.29 (curve (b)), after Trutna and Byer, in each case modified to include transience, and for the 30 MHz linewidth only.*

Byer (equation 4.29), in each case adapted to include transience. An interesting result is the convergence of the two curves for the broad and narrow linewidths as the pressure increases. Thus, at 22 atmospheres, there is a factor of 2 between the thresholds, while at 50 atmospheres the factor is reduced to 1.3. This can be explained qualitatively as follows. The gain length required to reach threshold, defined by $L = \frac{30}{gI}$, was 5cm at 30 atmospheres pressure for the single mode pump, the threshold power being 0.5 MW in a spot size of ~ 150 μm and the gain g = 0.008 cm/MW. At 50 atmospheres, when g = 0.023 cm/MW, the threshold power was 0.24 MW, giving a gain length of ~ 4cm for the single mode pump. Thus, the temporal structure of the broader linewidth pump is larger, relative to the threshold gain length, at 50 atmospheres than it is at 30 atmospheres. Hence, the higher the pressure, the closer the broader linewidth pulse is to steady state conditions, and the closer the threshold power is to that for the single mode pump.

5.2. Measurements made on the two-pass amplifier arrangement

The performances of the phase conjugator and of the two-pass amplifier, with and without phase conjugation, were quantified by making the following measurements.

5.2.1. Energy and Power

The output energy of the system was measured using a cone calorimeter. The output power was then deduced by photographing the pulse on a fast storage oscilliscope and measuring the duration. Pulse shapes were monitored using a vacuum photodiode with a rise time of 100 ps.

5.2.2. Beam Divergence

Measurement of beam divergence required some care because a large spot size in the far field does not necessarily indicate that a beam is significantly worse than diffraction-limited. For example, if a pure Gaussian input to the amplifier were not exactly collimated and/or the amplifier rod possessed distortion in the form of pure spherical lensing, then the output, despite still being diffraction limited, could have a divergence quite different to that expected, assuming that there was a beam waist at the output. To avoid any uncertainty the output beam was deliberately focussed to form a waist (as in Figure 5.4.), the size of which was measured using the diode array. The array consisted of 128 photodiodes in a line 1cm long, allowing spot size measurements down to about $w = 0.4mm$. The beam divergence from this waist was then determined by measuring the spot size at some known distance many confocal parameters from the waist. The factor by which this divergence exceeded that calculated from the measured waist spot size (assuming a Gaussian beam) was the factor by which the output beam exceeded the diffraction limit.

5.2.3. Beam Quality

The transverse spatial quality of the beam was assessed at various distances from the output coupler using two techniques.

Firstly, the beam was allowed to fall on 'burn paper' - exposed and developed photographic paper. Although the burning is not necessarily a linear function of laser intensity, and cannot therefore give a straightforward reading of the absolute value of intensity at any point,

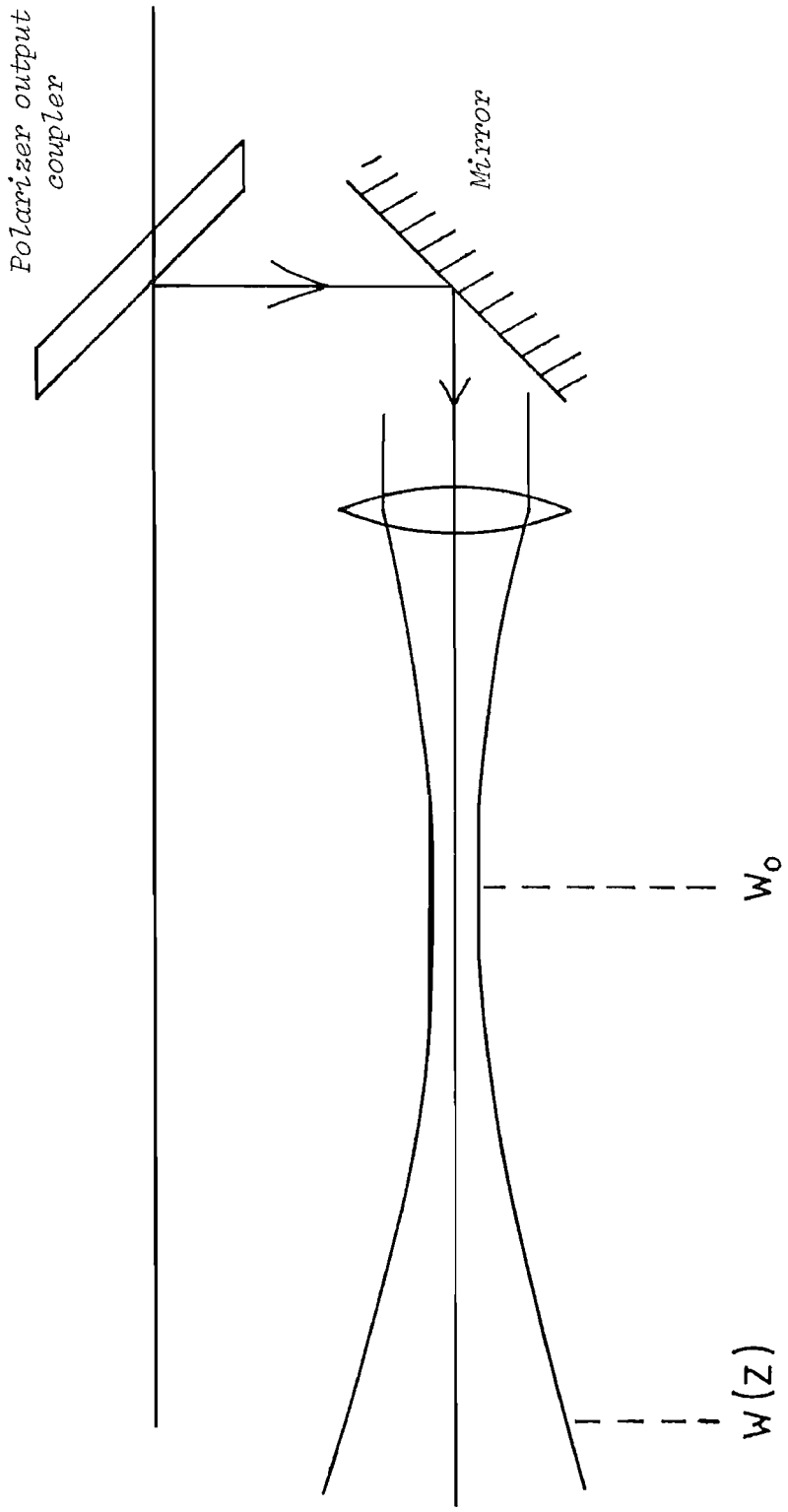

Figure 5.4 Measuring the beam divergence.

this method does show up the transverse structure and the shape of the beam.

Secondly, the diode array (described above) was used to display the transverse intensity profile on a storage oscilloscope, so that the profile could be photographed. Having a linear response, the array could be used for direct examination of the detailed structure of the beam. Rotation and translation of the array allowed the display of the profile along any chosen line across the cross section of the beam.

5.2.4. Depolarization Loss

Ideally, all the energy incident on the polarizer after the second pass through the amplifier should be vertically polarized and therefore reflected off the polarizer as output (Figure 5.1.). However, as already mentioned, depolarization can occur both in the amplifier rod and in the phase conjugate cell, so that some component of the beam could be horizontally polarized. This component would be transmitted by the polarizer and travel back towards the oscillator. This represents both an energy loss and a spatial beam distortion - since the depolarization is spatially dependent, some parts of the output will lose more energy than others.

As described in Chapter 3, a horizontally polarized ray passing through a point in the amplifier rod cross section and travelling along a path parallel to the rod axis will see two indices of refraction for the radial and tangential directions of polarization (Figure 3.3.). The ray will, in general, have components along these fast and slow axes which emerge from the rod with some phase difference, giving elliptical polarization. By

placing the Faraday rotator between the amplifier and the plane mirror, the amplifier birefringence can in principle be cancelled out as follows. The ray returning through the amplifier on the second pass has the two fast and slow components each rotated by 90^{o}, so that the polarization component which, on the first pass, was parallel to the fast axis, is parallel to the slow axis on the second pass, and **vice versa.** Thus, in traversing the amplifier on the second pass, the phase difference between the components is cancelled out and they emerge in phase, resulting in vertically plane polarized light. The process is illustrated in Figure 5.5., which shows the rod viewed along its length. The success of this scheme depends upon the requirement that a ray passing along any particular path P in the rod must return along exactly the same path, for along any other path the directions of the fast and slow axes will differ, as will the phase difference for the two components. In this case, exact cancellation of the birefringence seen on the first pass will not occur on the second pass. This exact ray retracing may not occur if the amplifier shows significant lensing, or if the input beam is not collimated. The scheme will also work less than perfectly if any further polarization change takes place between the first and second passes of the amplifier and this may occur in an SBS phase conjugator, even though the use of a phase conjugate mirror should, in principle, ensure exact ray retracing.

An additional feature of the scheme is that the laser beam, after a double pass through the rod, is no longer brought to two foci (for the radial and transverse polarizations) given by equations 3.3.2. and 3.3.3. We illustrate this in Figure 5.6., which shows a plane horizontally polarized beam travelling through the rod cross section. Notice that those parts of the beam

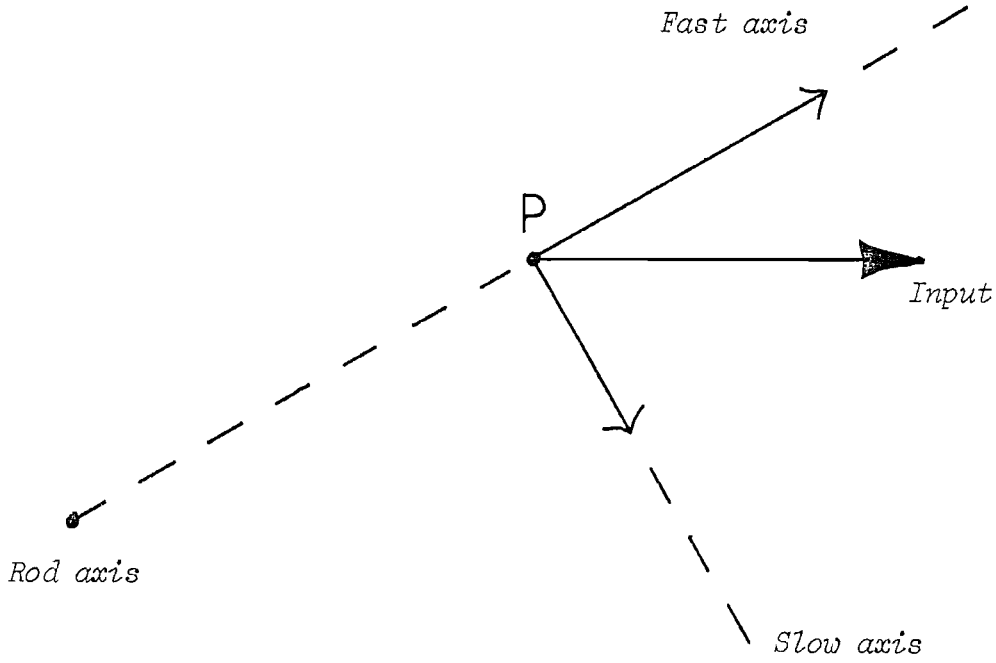

FIRST PASS

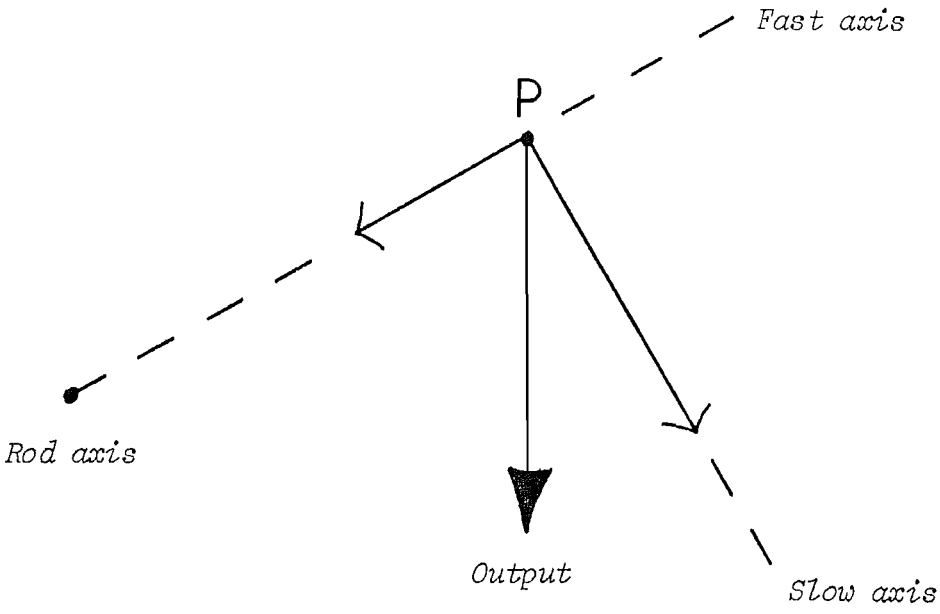

SECOND PASS

Figure 5.5 *Compensation of amplifier birefringence by Faraday rotation of the polarization components by 90 degrees.*

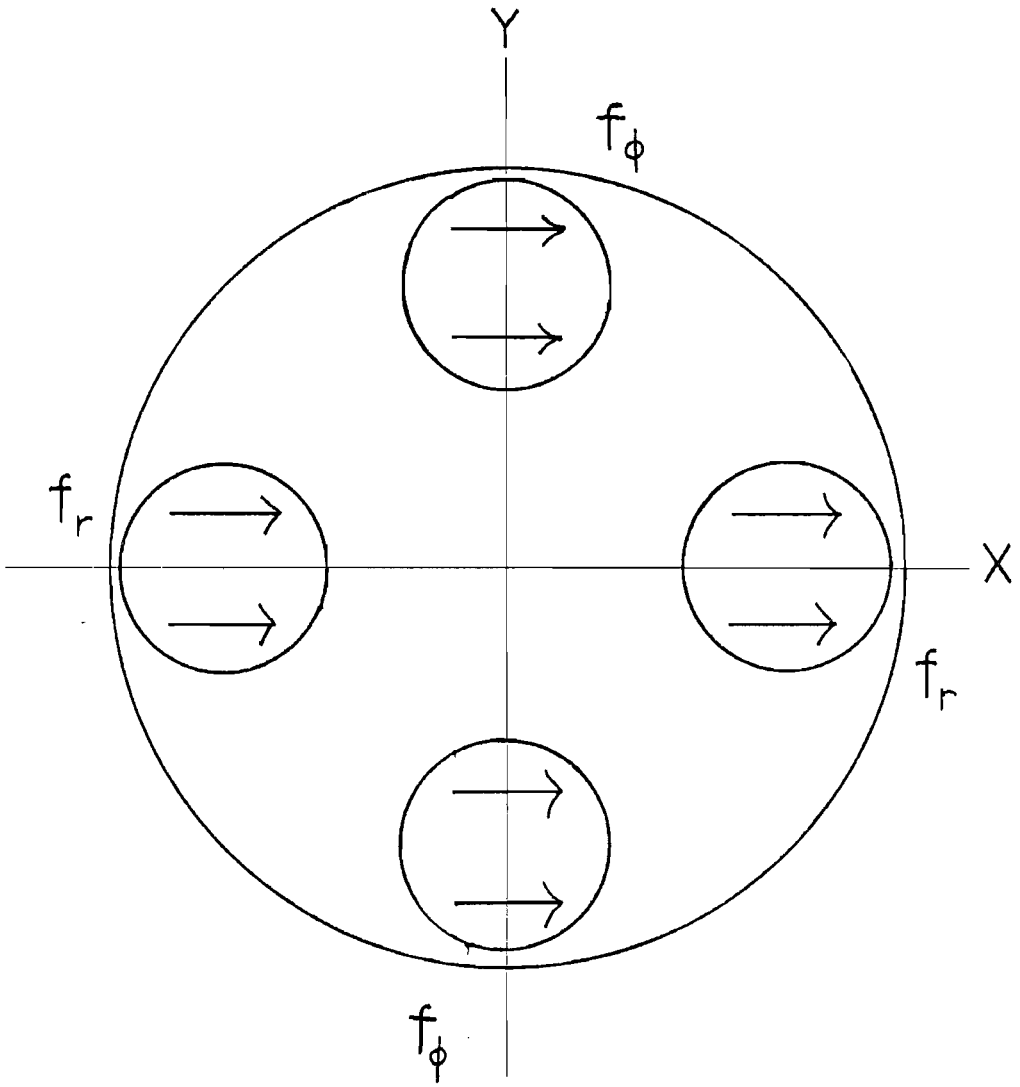

Figure 5.6 *A horizontally polarised beam travelling through a birefringent rod. Those parts of the beam near the Y axis see a refractive index n_ϕ, while those parts near the X axis see an index n_r.*

lying along the x axis see a refractive index n_r and the rod has focal length f_r, while those parts of the beam along the y axes see a refractive index n_ϕ, and for these parts the focal length is f_ϕ. If, on the second pass, the beam polarization is rotated by 90^o, the focal lengths are interchanged, and the effective focal length seen by any part of the beam will be constant. This statement is also subject to the condition that rays retrace their paths exactly.

A commonly used technique for polarization rotation of 90^o in a double pass is a quarter wave plate, for example placed at locations 1 or 2 in Figure 5.1. However, this scheme cannot compensate for birefringence in the same way that a Faraday rotator can, because a quarter wave plate does not simply rotate the polarization, but is a birefringent component itself. It is possible to calculate the depolarization loss for the case of Nd:YAG amplifier double passed with a plane mirror and a quarter wave plate. This was done for various input pump powers to the amplifier, using an extension of the theory of rod birefringence presented in Chapter 3. Details are given in Appendix III and the results are given with the experimentally measured loss later in this Chapter.

The birefringence loss was measured experimentally for the four double pass configurations - Faraday rotator or quarter wave plate with plane mirror or phase conjugate mirror - at various pulse repetition rates. The depolarization loss was measured by placing a beam splitting mirror in the beam between the oscillator and polarizer, as shown in Figure 5.7. This mirror was usually a plane/plane 30%/AR placed almost perpendicular to the beam, so that the beam would not be translated laterally by any significant amount. The birefringence

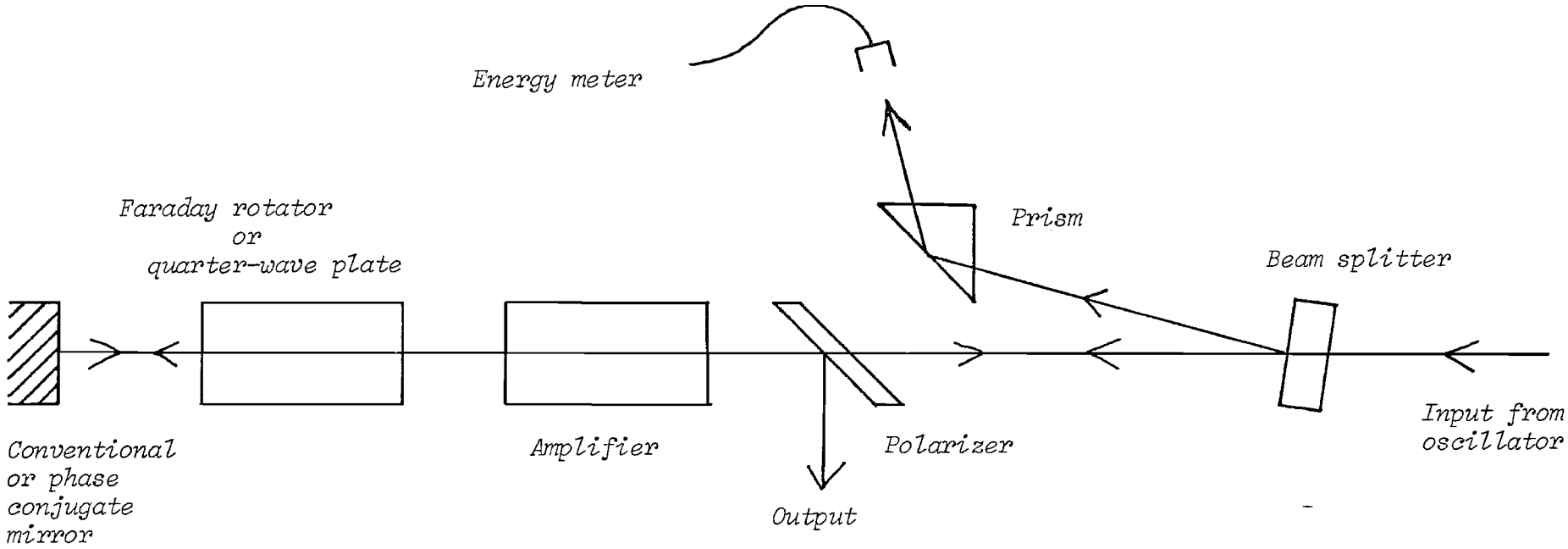

Figure 5.7 Method used for measuring theamount of energy lost due to depolarization of the beam in the amplifier.

loss, transmitted by the polarizer back in the direction of the oscillator, could be calculated by measuring the energy reflected from this beam splitter via a prism, as shown in the Figure.

5.2.5. Linewidth Measurement

The linewidth of the laser was first measured for the oscillator alone, then when the amplifier was double passed using the plane mirror, and later when the phase conjugate mirror was employed. Thus any increase in linewidth due firstly to amplification, and secondly due to the SBS process - the broadening of a single line or the appearance of new frequencies - could be observed.

The bandwidth limit of a 30 ns Gaussian pulse is ~ 15 MHz. A measurement of its linewidth therefore requires an instrument with a resolving power of possibly as much as $\frac{\nu}{\Delta\nu} = \frac{3 \times 10^{14}}{15 \times 10^{6}} = 2 \times 10^{7}$ at a wavelength of ~ 1 μm. The only type of spectrometer with this resolving power that is convenient to use is the Fabry-Perot interferometer, in particular the spherical-mirror confocal Fabry-Perot (Bradley and Mitchell, 1968, Bradley et al, 1968, Hercher, 1968). An instrument of this type was available with mirrors coated for visible light in the green part of the spectrum, so for this reason and for the general convenience of working with visible light, the 1.06 μm laser output was frequency doubled to 532 nm.

To check the single mode operation of the oscillator one must also ensure that the free spectral range of the etalon comfortably exceeds the adjacent mode frequency spacing of the laser resonator, which was ~ 150 MHz.

The etalon used had a spacing of 5cm between mirrors with radius of curvature 5cm, giving a free spectral range of 1500 MHz, i.e. ten longitudinal mode spacings of the oscillator. The mirror reflectivity R was ~ 97% at 532nm, giving a finesse $F = \frac{\pi\sqrt{R}}{1-R} \simeq 100$. Thus the pass bandwidth was ~ 15 MHz. One of the etalon mirrors was on a piezoelectric mount, allowing precise control or scanning of the mirror spacing.

Initially the etalon was set up as shown in Figure 5.8. to display the characteristic ring pattern. The laser output was attenuated with two beam splitters before being frequency doubled. A 1.06 μm absorbing filter was placed immediately after the doubler. The interference fringes of the etalon are localised at or close to the midplane of the instrument, as indicated in the Figure. These were imaged upon a screen, where they could be observed visually. In this way the performance of the laser could be seen directly, both in terms of the number of modes oscillating and the stability; the performance was observed for fast Q-switching, pre-lase Q-switching and pre-lase Q-switching with the beat detector circuit. The results of these observations were as follow.

When the oscillator was fast Q-switched with the etalon and resonant reflector, the ring pattern consisted of sets of approximately five rings, each set separated by one free spectral range of the etalon. The exact number of rings was difficult to count because the intensity of each ring varied considerably from shot to shot in a random fashion (the oscillator was run at 5 Hz for all the linewidth measurements). This number of rings suggested that the laser was oscillating on three longitudinal modes most of the time. (Note that if n fundamental frequencies w, $w+\Delta$, $w+2\Delta$, ... $w+(n-1)\Delta$ are frequency doubled, the number of new frequencies

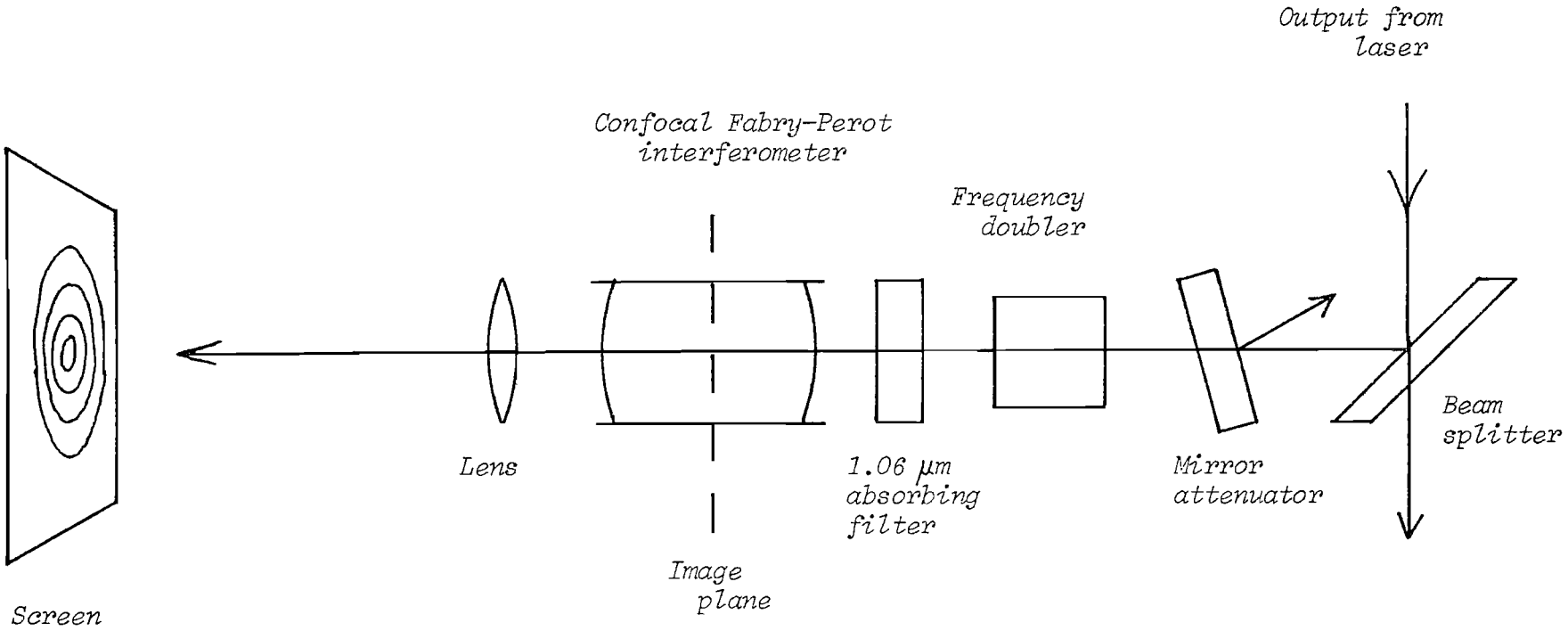

Figure 5.8 Experimental set-up for visual observation of the longitudinal mode behaviour of the oscillator.

generated is 2n-1.) This is roughly consistent with the calculated linewidth of 210 MHz.

When the laser was pre-lase Q-switched, there were single rings separated by the etalon's free spectral range, though for about 30% of the time there were three rings. This pattern indicates single-longitudinal mode performance breaking into two-mode oscillation for periods. Once 'warmed up' the laser would typically run on one mode for a couple of minutes, then on two modes for about half a minute.

When the beat detector was in use the three ring pattern never appeared, the laser running always on a single longitudinal mode. Although the beat detector always ensures SLM operation, the frequency of this mode is decided by the cavity length. Drifts in the cavity length therefore cause drifting of the laser frequency and this could be seen sometimes - the ring would slowly collapse towards or expand from the centre. However, it never moved more than a distance corresponding to approximately half a longitudinal mode spacing, i.e. 75 MHz, when the laser would jump frequency to the next adjacent mode, this new mode frequency having moved closer to the peak of the etalon transmission band. A typical rate of frequency drift was estimated at 1-2 MHz/sec, although when the laser was run for long periods it would run on the same mode for many minutes at a time.

Having seen that the laser could be run on one mode reliably, a scheme was devised for quantitative measurement of its linewidth. A single shot linewidth measurement is difficult, because it involves recording the spatial intensity distribution of the ring pattern with, for example, a diode array or a photographic method. Such methods suffer from limitations of

resolution or non-linearity of photographic materials. An important feature of a Fabry-Perot etalon is the ability to scan a narrow wavelength range using the piezoelectric control of mirror separation, and this feature was exploited using a multiple shot measurement, shown in Figure 5.9. A voltage ramp generator sweeping from 0 to 1000 V with a minimum sweep rate of 10 V/sec was used to drive the etalon. It was found that one free spectral range of the etalon was swept by a voltage change of 62V, therefore this would be swept in ~ 6 seconds, or 30 shots at 5 Hz. To increase the sweep time and the number of shots recorded, a variable voltage divider was made to step the voltage down by a factor of 8-16, so that the full 1000 V sweep of the generator swept one FSR in 50-100 seconds, i.e. 250-500 shots. In terms of frequency this corresponds to a laser shot every 6-3 MHz of sweep. The central spot of the ring pattern was monitored with a small area photodiode (of dimensions 0.5 x 0.5mm) and the signal fed to a boxcar detector used as a sample and hold circuit. This was used to hold the signal from one shot until the next one arrived. The sample and hold circuit was triggered by the signal from a second photodetector, looking at the laser output pulse. The output of the circuit was fed to the Y input of an XY plotter. The X input was driven by a 0-10 V reference voltage from the ramp generator. Thus the plotter recorded the transmitted intensity of the etalon versus its mirror spacing. With suitable adjustment of the voltage divider and the initial mirror spacing, it was possible to obtain transmission scans over one FSR of the etalon.

Typical scans are shown in figure 5.10, for the oscillator/amplifier with plane mirror and with phase conjugate mirror. Each curve results from ~ 100 laser shots. The linewidth is given by the ratio of the FWHM

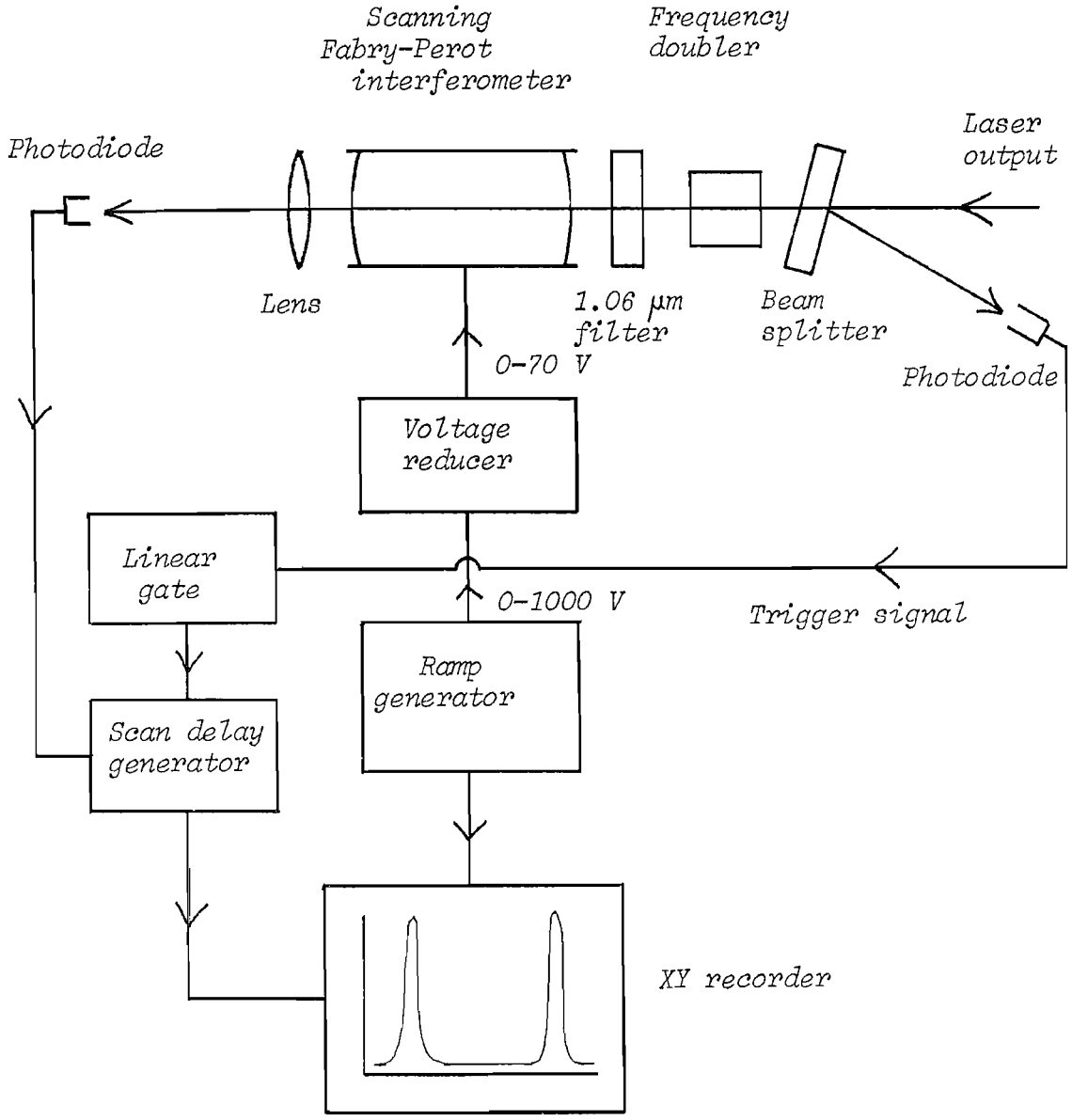

Figure 5.9 *Arrangement used for quantitative measurement of the single longitudinal mode linewidth.*

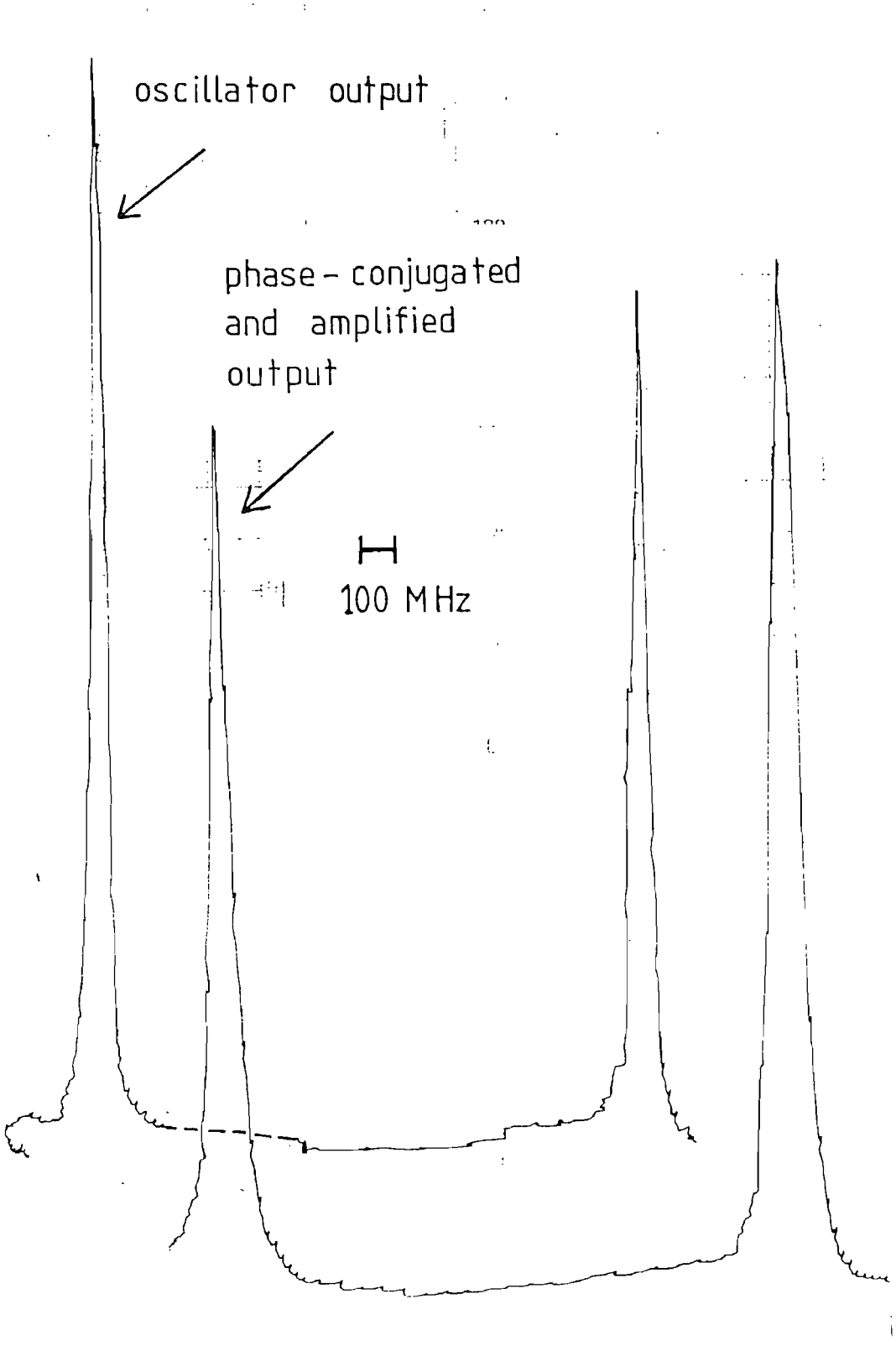

Figure 5.10 *Fabry-Perot transmission scans of the frequency doubled oscillator output and the phase conjugated and amplified output*

of each 'spike' to the spike separation multiplied by 1500 MHz. For the oscillator alone this was 45 MHz, which for the fundamental frequency corresponds to a width of $\frac{45}{\sqrt{2}}$ MHz = 33 MHz. Any broadening introduced in the amplifier when double passed with the plane mirror was negligible compared with the experimental error. When the SBS mirror was used the linewidth at 532 nm increased to 60 MHz, or approximately 45 MHz at the fundamental (the factor between the widths at 532 nm and 1.06 μm may no longer be exactly $\sqrt{2}$, since the pulse is not Gaussian in shape). The estimated error on these measurements was $\pm$ 5 MHz, given by the variation in the width of the spikes.

The increased linewidth of the Brillouin pulse is consistent with its shorter duration. From the results above, one can conclude that the SBS process did not cause significant linewidth broadening. The system was still a 'single mode' laser and no new frequency components were introduced. Thus a laser incorporating such an SBS mirror could be used where narror linewidth operation is a pre-requisite, such as in holographic applications.

5.3. Results for the two-pass amplifier

5.3.1. Comments on the methane cell as a reflector

Before comparing the output of the laser with and without phase conjugation, we make some observations regarding the use of the SBS cell simply as a mirror, not yet concerning ourselves with its performance as a phase conjugator.

The laser was usually run so that the input to the cell before the focussing lens was ~ 185 mJ, and the reflected energy was 100 mJ (measured using a beam splitter), giving a reflectivity of 55% for the cell plus lens. The reflectivity was measured down to input energies of 144 mJ at 30 atmospheres and 75 mJ at 50 atmospheres pressure and was constant over this range at 55%. This is consistent with the findings of Maier (1968) (section 4.5.1. Chapter 4), who found that the efficiency of SBS became independent of the input energy for inputs well above threshold (At 50 atmospheres 75 mJ is still ten times the threshold energy). If allowance is made for a 4% loss at the four uncoated glass/gas surfaces, the efficiency in the gas itself is found to be 63%.

A problem encountered with the cell after several weeks of use was a build up of a sooty substance on the cell wall around the beam focus, suggesting that gas breakdown was occurring, though no cracking noise could be heard when an ear was placed on the cell. Of more seriousness was a similar deposit on the inside surface of the entrance window, which led to minor damage to the window surface with subsequent absorption of laser light and major damage. The peak laser intensity on the window is ~ 300 MW cm^{-2}, which is well below the maximum threshold for spectrosil B of 5 GW cm^{-2}, so that the soot was apparently the cause of the problem. The peak laser intensity at the focus was 7.5 GW cm^{-2} averaged over the beam area πw_o^2. The mechanisms of gas breakdown are varied and complex, depending upon pressure, pulse duration, intensity, wavelength and focussing conditions (e.g. see Grey Morgan, 1978). Unfortunately, there is a lack of data for the conditions of our experiment. The breakdown intensity of methane at 30 atmospheres pressure has been measured at a wavelength of 249 nm and was found to be 6.5 GW cm^{-2} (J. Murray), but

this result cannot be extrapolated reliably to the wavelength of 1.06 μm. Using a 30cm lens to focus the beam to a spot size of ~90 μm giving a threefold increase in intensity to 22 GW cm^{-2} caused an audible spark. It would have been an advantage to have a spot size larger than 150 μm to decrease the focal intensity further. This could only have been achieved by using a longer focal length lens, of say 75cm or 1m. However, the focus would then have been so close to the rear cell window, that damage could have ensued there. Alternatively, the lens could have been moved further from the cell to keep the focus at the cell centre, in which case the spot size on the front window would have been too small. Thus, the 50cm lens was retained, damage to the gas being less inconvenient than damage to the windows! Although the observed gas breakdown threshold did not seem unreasonable in the light of Murray's measurement, the appearance of soot on the window effectively prevented long term operation of the cell. It was suggested (Dr. F. O'Neill, personal communication) that this was due to organic impurities in the gas in the form of large molecules with low dissociation energy. To try and eliminate these a filter with pore size 0.22 μm (manufactured by Millipore) was added to the gas supply line. It proved successful in reducing the quantity of soot appearing in the cell and the associated damage problems to a negligible level.

5.3.2. Performance of the two pass amplifier

We now compare the performances of the various configurations of the two pass amplifier.

For the plane mirror version with the Faraday rotator, the output energy at 5 Hz repetition rate was 400 mJ in a

30 ns pulse, at the maximum amplifier pump energy of 72J. Higher pump energies led to superradiance in the amplifier rod with no further increase in laser output.

The beam quality can be judged from figures 5.11 and 5.12 , which show burn marks and diode array profiles made at various distances from the output coupler. In 5.11 the repetition rate was 5 Hz, at this mean pump power (360 W) the profile showed modulation of the order of 20% on the envelope. The beam was measured to be essentially diffraction-limited within the experimental accuracy.

At a repetition rate of 15 Hz (a mean pump power of 1.08 kW), the beam showed significant aberration, as shown in Figure 5.12 . Firstly, the strong thermal lensing of the amplifier rod brought the beam to a focus at about 2m from the output. We can calculate a theoretical value for the position of the focus. Using equations 3.32 and 3.33 we find the rod focal length was $f_R = 3.5$m. Thus, after a double pass through it the beam would be expected to focus at a distance of ~ 1.8m from the amplifier. Secondly, the beam was astigmatic; the first focal line being 1.5m from the output and orientated at 45^o to the horizontal, the second being at 2.5m and perpendicular to the first line. An explanation for this astigmatism, especially the 45^o orientation of the focal lines in a system which appears to be symmetrical about a vertical plane, has to date eluded the Author. Thirdly, the beam begins to break up in the far field losing its last vestiges of circular symmetry.

Despite the grotesque appearance of the beam, its divergence was only approximately twice diffraction

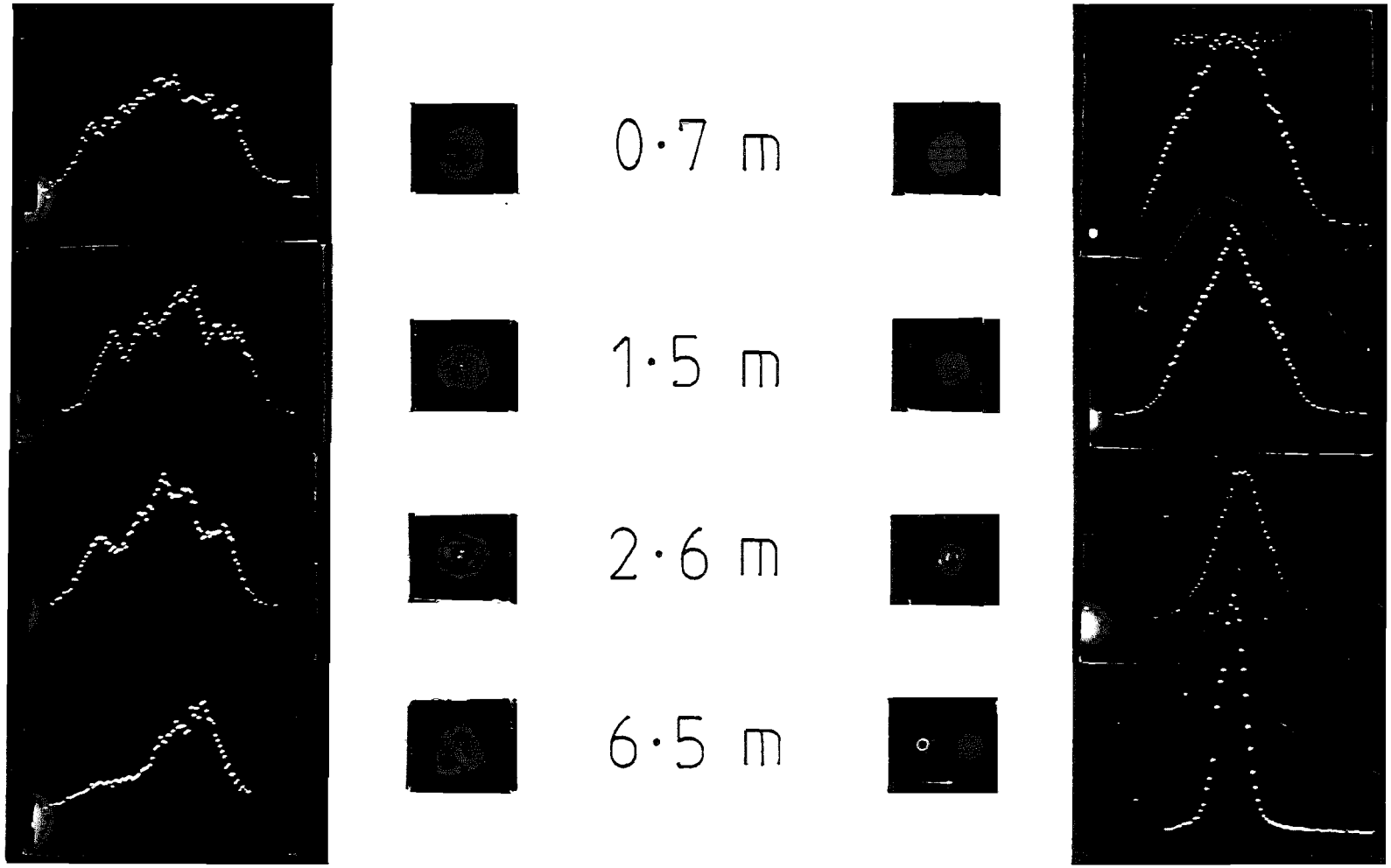

Figure 5.11 *Beam profiles and burn marks at various distances from the two-pass amplifier, at 5 Hz repetition rate, either with phase conjugation (right-hand photos) or without phase conjugation (left-hand photos).*

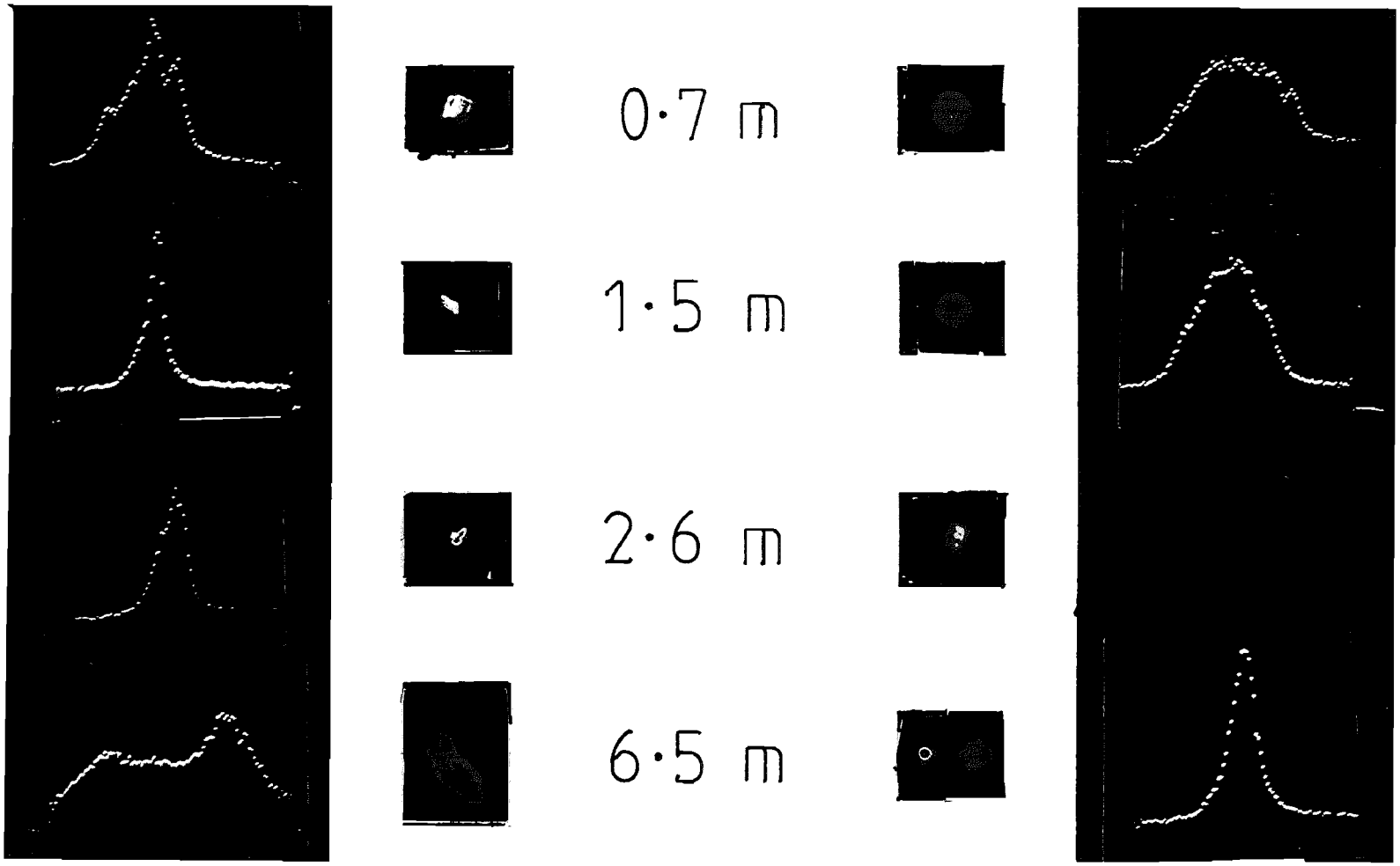

Figure 5.12 *Beam profiles at various distances from the two-pass amplifier, at 15 Hz repetition rate, either with phase conjugation (right-hand photos) or without phase conjugation (left-hand photos).*

limited. This result is perhaps surprising and suggests that beam divergence alone is not an adequate guide to beam spatial quality.

When the plane mirror was replaced by the SBS cell the energy dropped by 20% to 330 mJ. Thus, even though the cell has only a 50% reflectivity, the output drops by much less than this, implying that the amplifier is less saturated on the second pass when the cell is used - i.e. there is more gain.

The pulse shapes at various points in the laser are shown in Figure 5.13, which shows the 30 ns oscillator pulse, the output of the complete system, and the throughput of the SBS cell. The output exhibits a very rapid rising edge 2ns long and thereafter approximates the shape of the input pulse. The lower picture shows the transmission through the cell, and here the pulse has the rising curve of the input and then drops rapidly (corresponding to the rise of the reflected pulse) to a low level which decreases gradually to zero over 20ns. It appears that once the Brillouin process is set up, the efficiency rises to a high value very quickly. The instantaneous power of the input pulse when this occurs is approximately ten times the measured threshold power of 0.5 MW for a 30 ns pulse (at 30 atmospheres), which shows that a certain time is required to set up the process, rather than a certain power level. The sudden fall in the throughput occurs $\sim$10 ns after the leading edge of the input pulse arrives, which is of the same order of magnitude as the phonon lifetime of 10 ns. The output pulse is shortened by the loss of the front part of the input to 16 ns, giving a pulse power of 20 MW as opposed to 13 MW for the 400 mJ, 30 ns pulse obtained using the conventional mirror.

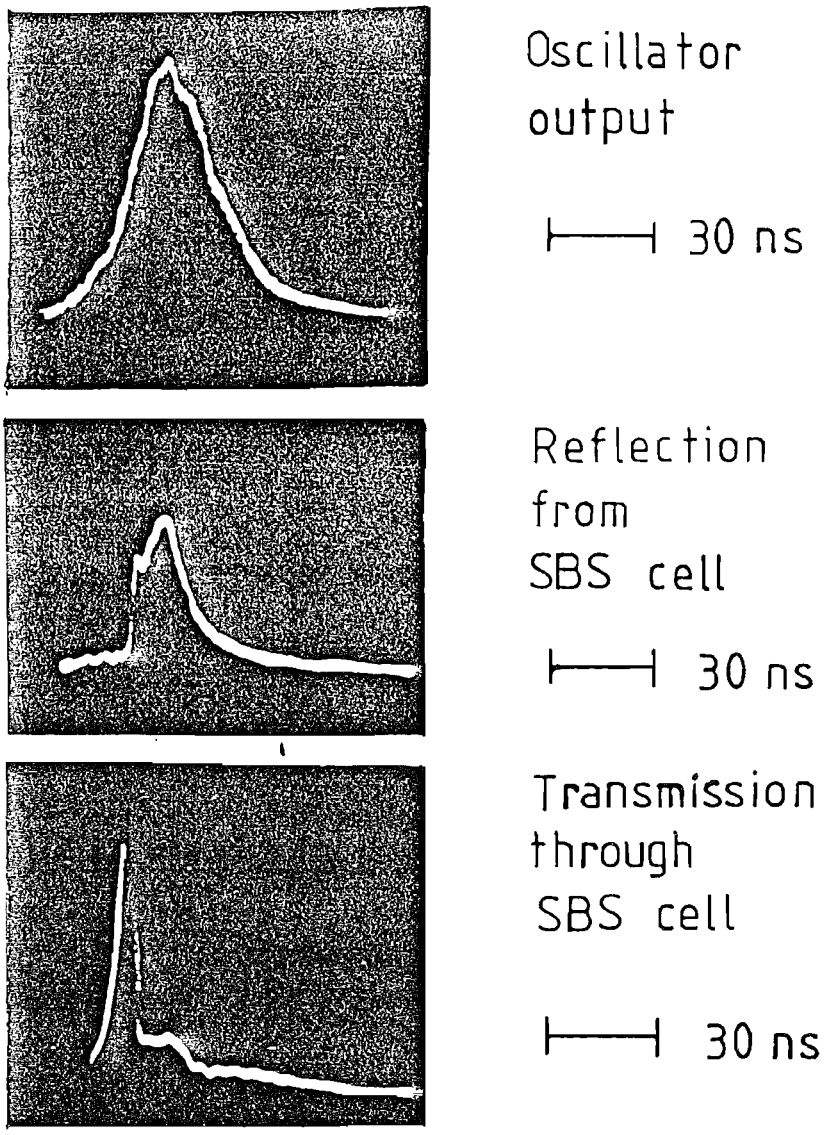

Figure 5.13 *Pulse shapes at various positions in the two pass amplifier.*

The beam quality with the phase conjugator is shown for direct comparison with the plane mirror in Figures 5.11 at 5 Hz and 5.12 at 15 Hz repetition rate. The profiles, though not as smooth as the input to the amplifier, are very much smoother than those obtained with the plane mirror and the burn marks are much more circular. Most dramatic is the improvement over the plane mirror at 15 Hz, the strong focussing, astigmatism and beam break up no longer appearing. The slight focussing of the phase conjugate beam was due to a small divergence of the beam entering the amplifier from the beam expansion telescope. This caused negligible change in the spot size over the length of the amplifier and Faraday rotator and indeed this imperfect collimation was not noticeable until the phase conjugator was used. (In fact slight divergence of the beam entering the amplifier will partly compensate the thermal lensing anyway). The burn marks of the phase conjugate beam show four slight 'blips' on the edges of the intense circular central spot, which are indicative of uncompensated birefringence. These were not visible, however, on the diode array. The magnitude of the depolarization loss will be given in the next section, and the energy in the blips was also measured directly in the following way. The diode array profile in the far field showed a Gaussian profile, the spot size w of which was measured. An aperture of diameter 3w, through which essentially all the energy of a pure Gaussian of spot size w should have passed, was placed in the beam. By measuring the energy both before and after the aperture, the proportion of energy in the 'wings' of the beam could be found. The energy measured at the system output was also compared with the far field energy in case beam components with large angular divergence were present, which would not enter the calorimeter in the far field. This way it was estimated that 90% of the beam energy was in the diffraction-limited part.

The performance of the phase conjugator was also briefly tested with the oscillator running multimode to give a broader linewidth. Firstly, it was run fast Q-switched to give a 200 MHz linewidth, when it ran on two or three modes (Figure 5.14 (a) and (b)) and the output pulse was observed. Typical examples of two and three mode outputs are shown in Figures 5.14 (c) and (d), together with the superimposed single-mode output for comparison. It is interesting to see that once the SBS process is set up the reflected pulse still follows the shape of the input, despite the large intensity fluctuations which go right down to the baseline. An examination of the far field beam profile revealed a consistently smooth Gaussian for both two and three mode operation.

When the linewidth was increased to 400 MHz the Brillouin pulse still appeared to follow the input as shown in Figure 5.15, even though the individual oscillations were only ~ 2 ns wide, and the SBS process still seemed to 'switch on' after 10 ns as for the single mode pump. The output beam quality remained good.

Broadening the linewidth to 2000 MHz did have an effect on the phase conjugate beam - its shape and divergence changed from shot to shot; and the energy was reduced and fluctuated by large amounts, sometimes falling to almost zero. It was difficult to compare the output pulse shape with the input because the structure was very fine and varied greatly from one shot to the next. The coherence length of the beam at this linewidth was 15cm, which was approximately equal to the confocal parameter. In fact, the effective overlap length between the pump and back-scattered Stokes waves is half this value, because they travel in opposing directions. For a single mode pump of linewidth 33 MHz, the threshold power in methane at 30 atmospheres pressure was 0.5 MW,

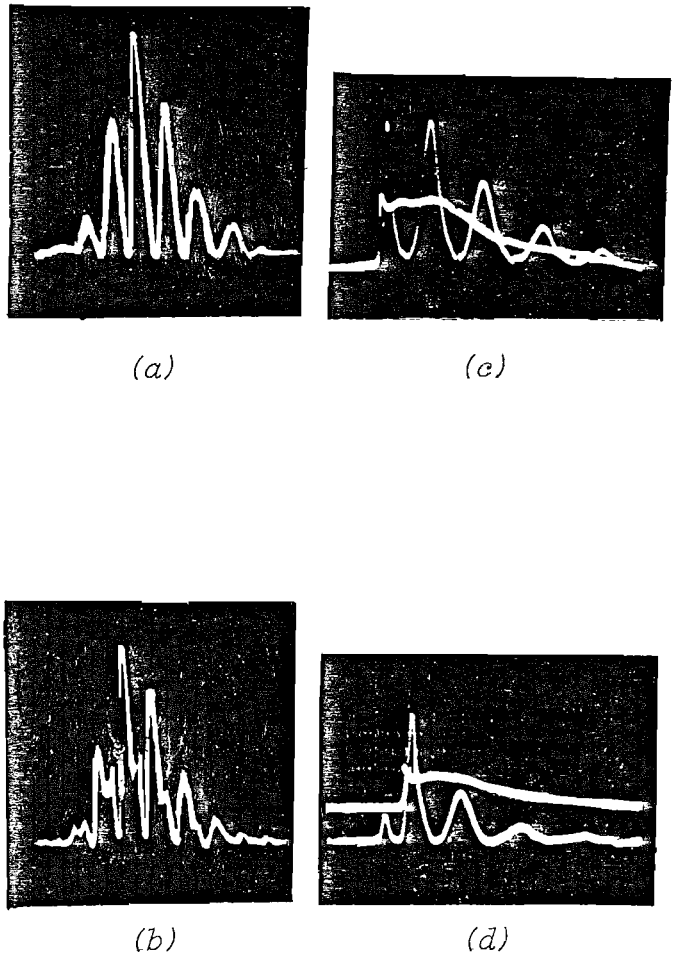

Figure 5.14 *Output pulse shapes of the oscillator (a) and (b) when running on two and three modes respectively, and of the two pass amplifier with phase conjugation (c) and (d). The single mode output is superimposed upon the latter two traces for comparison.*

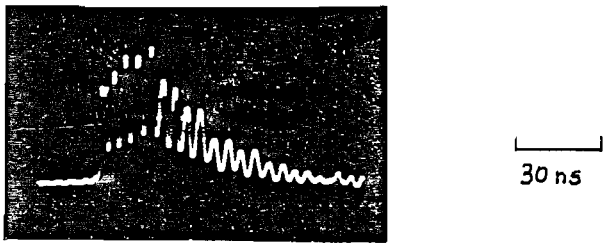

Figure 5.15 The reflected Brillouin pulse for a linewidth of 400 MHz.

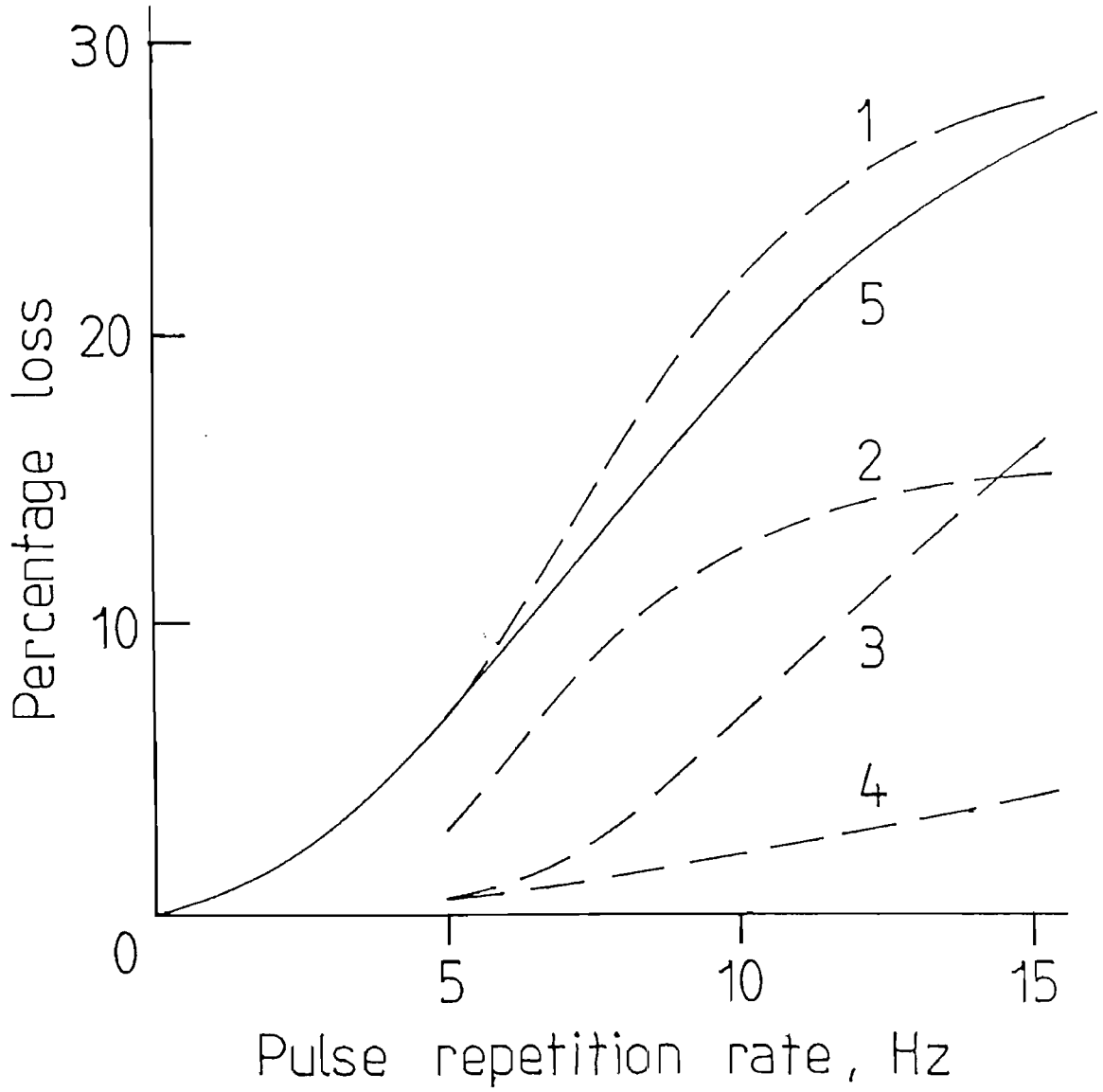

Figure 5.16 Depolarisation loss for the two pass amplifier as a function of pulse repetition rate.
Curve 1 is for plane mirror with quarter wave plate
2 is for the SBS mirror with quarter wave plate
3 is for plane mirror with Faraday rotator
4 is for the SBS mirror with Faraday rotator
Curve 5 is a theoretical calculation of curve 1.

in a spot size of 150 μm. Hence the gain length required for threshold to be reached, $l = \frac{30}{gI}$, was ~ 5cm. Thus, the effective overlap length at a linewidth of 2000 MHz had become comparable to this threshold gain length, which explains qualitatively why the SBS efficiency was reduced.

5.3.3. Depolarization Loss

The results for the depolarization loss measurements are displayed in Figure 5.16. The percentage of the total energy incident on the polarizer after the second amplifier pass, which was transmitted by the polarizer, is shown versus the pulse repetition rate for a pump energy of 72 J. Curve (1) is for the plane mirror used with a quarter wave-plate, and the loss reaches a value of ~ 30% at the maximum pump power, which in terms of pulse energy is 120 mJ, reducing the output energy to approximately 300 mJ. Also shown (Curve (5)) is the theoretical loss for this configuration, as calculated in Appendix III, the agreement with the measured results is excellent. The curve tends asymptotically to a maximum value of 44%. Curve (2) results from the SBS mirror used with the quarter wave plate. Curves (3) and (4) result from the plane mirror and SBS mirror respectively, each with the Faraday rotator.

Comparing curve (1) with (3) shows that the Faraday rotator does give significant improvement (by a factor of ~2) over the quarter wave plate, as one would expect. Under ideal conditions the loss for curve (3) would be zero. Indeed, it is very low at the small pump powers. The rapid increase in loss as the repetition rate increases can be explained by the fact that not only does the magnitude of the birefringence at any point in

the rod increase, but the increasing thermal lensing means that reflected rays retrace their incident paths through the amplifier rod less and less precisely. Cancellation of the birefringence can only occur for rays that do retrace their paths exactly, as explained in Section 5.2.4.

Comparison of curve (3) with (4) shows a further reduction at higher pump powers by a factor of ~ 4 in loss for the SBS mirror over the plane mirror. This is because rays now retrace their paths more exactly through the amplifier. The two curves converge at low pump powers because the thermal lensing becomes negligible (f_R = 10.5m at 5 Hz). What is not clear is how much further depolarization of the beam, in addition to that caused by the rod, occurs in the SBS cell (see Section 4.5.5.). The depolarization of the input to the cell can be found by calculating the single pass depolarization in the amplifier rod, which is 0.8%, 2.8% or 5.5% at pulse repetition rates of 5, 10 and 15 Hz respectively. The loss of curve (4) presumably comprises a part due to imperfect ray-retracing through the rod (i.e. imperfect wavefront reversal) and a part due to change of polarization state in the SBS cell. Since these two parts cannot be differentiated, it is difficult to say more. However, the purpose of the experiment was to evaluate the scheme of the SBS cell used with the Faraday rotator, and it most certainly works significantly better than the other three variations.

The results for the two pass amplifier are summarised in Table 5.3. At 5 Hz repetition rate the degradation of the beam by the amplifier was only slight and so, apart from the cleaner appearance of the beam, the phase conjugator did not make a significant difference. At

TABLE 5.3.

	Two pass amplifier	
	Without phase conjugation	With phase conjugation
Energy	400 mJ	330 mJ
Beam quality — 5 Hz	Scruffy profile but diffraction limited	Very clean profile, diffraction limited
Beam quality — 15 Hz	Very scruffy profile twice diffraction limited	Clean profile, diffraction limited
Pulse duration	30 ns	16 ns
Linewidth	33 MHz	50 MHz

15 Hz the value of the conjugator was much more apparent, giving a factor of 4 increase in beam brightness, or 6 if the pulse shortening is taken into account.

5.4. Four-pass amplifier scheme

The main idea behind the four-pass amplifier was simply to attain higher output energies, since it appeared that two passes through the amplifier were not sufficient to extract all the energy. Additionally, it was hoped that birefringence compensation could be applied before the phase conjugator, so that plane polarized light could be presented to it, avoiding possible depolarization in the conjugator. Other potential advantages of the system were a lower input energy requirement from the oscillator, or satisfactory energy extraction with lower input to the conjugator, or with a lower efficiency conjugator.

5.4.1. The basic experimental arrangement

The layout of the four-pass scheme is shown in Figure 5.17. Horizontally polarized light from the oscillator is transmitted by polarizer 1 and is then subjected to opposite 45^{o} rotations by a Faraday rotator and a half-wave plate. After traversing polarizer 2, and then the birefringent amplifier, it enters a ring arrangement which both reflects the beam and interchanges the polarization components (rather as the plane mirror and Faraday rotator did in the previous experiment). This is achieved by splitting the beam into the two orthogonal polarization components using polarizer 3. These components counterpropogate around the ring and each is given a 90^{o} rotation by a half wave plate. They recombine into a single beam at polarizer 3 which, after traversing the amplifier a second time, is in principle

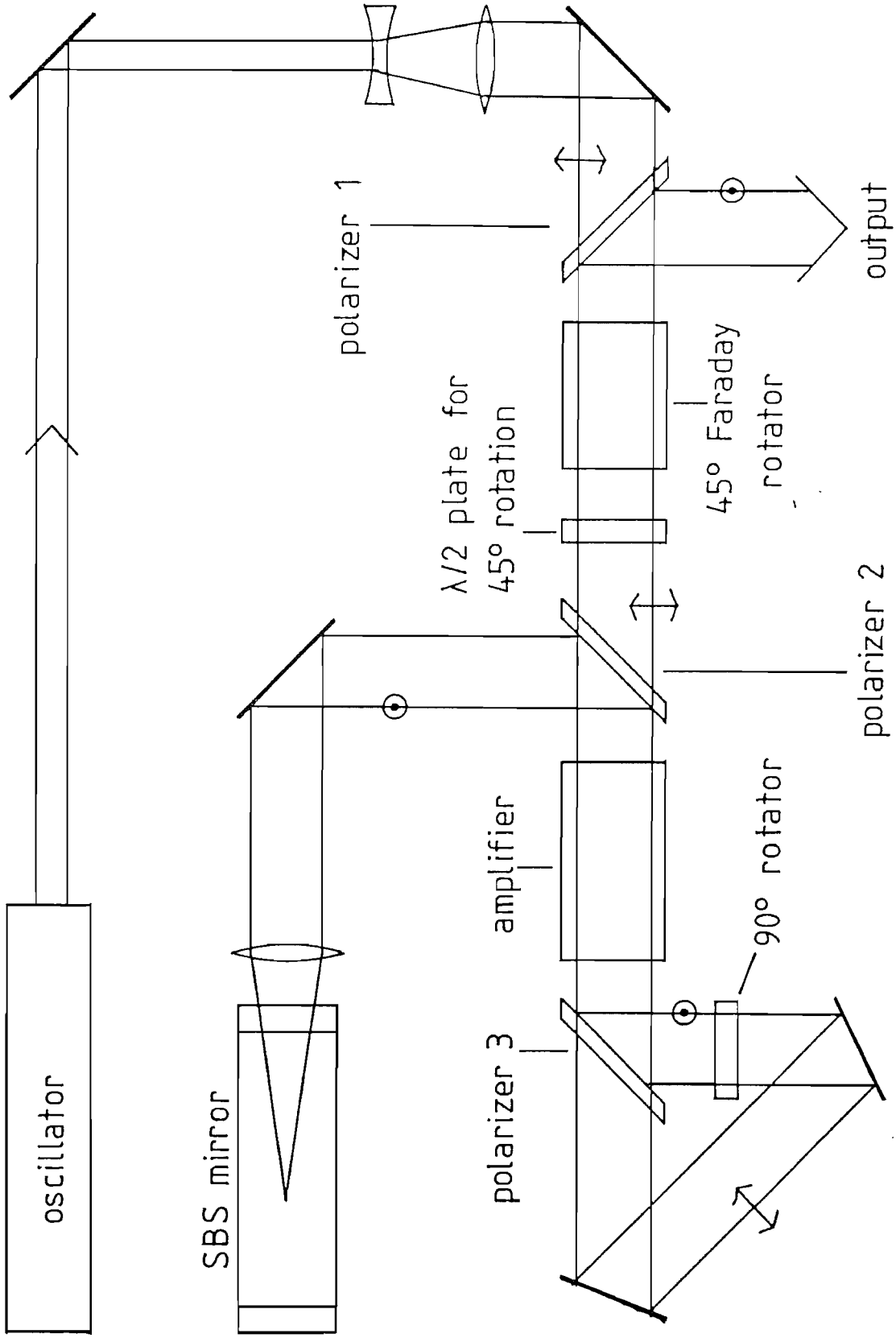

Figure 5.17 The four-pass amplifier arrangement

completely vertically polarized. (We acknowledge Dr. C. L. M. Ireland for pointing out the polarizing properties of this ring configuration. We also note that Richards (1983) used an equivalent arrangement in a special Pockels cell Q-switch device.) This beam is therefore reflected by polarizer 2 into the SBS cell. After conjugation the process is reversed, so that after the fourth amplifier pass the beam is horizontally polarized and is transmitted by polarizer 2. Travelling from left to right, the beam experiences two 45^{0} rotations in the same sense as it passes the half wave plate and Faraday rotator and it is reflected from polarizer 1 as output. A plane mirror was also tried in place of the phase conjugator. The latter was the methane cell as used previously with similar focussing conditions.

5.4.2. Setting up the experiment

Techniques similar to those described in Section 5.1.4. were used for setting spot sizes and orientating the half wave plates. The ring, however, demanded a careful alignment procedure to obtain a good beam from the system. The problem was that adjustment of the mirrors influenced not only the direction of the reflected beam, but also its position within the rod - if the reflected beam was parallel to the incident beam it was not necessarily colinear with it. Figure 5.18 shows the set up for aligning the ring. The phase conjugator was blocked off, the Faraday rotator was switched off and the half wave plate beside it was removed. It was found that a weak beam (due to uncompensated rod birefringence after a double pass) then returned back towards the oscillator. The energy in this beam was monitored by allowing it to fall on a holed card positioned at the oscillator output. Some of the light scattered from the

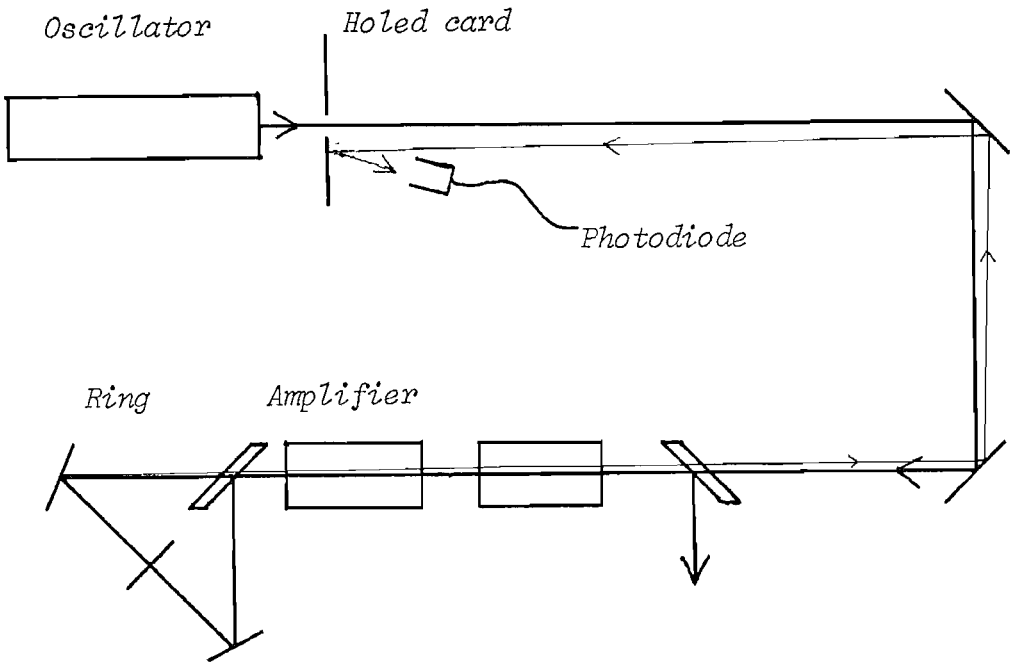

Figure 5.18 *Method for aligning the ring in the four-pass amplifier arrangement.*

card fell upon a photodiode. Maximising the signal from the photodiode by adjustment of the mirrors ensured that the reflected beam travelled through the centre of the amplifier and in the correct direction. It was not allowed right back into the oscillator in case damage occurred there when the laser was Q-switched. The mirrors used in the ring were designed as 45^{o} turning mirrors, but had a reflectivity of ~97% at the 28^{o} angle of incidence used.

5.4.3. Measurements made on the four-pass amplifier arrangement

The performance of the four-pass amplifier was assessed by making measurements similar to those for the two-pass arrangement. However, a significant difference between the two systems is that in the four-pass scheme some of the energy lost as a result of uncompensated amplifier birefringence appears as part of the output beam instead of travelling back towards the oscillator as it does in the two-pass arrangement. A glance at Figure 5.17 shows that, after the first two amplifier passes, any uncompensated birefringence results in a horizontally polarized beam component, which is transmitted by polarizer 2 (instead of reflected into the SBS cell) and reflected by polarizer 1. Thus, it mixes with the main output, which has made four passes. This could not only degrade the spatial quality of the output; but since these two components are of different frequencies separated by the Brillouin shift, (811 MHz in methane), it could broaden the linewidth and cause temporal modulation of the output pulse. Furthermore, another undesirable effect could result from uncompensated birefringence on the third and fourth passes of the amplifier. The reflection from the SBS cell is

vertically polarized and if, after the third and fourth passes, there is still a vertically polarized component, this re-enters the SBS cell a second time and is reflected. Thus oscillation could be set up between the SBS cell and the ring. In fact, during the course of this work, it was reported by Dr. A. Scott (personal communication) that a four-pass scheme incorporating a plane mirror and quarter wave plate in place of the ring went into oscillation in this way.

The depolarization loss was estimated by measuring the signal, emerging off polarizer 1, that had made two passes of the amplifier. An attempt was made to reduce the loss at the highest repetition rate of 15 Hz, by inserting a negative lens in the ring to compensate for thermal lensing of the amplifier rod.

5.4.4. Performance of the four pass amplifier

The total output energy of the laser was 440 mJ for an amplifier pump input of 72 J. Interestingly the output remained constant for signal inputs ranging from the maximum 80 mJ down to approximately half this value. This was probably a consequence of the fact that, as the input signal increased, more energy was incident on the phase conjugator, of which roughly half was lost; the reflection would then also experience lower gain on the third and fourth passes because more energy had been extracted from the amplifier on the first two passes. Such an output, which is independent of the input energy, would be useful for a system where the oscillator output energy was variable.

The output pulse shape is shown in Figure 5.19 (a) and shows considerable compression down to a duration of

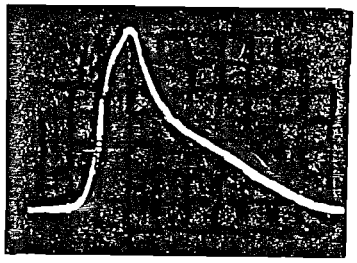

(a) Output pulse

6 ns

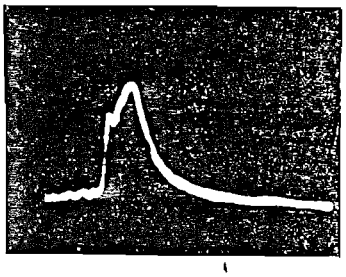

(b) Pulse reflected from the SBS cell before the third pass of the amplifier.

30 ns

Figure 5.19 Pulse shapes in the four pass amplifier.

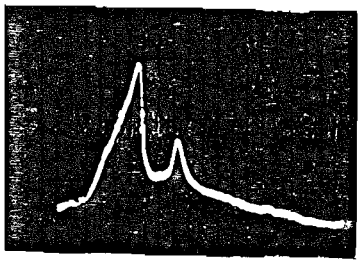

12 ns

Figure 5.20 The pulse transmitted through the SBS cell in the four pass amplifier. The second peak is due to uncompensated amplifier birefringence.

approximately 6 ns, implying a power of 70 MW. This degree of compression had not been seen in the two-pass amplifier and so it was doubted that this could be occurring in the SBS cell. To check this the signal reflected from the cell was observed and it was found to be much like the output from the two-pass amplifier, which is reproduced in Figure 5.19 (b). This signal was therefore being compressed in the third and fourth amplifier passes, due to saturation, as described in Chapter 3. Because the pulse has a fast rising edge, this leading edge receives higher gain than the trailing edge. In Appendix I a calculation is performed to find the expected degree of compression under these conditions.

We note that in 1966 Ambartsumyan et al devised an oscillator - amplifier system for the production of short pulses, in which the front end of the Q-switched oscillator output pulse was chopped off with a shutter to give it a steep rising edge for subsequent compression in a saturated amplifier. In our experiment this occurs in a simple and automatic fashion as a result of the SBS process.

The output pulse shows no sign of beating at 800 MHz between the Brillouin-shifted and unshifted components, which suggests that the unshifted component was much weaker and that the output was essentially single frequency. Another indication that birefringence compensation was adequate (if not necessarily perfect) was the absence of any oscillation between the ring and the SBS cell. The "cavity length" between these components was 1.8m, giving a round trip time of 12 ns. Thus oscillation would have been revealed as a series of pulses at intervals of 12 ns after the first output peak. No such pulses were seen.

Oscillation was seen when the phase conjugator was replaced with a plane 100% mirror. In this situation the birefringence compensation has to be sufficient to prevent oscillation between two 100% mirrors. The output consisted of relaxation oscillations lasting for 100 μs during the pump pulse, a feeble Q-switched pulse, then further oscillations due to the Q-switched pulse bouncing between the ring and 100% mirror. This illustrates the usefulness of the SBS cell in high-gain situations, where its reflectivity is zero until the arrival of the Q-switched pulse.

It may appear that there is a discrepancy here because oscillation did not occur after the first Q-switched pulse with the SBS cell. It was suspected that this was because the first pulse extracted virtually all the energy from the amplifier, reducing the gain far enough to prevent further oscillation. An inspection was therefore made of the transmission through the SBS cell, which showed that there was a second pulse incident on the cell due to uncompensated birefringence when the repetition rate was 15 Hz, and it was indeed 12 ns after the peak of the first pulse (which corresponds to the falling edge of the transmitted pulse). This is shown in Figure 5.20, the first peak being the leading edge of the input. The reflection of this second pulse suffered loss and little or no amplification on the fifth and sixth passes, so emerged from the laser too weak to be visible.

The beam quality from the laser is shown in Figure 5.21, for repetition rates of 5 Hz and 15 Hz, in the near and far fields. The fraction of the beam in the diffraction limited part was measured to be 80%, or 350 mJ. At 5 Hz the near field shows slight modulation, but the far field profile is smooth. The profile at 15 Hz is more

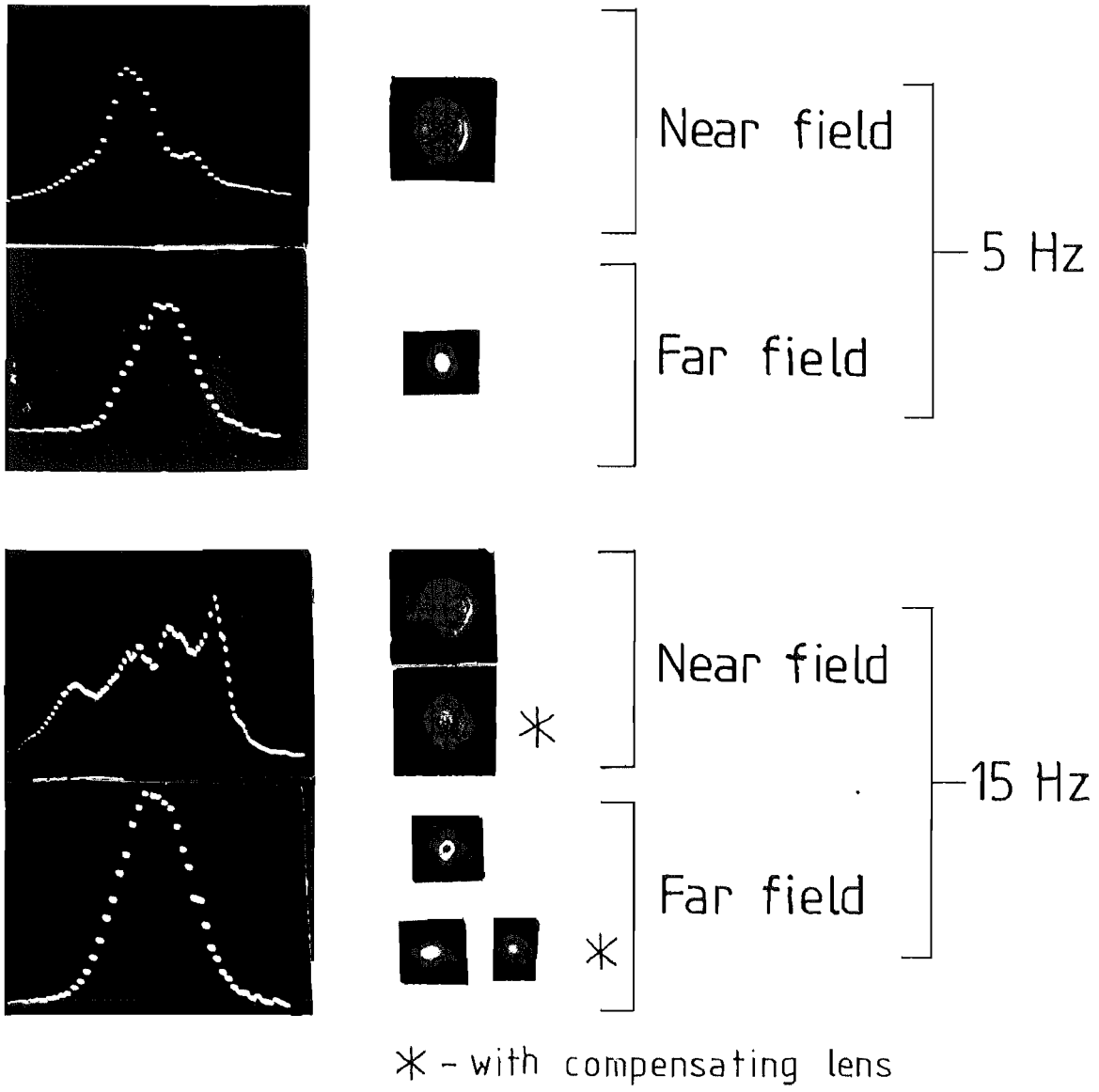

Figure 5.21 *Near field and far field beam profiles for the four-pass amplifier with phase conjugation, at 5 Hz and 15 Hz repetition rate. The effect of adding a compensating lens is shown.*

interesting, in that the near field shows large modulation and asymmetry, and yet the far field is again a smooth bell shape. This can be explained with the aid of Lehmberg's work of 1982, in which he shows with a computer simulation that, even for a fidelity of 99%, the near field beam profile can show modulation of up to 20%. The burn marks made with the compensating lens will be explained later.

The depolarization loss is shown in Figure 5.22. This was measured by blocking off the phase conjugator and taking the ratio of energy emerging off polarizer 1 (in the 'wrong' polarization) to the sum of this and the energy reflected off polarizer 2 (in the 'right' polarization) after two passes.

The depolarized beam reflected from polarizer 1 after two amplifier passes had a higher divergence and a slightly different direction to the phase conjugated output when the SBS cell was uncovered, so the two signals could be separated and observed independently. Observation of the former signal with the SBS cell covered or uncovered revealed an interesting mechanism in the operation of the four-pass amplifier, which acted to enhance the pulse compression over that due purely to saturation of the amplifier. The mechanism was a consequence of the input pulse length (of ~9m FWHM) being greater than the round trip distance bwtween the SBS cell and the ring. When the SBS cell was covered up, the depolarized beam had the roughly Gaussian temporal pulse shape of the input. When the cell was uncovered the conjugated four-pass signal was seen to have a position relative to this Gaussian as shown in Figure 5.23 (a), with the front edge of the main output approximately at the midpoint of the Gaussian. (Note the vertical scales of the two signals are different). This showed that the main output signal

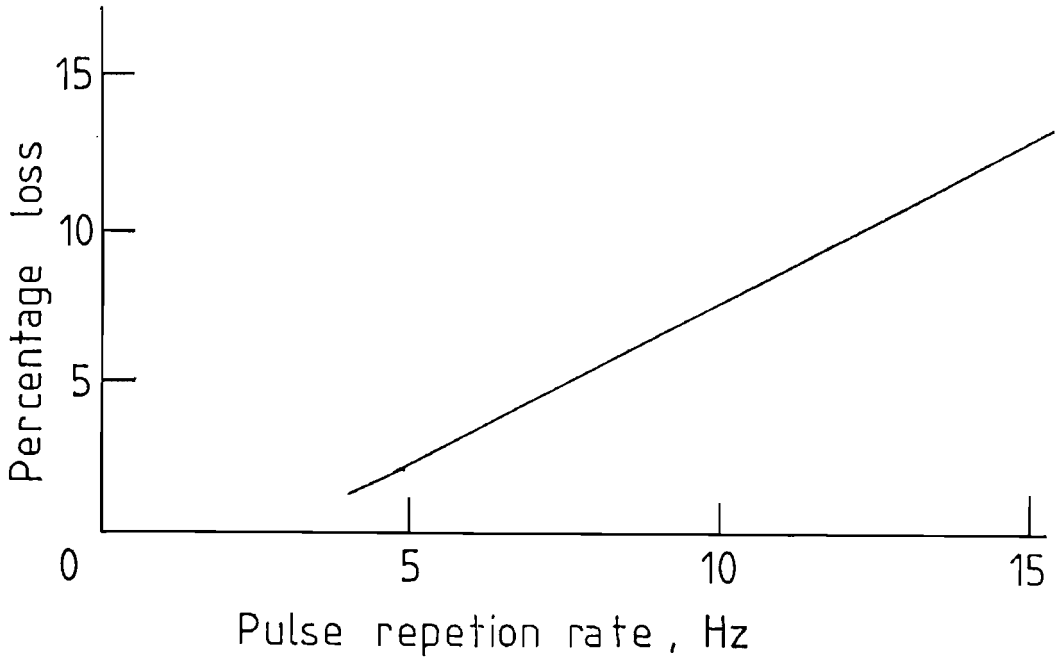

Figure 5.22 *Depolarisation loss versus pulse repetition rate for the four pass amplifier.*

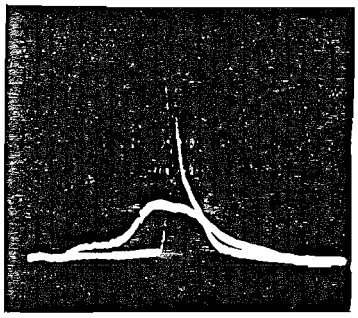

Figure 5.23(a) *Showing the relative positions of the depolarised signal in the absence of phase conjugation (SBS cell blocked) and the conjugated output signal, in the four pass amplifier.*

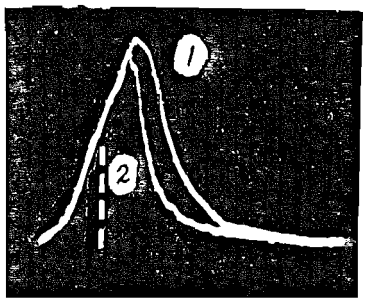

Figure 5.23(b) *The depolarised signal in the absence of,(1), or the presence of,(2), the phase conjugated signal, showing how the tail of the pulse is depleted in the latter situation.*

overlapped the tail end of the input signal in the amplifier, and would therefore deplete the inversion and reduce the gain for this part of the input over the first two passes. This was verified by looking at the depolarized signal when the conjugate signal was present and this is shown in Figure 5.23 (b) superimposed with the Gaussian. It can be seen that the tail of the depolarized signal is amplified much less on its two passes when the conjugate wave is making the third and fourth passes at the same time. Now this birefringence signal is proportional to the input to the SBS cell, so this is also the pulse shape incident on the cell. The reflected pulse also loses the front end up to the dotted line in Figure 5.23 (b), and this shape is very similar to the reflected pulse observed in Figure 5.19 (b). (That this shape is similar to the output of the two pass amplifier suggests that a similar process may have been occuring then). Thus there are three pulse shortening mechanisms in operation: the leading edge of the input is lost in setting up the SBS process; the reflected pulse is shortened in the saturated amplifier and, at the same time, depletes its own trailing edge.

The depolarization loss of Figure 5.22 is close to that for the equivalent arrangement of Faraday rotator and plane mirror used in the two-pass arrangement, and it occurs because rays retrace their paths less exactly through the amplifier as it lenses more strongly. To try and compensate for this and improve the beam quality, a lens was inserted into the ring to partially compensate for the thermal lensing of the amplifier rod. A calculation using ray transfer matrices shows that, if the distance from the amplifier rod of focal length f_R round the ring and back is 2d, then the focal length f required to give a parallel reflected beam for parallel input is $f = (d - f_R)/2$. At 15 Hz repetition rate

$f_R \simeq$ 2.7m (from equations 3.32, 3.33), so f = -1.18m. The closest available lens was f = -1m. This reduced the birefringence loss from 13% to 6.5% and improved the beam quality, which is shown by the burn marks in Figure 5.21. Not being anti-reflection coated it also reduced the output energy somewhat.

To summarize the performance of the four pass amplifier we note that it produced 350 mJ of diffraction limited output in a 6 ns pulse, giving a beam brightness 16 times that of the two pass amplifier used without phase conjugation. The phase conjugator is essential for the operation of the four-pass arrangement.

5.5. Two-pass amplifier scheme incorporating four-wave Brillouin mixing

We have seen from other workers' reports (see Section 4.5.5.) that a depolarized pump is not, in general, accurately phase conjugated in stimulated scattering. The evidence of the results from the two-pass amplifier (Section 5.3.3.) does not contradict this, but it is difficult to isolate the effects of depolarization from other possible causes of imperfect conjugation. In the four-pass amplifier arrangement uniform polarization is presented to the SBS cell but, if the birefringence compensation is not complete, part of the beam is lost before conjugation takes place. By setting up a laser system incorporating a four-wave mixing scheme along the lines of Basov et al (1978) it was hoped to reduce the depolarization loss even below the 5% (at 15 Hz repetition rate) already achieved. In this scheme the light after the first amplifier pass is separated into two orthogonal components using a polarizer, one of which is rotated by 90^0, and then the two components, having the same polarization, are conjugated together.

5.5.1. The experimental arrangement

Previous experimenters have used a waveguide for mixing the two inputs, but it was decided that, initially, the usual methane cell would be tried with the two beams focussed together. If the reflectivities for both beams were the same (they may not necessarily have been, however) then the losses in each beam path would have to be equal. Provision was also made for some variation in the ratio of energies in the two beam components. The set up is shown in Figure 5.24. The energy ratio between the horizontal and vertical polarization components was varied by rotation of half wave plate 'A', the Faraday rotator giving 45^{o} of rotation per pass. The components were split at polarizer P2, and the horizontal component rotated by 90^{o} by half wave plate 'B'. The vertically polarized beams were then directed via prisms 'X' and 'Y' (with 60^{o} angles) and polarizer 3 through the optics which focussed them at the centre of the cell. After reflection the process was reversed and the output appeared from polarizer 1. The focussing optics consisted of a telescope giving beam reduction of 1.7, followed by a 1m focal length lens. By placing the lens 50cm from the cell, it was possible to squeeze both beams through the window and still focus them at the cell centre. The spot size on the window was 1.3mm, giving a maximum mean power density of 120 MW cm^{-2}, still comfortably below the damage threshold.

5.2.2. Results and Discussion

To begin with, the system was set up with half wave plate 'A' orientated to give approximately equal intensity beams into the SBS cell. This was a demanding test of the four wave mixing scheme, because both beams were well

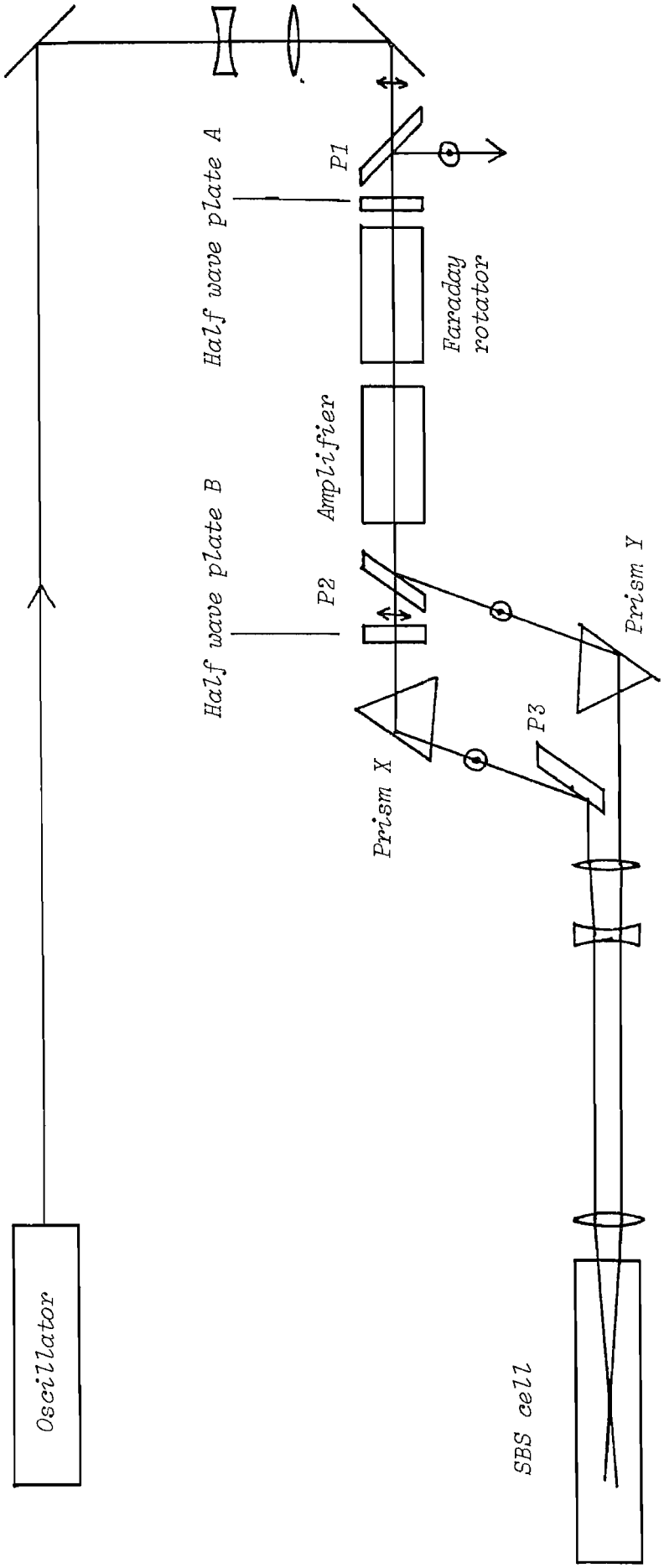

Figure 5.24 Two pass amplifier scheme incorporating four-wave Brillouin mixing.

above the threshold intensity, and therefore capable of being phase conjugated independently. The behaviour of the system was evaluated by monitoring the temporal shapes of both the output pulse and the pulse returning towards the oscillator (via a beam splitter) due to depolarization. The overlap of the beams at their focus was first set up without the SBS cell in place. After the cell was put back, fine adjustments were made to prism 'Y' while watching the pulse shapes.

The laser output when the beams did not overlap is shown in Figure 5.25 (a) and shows wide, apparently random, variation from shot to shot, the maximum energy being roughly four times the minimum energy. Figure 5.25 (b) shows the corresponding depolarization signal which has a larger fractional variation.

These observations can be explained as follows. The input beam, after passing through the Faraday rotator, is plane polarized at 45^{o} to the horizontal, so is split into two equal horizontal and vertical components which are in phase. These components are conjugated independently and then return to the Faraday rotator. In order to be extracted as output, these components must return in phase to again give the same plane 45^{o} polarization, as well as being accurately conjugated. If they do not return in phase, then the energy will be split between the output beam and the beam returning to the oscillator. For a phase difference of π all the energy would return towards the oscillator and there would be no output, assuming perfect phase conjugation. Since the two beams are conjugated independently,there is no reason why they should retain their initial phase relationship. The large variation in output energy confirmed that the phase between the beams varied, although only up to a limited amount, because the energy

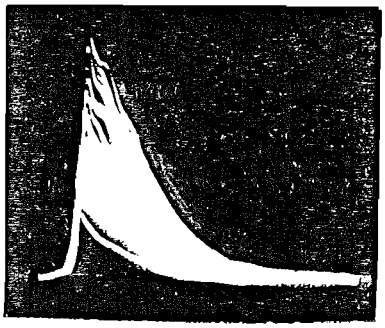

(a) *Output pulse, no overlap of the beams entering the SBS cell. 60 shots.*

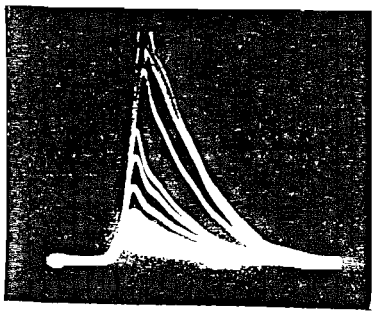

(b) *Depolarised pulse, no overlap of the beams entering the SBS cell.*

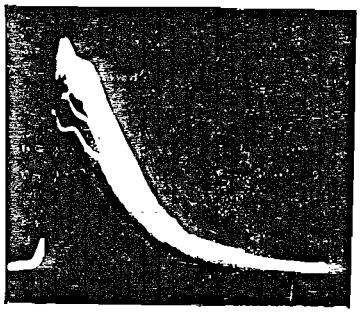

(c) *Output pulse with overlap of beams in the cell, 60 shots.*

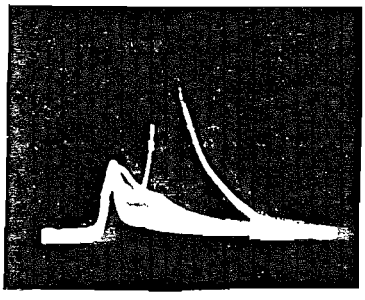

(d) *Depolarised pulse with overlap of the beams in the cell.*

Figure 5.25 *Pulse shapes seen in the four pass amplifier with the four wave Brillouin mixing scheme, with equal intensity beams entering the SBS cell.*

never dropped below a certain level (in other words it wasn't completely random). The pulse returning to the oscillator showed larger fractional variation, because it dropped to a very low level when the two beams were in phase and nearly all the energy appeared as output. The maximum pulse energy returning to the oscillator contained ~75% of the total energy, when the two beams were at their largest phase difference. The constant pulse shape implies that, although the initial phase difference varies, the phase difference during the rest of the pulse is constant.

Figure 5.25 (c) and (d) show the output pulse and depolarized pulse when the two beams overlap at the focus. For this case most of the energy appeared as output on the majority of shots, but approximately 20% of pulses had reduced energy, falling to roughly half the maximum. Correspondingly, the depolarized pulse contained little energy (estimated at 10% of the total energy) on most shots, but for ~ 20% of the time was of higher energy, occasionally up to ~ 50% of the total. Additionally, this pulse showed temporal modulation. These results suggest that, for most of the time, the phases of the two beams reflected from the SBS cell remained locked together, but sometimes they were out of phase, and that when this happened the phase also varied during the pulse. Since both beams were capable of reaching threshold independently, it is not surprising that their phase relationship was sometimes lost - this might happen for example if SBS took place before the overlapping foci in one or both beams. If SBS occurred at the foci as well, where the beams interacted, this could account for a phase change during one or both reflected pulses. The resulting temporal modulation was more prominent on the depolarized signal than the output, because the former was of lower energy.

Although the scheme did work for some of the time, it was certainly not reliable enough. It was altered to give one strong and one weak input to the cell which, it was hoped, would give better performance.

The half wave plate 'A' was re-orientated so that the light emerging from the amplifier after the first pass was predominantly horizontally polarized with a small fraction (5% at a repetition rate of 15 Hz) in the vertical polarization due to amplifier birefringence. Thus the input to the cell consisted of a strong beam (via prism X), roughly Gaussian in transverse profile, with a weak beam (via prism Y) having four lobes characteristic of such a birefringence signal.

The strong beam was first blocked, and a beam splitter was temporarily placed in the weak beam before it entered the cell, to monitor the weak reflection. It was found that this beam was below the threshold for SBS. However, when the strong beam was allowed to enter the cell, the weak beam <u>was</u> reflected. Thus, four wave Brillouin mixing was taking place.

The beam splitter was removed and, as before, the output and depolarized pulses were observed after the double pass. These are shown in Figure 5.26 (a) and (b). The output stability was much improved. The depolarized pulses in 5.26 (b) are with the weak beam blocked (1) and then with it entering the SBS cell (2). They illustrate very convincingly the working of the scheme, even though it was not perfect. When the weak beam was present <u>more</u> energy was incident on polarizer 1 after the second amplifier pass, but <u>less</u> energy was transmitted by it in the wrong polarization. The reduction in loss was by roughly a factor of two, down to a measured value of 2%. When the weak beam was blocked, the depolari-

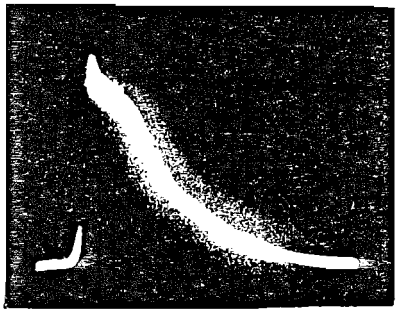

(a) Output pulse, 80 shots superimposed.

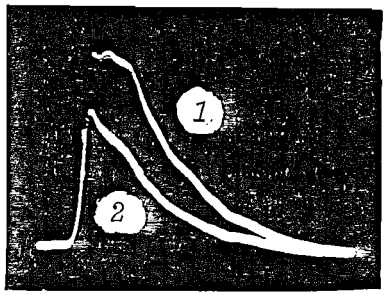

(b) Signal returning towards the oscillator
1 With weak beam blocked
2 With weak beam present.

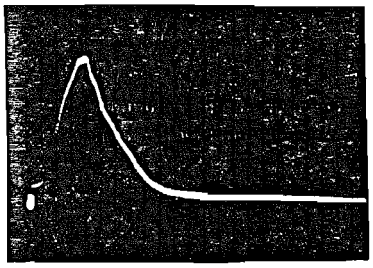

(c) Weak pulse reflected from the SBS cell.

15 ns

Figure 5.26 Pulse shapes seen in the two pass amplifier with the four wave Brillouin mixing scheme, with one weak and one strong beam entering the SBS cell.

zation loss was measured as 5%, which is close to the single pass birefringence loss. This was to be expected, since linearly polarized light was incident on the amplifier for the second pass. The amplitude variation on the depolarized pulse was ~10%. The improved output stability of the laser was because the weak beam could only be phase conjugated in the overlap region where it had a definite phase relationship to the strong beam - the beams could not be conjugated independently.

The output energy from this laser was 230 mJ, of which 95% was measured to be in the diffraction limited part. It is anticipated that this energy could be increased, using AR coated prisms, or mirrors, in place of the uncoated prisms X and Y. The beam quality is shown in Figure 5.27. The burn marks showed slight modulation in the near field, but the diode array profiles are extremely smooth, both in the far and near fields.

The less than perfect performance of the birefringence compensation in this laser was, it was suspected, due to limited overlap of the two beams in the SBS cell. This raised many questions regarding the effect of the length of the overlap region, its transverse dimensions, the tightness of focussing, the effect of time delay between the strong and weak pulses and the possible use of waveguides.

Observation of the weak pulse reflected from the cell (Figure 5.26 (c)) showed that it differed slightly in shape from the strong pulse, having a less steep rising edge. A possible reason for the less efficient conjugation of the weak beam was that, having originated from birefringence in the amplifier, it had a weak central part and strong edge lobes, giving poor overlap

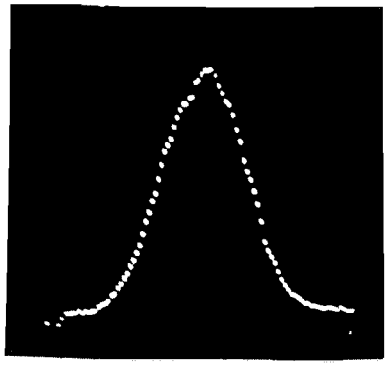

Near field

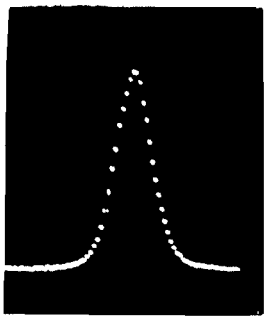

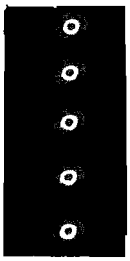

Far field

Figure 5.27 *Near field and far field profiles and burn marks for the two-pass amplifier with four-wave Brillouin mixing.*

with the strong beam, which had a strong central spot and weaker wings. By changing the relative transverse dimensions of the two beams, it was hoped that the effective overlap volume of the two beams could be increased, leading to better conjugation of the weak beam. The set up for this is shown in Figure 5.28. Each beam is provided with its own focussing optics. Had the beams both been Gaussian, the spot sizes at the foci would have been 150μm via prism X and the 50cm lens, and 300 μm via prism Y and the 1m lens. By rotating the half wave plate A it was possible to make either of the beams strong, with the other weak.

The result of this experiment was somewhat unexpected. When the strong beam was focussed less tightly (i.e. to a larger waist size) than the weak beam, no conjugation of the weak beam occurred at all. However, when the strong beam was focussed more tightly, conjugation of the weak beam did occur, and the depolarization loss of the system dropped to a measured value of less than 2%.

Thus it would seem that the focussing conditions are important. At present there is no explanation for the behaviour described above and further experiments are planned to elucidate it.

A further possibility is the application of the four wave Brillouin mixing scheme to a four-pass amplifier arrangement.

To summarise this section, we note that the four wave Brillouin mixing scheme, when applied to the two pass amplifier, further improved the beam quality to give 95% of the output in the diffraction limited part, with smooth beam profiles in the near as well as the far field; and reduced the double pass birefringence loss to 2% at the maximum input pump power.

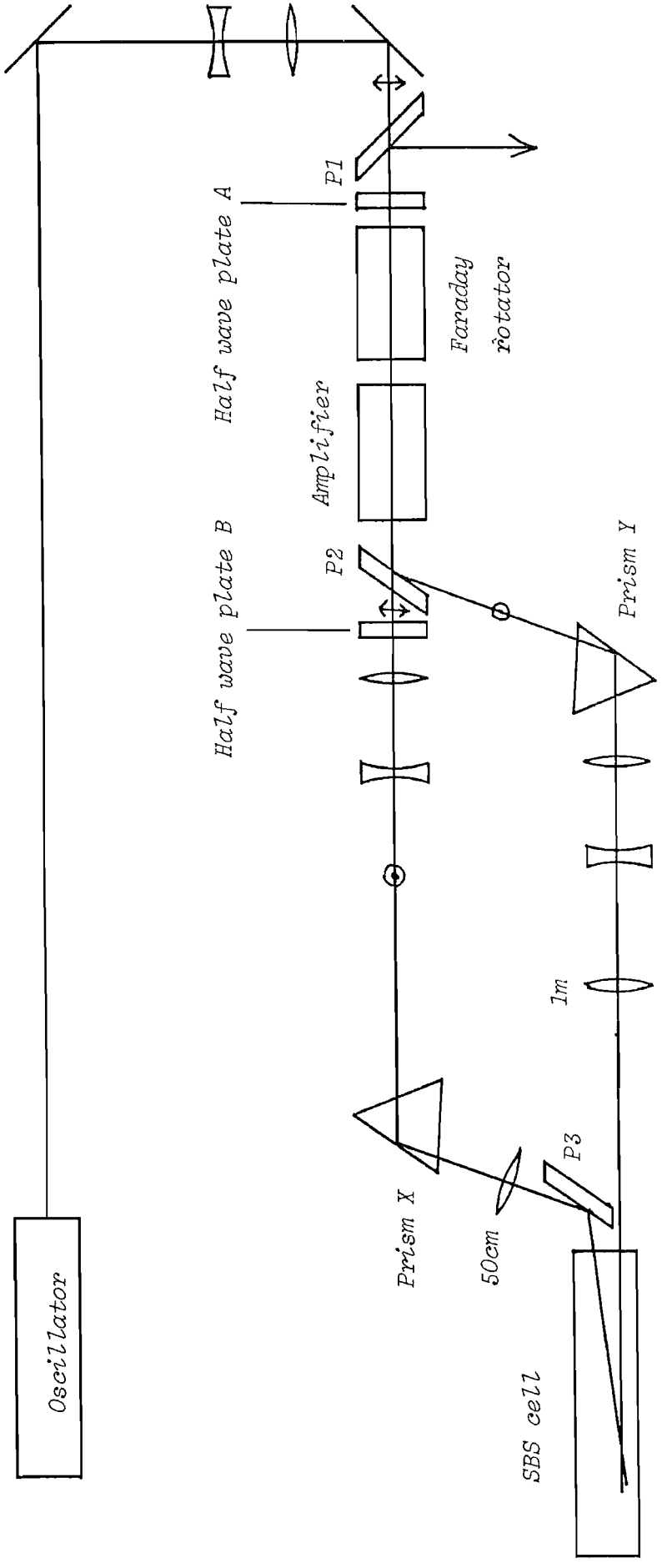

Figure 5.28 Two pass amplifier incorporating four-wave Brillouin mixing, with different focussing conditions for the two beams entering the SBS cell.

CHAPTER 6

Conclusions

The work described in this thesis clearly demonstrates that phase conjugation via stimulated Brillouin scattering can be successfully and usefully applied to typical Nd:YAG oscillator/amplifiers suffering from moderate, but troublesome, beam aberrations. The improvements in performance are particularly apparent under conditions of high average input pump powers to the amplifier. A simple high pressure gas cell into which the beam is focussed is all that is required to give good phase conjugation and this has the added convenience of being easy to align.

For the two pass amplifier arrangement with a conventional mirror the beam was only slightly aberrated at pulse repetition rates of less than 5 Hz, having an irregular transverse profile but being essentially diffraction limited. It is therefore debatable whether the improvement in beam profile - although apparent - justifies the application of phase conjugation in this régime. At higher repetition rates, however, thermal distortions in the amplifier become sufficient to increase the divergence beyond the diffraction limit and the beam is seen to break up. Under these conditions the benefit of phase conjugation - giving a sixfold increase in beam brightness - is indisputable.

A further important conclusion is that the stimulated Brillouin scattering process does not introduce new frequency components or cause significant broadening when the pump beam originates from a single longitudinal mode oscillator. Thus, an oscillator/amplifier incorporating phase conjugation via this process retains its single mode performance. Where single mode operation is not a pre-requisite, good phase conjugation occurs even for a multimode pump having a linewidth up to 400 MHz under our experimental conditions. Hence an oscillator/amplifier beam with high spatial coherence is attainable without severe constraints being placed upon the temporal coherence of the oscillator output.

The depolarization loss associated with thermally induced amplifier birefringence was significantly lower when phase conjugation was employed than when a conventional mirror was used. At pulse repetition rates greater than 10 Hz this reduction was by a factor of four, dropping from 16% to 4% at the maximum rate of 15 Hz. Therefore, although phase conjugation of the depolarized pump was not perfect, it still gave a worthwhile improvement over the use of a conventional mirror. The depolarization loss can be further reduced, if desired, to $\sim 2\%$ at 15 Hz, using the four-wave Brillouin mixing scheme.

The value of phase conjugation becomes even more apparent in the case of the four-pass amplifier. Even at low repetition rates an increase in beam brightness by a factor of four was attained over the two pass amplifier incorporating a plane mirror. At the high repetition rates, this factor increased to sixteen.

It is anticipated that further improvements will be made to the performance of the oscillator/amplifier in the future, for example by using a waveguide for efficient beam overlap in the four wave Brillouin mixing arrangement. It is also anticipated that the phase conjugation schemes described in this thesis will be applied equally successfully to other types of laser, such as the ruby laser.

APPENDIX I

Optical and Quantum Electronics 15 (1983) 447–450

A prism reflector of anti-resonant ring configuration

I. D. CARR, D. C. HANNA
Department of Physics, University of Southampton, Highfield, Southampton, UK

Received 5 January 1983

Two identical prisms are combined to form an anti-resonant ring reflector, giving total reflection without the use of coatings or roof edges. When used as the total reflector in a Q-switched NdYAG laser this device has shown a damage threshold twice that of a multilayer reflector.

The concept of the anti-resonant ring interferometer first gained prominence in a laser context when, in 1972, Siegman [1] indicated a number of its potential uses. An early demonstration of its use was in cavity dumping [2]. More recently [3, 4] it has excited interest as a means of providing a colliding-pulse configuration, which has been shown to possess advantages in passive mode-locking [5]. It is interesting to note that McGeoch, in 1970 [6], had used a prism reflector device based on the anti-resonant ring principle and had, in addition, exploited its colliding-pulse configuration in a mode-locked ruby laser. The primary motivation behind McGeoch's prism reflector design was the need to overcome damage limitations imposed by multilayer dielectric reflectors while avoiding also the disadvantages of internal reflection at a prism roof-edge. Subsequent improvements in the power handling capability of multilayer coatings then diminished the attractions of this prism reflector. Recently, however, Vanherzeele [7] has drawn attention to the possibility of using the McGeoch prism reflector to provide a compact device suitable for a colliding pulse mode-locking set-up. Our own re-examination of this prism reflector has been motivated in part by a renewed interest in reflectors of high damage threshold since the output power capability of a Q-switched TEM_{00} mode NdYAG laser employing a telescopic resonator [8–10] is determined by damage to the reflector in the contracted beam.

We describe here the design and performance of a modified version of the McGeoch reflector. We have confirmed by measurement that it has a damage threshold twice that of a multilayer reflector when used as the total reflector of a Q-switched NdYAG laser. An important difference from the McGeoch design is that the beam splitting surface does not involve frustrated total internal reflection (FTIR) to achieve the required 50% reflectivity and the device can therefore be realized with less exacting requirements on the prism spacing*. In fact, this increased design freedom suggests other possibilities, such as controllably varying the prism spacing and thus achieving a reflectivity adjustable between zero and 100% for any wavelength within the transmission range of the prism material.

The basic arrangement of an anti-resonant ring is shown in Fig. 1. The beam splitter divides the incident beam into two counter-propagating beams which then recombine at the beam splitter. The transmitted beam is the superposition of a contribution from the clockwise circulating beam, which undergoes two reflections at the beam splitter (one from each side) and a contribution from the anti-clockwise beam which undergoes two transmissions through the beam splitter. These two contributions to the transmitted beam are therefore in exact antiphase, regardless of the angle of incidence at the beam splitter. Thus if the beam splitter has 50% power reflectivity the counter-

*We note that Vanherzeele has also chosen, like McGeoch, the more exacting option of using FTIR at the beam splitter interface.

0306-8919/83 $03.00 + .12

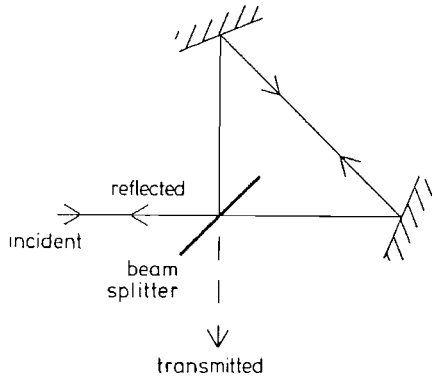

Figure 1 The anti-resonant ring.

propagating beams are of equal intensity, the transmitted beam is therefore of zero intensity, and the reflected beam carries all the incident power. The arrangement in Fig. 1 can be realized in a number of ways, using two identical prisms. Fig. 2a shows the design we have tested. The required 50% reflectivity at the beam splitter (which now consists of the two adjacent prism faces) can be achieved for a range of angles of incidence at the beam splitter. In fact the two faces act as a Fabry–Perot interferometer and given the angle of incidence one simply has to choose the appropriate spacing d (or vice versa) to achieve 50% reflectivity. It is also possible to use angles of incidence greater than the critical angle and thus involve FTIR. This is not necessary however since 50% reflectivity can be obtained from uncoated prism faces, for angles less than the critical angle, and the antiphase property remaining the same as for FTIR. The advantage of working at less than the critical angle is that the prism spacing can be much larger (and hence achieved more conveniently) than for FTIR. In fact one can exploit the interference behaviour of the beam splitter faces, whereby the reflectivity is the same for values of d differing by an integral multiple of $\lambda/2 \cos\theta$ where θ is the angle of incidence in the air gap between the prism. We have also used this interference behaviour to arrange for zero reflectivity where the beams cross the beam splitter at normal incidence, choosing $d = \lambda = 1.06\,\mu$m, this being the operating wavelength of the laser at which the 100% reflectivity was devised. Having chosen d, the angle of incidence at the interface was determined ($\theta = 40.56°$, the prism material being BK7 glass) and this in turn fixes α (6.98°, since a Brewster angle input was required) and β (110.28°).

The construction of this device calls for two identical prisms with all the reflecting faces arranged perpendicular to one plane. A single prism was first made (Fig. 2b) with the angles α, β as specified (tolerance ±1 min) and the bases ABCD, A′B′C′D′ perpendicular to the reflecting faces (tolerance ±2 sec on perpendicularity). This prism was then cut in half (along plane A″B″C″D″) and the bases ABCD, A′B′C′D′ placed in contact with the surface of an optical flat. To provide the correct prism spacing two thin strips of dielectric were evaporated onto the longest face of one prism (Fig. 2b) leaving the centre of the face clear. The entire assembly was then mounted in a conventional mirror mount having micrometer angular adjustments

The following tests were carried out to assess the performance of the reflector. First a visual observation was made of any fringes resulting from

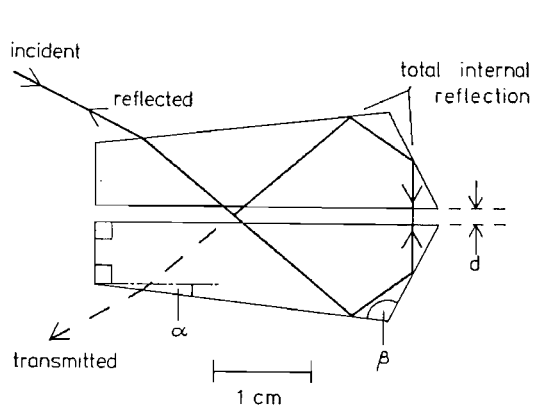

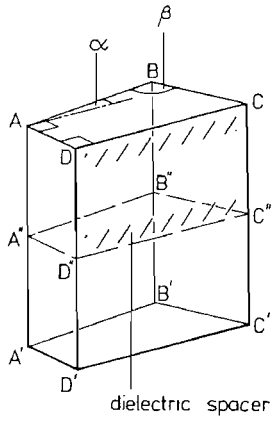

Figure 2 (a) A scale drawing of the actual reflector which was constructed and tested; $\alpha = 6.98°$, $\beta = 110.28°$, and $d = 1.06\,\mu$m (nominally). (b) Method of fabricating the identical prisms for the reflector.

imperfect parallelism between the beam splitter faces and between the prism bases ABCD, A′B′C′D′ and the optical flat. For the beam splitter faces excellent parallelism was easily achieved with no fringes visible across the face (of sides DC = 35.5 mm, CC″ = 15.0 mm). The parallelism between the prism bases and the optical flat to which they were contacted was found to be less good and it was estimated that the two prism bases were as much as 5 sec out of parallelism. The origin of this lack of parallelism is not certain, although it is probably due to imperfect contact with the optical flat. However, it does not appear to have significantly degraded the reflector performance. The reflectivity was measured in two ways: (1) using for the incident beam the horizontally polarized TEM_{00} output from a NdYAG laser, and (2) using the device as one of the reflectors of a NdYAG laser. In the first method the prism was aligned for retroreflection and a beam splitter was used for monitoring the incident and reflected beams. This measurement was of limited accuracy, but confirmed that the reflected beam had an intensity of $> 95\%$ of the incident beam. A small output was observed in the direction of the transmitted beam, $\sim 1\%$ of the incident beam and this was found to consist mostly of light polarized perpendicular to the plane of polarization of the incident light. These results suggest the presence of some strain-induced birefringence. In the second more accurate method, a measurement of threshold was made with the prism used as one reflector of a NdYAG laser, and a comparison with the threshold for a multilayer total reflector indicated a reflectivity of $> 99\%$.

To check the power handling capability of this reflector tests were made with a Q-switched NdYAG laser having a telescopic resonator configuration, the reflector being in the contracted beam [9]. The resonator dimensions differed somewhat from those of [9]; the rod diameter was 6 mm, the beam expansion telescope had x 3 magnification and the spacing between the telescope and the prism reflector was 0.35 m. The laser output was taken from the expanded beam end of the resonator, using a single uncoated glass surface as the output. Under these conditions it was found that a multilayer dielectric mirror used as a total reflector in the contracted beam would damage when a TEM_{00} output of 105 mJ was reached. This corresponded to a measured 26 mJ incident on the total reflector in a pulse of 25 ns duration with a beam of spot size $W_0 = 0.39$ mm. By contrast the prism reflector allowed a TEM_{00} output of 185 mJ to be reached before damage occurred. The energy incident on the reflector under these conditions was measured to be 47 mJ, i.e. approximately twice that which the multilayer mirror could sustain. The damage manifested itself as a very small speck at the interface where the beam division occurs. The vulnerability to damage at this location is probably a consequence of the standing waves formed at this interface [11].

The prism design of Fig. 2a is just one of a number of possibilities. McGeoch [6] and Vanherzeele [7] have used an arrangement where one has access to the location where the counter-propagating beams cross from one prism to the other (having exited from Brewster angle faces) as in Fig. 3. A passive mode-locking cell can then be placed at this location to allow colliding pulses. A further advantage of this prism arrangement is that it suppresses reflections where the beams cross. (If these are not suppressed then one cannot ensure equal amplitude counter-propagating waves recombining at the interface.) In our design the reflections were suppressed by using an appropriate choice of the interface spacing, however if one is free from this design constraint then one can consider the possibility of a variable spacing between the two prisms, controlled for example by piezoelectricity.

Such spacing control is made much more practical by avoiding the exacting requirements on spacing that are implied by FTIR beam splitting. By ranging the spacing the reflectivity can be adjusted, at any operating wavelength, from zero

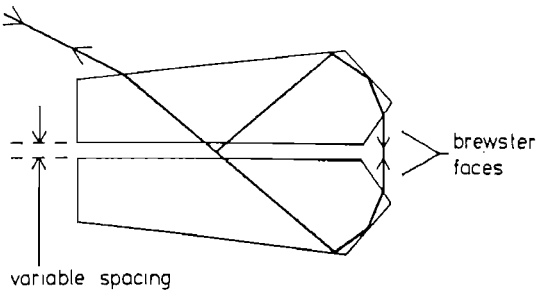

Figure 3 A reflector design tunable over the transmission range of the prism material.

to 100%. The range of operating wavelengths is determined by the transmission range of the prism material. Thus in the case of fused silica this would offer a tunable reflectivity from the UV to the near IR with a damage threshold in excess of that offered by multilayer reflection.

In conclusion we have constructed and tested an anti-resonant ring prism reflector of high reflectivity and high damage threshold. Used as the total reflector in a telescopic resonator it has allowed 150 mJ TEM_{00} output to be reliably achieved in a Q-switched NdYAG laser. Damage to the prism did not occur until the output energy reached a level of 185 mJ. The damage threshold under these conditions is approximately twice that of the best available multilayer reflector. By avoiding reliance on frustrated total internal reflection at the beam splitter interface a greater design freedom is achieved, and by providing a variable gap between the prisms this device could offer a reflectivity which is controllably variable between zero and 100% for any wavelength within the transmission range of the prism material.

Acknowledgements

This work has been supported in part by the SERC and by Marchwood Engineering Laboratories. I. D. Carr holds a CASE studentship, sponsored by MEL. We also wish to acknowledge I.C. Optical Systems for carrying out the prism construction and J.K. Lasers Ltd for the deposition of the dielectric spacer.

References

1. A. E. SIEGMAN, *IEEE J. Quant. Elect.* QE-9 (1973) 247–50.
2. R. TRUTNA and A. E. SIEGMAN, *ibid.* QE-13 (1977) 955–62.
3. A. E. SIEGMAN, *Opt. Lett.* 6 (1981) 334–5.
4. H. VANHERZEELE, J. L. VAN ECK and A. E. SIEGMAN, *Appl. Opt.* 20 (1981) 3484–6.
5. R. L. FORK, B. I. GREENE and C. V. SHANK, *Appl. Phys. Lett.* 38 (1981) 671–2.
6. M. McGEOCH, *Opt.-Elect.* 2 (1970) 85–9.
7. H. VANHERZEELE, *Rev. Sci. Instrum.* 53 (1982) 1095–6.
8. P. H. SARKIES, *Opt. Commun.* 31 (1979) 189–91.
9. D. C. HANNA, C. G. SAWYERS and M. A. YURATICH, *ibid.* 37 (1981) 359–62.
10. *Idem, Opt. Quant. Elect.* 13 (1981) 493–507.
11. N. L. BOLING, M. D. CRISP and G. DUBÉ, *Appl. Opt.* 12 (1973) 650–60.

APPENDIX II

Losses and intensity - length products for waveguides versus tight focussing

To maximise the gain $G = gIL$ in stimulated scattering, the product IL can be made very large by using a waveguide instead of focussing the beam. It is useful to know the expected gain enhancement as a function of waveguide dimensions and beam parameters.

The product IL for a focussed Gaussian beam may be approximated by the product of intensity at the waist and the confocal parameter b:

$$IL \simeq \frac{P}{\pi w_o^2} \cdot b \qquad \text{II.1.}$$

where P is the power. For an $M\times$ diffraction limited beam the divergence angle is $\theta' = M\lambda/\pi w_o$ and the confocal parameter is given by $b\,\theta' = 2w_0$, i.e. $b = \frac{2\pi w_o^2}{M\lambda}$. The intensity-length product is therefore approximately

$$IL \simeq \frac{2P}{M\lambda} \qquad \text{II.2.}$$

To calculate the intensity-length product for a waveguide, it is necessary to know the loss. If a beam with divergence $M\theta_0$ is focussed to a radius 'a' at the entrance to a guide of diameter D and length L, the loss l is (D.C. Hanna, personal communication; Marcatili and Schmeltzer, 1964)

$$l \simeq \frac{M^2\lambda^2 L}{a^2 D} \qquad \text{II.3.}$$

If the input power is P, the output power from the far end of the guide is P (1-l). If l is small, then the mean power is approximately:

$$P_m = \frac{1}{2}\left[P + P(1-l)\right] = \frac{P}{2}(2-l)$$

$$= \frac{P}{2}\left(2 - \frac{M^2\lambda^2 L}{a^2 D}\right) \qquad \text{II.4.}$$

The intensity length product is then:

$$IL = \frac{4 P_m L}{\pi D^2} = \frac{2PL}{\pi D^2}\left(2 - \frac{M^2\lambda^2 L}{a^2 D}\right) \qquad 11.5.$$

The enhancement ratio $\mathcal{E} = \frac{IL\ (waveguide)}{IL\ (focussing)}$ is therefore:

$$\mathcal{E} = \frac{M\lambda L}{\pi D^2}\left(2 - \frac{M^2\lambda^2 L}{a^2 D}\right) \qquad 11.6.$$

If the loss l is negligible this becomes:

$$\mathcal{E} = \frac{M\lambda L}{\pi D^2} \qquad 11.7.$$

APPENDIX III

Depolarization loss when double-passing an amplifier using a plane mirror and a quarter wave plate

The experimental arrangement is shown in Figure A3.1(a), and its equivalent single pass geometry in Figure A3.1(b). The input field E_{ix} is horizontally polarized in the xz plane. The transmitted loss is found by calculating the transmitted field E_t, and integrating this over the rod cross section for a plane wave (representing a multimode beam) or for a TEMoo Gaussian beam.

We calculate the transmitted field E_t using Jones matrices (see Gerrard and Burch, 1975). E_t is given by $E_t = ME_i$, where E_t and E_i are column vectors containing the x and y components and M is a 2 x 2 matrix describing the system. If B, C, D...N are the matrices for the individual components of the system, then M = N..DCB. The Jones matrices for each component are:

Polarizer transmitting the horizontal (xz plane) polarization:

$$P = \begin{bmatrix} 1 & 0 \\ 0 & 0 \end{bmatrix} \qquad \text{III.1.}$$

Birefringent plate causing phase shift δ between the fast axis (orientated at an angle θ to the x axis) and the slow axis:

$$A = \begin{bmatrix} c^2 + s^2 e^{-i\delta} & cs(1 - e^{-i\delta}) \\ cs(1 - e^{-i\delta}) & c^2 e^{-i\delta} + s^2 \end{bmatrix} \qquad \text{III.2.}$$

where $s = \sin\theta$, $c = \cos\theta$. This represents the amplifier, for which θ and δ are functions of position in the cross-section (see Figure 3.3).

Half wave plate with principle axes at 45^0 to the horizontal:

$$H = \begin{bmatrix} 0 & 1 \\ 1 & 0 \end{bmatrix} \qquad \text{III.3.}$$

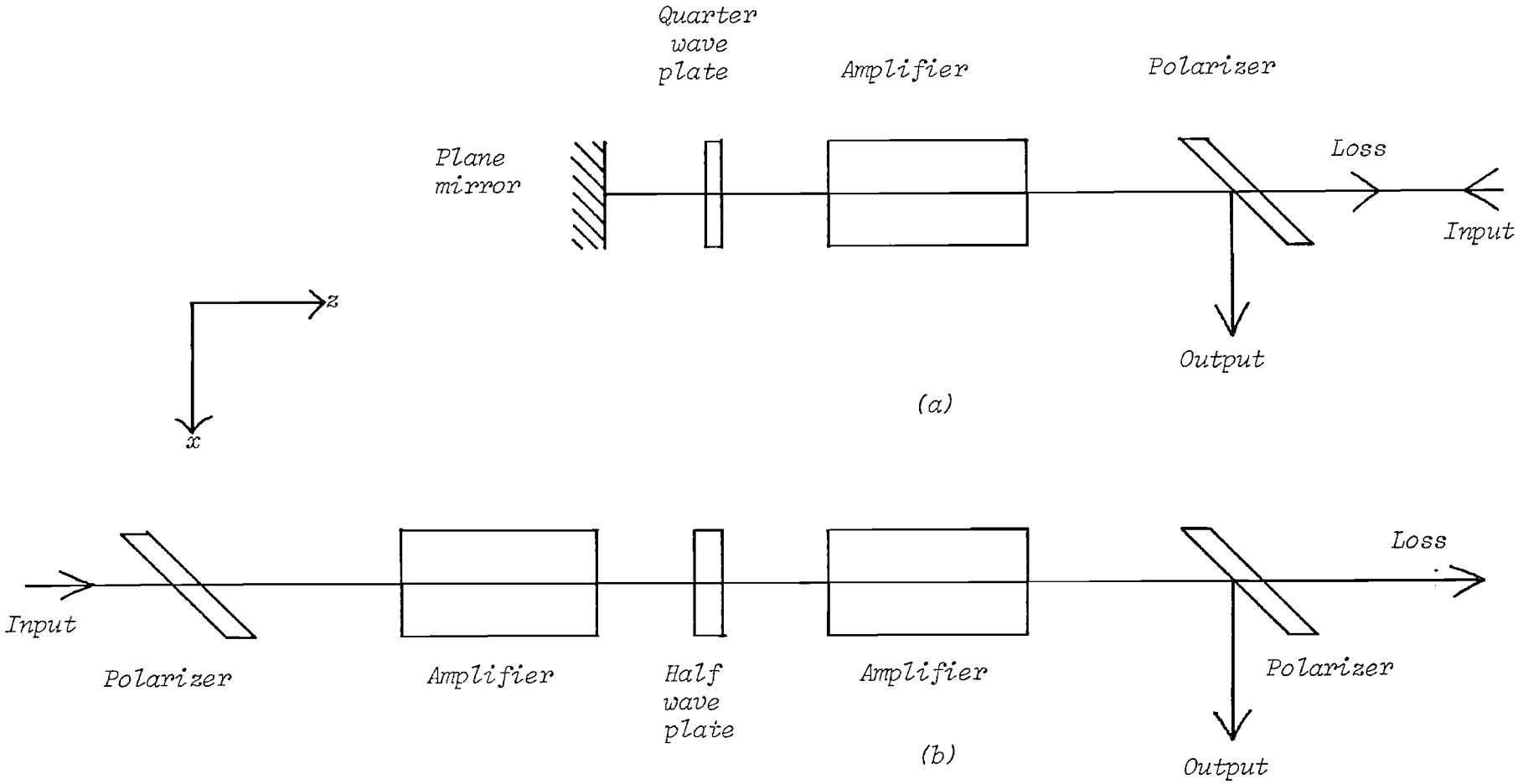

Figure A3.1 *The experimental arrangement for double passing an amplifier using a plane mirror and quarter wave plate, (a), and the equivalent unfolded arrangemant (b).*

The total matrix for the system is thus:

$$M = PAHAP \qquad \text{III.4.}$$

After performing the algebra we find that:

$$M = \begin{bmatrix} 2cs\,(1-e^{-i\delta})(c^2+s^2e^{-i\delta}) & 0 \\ 0 & 0 \end{bmatrix} \qquad \text{III.5.}$$

The input field is $E_i = \begin{bmatrix} E \\ 0 \end{bmatrix}$ so the output is

$$E_{out} = M \begin{bmatrix} E \\ 0 \end{bmatrix} = E_x \quad , \qquad \text{hence}$$

$$\frac{E_x}{E} = 2cs\,(1-e^{-i\delta})(c^2+s^2e^{-i\delta}) = E_1 \qquad \text{III.6.}$$

The loss is then given by $E_1E_1^*$ integrated over the cross section of the rod.

It turns out that

$$E_1E_1^* = (2c^4s^4 - c^6s^2 - c^2s^6)(8\cos\delta - 8) + 16\,c^4s^4\sin^2\delta \qquad \text{III.7.}$$

Re-writing equation III.7. only in terms of $\cos\theta$ makes it easier to integrate:

$$E_1E_1^* = 8(4c^8 - 8c^6 + 5c^4 - c^2)(\cos\delta - 1) + 16(c^8 - 2c^6 + c^4)\sin^2\delta \qquad \text{III.8.}$$

The depolarization loss L is given by:

$$L = \frac{1}{\pi r_o^2} \int_{\theta=0}^{2\pi} \int_{r=0}^{r_o} E_1E_1^*\, r\,dr\,d\theta \qquad \text{III.9.}$$

for a plane wave input, where r_o is the radius of the rod. Inserting III.8 in III.9 we have

$$L = \frac{8}{\pi r_o^2} \int_{\theta=0}^{2\pi} (4c^8 - 8c^6 + 5c^4 - c^2)\,d\theta \int_{r=0}^{r_o} (\cos\delta - 1)\,r\,dr$$

$$+ \frac{16}{\pi r_o^2} \int_{\theta=0}^{2\pi} (c^8 - 2c^6 + c^4)\,d\theta \int_{r=0}^{r_o} r\sin^2\delta\,dr \qquad \text{III.10.}$$

We saw in Chapter 3, equation 3.35, that the phase shift δ is proportional to r^2 :

$$\delta = k r^2 \qquad \text{III.11.}$$

where k is a constant for a given pump input power and rod radius.

Evaluating the radial and angular integrals gives the plane wave depolarization loss

$$L_{PW} = \frac{7}{16} - \frac{1}{4kr_o^2} \cdot \left[\sin(kr_o^2) + \frac{3}{8} \sin(2kr_o^2) \right] \qquad \text{III.12.}$$

To use this we need to know k. From equation 3.35 we have

$$kr_o^2 = C_T P_a \qquad \text{III.13.}$$

where $$C_T = \frac{2 n_o^3 \alpha C_B}{\lambda K} \qquad \text{III.14.}$$

and $$C_B = \frac{C_\phi - C_r}{2} = -0.0097 \quad \text{for Nd:YAG.} \qquad \text{III.15.}$$

P_a is the total heat power dissipated by the rod, which is proportional to the input pump power P_{in}:

$$P_a = \eta P_{in} \qquad \text{III.16.}$$

For Nd:YAG $\eta \simeq 0.05$. Inserting the material and rod parameters into III.13. and III.12. gives an expression for the plane wave loss as a function of pulse repetition rate R for our amplifier:

$$L_{PW} = 0.438 - \frac{0.877}{R} \left[\sin(0.285\,R) + 0.375 \sin(0.570\,R) \right] \qquad \text{III.17.}$$

To extend this theory to the case of a Gaussian TEMoo input beam, an extra radial term describing the input profile is inserted into III.9 and III.10. The field has the form:

$$E(r) = E_1 \exp\left(-\frac{r^2}{W^2}\right) \qquad \text{III.18.}$$

so that in equation III.9 the integrand is multiplied by N exp $(-r^2/w^2)$. N is a normalization constant defined by:

$$\int_{\theta=0}^{2\pi} d\theta \int_{r=0}^{r_o} N \exp\left(-\frac{2r^2}{w^2}\right) r\,dr = 1 \qquad \text{III.19.}$$

which, when evaluated, gives

$$N = \frac{-2}{\pi w^2}\left[\exp\left(\frac{-2r^2}{w^2}\right) - 1\right]^{-1} \qquad \text{III.20.}$$

(Note that for the plane wave the normalization constant was πr_o^2).

In equation III.10 the radial integrals are therefore modified to:

$$N\int_{r=0}^{r_o}\left[\cos\left(kr_o^2\right)-1\right].r\exp\left(\frac{-2r^2}{w^2}\right)dr \qquad \text{III.21.}$$

and

$$N\int_{r=0}^{r_o}\sin^2\left(kr_o^2\right).r\exp\left(\frac{-2r^2}{w^2}\right)dr \qquad \text{III.22.}$$

Performing these two integrals and inserting them in III.10 in place of the plane wave radial integral gives the TEMoo depolarization loss:

$$L_{oo} = \frac{-N\pi}{2}\left\{\frac{w^2}{2(4+k^2w^4)}\left[e^{-b}\left(kw^2\sin kr_o^2\right) - 2\cos\left(kr_o^2\right) + 2\right]\right.$$
$$\left. + \frac{w^2}{4}\left[e^{-b}-1\right]\right\}$$
$$+ \frac{3N\pi}{4}\left\{\frac{-w^2}{4(1+k^2w^4)}\left[e^{-b}\sin\left(kr_o^2\right)\left[\sin\left(kr_o^2\right)+ w^2k\cos\left(kr_o^2\right)\right]\right]\right.$$
$$\left. - \frac{k^2w^6}{8(1+k^2w^4)}\left[e^{-b}-1\right]\right\} \qquad \text{III.23.}$$

where $b = \frac{2r_o^2}{w^2}$; $N = \frac{-2}{\pi w^2}\left(e^{-b}-1\right)^{-1}$.

Equation III.23 is the final result. Note that as $k \to \infty$, both L_{PW} and $L_{oo} \to \frac{7}{16}$.

In the experiment the spot size W was set so that $2r_o = 3w$, so exp $(-\frac{2r^2}{w^2}) = 0.0111$. Putting all other relevant values into III.23 gives the TEMoo loss as a function of repetition rate R for the amplifier:

$$L_{oo} = -0.0112\left\{\frac{4.5}{4+0.0161R^2}\left[0.0111\left[0.127R\sin(0.285R) - 2\cos(0.285R)\right]+2\right] - 2.23\right\}$$

$$-0.168\left\{\frac{-2.25}{1+1.0161R^2}\left[0.0111\sin(0.285R)\left[\sin(0.285R)+0.127R\cos(0.285R)\right]\right] + \frac{0.0179R^2}{1+0.0161R^2}\right\} \qquad \text{III.24.}$$

Plots of equations III.17 and III.24 are shown in Figure A.3.2., together with the experimental results for the TEMoo input.

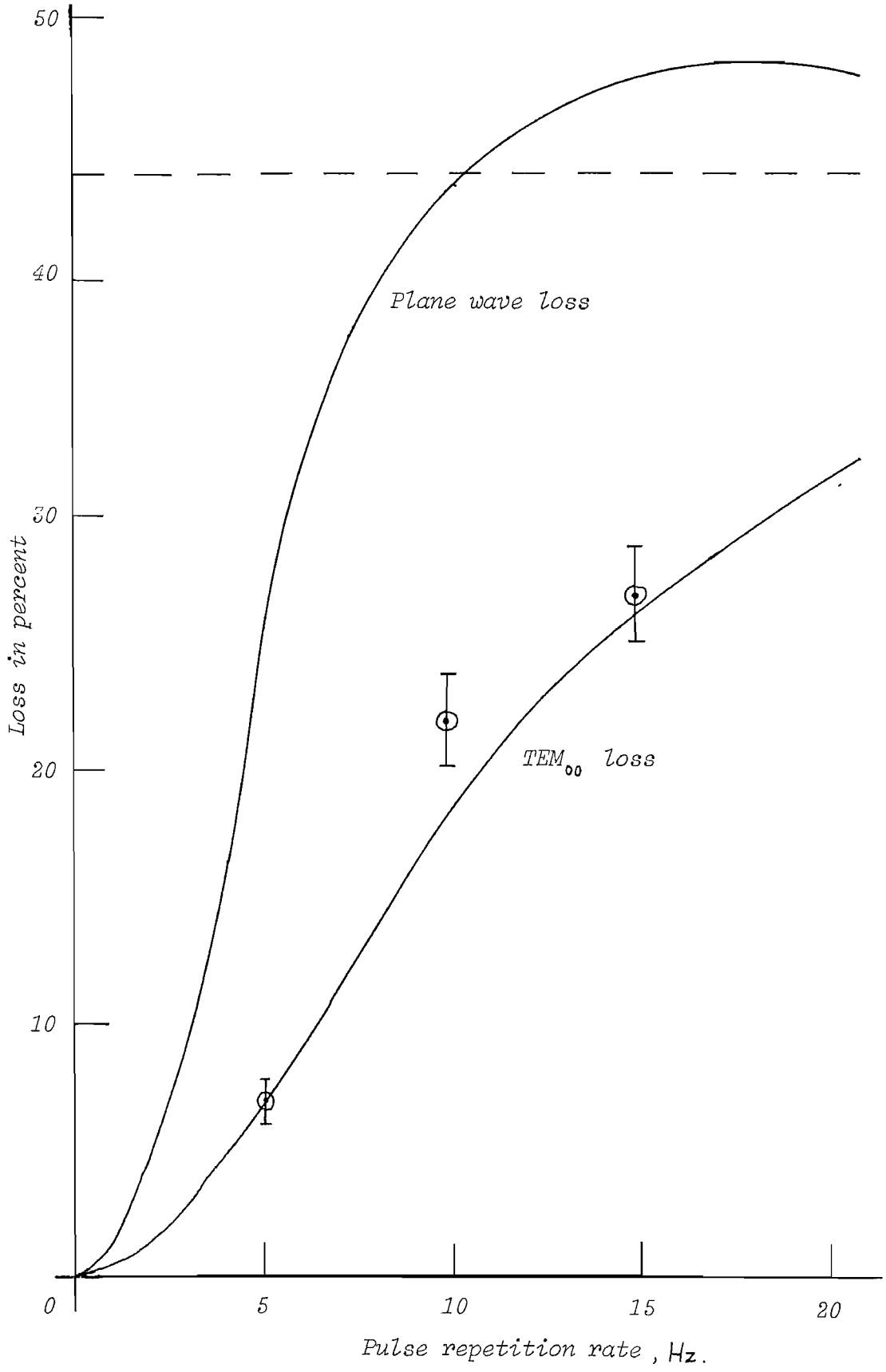

Figure A. 3 .2 *The birefringence loss in percent as a function of the pulse repetition rate for the amplifier double passed using a quarter wave plate and a plane mirror. Both curves tend assymptotically to the dashed line.*

APPENDIX IV

Laser pulse compression in a saturated amplifier

Below we estimate the expected compression of the pulse reflected from the SBS cell as it makes the third and fourth passes in the four pass amplifier. We approximate the reflected pulse shape by a plane wave square pulse of photon density n_o and duration τ (eqn 3.7). The amplified shape is then given by 3.11:

$$n_L(t) = \frac{n_o}{1-[1-\exp(-\sigma N_o L)].\exp(-\sigma\eta t/\tau)} \qquad \text{IV.1.}$$

To use this equation we need to know the initial population inversion N_o and the incident number of photons per unit area, $\eta = n_o c \tau$. We calculated the population inversion in Chapter 3, equation 3.17, for the maximum 100 J pump input, finding $N_{max} = 1{\cdot}1 \times 10^{18}$ cm^{-3}. Thus, at the usual 72 J pump energy, $N = 7.9 \times 10^{17}$ cm^{-3}, giving a stored energy in the 75cm x 9mm rod of ~800 mJ. Now N_o is the inversion remaining in the rod after the first and second passes. We can estimate this knowing firstly that 300 mJ were extracted after two passes with the SBS cell removed. Secondly, we note that when the SBS cell <u>is</u> in place, the reflected pulse arrives at the amplifier for the third pass at approximately the mid point of the input Gaussian pulse (see Figure 5.23(a)). Thus, at this time, only approximately half the 300 mJ quoted above has been extracted, i.e. ~150 mJ, leaving ~650 mJ in the rod, corresponding to an inversion of 7.1×10^{17} cm^{-3}. In fact, the inversion at the fourth pass will be lower than this, since energy is extracted on the third pass, so a more realistic working value for the third and fourth passes would be, say, $N_o \simeq 5 \times 10^{17}$ cm^{-3}. We take this value for an effective amplifier length of 15cm, this approximation being more straightforward than a calculation involving beams propagating in both directions at once in the amplifier.

To estimate η, we know that the efficiency of the SBS cell is ~0.5, so 150 mJ are reflected from it in a spot size of w = 3mm. The

number of photons per unit area is:

$$\eta \simeq \frac{E_i}{E_p \pi w^2} \qquad \text{IV.2.}$$

where E_i is the pulse energy and E_p is the photon energy. We find $\eta = 2.8 \times 10^{18}$ cm^{-2}.

The reflected pulse length was $\tau = 16$ ns, giving $n_o = \eta/c\tau = 5.8 \times 10^{15}$ cm^{-3}.

Inserting the values for N_o, η and n_o, and $\sigma = 3.5 \times 10^{19}$ cm^2 into IV.1 gives

$$\frac{n_L(t)}{n_o} = \left[1 - 0{\cdot}927 . \exp\left(-0{\cdot}061\, t\right)\right]^{-1} \qquad \text{IV.3.}$$

This curve is plotted in Figure A4.1. A significant approximation in the calculation is that the leading edge of the actual pulse rises in $\sim$ 2ns, not instantaneously as for the assumed pulse. Allowance for this would give a pulse duration of the order of 5 ns (see Figure A.4.1) which is close to the observed value of 6 ns. Another estimate for the expected pulse duration can be made by assuming only a third pass (and no fourth pass) through the amplifier of length 7.5cm, with the initial inversion $N_o = 7.1 \times 10^{17}$ cm^{-3}. Equation IV.1. then becomes

$$\frac{n_L(t)}{n_o} = \left[1 - 0{\cdot}840 . \exp\left(-0{\cdot}061\, t\right)\right]^{-1} \qquad \text{IV.4.}$$

giving a pulse duration of 6.5 ns, which is closer to the observed value. A further approximation, in addition to that of the pulse temporal shape, is that of a plane wavefront instead of the Gaussian transverse profile in the experimental situation.

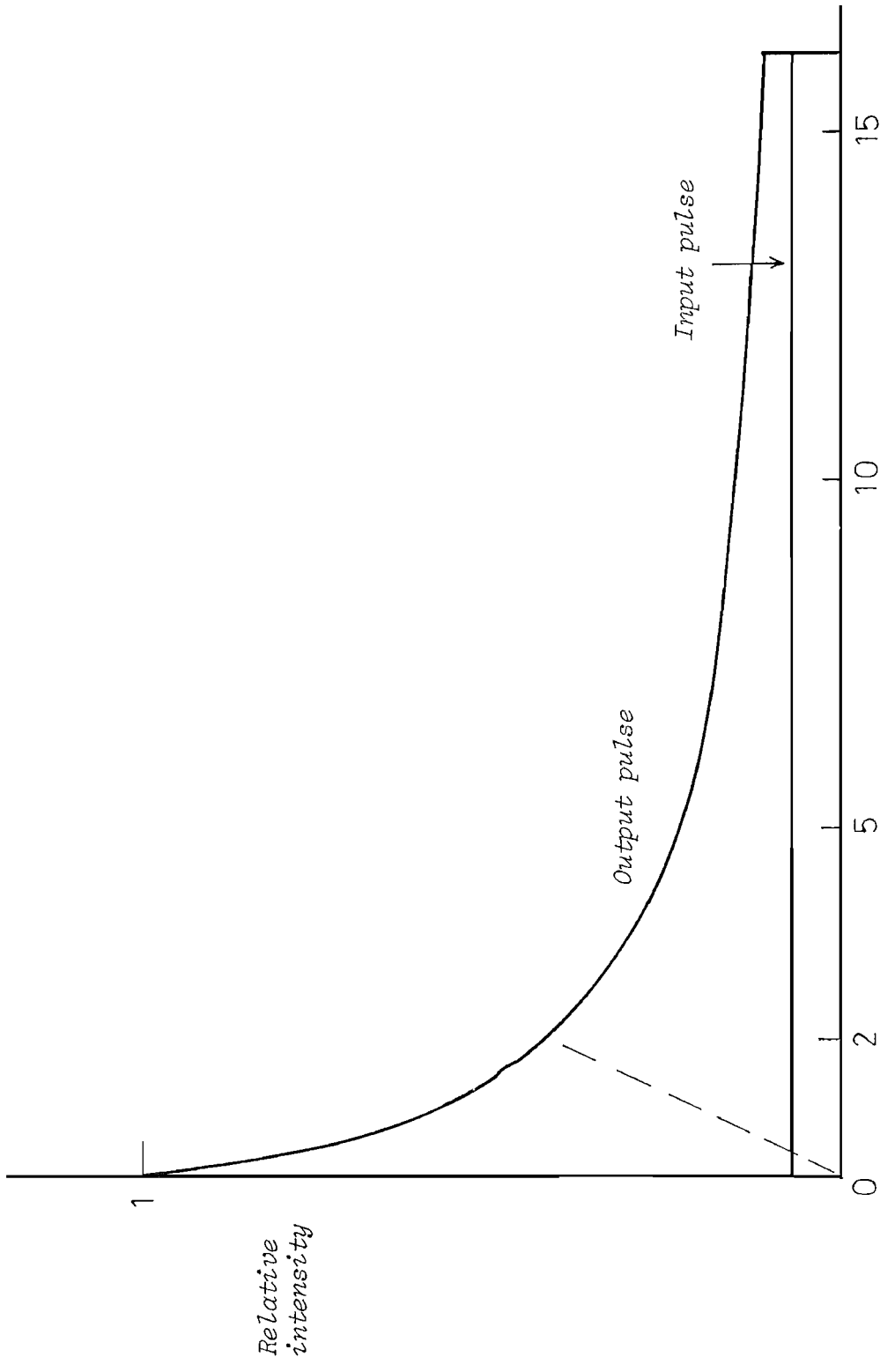

Figure A4.1 Pulse distortion in the saturated amplifier.

APPENDIX V

Appl. Phys. B 36, 83–92 (1985)

Applied Physics B Photophysics and Laser Chemistry

Performance of a Nd:YAG Oscillator/Amplifier with Phase-Conjugation via Stimulated Brillouin Scattering

I. D. Carr and D. C. Hanna

Department of Physics, University of Southampton, Southampton SO9 5NH, UK

Received 5 July 1984/Accepted 6 August 1984

Abstract. Phase conjugation via stimulated Brillouin scattering in CH_4 gas has been used to correct amplifier aberrations in a Nd : YAG oscillator/amplifier system. The single amplifier stage has been used in two-pass and four-pass arrangements. Using the four-pass arrangement incorporating compensation for thermal birefringence, a single-frequency diffraction-limited output of 350 mJ, in a compressed 6 ns pulse is achieved at 15 Hz repetition rate.

PACS: 42.60, 42.65F, 62.65C

Nonlinear optical phase-conjugation (NOPC) via stimulated Brillouin scattering has received considerable theoretical and experimental attention since the initial work of Zel'dovich et al. [1, 2] (see [3] for extensive reviews). An interesting application of NOPC is in the correction of optical aberrations produced by a laser amplifier stage (or stages). A great deal of the work in this area has been performed with high power glass laser systems (many references in [3]) but there has been little published work based on the Nd : YAG laser, despite its being the most widely used solid-state laser. Exceptions to this are the work of Zubarev et al. [4] and Hon [5]. Zubarev et al. demonstrated a considerable improvement in output beam quality from a Nd : YAG oscillator/amplifier using SBS phase-conjugation. However, the Nd : YAG crystals used in that experiment were of poor optical quality and distorted the beam to a much worse degree than would crystals of typical quality. Furthermore, the final output energy was only at the level (~ 100 mJ) that can be achieved from a TEM_{00} oscillator of suitable design [6, 7] with crystals of typical quality. Hon's work [5] demonstrated the successful application of NOPC to a Nd:YAG system consisting of a Q-switched oscillator with two amplifier stages, leading to ~ 700 mJ of diffraction-limited output. Additional aberration was introduced into the amplifier chain in the form of a Nd : YAG rod subjected to strong continuous pumping. The ability to correct severe pump-induced aberrations was thus demonstrated. In fact, it is also a feature of many NOPC experiments that aberrations are deliberately introduced on the basis that this produces better fidelity in the wavefront reconstruction [8]. However, this can complicate the NOPC set-up since the extra beam distortion raises the SBS threshold and a lightguide arrangement is then needed to reduce the threshold. Meanwhile, the question that needs to be answered for the user of a typical pulsed Nd : YAG laser is whether the additional complexity of a NOPC set-up is worthwhile and how much complexity is necessary (e.g., introduction of aberrator, lightguide, single-mode operation of the oscillator), when the requirement is simply to remove the relatively modest, but still troublesome aberrations associated with the amplifier stage. This paper reports results obtained in an attempt to answer that question. To summarise, we have found that

(i) effective NOPC can be achieved using a simple cell containing high pressure CH_4 gas but not involving the use of a light guide,

(ii) effective NOPC can be achieved even with the oscillator operating on a few longitudinal modes,

(iii) by incorporating birefringence compensation we can successfully use a single amplifier in a four-pass configuration,

(iv) with this four-pass arrangement, a single frequency TEM_{00} output of 350 mJ is obtained in a pulse of 6 ns, compressed temporally from the input pulse duration of 30 ns,
(v) we find that most of this pulse compression occurs in the last two passes of the amplifier rather than (as in the experiments of [9–11]) in the SBS medium.

1. Experimental Details

1.1. Amplifier Configurations

The Nd : YAG laser system consisted of an oscillator (3″ × 1/4″ rod with single flashlamp) and an amplifier (3″ × 3/8″ rod, with twin flashlamps), capable of operating at up to 15 Hz repetition rate, with maximum flashlamp input energies of 50 J to the oscillator and 100 J to the amplifier. The TEM_{00} mode oscillator used a telescopic resonator, similar to that described in [6, 7], with a X3 telescope magnification and a spacing of 0.35 m between the telescope and the resonant reflector output coupler. The oscillator was operated on a single longitudinal mode on every shot, using the technique described in [12], and produced up to 100 mJ output in a 30 ns pulse. When multi-longitudinal mode operation was required, the conventional fast Q-switched arrangement was used, or the mode-selection etalon was removed, or (for the broadest linewidth) both of these measures were adopted. The beam from the oscillator was expanded by a telescope to produce a spot-size (TEM_{00}, radial spot-size w) of 2.8 mm in the amplifier rod, this being close to the maximum size ($3w$ = rod diameter) possible without significant truncation.

We have examined two different experimental arrangements, involving either two passes through the amplifier (Fig. 1a) or four passes through the amplifier (Fig. 1b). We consider the two-pass arrangement first. To assess the effectiveness of phase-conjugation the performance with the SBS "mirror" was compared with that obtained using a conventional plane mirror of 100% reflectivity. With the latter arrangement, various schemes can (in principle) be used to isolate the oscillator from the return beam and at the same time enable the amplifier output to be extracted. The simplest involves a polariser followed by a quarter wave plate (Fig. 1a) which can be located on either side of the amplifier (location 1 or 2 in Fig. 1a). In either

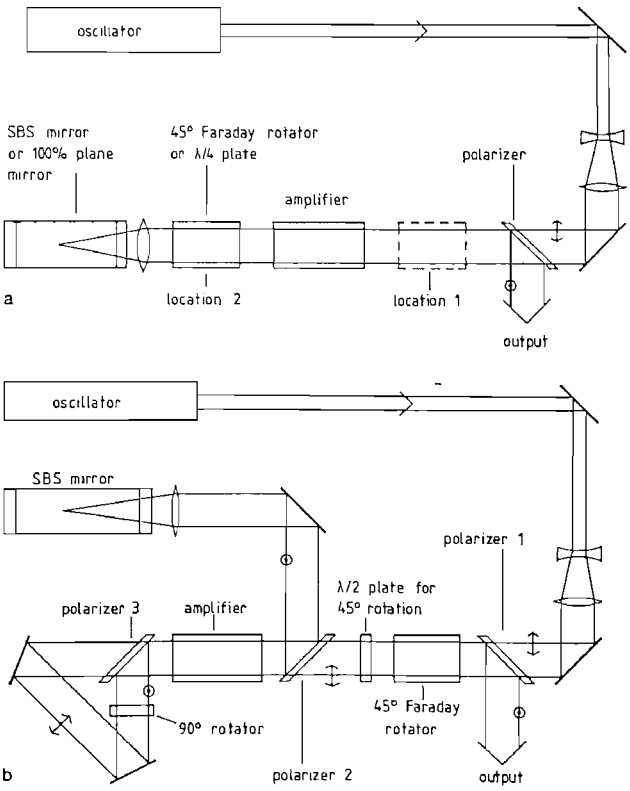

Fig. 1. (a) Two-pass amplifier configuration. For isolation of the oscillator from the amplifier beam a quarter wave plate or 45° Faraday rotator can be placed at location 1 or 2. (b) Four-pass amplifier configuration. The Faraday rotator and $\lambda/2$ plate give zero net rotation for light from right to left but 90° rotation for light from left to right. Details of the polarisation changes after polariser 2 are given in the text

case, one is relying on there being no additional polarising elements following the polariser. In fact, however, the laser rod suffers from thermally induced birefringence [13] which not only introduces an extra polarising element, but one which has a birefringence behaviour distributed non-uniformly over the rod cross section. This has the undesirable effects of i) coupling power back to the oscillator, representing both a source of loss and a damage risk, and ii) producing phase and amplitude variations across the output beam which degrade the beam quality.

One means of compensating the birefringence is to use a Faraday rotator (45° rotation) placed after the first pass of the amplifier (location 2 in Fig. 1a). This arrangement is then equivalent to the unfolded arrangement, as actually used by Scott and DeWitt [14], in which a 90° rotator is placed between two identical amplifier stages. A ray passing through the amplifier has its field component along the fast birefringence axis rotated by 90° so that it lies along the slow axis in the second amplifier, and vice versa. Thus, regardless of the orientation of the fast and slow axes (they are, however, orthogonal to each other) the birefringence in one amplifier is cancelled in the second. (Note that a quarter wave plate at location 2 in Fig. 1a or equivalently a half-wave plate between two identical amplifiers does not achieve this birefringence compensation.) For the compensation to work effectively the following condition must be met: the two amplifiers must be closely matched, a situation that automatically results from double-passing a single amplifier: the beam passing through the amplifier should be collimated if the return mirror is a conventional mirror, so that identical paths are retraced on the second pass: the round-trip distance between the two amplifier passes should be kept short to minimise the effects of diffraction spread. A measure of the birefringence compensation is determined by comparing the power reflected by the polariser (this is the useful output) with that transmitted by the polariser (this is the depolarisation loss), after a double pass of the amplifier.

When the conventional mirror is replaced by the SBS mirror the conditions for birefringence compensation are no longer quite the same since the SBS process does not, in general, produce a Stokes wave with the same polarisation state as the pump wave [15]. However, for a *uniformly* polarised pump beam the SBS mirror has the same effect on polarisation state as a conventional mirror [5, 15] and therefore, in the absence of amplifier depolarisation, a quarter wave plate at location 1 or 2 in Fig. 1a would provide the desired isolation and beam extraction. The situation is more complicated when the amplifier introduces an inhomogeneous birefringence distribution. As discussed above, a 45° Faraday rotator placed at location 2 would correctly compensate the depolarisation if a conventional mirror were in use, but, as Zel'dovich and Shkunov [15] have shown in a theoretical analysis, when a depolarised pump is used the Brillouin Stokes wave can have a quite different polarisation state from that produced by a conventional mirror. One would expect, therefore, the wavefront reconstruction to be degraded as a result of the amplifier birefringence, but the analysis of Zel'dovich and Shkunov does not predict the extent of degradation. We have therefore carried out an experimental examination of the phase-conjugation behaviour with either a $\lambda/4$ plate or a 45° Faraday rotator, in each case placed at location 2 in Fig. 1a. We have found that the depolarisation loss is significantly lower with the Faraday rotator and that furthermore the loss is lower when the rotator is used in conjunction with the SBS mirror rather than the conventional mirror.

By going to a four-pass arrangement it is possible to introduce birefringence compensation prior to the phase-conjugation process and thus, in principle, present a uniformly polarised wave to the SBS mirror. Hon [5] used the equivalent unfolded arrangement by having two amplifier stages with a 90° rotator between them, and then followed by the SBS mirror. Our four-pass arrangement is shown in Fig. 1b. Horizontally polarised light (p-polarisation) from the oscillator is passed by polariser 1 and remains p-polarised after being subjected to opposite 45° rotations from the Faraday rotator and $\lambda/2$ plate. On the return path this arrangement produces a vertically polarised (s-polarisation) beam which is then reflected as output by polariser 1. The p-wave passing through polariser 2 enters the amplifier and then, emerging as a depolarised beam, is split into two orthogonally polarised waves at polariser 3. These waves conterpropagate around the ring configuration, each being subjected to a 90° rotation of polarisation on the way round. They recombine as a single beam at polariser 3. The effect of the ring is to interchange the field components for any two orthogonal polarisations (i.e., it acts like a double pass through a 45° Faraday rotator) and thus allows the rod birefringence to be compensated. The beam emerging from the second pass of the amplifier is now s-polarised and therefore reflected off polariser 2 into the phase-conjugator. After conjugation the entire process is repeated for the return beam which is p-polarised as it emerges from the fourth amplifier pass. (We are indebted to Dr. C. L. M. Ireland for pointing out the polarising properties of this ring configuration, and we also note that an equivalent arrangement is embodied in a special Pockels cell Q-switch device reported by Richards [16]).

Besides offering the ability to compensate rod depolarisation before phase-conjugation the four-pass amplifier offers additional potential advantages over the two-pass amplifier such as:

1) a lower input energy requirement from the master oscillator,
2) a better energy extraction from the amplifier, and
3) satisfactory energy extraction with a lower input energy to the phase-conjugator or with lower reflectivity from the conjugator.

1.2. The SBS Medium

We have confined our investigations to the use of high-pressure CH_4 gas as the SBS medium since it had been shown [5] to provide efficient SBS for a 1.06 μm pump. Other media, (see, e.g., [4] and the discussion in [10]) may also prove satisfactory but we have not tested these.

The threshold pump power for SBS is a parameter of practical importance and we now discuss how we have calculated this from the published data. We find good agreement between our calculated and measured values. Under steady state conditions, i.e. with a pump pulse whose bandwidth $\Delta\nu_p$ is such that $(\Delta\nu_p)^{-1} \gg \tau_B$, where τ_B is the acoustic phonon damping time, the gain of the Stokes wave over a length l of medium for a plane wave pump of intensity I_p is $\exp\{g_B I_p l\}$. We define threshold as the condition when the gain reaches exp(30). Hence the threshold pump power $P_{p,th}$ is given by

$$P_{p,th} = \frac{30 A_p}{g_B l} p , \tag{1}$$

where A_p is the area of the pump beam. This simple expression for the pump threshold becomes modified in a number of ways when account is taken of the non-plane-wave nature of the pump (including the possibility of an aberrated pump beam) and the transient nature of the process when $(\Delta\nu_p)^{-1} \leqq \tau_B$. The latter condition can arise either because the overall pump envelope is shorter than τ_B or because the envelope contains fluctuations on a short time scale, e.g. when a multimode pump is used.

To calculate the steady-stade threshold for a Gaussian pump beam we have used the analysis of Cotter et al. [17] which, for a pump beam waist w_p (confocal parameter $b_p = 2\pi w_p^2/\lambda_p$) at the centre of a SBS medium of length L yields a threshold pump power

$$P_{p,th} = \frac{\lambda_p}{4 g_B} \{1 + [1 + 30/\arctan(L/b_p)]^{1/2}\}^2 . \tag{2}$$

The typical parameters relevant to our experiment are $w_p = 150$ μm, hence $b_p = 0.13$ m, and the cell length $L = 1$ m. The dependences of g_B and τ_B on gas pressure p and laser wavelength λ_p are as follows [10], $g_B \propto p^2$, $\tau_B \propto p$, $\tau_B \propto \lambda_p^2$ and g_B is essentially independent of λ_p. For 30 atmospheres pressure (as used in our experiments) $g_B = 8 \times 10^{-5}$ m/Mw and for a 1.06 μm pump, $\tau_B \sim 6$ ns. These values, with (2) yield a calculated steady state threshold pump power $P_{p,th} = 100$ kW. In fact, however, the pump pulse duration τ_p of 30 ns (FWHM) is sufficiently close to the phonon lifetime τ_B for a significant departure from the steady state threshold and with our values $\tau_p/\tau_B = 5$ the threshold power is then predicted [18] to be ~ 2.5 times greater than the steady state value, i.e. ~ 250 kW. The actually observed threshold was 400 kW for single-mode pumping. Note that this threshold cannot be significantly reduced by altering the focussing condition since the best that can be achieved is to make $\arctan(L/b_p) = \pi/2$. On the other hand, it can be reduced using an optical waveguide capillary [19, 20], and a threshold reduction of an order of magnitude has been obtained in this way [21]. A threshold reduction can also be achieved by operating at higher pressure p, where the fact that the process becomes more transient ($\tau_B \propto p$) is offset by the fact that $g_B \propto p^2$. Thus at 50 atmospheres we observed a threshold of 230 kW for an unguided single frequency, Gaussian pump beam.

To estimate the threshold for a beam which is not diffraction-limited, we note that the product of intensity I_p and the length of medium over which this intensity is maintained (i.e., the Rayleigh range) is smaller by a factor M for a beam whose divergence is M times greater than the diffraction limit. This result would appear to suggest that the threshold is M times greater, however it has to be remembered that the phase-conjugate beam can experience a gain exponent of $\sim$ twice that which would result from a single spatial mode of the same spatially averaged intensity [22]. The minimum threshold power for the aberrated beam is therefore $\sim M/2$ greater than for the diffraction limited pump beam.

The effect on threshold of using a noisy pump (i.e., multi frequency) has been discussed in detail by Akhmanov et al. [23]. The following conclusion can be drawn; the SBS gain with a noisy pump of mean intensity I_p is the same as for a monochromatic pump of the same mean intensity provided the length of medium, $30/(g_B I_p)$, over which an exp(30) fold Stokes growth occurs is much less than the coherence length $(c/\Delta\nu_p)$ of the pump. In practice this means that the confocal parameter of the focussed pump should be less than the pump coherence length; i.e.

$$b_p \ll l_{\mathrm{coh}} . \tag{3}$$

The analysis of Akhmanov et al. also allows an estimate to be made of the threshold increase due to a noisy pump where this condition is not met. With our

typical operating conditions, $b_p = 0.13$ m, and with a single mode pump, $l_{coh} \simeq 6$ m, the condition is clearly satisfied. With n longitudinal modes, $l_{coh} = 2L_{laser}/n$, and since for our laser, $L_{laser} \sim 1$ m, the condition $b_p \ll l_{coh}$ is maintained even for 3 or 4 mode operation. This is confirmed by the observation that the threshold and phase-conjugation behaviour are little affected even when a few modes oscillate. However, when the laser oscillated with a bandwidth of ~ 2 GHz ($l_{coh} \sim 0.15$ m, $n \sim 15$ modes) the threshold, at 30 atmospheres, was increased by $\sim 75\%$, a result consistent with the analysis of Akhmanov. Under these conditions phase-conjugation still occurred but it was noticeably less reliable and gave poorer beam reconstruction. We also noted that at a gas pressure of ~ 50 atmospheres, (thus increasing g_B), the threshold for the noisy pump was only slightly greater than for the single mode pump, a result in accord with the requirement $30/(g_b Ip) \ll l_{coh}$ and confirmed by Akhmanov's analysis.

2. Experimental Results

The experimental parameters of most interest are the output energy and the beam quality. We have measured beam profiles using a diode array and at the same time a qualitative assessment of the beam has been made by observing the burn patterns on photographic paper. There are some possible pitfalls where beam quality measurements are concerned so we point these out and explain our measurement procedure in some detail.

First we note that an irregular burn pattern in the near field is not necessarily indicative of a poor beam quality since it may be that most of the beam energy is in a diffraction-limited component but mixed with a small component having different beam profile. This sensitivity of the spatial profile to a small admixture is analogous to the sensitive detection of beats when a dominant longitudinal mode is in the presence of a much weaker mode [24]. Lehmberg [25] has confirmed in a numerical calculation that the near-field beam profile in a phase-conjugation set-up may suffer large amplitude modulation when even a small non-phase-conjugate component is present.

Secondly, we note that in comparing the beam quality obtained with and without the phase-conjugator one cannot draw conclusions on beam quality simply from an observation of difference in far-field beam dimensions for these two cases. For example, if the amplifier distortion was in the form of pure spherical lensing or if the input to the amplifier was not collimated, then the two cases would produce quite different output beam focussing, and hence divergence, while both would be diffraction-limited. To remove any uncertainty we have deliberately used a lens to focus the output beam to form a new waist, whose size was then measured using the diode array. The beam divergence from this waist was then determined using the diode array to measure a spot-size in the far field (i.e., many confocal parameters from the waist). The ratio of the measured beam divergence to that calculated from the measured waist yields the factor by which the output beam exceeds the diffraction-limit.

Thirdly, we note that since some of the output beam energy may be in the form of a non-phase-conjugate component of higher divergence, the far-field pattern as indicated either by burn marks or by a diode array may not reveal these low-intensity wings of the spatial profile even if they contain a significant fraction of the total energy. We have therefore measured the energy in the central diffraction-limited part of the profile after first passing the far-field beam through a circular aperture. The aperture size was chosen to have a diameter three times the measured spot-size w of this central diffraction-limited spot.

The results on beam quality can be summarised as follows. With the two-pass amplifier arrangement of Fig. 1a using a plane 100% reflector in place of the SBS cell an output energy of ~ 400 mJ could be obtained in a 30 ns pulse. The output beam quality worsened as the mean power into the amplifier was increased. This is clearly seen in Fig. 2a and b which show burn patterns and profiles monitored by the diode array at various distances from the amplifier. Despite the somewhat ragged appearance of the burn pattern at 5 Hz, the diode array indicated that the beam was essentially diffraction-limited and even the severely distorted patterns at 15 Hz were found to correspond to only a factor of ~ 2 greater divergence than the diffraction limit. Also shown in Fig. 2a and b are the corresponding beam profiles for the two-pass amplifier with the SBS cell. In this case, a total output energy of ~ 330 mJ was obtained in a 16 ns pulse and $\sim 90\%$ of this energy was transmitted by the far-field aperture. Thus ~ 300 mJ of diffraction-limited output was obtained. The output-beam brightness at 15 Hz is therefore improved by a factor of 3 as a result of phase conjugation (or a factor of ~ 6 if one includes the increase of power due to the reduction of pulse length by a factor of ~ 2). At 5 Hz there is only a slight degradation of the beam by the amplifier and so apart from the cleaner appearance of the burn pattern the use of the phase-conjugator does not offer much benefit. At 15 Hz the value of the phase-conjugator is much more apparent and the far-field spots have a clean circular appearance apart from the small degree of square-shaped truncation due to thermal birefringence effects.

The output beams shown in Fig. 2a and b have not been modified by any focussing elements after leaving the

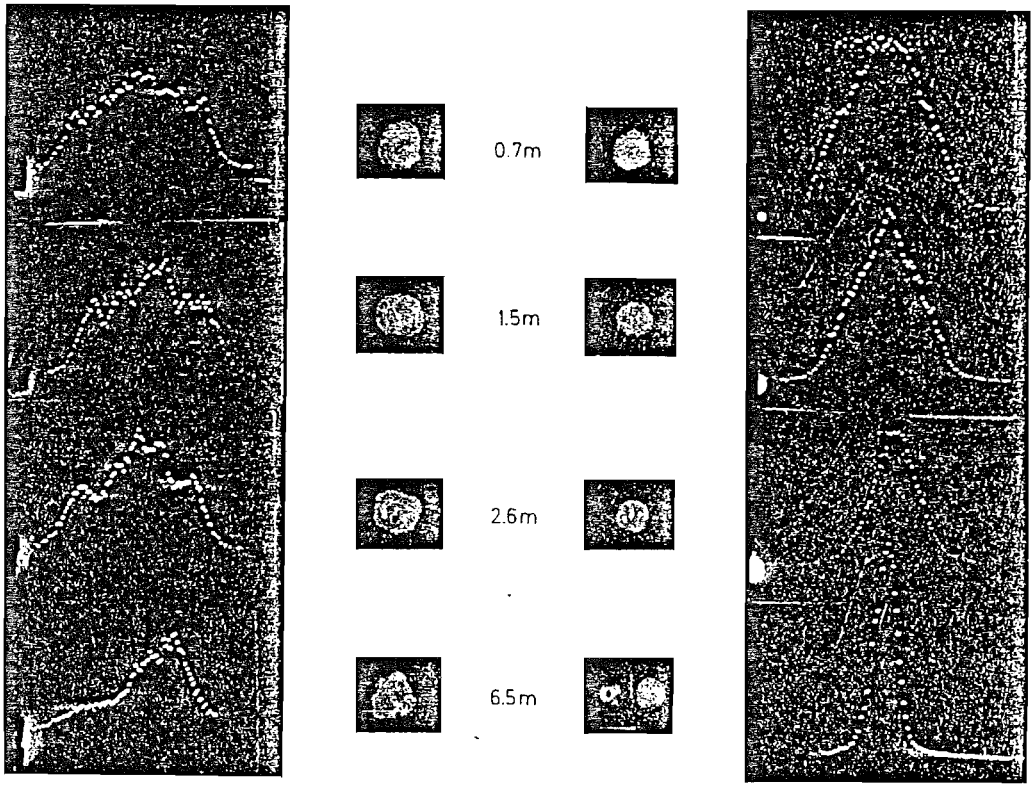

Fig. 2. (a) Beam profiles at various distances from two-pass amplifier, at 5 Hz rep. rate, either with phase-conjugation (right-hand photos) or without phase-conjugation (left-hand photos).

amplifier. The focussing behaviour observed at 15 Hz in the non-phase-conjugated beam, due to amplifier lensing, shows strong astigmatism with the beam coming to foci between 1.5 and 2.5 m from the amplifier. This amplifier lensing effect is removed in the phase-conjugate beam. The focussing behaviour of the phase-conjugate beam is simply due to the fact that the input to the amplifier was slightly divergent and hence the conjugate return beam has an opposite convergence. An enlarged version of the phase-conjugate beam 6 m from the amplifier is also shown, obtained by expanding the beam with a negative lens.

Using the four-pass amplifier arrangement similar results were obtained although at somewhat higher output energies. Measurements were only made with the SBS cell in this case since a conventional mirror in place of the SBS cell led to oscillaton (as a result of depolarisation caused by thermal birefringence in the amplifier). Output energies up to ~440 mJ were obtained, of which ~350 mJ (i.e. 80%) was diffraction-limited. Figure 3 shows the near-field and far-field output beam profiles at 5 and 15 Hz. The pulse duration of the output beam was considerably compressed, from an initial 30 to ~6 ns. Figure 4 shows the pulse shapes at various stages in the amplification process. The reflected SBS pulse shows a sharp leading edge, (rise: ~2 ns) and is truncated to ~20 ns duration. This reflected pulse after the two return passes through the amplifier is further shortened to ~6 ns as a result of saturation in the amplifier. This degree of pulse compression in the amplifier is consistent with calculations following the work of Frantz and Nodvik [26]. We note that Ambartsumyan et al. [27] have used a shutter to deliberately generate a steep leading edge to a Q-switched pulse for subsequent compression in a saturated amplifier. The SBS process achieves this in a simple and automatic fashion.

The shortened pulse duration must lead to some degree of spectral broadening. Direct confirmation of this was made for the two-pass amplifier configuration where the linewidths of the input and output to the amplifier were measured. The measurement was made

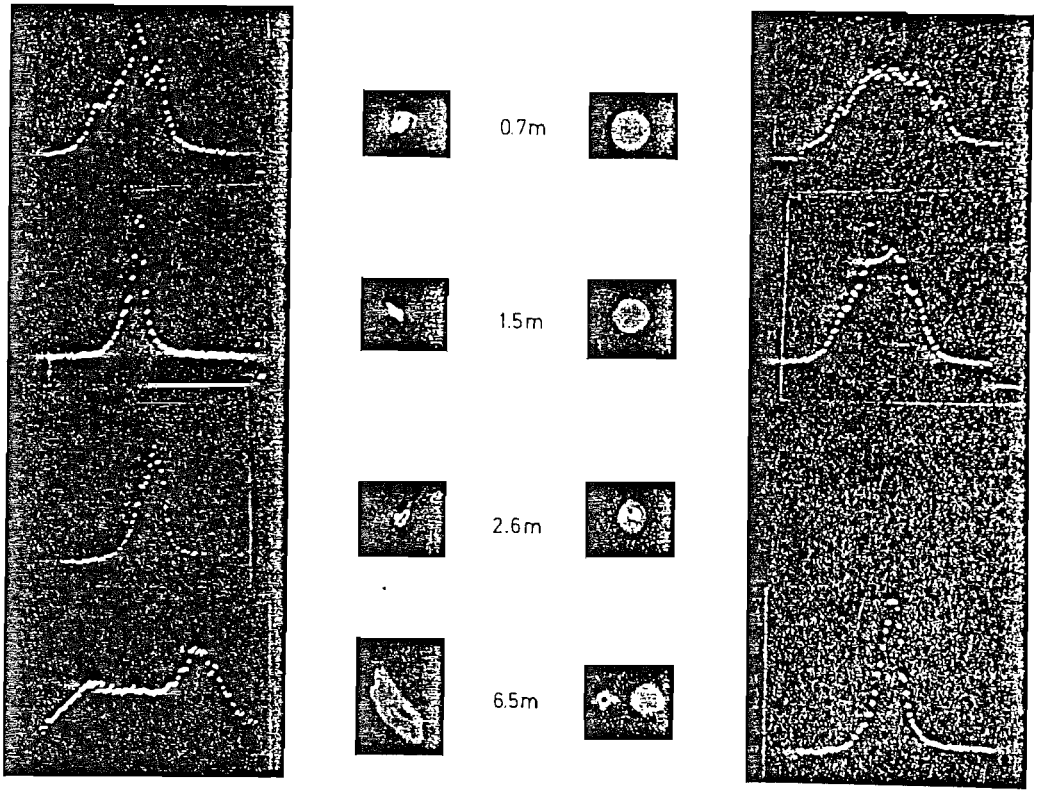

Fig. 2. (b) Beam profiles at various distances from two-pass amplifier, at 15 Hz rep. rate, either with phase-conjugation (right-hand photos) or without phase-conjugation (left-hand photos)

by converting the 1.06 μm radiation to its second harmonic and examining the linewidth of the green light using a scanning confocal Fabry-Perot interferometer. Figure 5 shows scans obtained for the input and output linewidths. After allowing for the spectral modification arising from the harmonic generation we deduce that the linewidth of the SLM input was 33 MHz (i.e., somewhat broader than the bandwidth limit for a 30 ns pulse) and the Brillouin shifted output linewidth was 50 MHz.

In the four-pass amplifier configuration it is, in principle, possible for an unshifted component (i.e., not phase-conjugated) and the Brillouin-shifted component to be both present in the output. The unshifted component is the result of uncorrected depolarisation of the beam after the first two amplifier passes, thus producing some output without undergoing phase-conjugation. However, an examination of the temporal behaviour of the output beam failed to reveal any beats (at ~800 MHz) between the Brillouin-shifted and unshifted components, suggesting that the unshifted component is much weaker and that the output can be regarded as essentially single-frequency. We have also examined the output to see if there is any evidence of oscillation from the SBS mirror once this is established. This could result if uncompensated amplifier depolarisation coupled enough radiation back to the SBS mirror after the fourth amplifier pass, rather than passing through polariser 2. No sign of such an oscillation was found, its absence being an indicator that our birefringence compensation was sufficient.

A measurement of depolarization losses give a useful guide to the success of any birefringence compensation scheme. We have determined these losses by measuring the fraction of the return beam which passes back through polariser 1 (Fig. 1) rather than being reflected as output. Figure 6 shows the results obtained at 5, 10, 15 Hz for four different arrangements of the two-pass amplifier, viz. plane mirror plus $\lambda/4$ plate, plane mirror plus Faraday rotator (FR), phase-conjugate mirror (PCM) plus $\lambda/4$ plate, and PCM plus FR. In

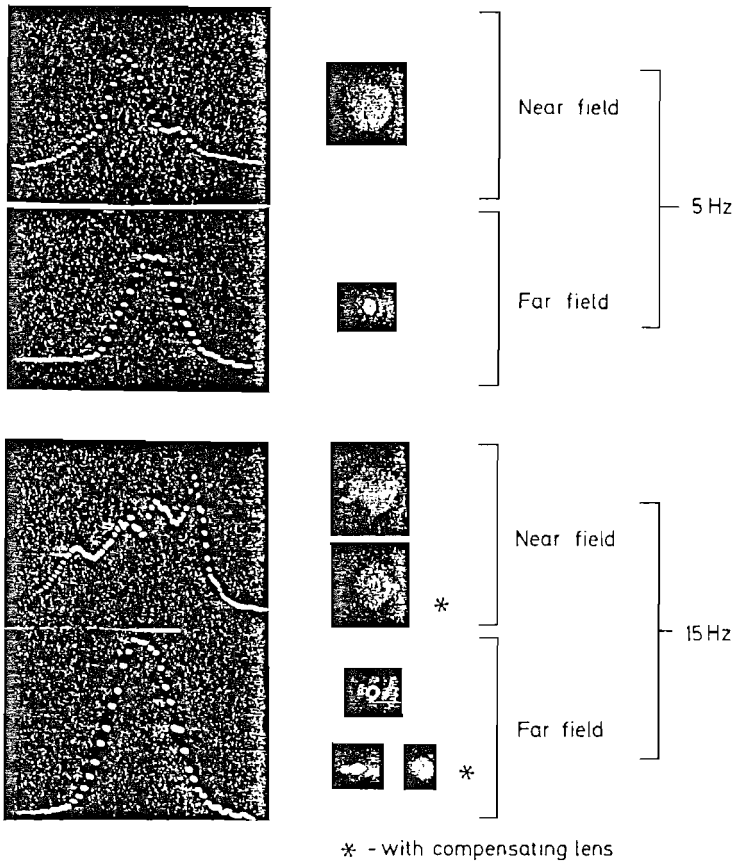

Fig. 3. Near field and far field beam profiles for the four-pass amplifier with phase-conjugation, at 5 and 15 Hz. The effect of adding a compensating lens is shown (see text)

each case, the $\lambda/4$ plate or FR was placed at location 2 in Fig. 1a. The increase of loss with repetition rate is expected since this increases the thermally-induced birefringence. It is interesting to see that the depolarisation losses for the configuration of plane mirror plus $\lambda/4$ plate can be calculated with good accuracy (using an extension of the analysis in[13]). The FR plus plane mirror gave a good performance at 5 Hz but were less effective than anticipated at 15 Hz. However, we conclude that this is because the considerable thermal lensing at 15 Hz upsets the requirement that the return rays should retrace identical paths. Evidence for this was also found in the four-pass amplifier scheme, where the ring configuration plays the role of Faraday rotator. Figure 7 shows the measured depolarisation loss in this arrangement, also increasing rapidly with repetition rate. However, when operating at 15 Hz, placing a negative lens in the ring, whose effect was to recollimate the beam for its return path through the amplifier, the depolarisation loss fell from ~15% to ~5%. This result emphasises the importance of obtaining good birefringence compensation. It also shows that while the arrangement we have used is adequate for the conditions in our laser it is clear that an improved scheme is needed to cope with more severe birefringence such as in a Nd glass laser. The scheme described by Basov et al. [28] looks attractive in this respect. We have conducted preliminary tests of this scheme, which show that a further reduction of depolarization loss can be achieved (down to less than 2% at the maximum pumping rate of the amplifier). Detailed results of this work will be reported in a later publication.

3. Conclusion

We have shown that a simple phase conjugation scheme can produce a significant improvement in the output beam quality from a Nd:YAG oscillator/amplifier system. While the benefits of introducing the phase conjugator are marginal at the 5 Hz repetition rate the technique is certainly worthwhile at 15 Hz,

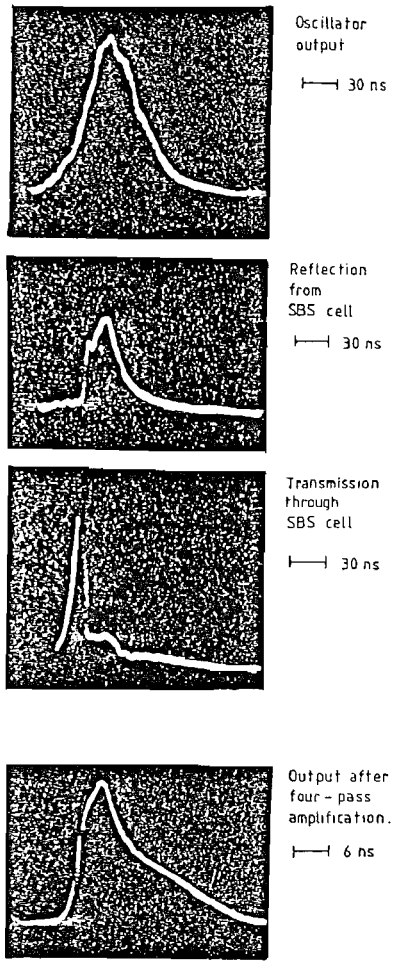

Fig. 4. Pulse shapes at various stages in the amplification process

giving a factor of 3 improvement in beam brightness. This factor does not include any allowance for the increase in power due to pulse compression. If this is included, the four-pass amplifier with phase-conjugator has led to a factor of ~15 improvement in beam brightness.

Besides the improvement in beam brightness the profile of the phase-conjugated beam had a much cleaner appearance, an important feature where accurate measurements are needed. Furthermore, we were able to vary the flashlamp input to the amplifier (as a means of varying the output energy) without causing variations in the output beam as a result of varying thermal conditions in the amplifier. Such output beam variations are a nuisance in conventional oscillator/amplifier systems.

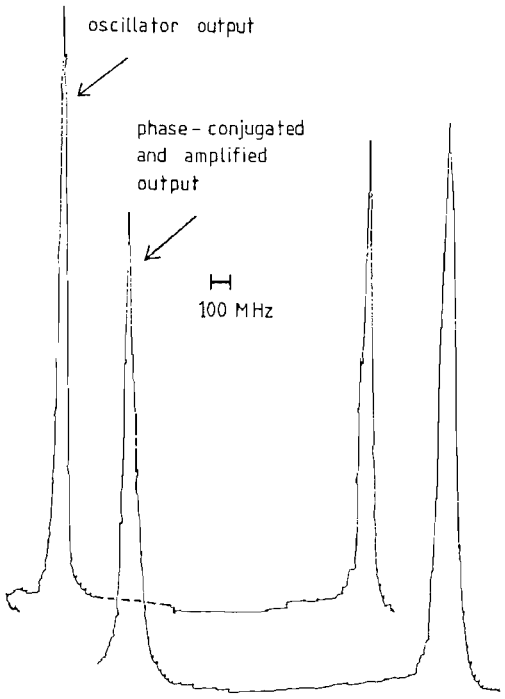

Fig. 5. Transmission Scans from scanning Fabry-Perot interferometer, using second harmonic of the Nd:YAG laser

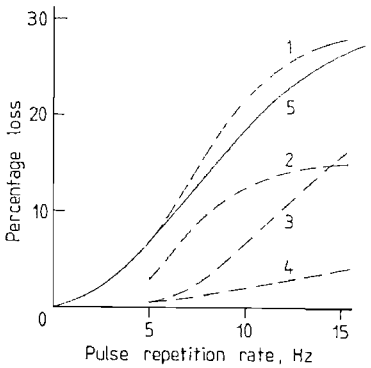

Fig. 6. Birefringence loss versus pump repetition rate for a constant 72 J pump energy per pulse to the amplifier, used in double pass. Curve (1) plane mirror with $\lambda/4$ plate; Curve (2) SBS mirror with $\lambda/4$ plate; Curve (3) plane mirror with Faraday rotator; Curve (4) SBS mirror with Faraday rotator; Curve (5) is calculated for the case of plane mirror with $\lambda/4$ plate

While our results show that a significant improvement in laser performance can be gained without undue complexity we have not made an exhaustive study, either of optimisation or of the degree to which certain conditions can be relaxed without prejudice to the

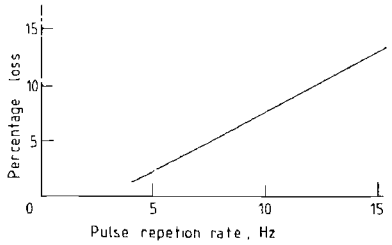

Fig. 7. Birefringence loss versus pump repetition rate for 72 J pump energy per pulse to the amplifier, used in the four-pass configuration

fidelity of the wavefront reconstruction. Certainly however we have seen that single-longitudinal mode operation can be relaxed to some extent and we have seen that a light guide is not essential. Without doubt further improvements in performance should be possible with detailed optimisation. It is also likely that improved schemes for birefringence compensation [28] or possibly a combination of phase-conjugation with a slab laser configuration will lead to similar improvements in the performance of Nd:glass systems.

Acknowledgements. This work has been supported by SERC and one of us (I.D. Carr) wishes to acknowledge SERC/CEGB for support in the form of a CASE Studentship.

References

1. B.Ya. Zel'dovich, V.I. Popovichev, V.V. Ragul'skii, F.S. Faizullov: J.E.T.P. Lett **15**, 109 (1972)
2. B.Ya. Zel'dovich, N. Pilipetskii, V.V. Shkunov: *Principles of Phase Conjugation*, Springer Ser. Opt. Sci. **42** (Springer, Berlin, Heidelberg, New York, Tokyo 1985)
3. D.M. Pepper: Optical Engineering **21**, 156–183 (1982) R.A. Fisher (ed.): *Optical Phase-Conjugation* (Academic Press, New York 1983)
4. I.G. Zubarev, A.B. Mironov, S.I. Mikhailov: Sov. J. Quantum Electron. **10**, 1179 (1980)
5. D.T. Hon: Opt. Eng. **21**, 252–256 (1982)
6. D.C. Hanna, C.G. Sawyers, M.A. Yuratich: Opt. Commun. **37**, 359 (1981)
7. D.C. Hanna, C.G. Sawyers, M.A. Yuratich: Opt. Quantum Electron. **13**, 493 (1981)
8. B.Ya. Zel'dovich, N.F. Pilipetskii, V.V. Shkunov: In *Optical Phase-Conjugation*, ed. by R.A. Fisher (Academic Press, New York 1983) Chap. 6
9. D.T. Hon: Opt. Lett. **5**, 516 (1980)
10. M.J. Damzen, M.H.R. Hutchinson: IEEE J. QE-**19**, 7 (1983)
11. M.J. Damzen, M.H.R. Hutchinson: Opt. Lett. **8**, 313 (1983)
12. D.C. Hanna, Y.-W.J. Koo: Opt. Commun. **43**, 414 (1982)
13. W. Koechner: Solid-State Laser Engineering, Springer Ser. Opt. Sci. **1** (Springer, New York 1976)
14. W.C. Scott, M. DeWitt: Appl. Phys. Lett. **18**, 3 (1971)
15. B.Ya. Zel'dovich, V.V. Shkunov: Sov. Phys. JETP **48**, 214–219 (1978)
16. J. Richards: Appl. Opt. **22**, 1306–1308 (1983)
17. D. Cotter, D.C. Hanna, R. Wyatt: Appl. Phys. **8**, 333–340 (1975)
18. M. Maier, G. Renner: Phys. Lett. **34A**, 299–300 (1971)
19. A.J. Berry, D.C. Hanna, D.B. Hearn: Opt. Commun. **43**, 229–232 (1982)
20. A.J. Berry, D.C. Hanna: Opt. Commun. **45**, 357–360 (1983)
21. A.J. Berry: Ph. D. Thesis, University of Southampton (1983)
22. R.W. Hellwarth: J. Opt. Soc. Am. **68**, 1050–1056 (1978)
23. S.A. Akhmanov, Yu.E. D'yakov, L.I. Pavlov: Sov. Phys. JETP **39**, 249–256 (1974)
24. A.J. Berry, D.C. Hanna, C.G. Sawyers: Opt. Commun. **40**, 54–58 (1980)
25. R.H. Lehmberg: Opt. Commun. **43**, 369–374 (1982)
26. L.M. Frantz, J.S. Nodvik: J. Appl. Phys. **34**, 2346–2349 (1963)
27. R.V. Ambartsumyan, N.G. Basov, P.G. Kryukov, V.S. Letokhov: IEEE J. QE-**2**, 436–441 (1966)
28. N.G. Basov, V.F. Efimkov, I.G. Zubarev, A.V. Kotov, S.I. Mikhailov, M.G. Smirnov: JETP Lett. **28**, 197–201 (1978)

REFERENCES

S.A.Akhmanov, Yu.E.D'yakov, A.S.Chirkin: Sov.Phys. JETP. 32, 266, (1971).

S.A.Akhmanov, Yu.E.D'yakov, L.I.Pavlov: Sov.Phys.JETP 39, 249-256 (1974).

R.V.Ambartsumyan, N.G.Basov,V.S.Zuev,P.G.Kruykov,V.S.Letokov: IEEE.J QE-2, 436-441 (1966).

J.A.Arnaud, A.A.M.Saleh, J.T.Ruscio: IEEE. Trans. on Microwave Theory and Techniques, M.T.T. 22, 486, (1974).

N.B.Baranova, B.Ya.Zel'dovich, V.V.Shkunov:Sov.J.Quant.Elec.8, 559-566 (1978)

N.G.Basov et al: Sov. Phys. JETP. Lett. 28, 197-201, (1978).

N.G.Basov et al: Sov.Jnl.Quant.Elec. 9(4), 455-458, (1979)(a).

N.G.Basov, I.G.Zubarev, A.V.Kotov, S.I.Mikhailov, M.G.Smirnov, Sov.J.Quant.Elec. 9, 237-239, (1979)(b).

P.Baues: Opto-Electron. 1,37-44, (1969).

A.J.Berry: Ph.D. Thesis, University of Southampton, 1983.

V.N.Blaschuk et al: Opt.Commun. 27, 137, (1978).

N. Bloembergen: Am. J. Phys. 35, 989-1023, (1967).

N.L.Boling, M.D.Crisp, G.Dube: Appl.Opt.12,650-660, (1973).

D.J.Bradley et al: Phil.Trans.A., 225-237, (1968).

D.J.Bradley, C.J.Mitchell: Phil.Trans.A., 209-233, (1968).

R.L.Carman et al: Phys. Rev. A,2, 60-72, (1970).

D.Cotter, D.C.Hanna, R.Wyatt: Appl.Phys.8,333-340, (1975).

M.J.Damzen, M.H.R.Hutchinson: IEEE. J.Q.E.-19, 7-14, (1983).

Yu.V.Dologopolov: Sov.Phys.JETP. 49, 458-466, (1979).

V.F.Efimkov et al: Sov.Phys.JETP. 50, 267-272, (1979).

R A.Fisher (ed.): "Optical Phase-Conjugation", Academic Press, New York, 1983.

L.M.Frantz, J.S.Nodvik: J.Appl.Phys.34,2346-2349, (1963).

A.Gerrard and J.M.Birch: "Introduction to matrix methods in optics", Wiley, London, 1975.

A.Z.Grasyuk, I.G.Zubarev, N.V.Suyazov: JETP. Lett. 16, 166, (1972).

C.Grey-Morgan: Sci. Prog.,Oxf. 65, 31-50, (1978).

A.L.Gyulamiryan et al: Opt.Spectr.(USSR) 51, 113-114, (1981).

E.E.Hagenlocker, R.W.Minck, W.G.Rado: Phys. Rev.154, 226-233, (1967).

D.C.Hanna, B.Luther-Davies,R.C.Smith:Elect.Lett.8(15),269-370, (1972).

D.C.Hanna, B.Luther-Davies, R.C.Smith: Opto-Elect.4,249-256, (1972).

D.C.Hanna, Y-W.Koo, D.J.Pratt: Opt.Comm.44(3),188-191, (1983).

D.C.Hanna, Y-W.Koo: Opt.Comm.43(6),414-418, (1982).

D.C.Hanna, C.G.Sawyers, M.A.Yuratich: Optics Comm.37(5), 359-362, (1981).

R.W.Hellwarth: J.Opt.Soc.Am. 68, 1050-1056, (1978).

M.Hercher: Appl. Opt. 7, 951-966, (1968).

D.T.Hon: Opt.Eng. 21(2), 252-256, (1982).

W.Kaiser, M.Maier: In "Laser Handbook", F.T.Arrechi, E.O.Schultz-Dubois, Eds., North Holland, Amsterdam, 1077-1150, (1972).

G.G.Kochemasov, V.D.Nikolaev: Sov.Jnl.Quant.Elec. 9(9), 1155-1157, (1979).

W.Koechner: Appl. Opt. 9, 2548, (1970).

W.Koechner:"Solid-State Laser Engineering", Springer Series in Optical Sciences, Vol 1, 1976.

H.Kogelnik, T.Li: Appl.Opt. 5(10), 1550-1567, (1966).

N.M.Kroll: J.Appl.Phys. 36, 34, (1965).

R.H.Lehmberg, K.A.Holder: Phys. Rev. 22, 2156, (1980).

R.H.Lehmberg: Opt.Commun. 43, 369-374, (1982).

V.S.Letokhov: IEEE. J. Q.E.-2, 436-441, (1966).

T.Li: Bell Sys.Tech.Jnl. 44 ,917-932,(1965).

D.von der Linde, M.Maier, W.Kaiser: Phys.Rev.178(1),11-17, (1969).

M.Maier: Phys.Rev.166, 113-119, (1968).

M.Maier, W.Kaiser, J.A.Giordmaine: Phys.Rev.177(2), 580-599, (1969).

M.Maier, G.Renner: Opt.Commun. 3, 301-304, (1971).

E.A.J.Marcatili, R.A.Schmeltzer: Bell.Syst.Tech.Jnl. 43, 1783-1809, (1964).

R.Mays, R.J.Lysiak: Opt.Commun. 32, 354, (1980).

M.McGeoch, Opt.-Elect.2,85-89, (1970).

R.W.Minck, E.E.Hagenlocker, W.G.Rado:J.Appl.Phys.38(5), 2254-2260, (1967).

J.Murray, Lawrence Livermore Laboratory, Livermore, California.

D.M.Pepper: Opt.Engineering 21,156-183, (1982).

N.F.Pilipetskii, V.I.Popovichev, V.V.Ragulskii: Sov.Phys.Dokl. 24, 845, (1979)(a).

N.F.Pilipetskii, V.I.Popovichev, V.V.Ragulskii: Opt.Commun. 31, 97, (1979)(b).

A.S.Pine: Phys.Rev. 149, 113-117, (1966).

J.Richards: Appl.Opt. 22, 1306-1308, (1983).

C.G.Sawyers: Ph.D. Thesis, University of Southampton, (1981).

V.G.Sidorovich: Sov.Phys.Tech.Phys. 21, 1270, (1976).

A.I.Sokolovskaya, G.L.Brekhovskikh, A.D.Kudryavtseva: Opt.Comm.24, 74-76, (1978).

J.Steffen, J.P.Lörtscher, G.Hertziger: IEEE. Jnl. QE-8(2), 239-245, (1972).

O.Svelto: "Principles of Lasers", Plenum Press, New York, 1982.

T.Trenholme: Semiannual Report UCRL-50021-73-1, Lawrence

Livermore Lab.,Livermore, California.(1973).

W.R.Trutna, R.L.Byer: Appl. Opt. 19(2), 301-312, (1980).

H.Vanherzeele, J.L.Van Eck, A.E.Siegman, Appl. Opt. 20,3484-6, (1981).

Chen-Show Wang: Phys.Rev.182, 482-491, (1969).

T.A.Wiggins, R.V.Minck, D.H.Rank: Appl.Opt. 5, 1069, (1966).

T.A.Wiggins et al: J.Opt.Soc.Am. 57, 661, (1967).

A.Yariv: "Quantum Electronics", second edition, John Wiley and Sons Inc. (1975).

A.Yariv: Opt.Comm.25(1),23-25, (1978).

B.Ya Zel'dovich, V.I. Popovichev, V.V. Ragul'skii, F.S.Faizullov: Sov.Phys. JETP. 15, 109-112, (1972).

B.Ya.Zel'dovich, V.V.Shkunov: Sov.Jnl.Quant.Elec. 7, 610, (1977).

B.Ya.Zel'dovich, V.V.Shkunov: Sov.Jnl.Quant.Elec. 8, 15, (1978)(a).

B.Ya.Zel'dovich, V.V.Shkunov: Sov.Phys. JETP. 48, 214-219, (1978)(b).

I.G.Zubarev: Sov.J. Quant. Elec. 10, 1179-1181, (1980).

ACKNOWLEDGEMENTS

Firstly, I am indebted to my supervisor, Dr. David Hanna, for his invaluable advice and continuous encouragement during the period of this work. Many thanks are due to other members of the laser group at Southampton University, in particular Andrew Berry, David Hearn and Graham Smith during the early stages, Joseph Koo and David Pratt for help with electronics, Ruth Hodder for technical assistance, Marcos Pacheco, Kin Hung Wong, David Pointer and Dr. Allister Ferguson.

Financial support in the form of a CASE studentship was provided jointly by the Science and Engineering Research Council and the Central Electricity Generating Board.

Dr. Clive Ireland of J.K.Lasers loaned several pieces of equipment and gave helpful suggestions and services.

Lastly, to Marianne, without whom this thesis would surely have been completed many months ago!